takece.com
Continuing Education Simplified!

Course Title: Use of Ultrasound in Musculoskeletal Disorders

Topic List:-

Chapter

Musculoskeletal and Nerve Ultrasonography

Stefan Cristian Dinescu, Razvan Adrian Ionescu, Horatiu Valeriu Popoviciu, Claudiu Avram and Florentin Ananu Vreju

Abstract

Musculoskeletal ultrasound had gained more and more importance lately and there is no doubt now about its role in the diagnosis and management of rheumatic diseases such as rheumatoid arthritis, spondyloarthritis, osteoarthritis and crystal related arthropathies. We can say that now, US is a widely available, non-invasive, and cost-effective technique suitable for the evaluation of the articular and periarticular structures, such as joints, tendons, muscles, ligaments, and bursa. The real-time capabilities of the US allow continuous observation of those structures during movement and of the needle placement during musculoskeletal interventions. More than this, recently, ultrasonography (US) has gained its rights in the evaluation of Sjogren syndrome and giant cell arteritis. Thus, US can detect changes secondary to both inflammatory joint diseases, like synovitis, tenosynovitis or enthesitis, and to degenerative disease, like osteophytes or tendinosis. US can identify calcium pyrophosphate and urate deposits at the level of the cartilage and tendons and to recognize the changes at the level of the salivary glands in the context of the Sjogren's syndrome and the ones at the level of the temporal artery, secondary to giant cell arteritis.

Keywords: rheumatology ultrasound, musculoskeletal, synovitis, enthesitis, nerve

1. Introduction

Ultrasonography (US) has become an integral part of the clinical rheumatology practice. It provides relevant information in many aspects of patient management, both diagnostic and therapeutic. It is a safe, non-invasive and readily accessible imaging modality, with a lack of contraindications. In this respect, US carries significant advantages over other imaging tests, such as CT or MRI. Musculoskeletal ultrasound provides the physician with a real-time evaluation, allows for a dynamic view of target areas and simultaneous scanning of multiple anatomical structures. It is fairly easy to apply imaging techniques, although it requires a prolonged period of training to achieve expert-level assessments. Musculoskeletal ultrasound (MSUS) allows for a fast examination of small and large joints and can guide further diagnostic tests. One of the most important benefits of MSUS is early diagnosis of articular and periarticular inflammation; this is especially the case in rheumatoid arthritis and psoriatic arthritis where diagnostic delay from symptom onset can lead to significant structural progression and poor outcomes. US evaluation is included in the EULAR (European League Against Rheumatism) recommendations for use of imaging in

disease management for both RA and Spondyloarthritis (SpA) [1, 2]. Also, standardization of US procedure is provided through the EULAR standardized procedures for US imaging [3] and OMERACT (Outcome Measures in Rheumatoid Arthritis Clinical Trials) definitions of US pathology [4]. Apart from inflammatory and degenerative joint disease, US can also aid the rheumatologist in the diagnosis and management of connective tissue diseases such as systemic scleroderma, Sjögren's syndrome or vasculitis [5–7].

2. Principles of ultrasound examination in rheumatology

Ultrasonography enables detailed examination of anatomical structures, periarticular soft tissue and also blood flow using Doppler modalities. The 2017 EULAR standardized procedures for US [3] recommend the use of high-resolution linear transducers with a working frequency between 6 and 14 MHz for deeper structures and a frequency of ≥15 MHz for superficial areas. Probe compression can be used to distinguish compressible from non-compressible tissue, but should be avoided when examining blood flow. Images acquired in the long axis should be oriented with the proximal aspect to the left of the screen, while in the short axis, the structures of interest will be aligned just as the examiner is looking at the patient.

US evaluation can assess bone surface, cartilage, tendons, ligaments, synovial proliferation and bursal effusions. Additionally, soft tissue US will include examination of blood vessels, skin, adipose tissue, peripheral nerves for entrapment or tumors (**Figure 1**) and muscles that can be scanned for inflammation, lesions or fluid collections [8].

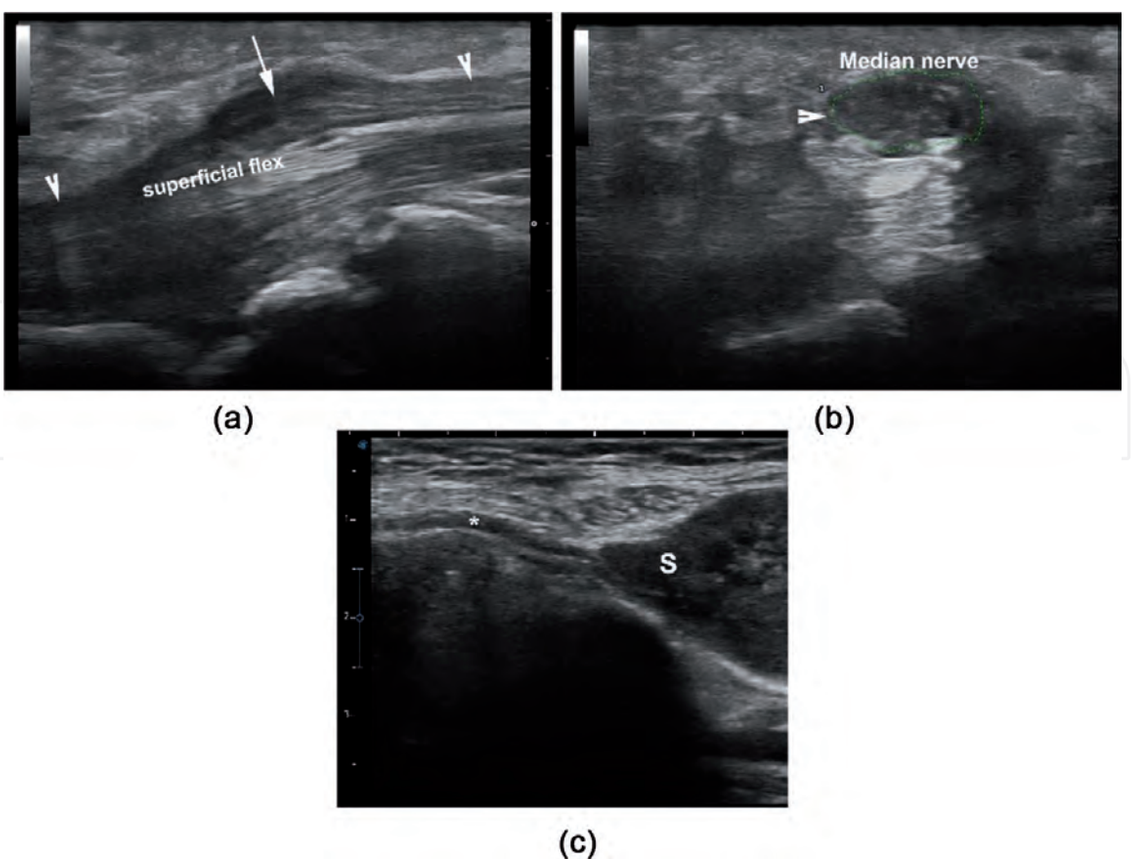

Figure 1.
Ultrasound GS images of a median nerve neuroma (a – Longitudinal, b - transverse) and a peroneal schwannoma (c - longitudinal). Arrowhead – Median nerve, arrow – Neuroma, asterisk – Peroneal nerve, S – Schwannoma.

The study of blood flow is important in detecting inflammatory activity and this can be performed using color Doppler or power Doppler modalities [9]. Because in the musculoskeletal US, the blood flow is very slow in the small new vessels formed by inflammatory angiogenesis, the pulse repetition frequency used is low, under 1KHz. Nevertheless, some small vessel blood flow is difficult to detect because the signal intensity can be lower than movement artifacts and will be filtered out [10].

Ultrasonography is examiner-dependent, thus a good clinical experience, knowledge of anatomy, good image acquisition and reading of the ultrasound images, together with pitfalls recognition are needed requirements for a quality examination. The OMERACT task-force group has developed standardized definitions to promote uniformity between US examiners' reports (see **Table 1**).

Additional information during US imaging can be obtained through sonoelastography and contrast-enhanced ultrasonography (CEUS) [11–15]. These two US techniques have been studied and proven their usefulness in certain rheumatic diseases, but nevertheless, they are not so widely used as conventional gray scale (GS) and Doppler modalities. Sonoelastography is used for measuring and quantifying tissue stiffness. This can be applied in various situations such as tendon lesions, myositis, and analysis of soft tissue formations such as gout tophi or rheumatoid nodules [16, 17]. Also, promising results are seen in studies of systemic scleroderma, where skin involvement is correlated with loss of dermal elasticity [5]. CEUS can assess joint inflammation and provides a view of the exact vascular patterns, which can also be visible in inflamed sacroiliac joints [10, 18]. Some studies report the superiority of CEUS compared to power Doppler US in detecting synovial hypervascularity [14, 15]. Compared to the known risks of using contrast agents in MRI and CT, contrast agents used in CEUS have no proof of significant side-effects.

Further use of ultrasonography in rheumatology practice resides in the ability to guide local procedures. These include synovial fluid aspiration, therapeutic injection, nerve blocks or soft tissue biopsy [19]. US guided infiltrations have proven to significantly increase the accuracy of medication placement when compared to infiltration guided by anatomical landmarks [20]. This is also the case in aspiration of small fluid effusions or fluid cavities which have multiple septa. Besides the accuracy of therapy injection, US-guided procedures have a reduced risk of damaging nearby nerves, tendons or blood vessels.

Bone Erosion	A step-down intraarticular discontinuity of the bone surface is visible in 2 perpendicular planes.
Synovial Fluid	Abnormal displaceable and compressible, hypoechoic or anechoic (in comparison to subdermal fat) intraarticular material, that does not exhibit Doppler signal. To note that sometimes it may be isoechoic or hyperechoic
Synovial Hypertrophy	Abnormal non-displaceable, but poorly compressible, hypoechoic intraarticular tissue (relative to subdermal fat), that may sometimes be isoechoic or hyperechoic. The Doppler signal might be present.
Tenosynovitis	The thickened tendon sheath, with hypoechoic or anechoic material inside, which is seen in 2 perpendicular planes, and which may exhibit Doppler signal. Also, fluid might be present.
Enthesopathy	Thickened tendon or ligament at its bony attachment, with loss of normal fibrillar architecture, looking abnormally hypoechoic (may contain calcifications, seen as hyperechoic foci and/or bony changes including enthesophytes, erosions, or irregularity), identified in 2 perpendicular planes. It may exhibit a Doppler signal.

Table 1.
OMERACT definitions of ultrasound lesions [4].

Despite being highly sensitive to inflammatory features, sometimes US cannot discriminate between underlying diseases, especially when suspecting septic arthritis. Here, arthrocentesis can aid the diagnosis through fluid analysis in Gram stain, culture, as well as polarized microscopy.

3. Pathology

3.1 Rheumatoid arthritis

Musculoskeletal ultrasound is frequently used in clinical practice when approaching a patient with joint pain or during the management of a patient with an established diagnosis of RA. US examination can provide valuable information and is often essential for differential diagnosis. Gutierez et al. established in a study on 204 patients with undifferentiated arthritis that US can help fulfill the ACR 2010 criteria and led to a modified diagnosis in 42.1% of cases [21]. This is very insightful because it points out to a significant proportion of patients, mainly seronegative cases with limited joint involvement that could be underdiagnosed within the first months from symptom onset. The 2013 EULAR recommendations for imaging in RA have taken this into account and highlighted the importance of early detection of inflammation and structural damage in patients with arthritis in at least one joint [1]. 9 out of 10 recommendations included the use of ultrasound. This stands for the potential benefit of US in the whole disease spectrum: detection of subclinical inflammation, prediction of progression, differential diagnosis and disease monitoring [22, 23].

The US features seen in RA include: synovial proliferation, joint effusion, cortical bone erosions (**Figure 2c** and **d**) and tenosynovitis. Among these, the presence of erosions and synovial proliferation are considered more specific (**Figure 2**). Moreover, synovial thickening with an increased power Doppler signal can differentiate between active and inactive inflammation [24]. The presence of active inflammation on US and bone marrow edema on MRI can predict risk for radiological progression even in asymptomatic joints. The potential for predicting erosive damage has also been proven for features of tenosynovitis [25].

There is significant evidence related to residual inflammation in clinical remission which in this case could be considered an unstable remission [26]. This can predict a disease flare or structural damage in asymptomatic cases within one year [27].

A more accurate evaluation of inflammatory features detected in RA patients will include a semi-quantified scoring system. This has proven to be correlated with disease activity and can aid the clinician in follow-up visits. The OMERACT study group provided grading systems for synovitis in both gray scale and Doppler mode [4] (see **Table 2**). In 2017, the EULAR-OMERACT study group integrated them into a combined scoring system for synovitis (see **Table 3**) [28].

For practical reasons, a physician should limit the number of joints included in one ultrasound examination. The exact number of joints that should be assessed will certainly depend on clinical presentation, but some studies have provided guidance for a more efficient imaging session. Naredo and colleagues proposed the examination of 12 joints using power Doppler which can provide an overall assessment of joint inflammation. The sites included bilateral wrists, second and third MCPs, and second and third PIPs of hands and knee joints [30]. In 2009, Backhaus and colleagues proposed a more limited number of joints which formed the German US7 score. This score included the wrists, II and III MCPs and PIPs, II and V MTPs joints of the clinically dominant hand and foot [31].

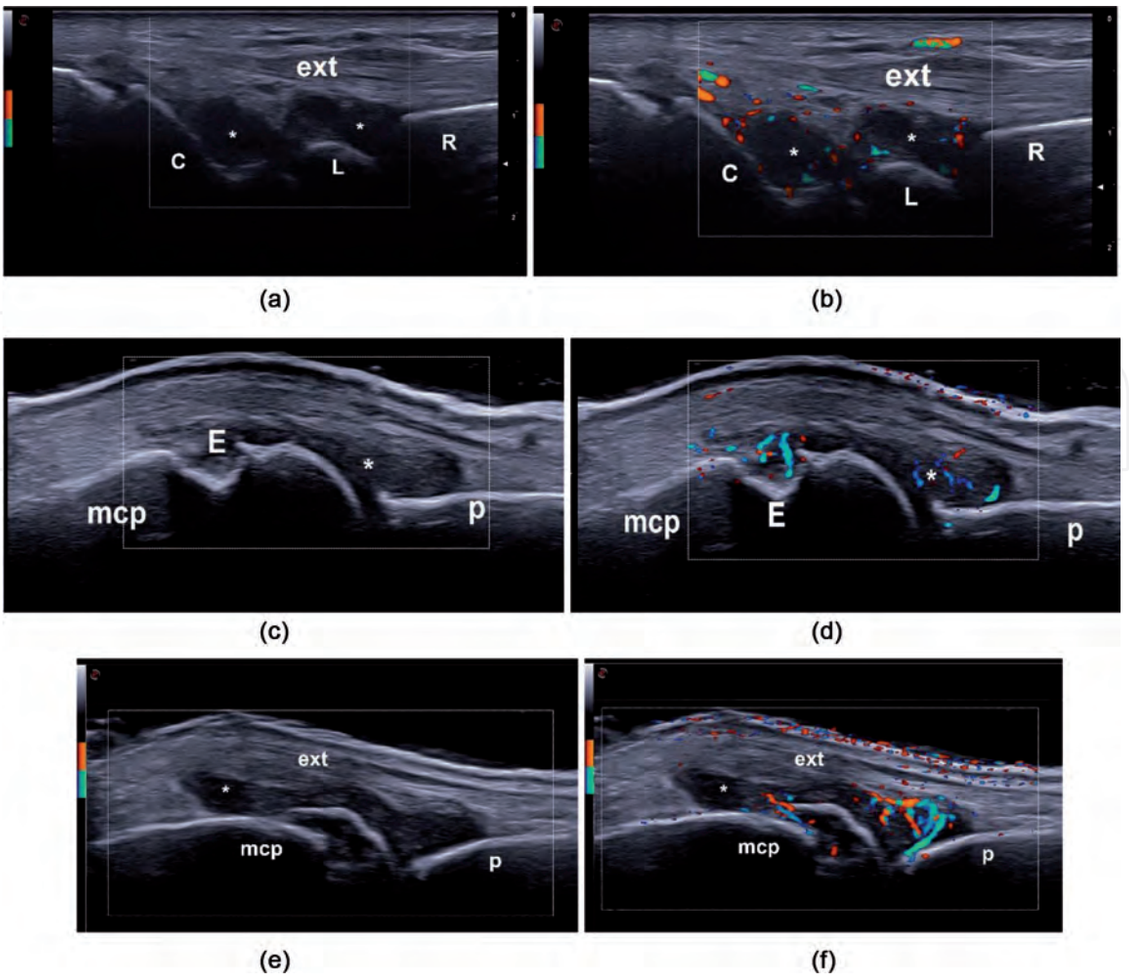

Figure 2.
Synovitis in GS (left images) and with power Doppler (right images) at the level of the wrist (a) and metacarpophalangeal joints (c-f). e – Erosions, ext. – Extensor tendons, mcp - metacarpal bone, p – Phalanx, asterisk – Synovitis.

GS	Grade 0: Normal joint (no synovial hypertrophy, no joint effusion)
	Grade 1: Minimal synovitis (minimal synovial hypertrophy, with or without minimal joint effusion)
	Grade 2: Moderate synovitis (moderate synovial hypertrophy, with or without minimal or moderate joint effusion)
	Grade 3: Severe synovitis (severe synovial hypertrophy, with or without severe joint effusion)
Power-Doppler	Grade 0: No vessels in the synovial membrane
	Grade 1: Up to 3 single color spots or 1 confluent spot plus other up to 2 single spots
	Grade 2: Doppler signal in <50% of the synovium
	Grade 3: Doppler signal in >50% of the synovium

Table 2.
OMERACT scoring system for synovitis [4].

Musculoskeletal ultrasound has proved a strong correlation with other disease activity markers such as the DAS28 score, ESR or CRP levels [32]. Nevertheless, detection of US inflammation is still possible in the context of DAS28 remission and this could influence treatment decisions [12]. US features are sensible to RA-specific

Grade 0: Normal joint	No synovial hypertrophy (SH) in GS and no PD signal (within the synovium)
Grade 1: Minimal synovitis	Grade 1 SH in GS and ≤ Grade 1 PD signal
Grade 2: Moderate synovitis	Grade 2 GS synovial hypertrophy and ≤ Grade 2 PD signal or Grade 1 SH in GS and a Grade 2 PD signal
Grade 3: Severe synovitis	GS grade 3 SH and ≤ Grade 3 PD signal or Grade 1 or 2 synovial hypertrophy in GS and a Grade 3 PD signal

SH – synovial hypertrophy; PD – power Doppler.
In addition, erosive changes have also been integrated into a 0–3 scale for each individual erosion, based on the maximum length. The scoring ultrasound structural erosion (ScUSSe) system is used as follows: 0 = no erosion, 1 = <2 mm, 2 = 2–3 mm, 3 = >3 mm [29].

Table 3.
EULAR-OMERACT combined scoring system for synovitis [28].

therapies and this has also been proven for local intraarticular steroid injections [24]. Thus, ultrasound is a helpful tool for monitoring treatment response.

3.2 Spondyloarthritis

Imaging tests commonly used in patients with axial spondyloarthritis are based mainly on the detection of sacroiliitis through conventional radiology or MRI. The use of ultrasound in SpA patients becomes relevant in peripheral involvement and especially in patients with psoriatic arthritis (PsA). US features seen in SpA patients include: arthritis, tenosynovitis, enthesitis and dactylitis. As in RA, Doppler mode is useful to confirm active inflammation in the articular and periarticular structures. Compared to RA, tenosynovitis (**Figure 3**) is more prevalent, while enthesitis and dactylitis are considered specific features of SpA.

The presence of the lesions on US can help differentiate PsA from early RA. Moreover, psoriatic arthritis patients have proven some other discriminative

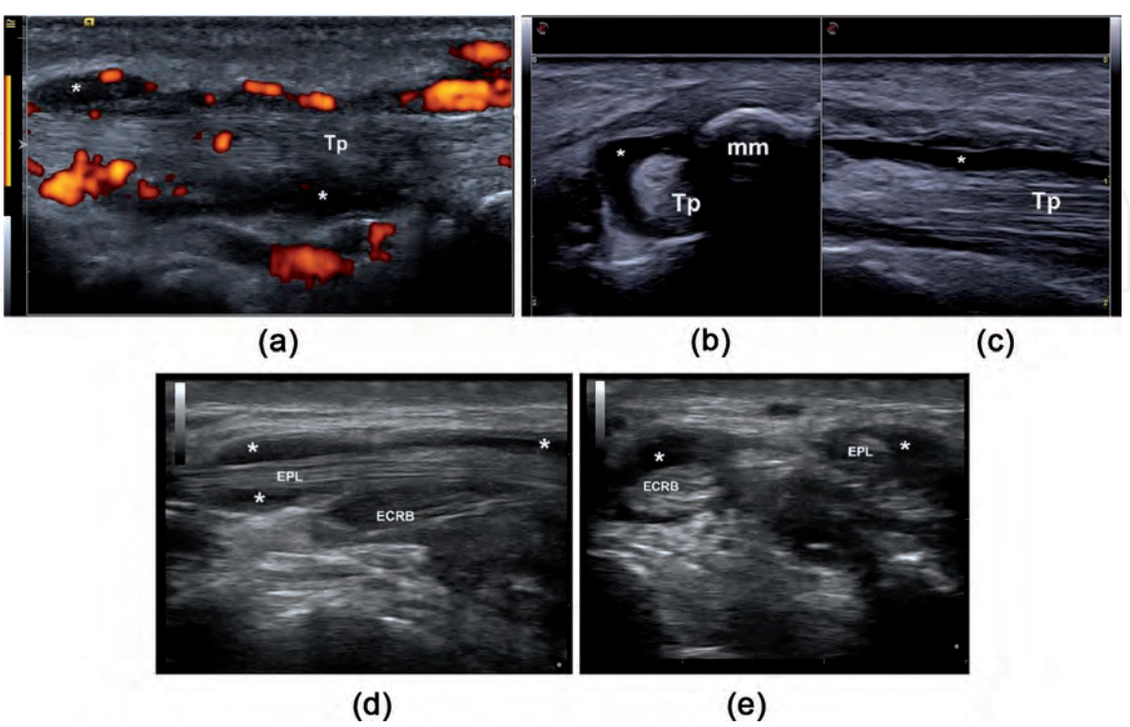

Figure 3.
Ultrasonography of the tibialis posterior (Tp) tenosynovitis (a-c, asterisk) and at the level of extensor carpi radialis brevis (ECRB) and extensor pollicis longus (EPL). mm – Medial malleolus.

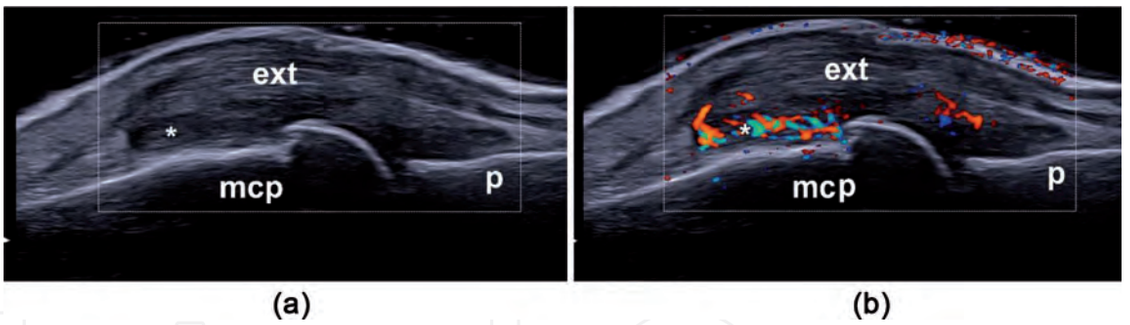

Figure 4.
Ultrasonography of the metacarpophalangeal joints in GS mode (left) and power Doppler (right), with periextensor tendon inflammation (PTI pattern - asterisk). mcp – Metacarpal bone, p – Phalanx, ext. – Extensor tendon.

features such as peritendon extensor digitorum tendon inflammation (**Figure 4**) and central slip enthesitis at the PIP joints [33].

The 2015 EULAR recommendations for the use of imaging in the diagnosis and management of SpA [2] have included ultrasound in three recommendations for peripheral SpA regarding diagnosis, monitoring activity and monitoring structural changes, as follows:

- *Recommendation 2 for peripheral SpA*

  Peripheral arthritis, tenosynovitis and bursitis may be **detected** by **US** or MRI. Furthermore, those imaging techniques may be used to detect peripheral enthesitis, which might support the **diagnosis** of SpA.

- *Recommendation 5 for peripheral SpA*

  US with high-frequency color or power Doppler and MRI may be used to **monitor disease activity** in peripheral SpA, the decision on when to repeat US/MRI depending on the clinical circumstances.

- *Recommendation 6 for peripheral SpA*

  When the clinical scenario requires monitoring of structural damage in peripheral SpA, MRI and/or **US might provide additional information**, besides conventional radiography.

The OMERACT Ultrasound Task Force published in 2013 a consensus regarding ultrasound score for tenosynovitis (see **Table 4**). A four grade-semiquantitative scoring system is proposed for both gray-scale (grade 0, normal; grade 1, minimal;

grade 0	no Doppler signal
grade 1	focal Doppler signal within the widened synovial sheath, identified in two perpendicular planes, excluding normal feeding vessels
grade 2	multifocal Doppler signal within the widened synovial sheath, seen in two perpendicular planes, excluding normal feeding vessels
grade 3	diffuse Doppler signal inside the widened synovial sheath, seen in two perpendicular planes, excluding normal feeding vessels

Table 4.
OMERACT ultrasound task force scoring system for tenosynovitis using Doppler mode [30].

grade 2, moderate; grade 3, severe) and Doppler mode (grade 0, no Doppler signal; grade 1, minimal; grade 2, moderate; grade 3, severe) [30].

Enthesitis is broadly defined as inflammation of the fibrocartilaginous tissue located at the insertion points of tendons (**Figure 5**), ligaments and the joint capsule on bone surface. US features related to enthesitis that have met the 2018 OMERACT consensus [34] include: hypoechogenicity, increased thickness of enthesis, erosions and calcifications/enthesophytes and Doppler signal at insertion. Increased tendon thickness, hypoechogenicity and shadowing of the fibrillar pattern are seen in earlier phases of enthesitis, while cortical bone changes, in the form of erosions and enthesophytes, are related to later stages [35]. Moreover, lesions should be restricted to <2 mm from cortical bone [34]. Nevertheless, distinguishing physiologic entheseal changes in active adults from disease-related lesions may be difficult. Also, lower extremity entheses are prone to mechanical loading, especially in obese patients [36].

When examining enthesis sites for inflammation, a selective approach is required. This will take into account the more accessible areas, present symptoms and potential confounding factors. Various research groups have proposed different sets of enthesis scoring systems. These include the: GUESS - Glasgow Ultrasound Enthesitis Score [37], MASEI - Madrid Sonography Enthesitis Index [38], GRAPPA US - proposed entheseal sites by the GRAPPA Ultrasound Working Group [39] and OMERACT US - proposed entheseal sites by the OMERACT Ultrasound Enthesitis Working Group [34].

New research revealed other areas in which we can find structures that can be assimilated to enthesis. Thus, we can consider as functional enthesis the areas of tendons or ligaments that are wrapped around by pulleys, without being attached to them and as articular fibrocartilaginous entheses, the synovial joints lined with fibrocartilage [40]. Inflammation of those entheses can be identified by US and can explain pain in specific areas.

Dactylitis, one of the more complex inflammatory lesions seen in SpA, is a pandigital disease that involves joint arthritis, tenosynovitis of the flexors, enthesitis of the

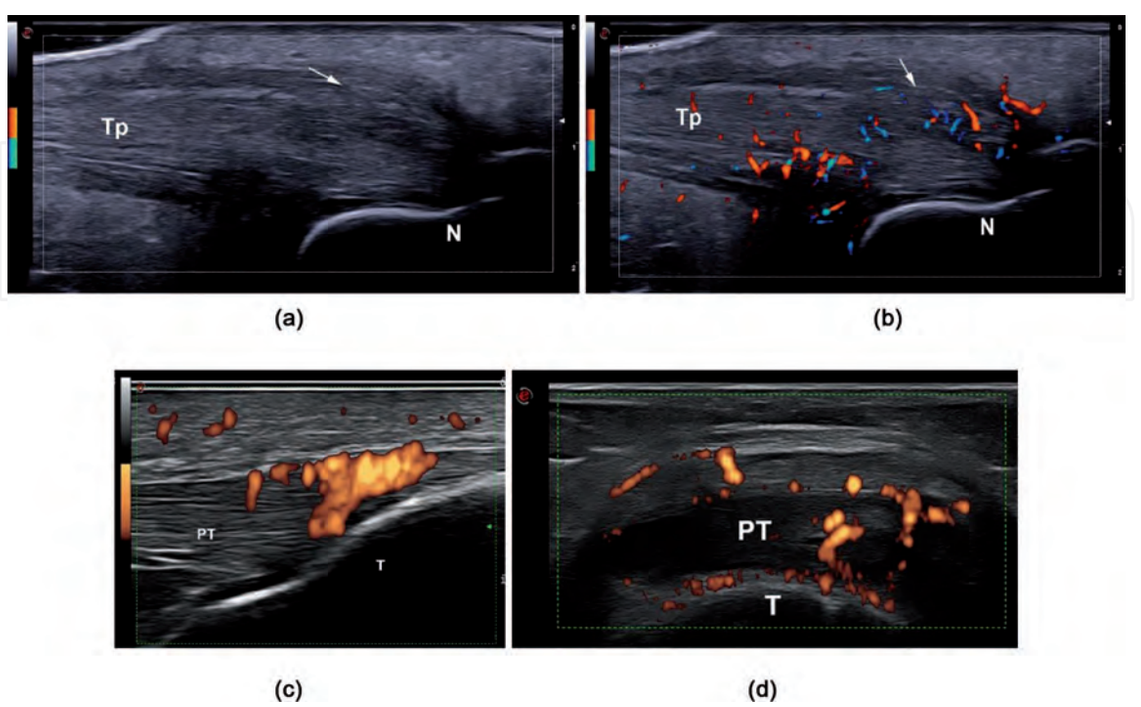

Figure 5.
Ultrasonography of the tibialis posterior (a, b – Longitudinal aspect) (Tp) enthesitis (arrow) at the level of the navicular tuberosity (N) in GS (left) and power Doppler modes (right) and enthesitis of the patellar tendon (c – longitudinal, d – transverse). PT – Patellar tendon, T – tibia.

superficial flexor of the finger, functional enthesitis, proximal to metacarpophalangeal joint (periextensor tendon inflammation) and soft tissue edema (**Figure 6**) [36, 41]. Of this spectrum of lesions, tenosynovitis (**Figure 5**) is considered the primary cause for the characteristic dactylitis or sausage-like appearance of the fingers. Flexor tenosynovitis and joint synovitis are the most frequent features seen in 90% of cases [11]. US lesions related to dactylitis evolve over time. Earlier phases are marked by tenosynovitis and lack of joint inflammation, while in later stages, joint synovitis is more prevalent in comparison to an absent or minimal tenosynovitis [42].

Dactylitis has a relevant role in the early diagnosis of PsA and has also been used as an outcome measure in clinical trials. This has prompted the development of sonographic scores for dactylitis, such as the DACTOS score. It is a composite score which includes the following: peritendinous inflammation of the extensors (PTI), evaluated in GS and PD at the MCP and PIP joints levels (with the maximum score of 4); soft tissue oedema; flexor tenosynovitis evaluated in GS and PD noted in the most severely affected area of the digit (with the maximum score of 6 for each); the combined score for synovitis (evaluated according to EULAR-OMERACT definitions) at the MCP, PIP, and DIP joints (maximum score of 9) [41]. DACTOS score is sensitive to treatment and correlates well with Leeds Dactylitis Index basic, as well as VAS for pain and functional impairment [43].

3.3 Crystal deposition disease

Gout and chondrocalcinosis are the two main forms of crystal deposition disease in which crystals of different compositions accumulate in the intraarticular space and periarticular soft tissue. In gout, raised uric acid levels in the serum to lead to deposition of monosodium urate (MSU) crystals. Chondrocalciosis, also called pseudogout, is characterized by the deposition of calcium pyrophosphate dihydrate (CPPD) crystals. Apart from the different chemical compositions, the both disorders have specific imaging features on ultrasound [17]. MSU crystals in gout generate a characteristic hyperechoic band on the cartilage surface [44], known as the "double contour sign" (**Figure 7**). The dynamic evaluation of the joint reveals the urate hyperechoic band moving together with the bone, thus confirming the belonging to the bone cartilage. This is observed in the majority of gout patients and is reversible with treatment.

MSU deposits can precipitate in the synovial membrane, in the joint cavity within synovial effusion (**Figure 8a–c**), in tendons, bursae and soft tissues. Gout tophi appear as a heterogeneous mass with intermittent hyperechoic foci and can

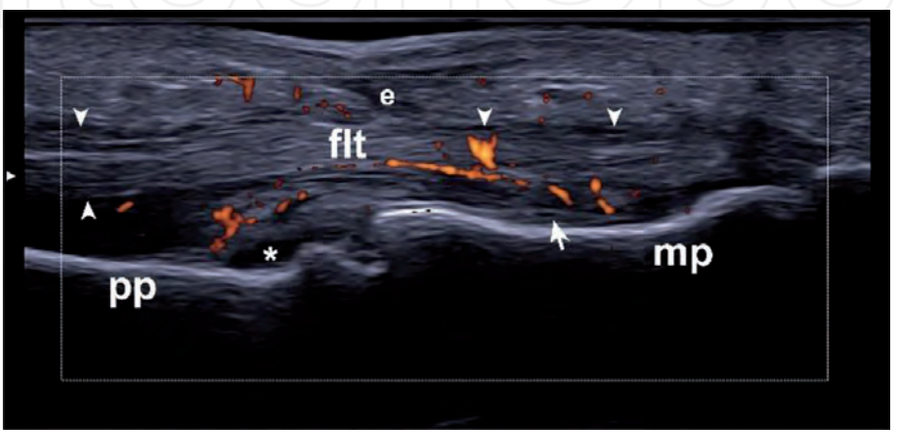

Figure 6.
Ultrasound image of a volar aspect of the finger, showing changes specific to dactylitis. pp – Proximal phalanx, mp – Medial phalanx, flt – Flexor tendon, asterisk – Synovitis, e - soft tissue oedema, arrow - enthesitis of the superficial flexor tendon, arrowheads – Flexor tenosynovitis.

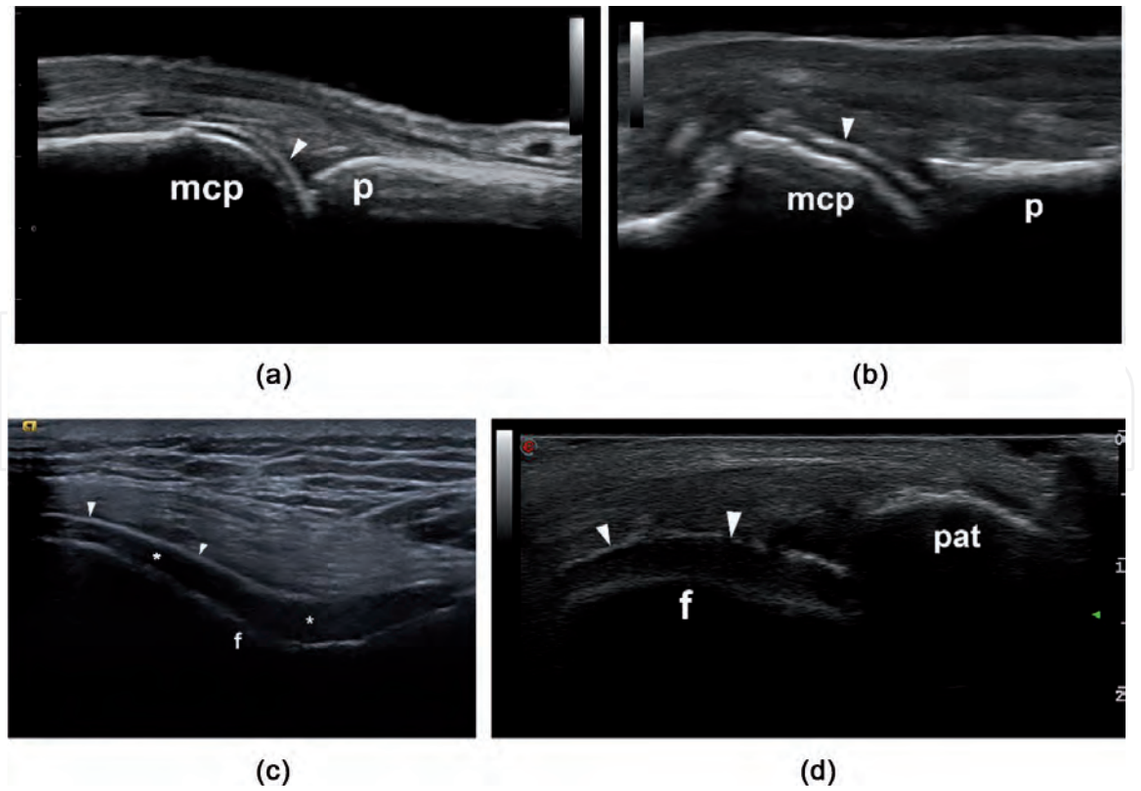

Figure 7.
"Double contour sign" (arrow head) in US of the metacarpophalangeal (a, b) and knee joints (c, d), in longitudinal (a, b, d) and transverse section (c). mcp – metacarpal bone, p – phalanx, f – femur, pat – patella, asterisk – hyalin cartilage.

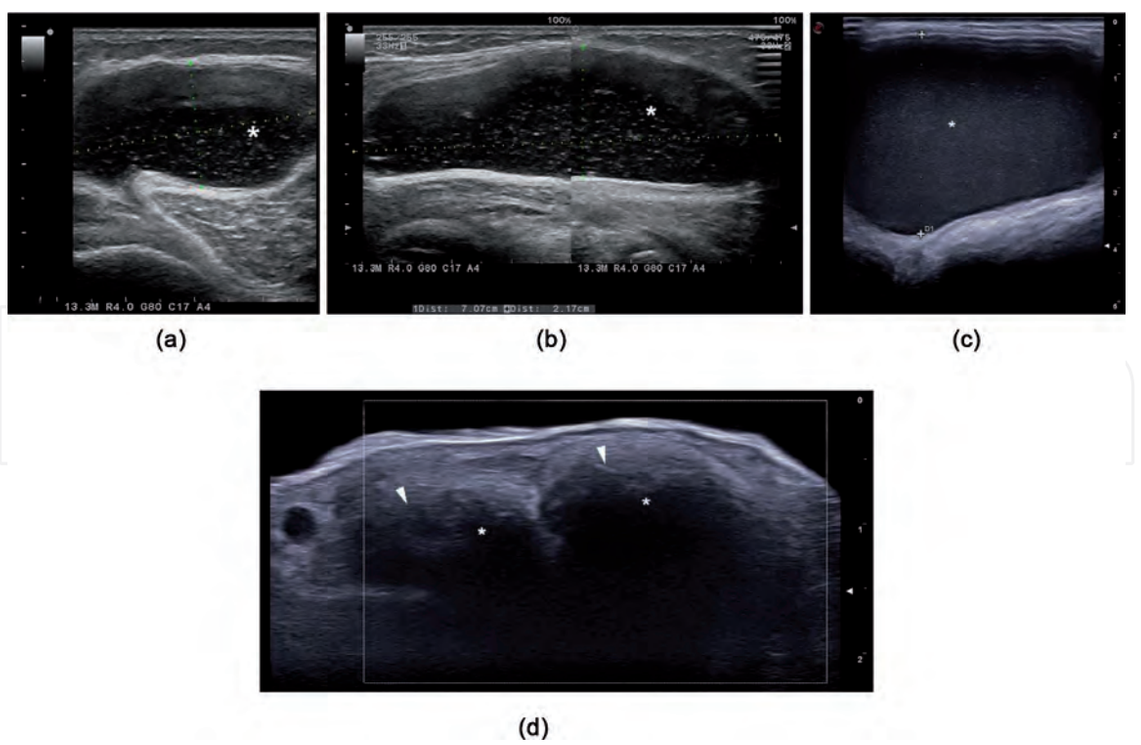

Figure 8.
a–c. Ultrasound images of gouty synovial effusion at the level of the posterior knee – Popliteal cyst (a - transverse, b - longitudinal) and of the olecranon bursa, with the aspect of the "snowstorm" (anechoic area with hyperechoic spots). d. Gouty tophus (arrowhead), with posterior acoustic shadowing (asterisk).

be distinguished from lipoma or rheumatoid nodules which are more hypoechoic and homogenous. Features of MSU crystal deposition inside tendons and joints and even tophi (**Figure 8d**) can be detected in the setting of asymptomatic

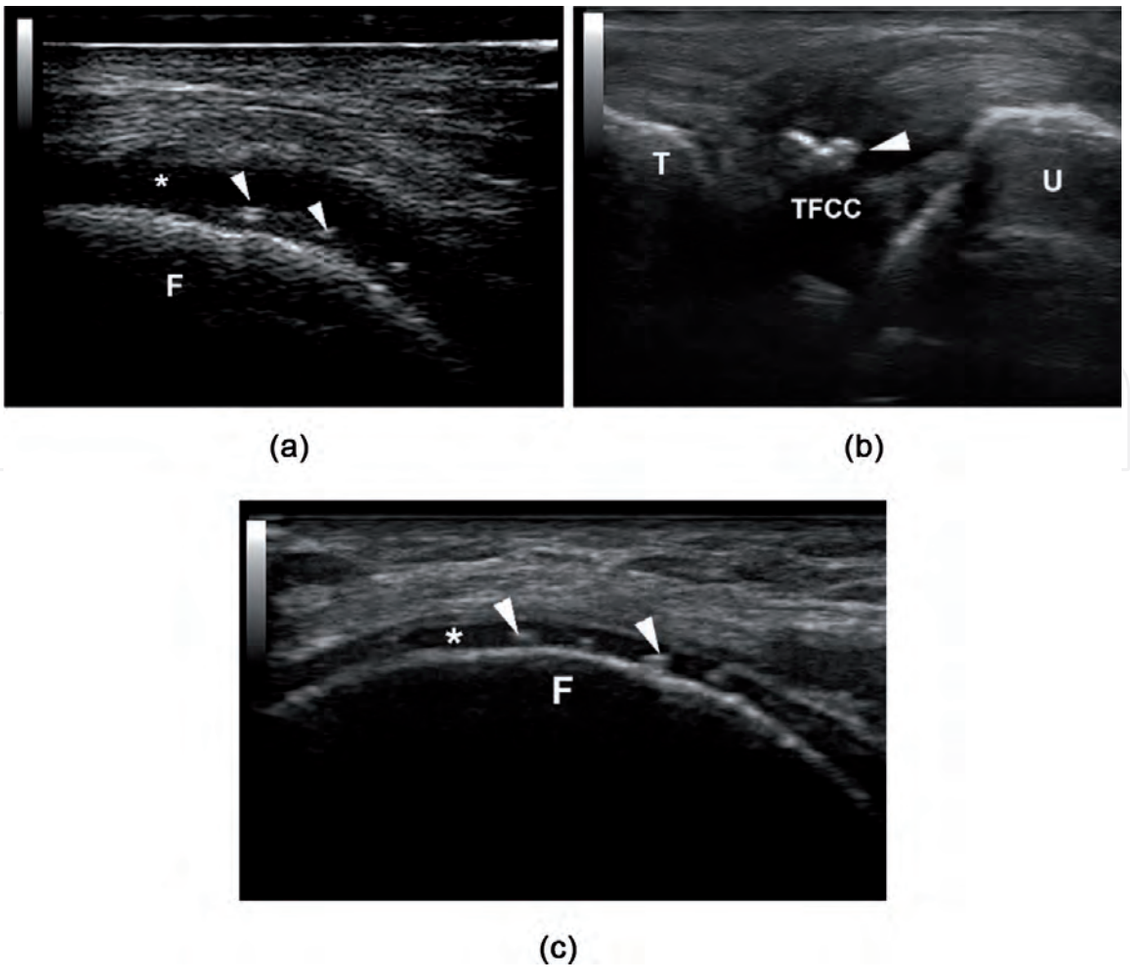

Figure 9.
Ultrasound images of calcium pyrophosphate deposits (arrowheads) in CPPD, inside the knee hyaline cartilage (a, c) and in the triangular fibrocartilage complex (b). F – Femur, TFCC - triangular fibrocartilage complex, asterisk – Hyaline cartilage.

hyperuricemia. EULAR and ACR recommendations support the use of ultrasound in gout and CPPD due to its high sensitivity and specificity [45–47]. The 2015 EULAR/ACR gout classification criteria recognize ultrasound and dual-energy computed tomography as the main imaging modalities used to accurately identify urate deposition [46].

The 2011 EULAR recommendations for calcium pyrophosphate deposition disease (CPPD) highlight the diagnostic potential of ultrasound with a high diagnosis likelihood ratio and possibly even better sensitivity than those of conventional x-rays [47]. The paper of Filippou demonstrated US to be an accurate tool for discriminating CPPD [48]. The OMERACT US group for CPPD has defined in 2017, the ultrasonographic characteristics of CPPD, in both joints and periarticular tissues [49, 50]. In contrast to gouty deposits appearance, at the surface of the cartilage, in CPPD the deposits are present inside the hyaline cartilage. The most important joints in which we can find CPPD deposits are the wrist (at the level of the triangular fibrocartilage), the knee (meniscus and hyaline cartilage) (**Figure 9**), acromioclavicular and hip joint [50].

3.4 Osteoarthritis

Features of degenerative joint disease are easily recognizable by ultrasound examination. Lesions related to osteoarthritis include varying degrees of cartilage damage and osteophyte formation. Although, conventional x-ray is also commonly used in osteoarthritis diagnosis, it can be fairly limited in earlier phases and lacks the capacity to directly visualize the articular hyaline cartilage. One of

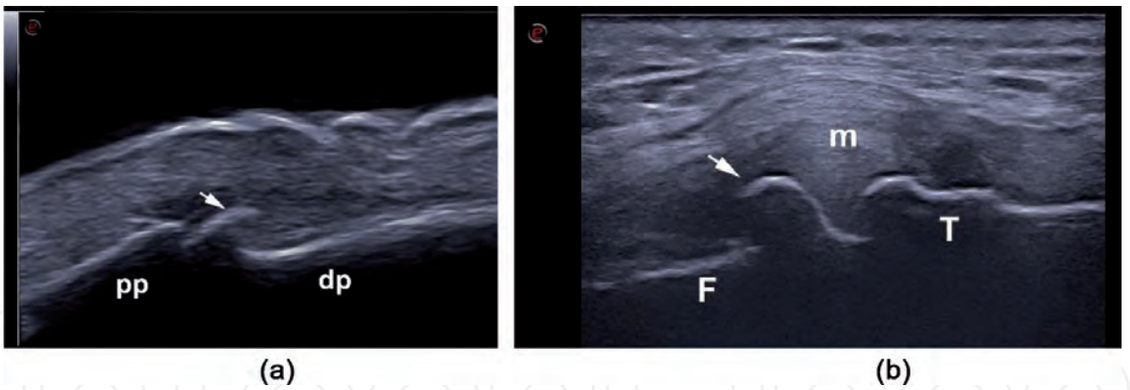

Figure 10.
Ultrasound images of step-up bony prominences, at the level of the interphalangeal (a) and femurotibial (b) joints, suggestive for osteophytes. pp – proximal phalanx, dp – distal phalanx, F – femur, T – tibia, m – meniscus, arrow - osteophyte.

the hallmarks of osteoarthritis US features is the diminished cartilage thickness. Normally, the hyaline cartilage appears as a well-defined anechoic band, due to increased water content, which lacks internal echoes [17]. US has proven to have higher sensitivity compared to conventional x-ray in the assessment of osteophytes and space narrowing. Early features of OA visible through US include: loss of the sharp contour, asymmetric thinning and changes in echogenicity of the cartilage matrix. Additionally, some forms of OA can display erosive and inflammatory changes [51]. Osteophytes are defined as step-up bony prominence seen in two perpendicular planes (**Figure 10**).

The presence of cortical bone irregularities and bony erosions can lead to difficulties in distinguishing osteophyte formations. Upon detection of osteophytes various scoring systems can be applied. This can be a simple semi-quantitative grading scale, as follows: 0 = No osteophyte, 1 = Marginal osteophyte, 2 = Medium osteophyte, 3 = Large osteophyte. Mortada and colleagues proposed a more detailed scoring system for the severity of knee osteoarthritis (see **Table 5**) [52].

The musculoskeletal US can also be applied for therapeutic purposes in degenerative diseases. Patients with OA can benefit from intra-articular infiltration with hyaluronic acid or glucocorticoid and this can be more accurately performed through ultrasound-guided injections. Besides the immediate release of synovial fluid visible during joint aspiration, inflammatory features have also proven to decrease posttreatment. Hence, ultrasound has become a useful tool in both local treatment and monitoring disease activity.

Grade 0		No osteophytes; regular end of femoral condyle without any projections.
Grade 1		Minor osteophyte; just a small projection from the femoral condyle.
Grade 2	2A	Small osteophytes; a projection from the femoral condyle that appears to have an inferior part in the joint space zone.
	2B	Large osteophyte appears to be separated from femoral condyle and to have an inferior part in joint space zone.
Grade 3		Large osteophyte appears to be separated from femoral condyle and to have an inferior part in joint space zone with small superior extension parallel to femoral bone.
Grade 4		Mainly superior osteophyte parallel to the femoral bone with or without an inferior part in joint space zone.

Table 5.
Ultrasonographic grading scale for severity of primary knee osteoarthritis by Mortada et al. [52].

3.5 Scleroderma

One of the most important clinical features of patients with systemic sclerosis (SSc) is the skin thickening. The extent of skin features in SSc is divided clinically into diffuse and limited involvement and is usually quantified using the Rodnan skin score. In addition to this, high-frequency ultrasound can also allow for a detailed assessment of skin involvement. The target measurement is the dermal thickness. For a correct assessment, the following interfaces need to be identified: surface–epidermis, epidermis–dermis and dermis–subcutis [53]. Skin features in SSc vary in time and this is detectable also through US. In the edematous phase, increased thickness associated with low echogenicity is seen due to water content. In time, fibrosis leads to increased echogenicity. Ultrasound measurements correlated well with histopathology, Rodnan skin score and EUSTAR disease activity index [5, 54]. Hongyan and colleagues defined an optimal cutoff point of 7.4 mm for skin thickness, with a sensitivity of 77.4% and specificity of 87.1% [54]. Quantitative studies of skin stiffness using sonoelastography yielded promising results. Research by Yang and colleagues indicates that Shear Wave Elastography can discriminate between SSc patients and controls (**Figure 11**), has good reliability and correlates well with skin thickness and modified Rodnan skin sore [55].

3.6 Sjögren's syndrome

Primary Sjögren's syndrome (pSS) is an autoimmune disease of the exocrine glands, which manifests mainly as hyposecretion of salivary and lacrimal glands. The diagnosis approach is generally focused on the detection of specific autoantibodies, positive ocular tests and findings of characteristic histopathological abnormalities. Sialography and scintigraphy are considered invasive and rarely used in everyday practice, while limited accessibility and the high cost of MRI also hinders its use. Studies on ultrasound have produced promising results for the assessment of major salivary glands (**Figure 12**) of pSS patients and offer a more accessible and less time-consuming alternative to other imaging tests. Still, the established

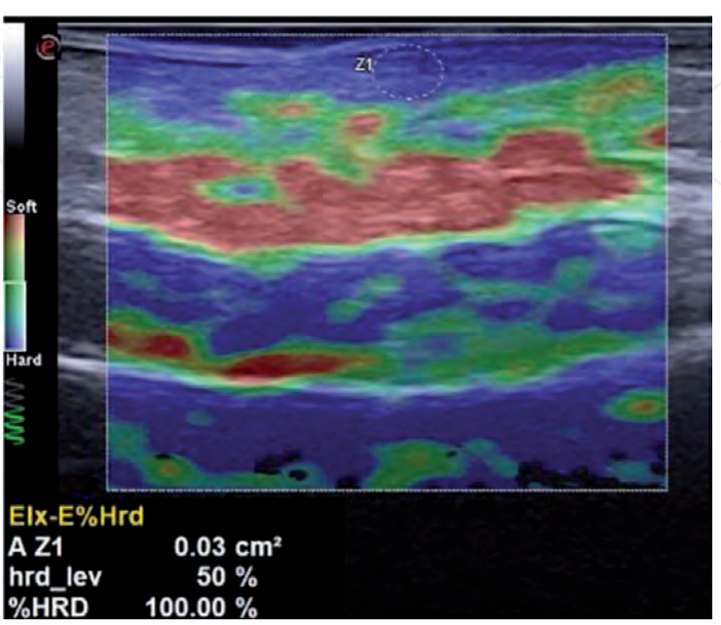

Figure 11.
Elastography of the finger volar aspect that shows the increased hardness of the epidermis and dermis, as shown by the blue color and the hardness percent.

diagnostic criteria developed up until now for pSS have not included ultrasonography as a recommended diagnostic tool.

The parotid and submandibular glands can be easily examined for certain structural abnormalities, such as: parenchymal inhomogeneity, hypo-anechoic or hyperechoic areas (**Figure 12b** and **c**) (produced by cysts or calcifications), surface irregularities and changes in glandular size, intra- or periglandular lymph nodes [56].

Additionally, the use of Doppler modes can identify glandular hypervascularization which has been consistently observed in pSS patients. In early phases, US is marked by an increase in glandular volume and high vascularity, while in later stages reduced volume and hypovascularization are characteristic [57]. Parenchymal inhomogeneity is the most recognizable term used in the development of numerous grading systems.

Research carried out by De Vita et al. [58], Hocevar et al. [59] and Salaffi et al. [60] provided some of the well-known semiquantitative scoring systems. All of these US scores proved high sensitivity and specificity for pSS. De Vita et al. developed a 0-3 scale for parenchymal inhomogeneity, while Hocevar et al. added 0-3 scales also for the number of hypoechogenic areas, hyperechogenic reflections and clearness of salivary gland border. Salaffi et al. proposed an extended 0-4 scale for parenchymal inhomogeneity which includes all of the features previously mentioned (see **Table 6**) [60].

Minor salivary gland biopsy remains the gold standard for diagnosis and is recommended in most patients with suspected pSS, especially in cases with positive autoantibodies. Studies evaluated the predictive value of salivary gland US for histopathology abnormalities. Miedany et al. [61] found a significant correlation between US score and histopathological score (r = 0.82). This supports the use of US when biopsy cannot be performed or in order to stratify the at-risk patients before ordering a biopsy.

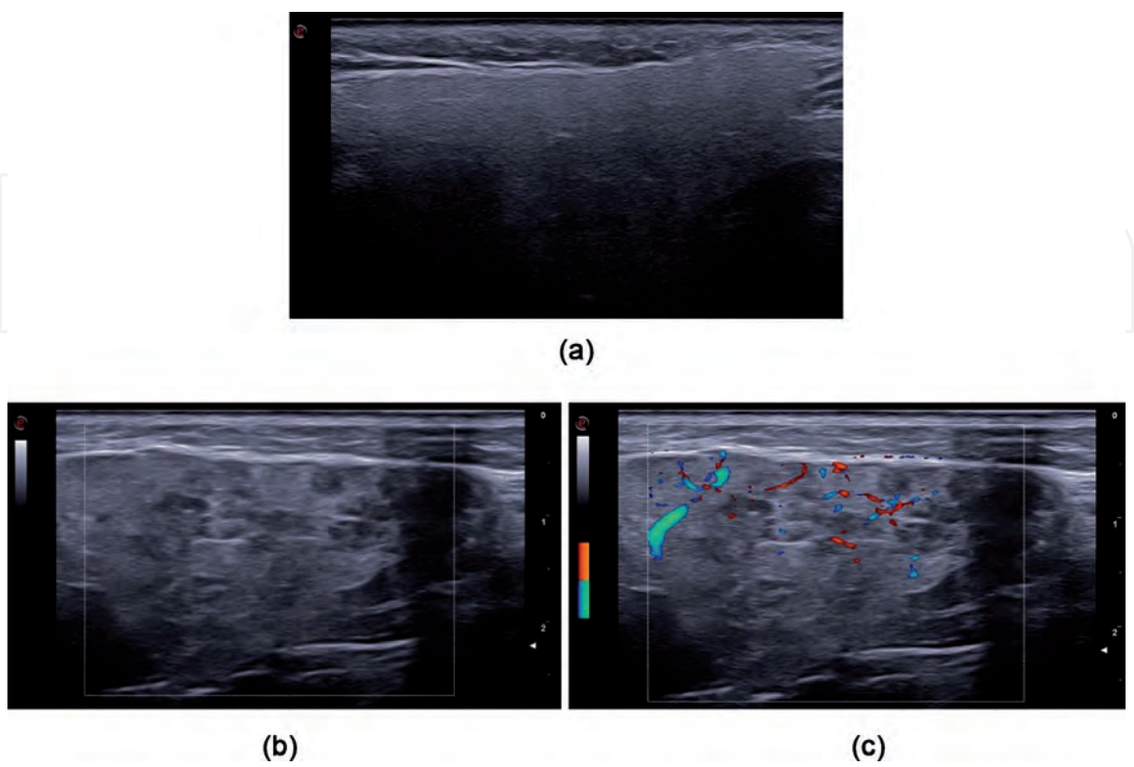

Figure 12.
a. Normal aspect of a parotid gland. b, c. Parotid gland US in GS (b) and PD (c) modes, with the inhomogeneous aspect, with multiple hypoechoic areas, suggestive for glandular inflammation.

Grade 0	normal US aspect of the glands
Grade 1	regular contour, small hypoechoic areas, without echogenic bands, normal or increased glandular volume (with mean values 20 + 3 mm for the parotids and 13 + 2 mm for the submandibular glands) and badly defined posterior border (definite echogenic border with respect to the neighboring structures)
Grade 2	regular contour, numerous dispersed hypoechogenic areas of variable size (<2 mm), without echogenic bands, normal or increased glandular volume and badly defined posterior border
Grade 3	irregular contour, multiple, moderate in size (2–6 mm), circumscribed or confluent hypoechogenic areas and/or multiple cysts, with echogenic bands, regular or decreased glandular volume and no visible posterior border
Grade 4	irregular contour, multiple, large (>6 mm), circumscribed or confluent hypoechogenic areas, and/or multiple cysts or multiple calcifications, with echogenic bands, resulting in severe change of the glandular architecture, decreased glandular volume and posterior glandular border not visible

Table 6.
Ultrasound semiquantitative scoring system for parenchymal inhomogeneity by Salaffi et al. [60].

3.7 Large vessel vasculitis

Ultrasound imaging can detect signs of arterial involvement in giant cell arteritis and Takayasu disease. The characteristic US features of large vessel vasculitis include the presence of a hypoechoic swollen artery wall which is surrounded by oedema, known as the halo sign (**Figure 13**).

The use of US has been studied more extensively in giant cell arteritis. Detection of the typical patchy inflammation seen in temporal arteritis can benefit greatly from ultrasound examination. Besides wall thickening, large vessel vasculitis can display lack of compressibility, stenosis and vessel occlusion [6]. Importantly, giant cell arteritis can spare the temporal arteries in some cases, and thus US examination should also include other large vessels such as the axillary or carotid arteries. The diagnostic value of US has been highlighted by its adoption in the 2018 Update of the EULAR recommendations for the management of large vessel vasculitis. Ultrasound examination is included in the imaging tests used to confirm the diagnosis when large vessel vasculitis is suspected [62].

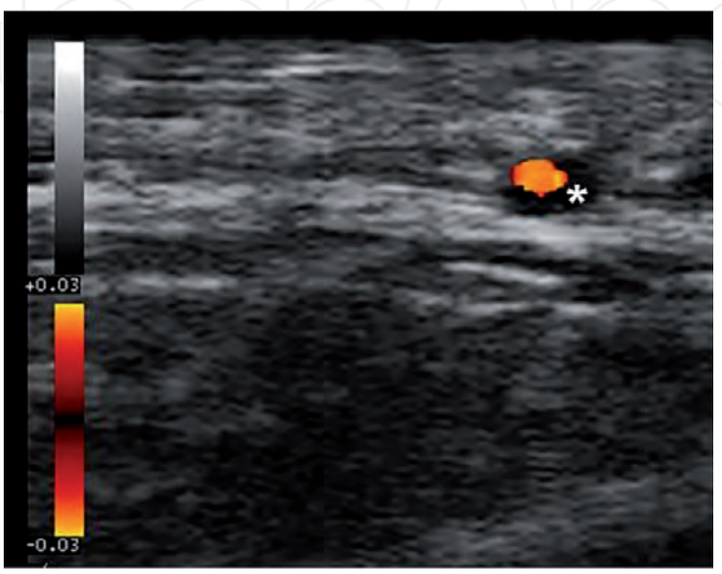

Figure 13.
Ultrasonography of the temporal artery showing a swollen hypoechoic wall – Halo sign (asterisk).

3.8 Muscular disease

Various muscle pathologies can be assessed using ultrasonography. It can detect partial and complete muscle ruptures, fluid collections, muscle infarctions or development of muscle tumors. Features of posttraumatic lesions vary by severity. Milder intensity trauma leads to interstitial hemorrhage which appears as poorly defined hyperechoic areas. In more severe trauma, an intramuscular hematoma can develop, and echogenicity will vary based on time of lesions, with a visible muscle blunt, with a "bell tongue" aspect (**Figure 14**).

On US examination, normal muscle is slightly hypoechogenic with hyperechoic septa and fascia [17]. In transverse plane, muscle tissue will normally have a "starry night appearance", while in long axis fibers run parallel to each other and at an angle towards the muscle insertion. Patients with inflammatory myopathies, such as polymyositis, dermatomyositis and inclusion body myositis, will display changes in muscle echogenicity. In acute phases, muscle edema will cause thickening and only slight increase in echogenicity which proves reversible to treatment [63]. In later

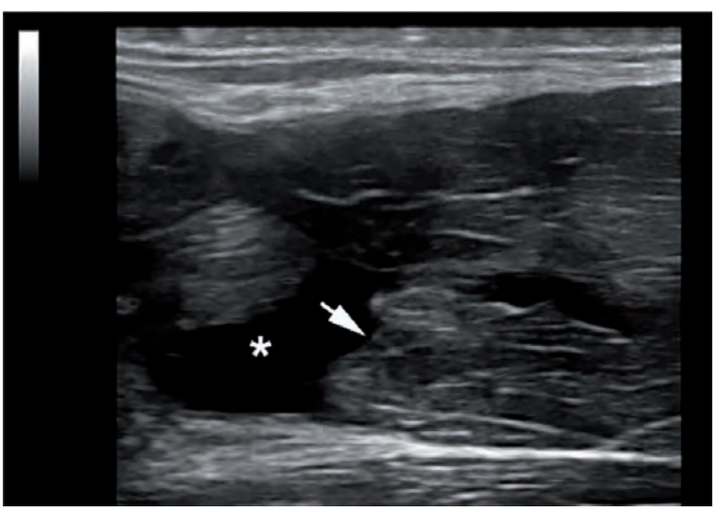

Figure 14.
Ultrasonography of the pectoralis major muscle with a lesion. Asterisk – Effusion secondary to the hemorrhage, arrow – The pectoralis muscle blunt ("bell tongue" aspect).

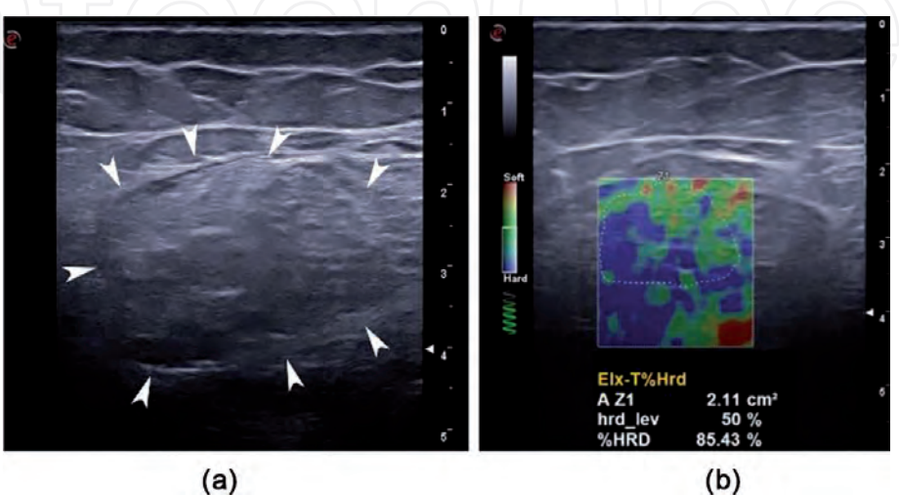

Figure 15.
Ultrasonography of the rectus femoris in a patient with polymyositis, that shows increased echogenicity and lack of the starry night appearance in GS mode (a), and decreased elasticity as showed by the blue color in elastography and the hardness percent (b).

stages, ultrasound will detect markedly increased echogenicity, muscle atrophy and reduced elasticity (**Figure 15**).

Studies have observed correlations between US and histopathology and also significant changes in muscle stiffness when applying elastographic modalities. Patients with active myositis display increased stiffness and this will be gradually reduced as more severe muscle weakness develops [64].

Author details

Stefan Cristian Dinescu[1], Razvan Adrian Ionescu[2], Horatiu Valeriu Popoviciu[3], Claudiu Avram[4] and Florentin Ananu Vreju[1*]

1 Department of Rheumatology, University of Medicine and Pharmacy of Craiova, Romania

2 3d Internal Medicine Department, Carol Davila University of Medicine and Pharmacy Bucuresti, Romania

3 Department of Rheumatology, BFK and Medical Rehabilitation, University of Medicine, Pharmacy, Science and Technology of Targu Mures, Targu Mures, Romania

4 Department of Physical Therapy and Special Motricity, West University of Timisoara, Timisoara, Romania

References

[1] Colebatch AN, Edwards CJ, Østergaard M, van der Heijde D, Balint PV, D'Agostino MA, et al. EULAR recommendations for the use of imaging of the joints in the clinical management of rheumatoid arthritis. Annals of the Rheumatic Diseases. 2013;**72**(6):804-814. DOI: 10.1136/annrheumdis-2012-203158

[2] Mandl P, Navarro-Compán V, Terslev L, Aegerter P, van der Heijde D, D'Agostino MA, et al. EULAR recommendations for the use of imaging in the diagnosis and management of spondyloarthritis in clinical practice. Annals of the Rheumatic Diseases. 2015;**74**(7):1327-1339

[3] Möller I, Janta I, Backhaus M, Ohrndorf S, Bong David A, Martinoli C, et al. The 2017 EULAR standardised procedures for ultrasound imaging in rheumatology. Annals of the Rheumatic Diseases. 2017;**0**:1-6

[4] Wakefield RJ, Balint PV, Szkudlarek M, Filippucci E, Backhaus M, D'agostino M-A, et al. Musculoskeletal ultrasound including definitions for Ultrasonographic pathology. The Journal of Rheumatology. 2005;**32**(12):2485-2487

[5] Chen C, Cheng Y, Zhu X, Cai Y, Xue Y, Kong N, et al. Ultrasound assessment of skin thickness and stiffness: The correlation with histology and clinical score in systemic sclerosis. Arthritis Research & Therapy. 2020;**22**(1):197. DOI: 10.1186/s13075-020-02285-x

[6] Schmidt WA. Ultrasound in the diagnosis and management of giant cell arteritis. Rheumatology. 2018;**57**(suppl_2):ii22-ii31

[7] Jousse-Joulin S, Milic V, Jonsson MV, Plagou A, Theander E, Luciano N, et al. Is salivary gland ultrasonography a useful tool in Sjögren's syndrome? A systematic review. Rheumatology. 2016;**55**(5):789-800

[8] Vreju FA, Ciurea ME, Popa D, Popa F, Parvanescu CD, Chisalau BA, et al. Ultrasonography in the diagnosis and management of non inflammatory conditions of the hand and wrist. Medical Ultrasonography. 2016;**18**(1):90-95

[9] Vreju F, Ciurea M, Roşu A, Muşetescu A, Grecu D, Ciurea P. Power Doppler sonography, a non-invasive method of assessment of the synovial inflammation in patients with early rheumatoid arthritis. Romanian Journal of Morphology and Embryology. 2011;**52**(2):637-643

[10] Zhao C-Y, Jiang Y-X, Li J-C, Xu Z-H, Zhang Q, Su N, et al. Role of contrast-enhanced ultrasound in the evaluation of inflammatory arthritis. Chinese Medical Journal. 2017;**130**(14):1722

[11] Bakewell CJ, Olivieri I, Aydin SZ, Dejaco C, Ikeda K, Gutierrez M, et al. Ultrasound and magnetic resonance imaging in the evaluation of psoriatic dactylitis: Status and perspectives. The Journal of Rheumatology. 2013;**40**(12):1951-1957. DOI: 10.3899/jrheum.130643

[12] Sifuentes-Cantú C, Contreras-Yáñez I, Saldarriaga L, Lozada AC, Gutiérrez M, Pascual-Ramos V. The added value of musculoskeletal ultrasound to clinical evaluation in the treatment decision of rheumatoid arthritis outpatients: Physician experience matters. BMC Musculoskeletal Disorders. 2017;**18**(1):1-10

[13] Klauser A, Halpern EJ, Frauscher F, Gvozdic D, Duftner C, Springer P, et al. Inflammatory low back pain: High negative predictive value of contrast-enhanced color Doppler ultrasound in the detection of inflamed sacroiliac

joints. Arthritis and Rheumatism. 2005;**53**(3):440-444. DOI: 10.1002/art.21161

[14] Klauser A, Demharter J, De Marchi A, Sureda D, Barile A, Masciocchi C, et al. Contrast enhanced gray-scale sonography in assessment of joint vascularity in rheumatoid arthritis: Results from the IACUS study group. European Radiology. 2005;**15**(12): 2404-2410

[15] Liu H, Huang C, Chen S, Zheng Q, Ye Y, Ye Z, et al. Value of contrast-enhanced ultrasound for detection of synovial vascularity in experimental rheumatoid arthritis: An exploratory study. The Journal of International Medical Research. 2019;**47**(11):5740-5751. DOI: 10.1177/0300060519874159

[16] Alfuraih AM, O'Connor P, Tan AL, Hensor EMA, Ladas A, Emery P, et al. Muscle shear wave elastography in idiopathic inflammatory myopathies: A case-control study with MRI correlation. Skeletal Radiology. 2019;**48**(8):1209-1219

[17] Kang T, Horton L, Emery P, Wakefield RJ. Value of ultrasound in rheumatologic diseases. Journal of Korean Medical Science. 2013;**28**: 497-507

[18] Ren J, Zhu J, Li D, Li W, Liu F. The value of contrast-enhanced ultrasonography to detect the sacroiliac joint for predicting relapse after discontinuation of anti-tumor necrosis factor therapy in patients with ankylosing spondylitis. Quantitative Imaging in Medicine and Surgery. 2019;**9**(6):1110

[19] Balea AM, Streba L, Vreju AF, Schenker M, Săndulescu DL, Bondari S, et al. Left gluteal metastasis from a hepatocellular carcinoma - an unusual finding. Romanian Journal of Morphology and Embryology. 2018;**59**(2):549-555

[20] Kane D, Grassi W, Sturrock R, Balint PV. Musculoskeletal ultrasound—A state of the art review in rheumatology. Part 2: Clinical indications for musculoskeletal ultrasound in rheumatology. Rheumatology. 2004;**43**(7):829-838

[21] Gutierrez M, Bertolazzi C, Castillo E, Reyes-Long S, Clavijo-Cornejo D, Santos-Moreno P. Ultrasound as a useful tool in the diagnosis of rheumatoid arthritis in patients with undifferentiated arthritis. Journal of Clinical Rheumatology. 2019;**25**(5):203-208

[22] Barbulescu AL, Ciurea PL, Mitran C, Chisalau BA, Parvanescu CD, Firulescu SC, et al. High frequency ultrasonography of the hand versus anti-RA33 evaluation in early rheumatoid arthritis - a pilot study. Medical Ultrasonography. 2017;**19**(2):166-171

[23] Di Matteo A, Mankia K, Azukizawa M, Wakefield RJ. The role of musculoskeletal ultrasound in the rheumatoid arthritis continuum. Current Rheumatology Reports. 2020;**22**(8):41. DOI: 10.1007/s11926-020-00911-w

[24] Iagnocco A, Ceccarelli F, Perricone C, Valesini G. The role of ultrasound in rheumatology. Seminars in Ultrasound, CT and MRI. 2011;**32**(2):66-73

[25] Lillegraven S, Bøyesen P, Hammer HB, Østergaard M, Uhlig T, Sesseng S, et al. Tenosynovitis of the extensor carpi ulnaris tendon predicts erosive progression in early rheumatoid arthritis. Annals of the Rheumatic Diseases. 2011;**70**(11):2049-2050

[26] Vreju FA, Filippucci E, Gutierrez M, di Geso L, Ciapetti A, Ciurea ME, et al. Subclinical ultrasound synovitis in a particular joint is associated with ultrasound evidence of bone erosions in that same joint in rheumatoid patients

in clinical remission. Clinical and Experimental Rheumatology. 2016;**34**:673-678

[27] Płaza M, Nowakowska-Płaza A, Pracoń G, Sudoł-Szopińska I. Role of ultrasonography in the diagnosis of rheumatic diseases in light of ACR/EULAR guidelines. Journal of Ultrasonography. 2016;**16**(64):55

[28] D'Agostino M-A, Terslev L, Aegerter P, Backhaus M, Balint P, Bruyn GA, et al. Original article: Scoring ultrasound synovitis in rheumatoid arthritis: A EULAR-OMERACT ultrasound taskforce—Part 1: Definition and development of a standardised, consensus-based scoring system. RMD Open. 2017;**3**(1):428

[29] Døhn UM, Terslev L, Szkudlarek M, Hansen MS, Hetland ML, Hansen A, et al. Detection, scoring and volume assessment of bone erosions by ultrasonography in rheumatoid arthritis: Comparison with CT. Annals of the Rheumatic Diseases. 2013;**72**(4): 530-534. DOI: 10.1136/annrheumdis-2011-201114

[30] Naredo E, D'Agostino MA, Wakefield RJ, Möller I, Balint PV, Filippucci E, et al. Reliability of a consensus-based ultrasound score for tenosynovitis in rheumatoid arthritis. Annals of the Rheumatic Diseases. 2013;**72**(8):1328-1334

[31] Backhaus M, Ohrndorf S, Kellner H, Strunk J, Backhaus TM, Hartung W, et al. Evaluation of a novel 7-joint ultrasound score in daily rheumatologic practice: A pilot project. Arthritis and Rheumatism. 2009;**61**(9):1194-1201. DOI: 10.1002/art.24646

[32] Damjanov N, Radunovic G, Prodanovic S, Vukovic V, Milic V, Simic Pasalic K, et al. Construct validity and reliability of ultrasound disease activity score in assessing joint inflammation in RA: Comparison with DAS-28. Rheumatology (Oxford, England). 2012;**51**(1):120-128. DOI: 10.1093/rheumatology/ker255

[33] Zabotti A, Salvin S, Quartuccio L, De Vita S. Differentiation between early rheumatoid and early psoriatic arthritis by the ultrasonographic study of the synovio-entheseal complex of the small joints of the hands. Clinical and Experimental Rheumatology. 2016;**34**(3):459-465

[34] Balint PV, Terslev L, Aegerter P, Bruyn GAW, Chary-Valckenaere I, Gandjbakhch F, et al. D'Agostino MA; OMERACT ultrasound task force members. Reliability of a consensus-based ultrasound definition and scoring for enthesitis in spondyloarthritis and psoriatic arthritis: An OMERACT US initiative. Annals of the Rheumatic Diseases. 2018;**77**(12):1730-1735. DOI: 10.1136/annrheumdis-2018-213609

[35] Gutierrez M, Filippucci E, De Angelis R, Filosa G, Kane D, Grassi W. A sonographic spectrum of psoriatic arthritis: "the five targets". Clinical Rheumatology. 2010;**29**(2):133-142. DOI: 10.1007/s10067-009-1292-y

[36] Kaeley GS. Enthesitis in psoriatic arthritis (part 2): Imaging. Rheumatology. 2020;**59** (Supplement_1):i15-i20

[37] Balint PV, Kane D, Wilson H, McInnes IB, Sturrock RD. Ultrasonography of entheseal insertions in the lower limb in spondyloarthropathy. Annals of the Rheumatic Diseases. 2002;**61**(10): 905-910. DOI: 10.1136/ard.61.10.905

[38] Macía-Villa C, Falcao S, Medina J, De Miguel E. Ultrasonography of enthesis in psoriatic arthritis: A descriptive and reliability analysis of elemental lesions and power Doppler subtypes. Scandinavian Journal of Rheumatology. 2019;**48**(6):454-459. DOI: 10.1080/03009742.2019.1602881

[39] Tom S, Zhong Y, Cook R, Aydin SZ, Kaeley G, Eder L. Development of a preliminary Ultrasonographic Enthesitis score in psoriatic arthritis - GRAPPA ultrasound working group. The Journal of Rheumatology. 2019;**46**(4):384-390. DOI: 10.3899/jrheum.171465

[40] Benjamin M, McGonagle D. The anatomical basis for disease localisation in seronegative spondyloarthropathy at entheses and related sites. Journal of Anatomy. 2001;**199**(Pt 5):503-526

[41] Zabotti A, Sakellariou G. Tinazzi I, et alNovel and reliable DACTylitis glObal sonographic (DACTOS) score in psoriatic arthritis. Annals of the Rheumatic Diseases. 2020;**79**:1037-1043

[42] Girolimetto N, Giovannini I, Crepaldi G, De MG, Tinazzi I, Possemato N, et al. Psoriatic Dactylitis: Current perspectives and new insights in ultrasonography and magnetic resonance imaging. Journal of Clinical Medicine. 2021;**10**(12):2604

[43] Girolimetto N, Zabotti A, Tinazzi I, Possemato N, Costa L, Batticciotto A, et al. Sensitivity to change and clinical correlations of the novel DACtylitis glObal sonographic (DACTOS) score in psoriatic arthritis. Rheumatology. 2021;**60**(9):4103-4111

[44] Grassi W, Meenagh G, Pascual E, Filippucci E. "Crystal clear"- sonographic assessment of gout and calcium pyrophosphate deposition disease. Seminars in Arthritis and Rheumatism. 2006;**36**:197-202

[45] Christiansen SN, Østergaard M, Terslev L. Ultrasonography in gout: Utility in diagnosis and monitoring. Clinical and Experimental Rheumatology. 2018;**36**:S61-S67

[46] Neogi T, Jansen TLTA, Dalbeth N, Fransen J, Schumacher HR, Berendsen D, et al. 2015 gout classification criteria: An American College of Rheumatology/European league against rheumatism collaborative initiative. Annals of the Rheumatic Diseases. 2015;**74**(10):1789-1798

[47] Zhang W, Doherty M, Bardin T, Barskova V, Guerne PA, Jansen TL, et al. European league against rheumatism recommendations for calcium pyrophosphate deposition. Part I: Terminology and diagnosis. Annals of the Rheumatic Diseases. 2011;**70**(4):563-570. DOI: 10.1136/ard.2010.139105

[48] Filippou G, Scanu A, Adinolfi A, Toscano C, Gambera D, Largo R, et al. Criterion validity of ultrasound in the identification of calcium pyrophosphate crystal deposits at the knee: An OMERACT ultrasound study. Annals of the Rheumatic Diseases. 2020;**80**(2): 261-267

[49] Filippou G, Scirè CA, Damjanov N, Adinolfi A, Carrara G, Picerno V, et al. Definition and reliability assessment of elementary ultrasonographic findings in calcium pyrophosphate deposition disease: A study by the OMERACT calcium pyrophosphate deposition disease ultrasound subtask force. The Journal of Rheumatology. 2017;**44**(11): 1744-1749

[50] Filippou G, Scirè CA, Adinolfi A, Damjanov NS, Carrara G, Bruyn GAW, et al. Identification of calcium pyrophosphate deposition disease (CPPD) by ultrasound: Reliability of the OMERACT definitions in an extended set of joints - an international multiobserver study by the OMERACT calcium pyrophosphate deposition disease ultrasound. Annals of the Rheumatic Diseases. 2018;**77**(8):1195-1200

[51] Amorese-O'Connell L, Gutierrez M, Reginato AM. General applications of ultrasound in rheumatology practice. Federal Practitioner. 2015; **32**(Suppl. 12):8S

[52] Mortada M, Zeid A, Al-Toukhy MAE-H, Ezzeldin N, Elgawish M.

Reliability of a proposed Ultrasonographic grading scale for severity of primary knee osteoarthritis. Clinical Medicine Insights: Arthritis and Musculoskeletal Disorders. 2016;**9**:161-166

[53] Moore TL, Lunt M, McManus B, Anderson ME, Herrick AL. Seventeen-point dermal ultrasound scoring system—A reliable measure of skin thickness in patients with systemic sclerosis. Rheumatology. 2003;**42**(12): 1559-1563

[54] Li H, Furst DE, Jin H, Sun C, Wang X, Yang L, et al. High-frequency ultrasound of the skin in systemic sclerosis: An exploratory study to examine correlation with disease activity and to define the minimally detectable difference. Arthritis Research & Therapy. 2018;**20**(1):1-8

[55] Yang Y, Qiu L, Wang L, Xiang X, Tang Y, Li H, et al. Quantitative assessment of skin stiffness using ultrasound shear wave Elastography in systemic sclerosis. Ultrasound in Medicine & Biology. 2019;**45**(4): 902-912. DOI: 10.1016/j.ultrasmedbio. 2018.11.015

[56] Carotti M, Salaffi F, Di Carlo M, Barile A, Giovagnoni A. Diagnostic value of major salivary gland ultrasonography in primary Sjögren's syndrome: The role of grey-scale and colour/power Doppler sonography. Gland Surgery. 2019;**8**(Suppl. 3):S159

[57] Lee KA, Lee SH, Kim HR. Diagnostic and predictive evaluation using salivary gland ultrasonography in primary Sjögren's syndrome. Clinical and Experimental Rheumatology. 2018;**36**:S165-S172

[58] De Vita S, Lorenzon G, Rossi G, Sabella M, Fossaluzza V. Salivary gland echography in primary and secondary Sjögren's syndrome. Clinical and Experimental Rheumatology. 1992;**10**(4):351-356

[59] Hočevar A, Ambrožič A, Rozman B, Kveder T, Tomšič M. Ultrasonographic changes of major salivary glands in primary Sjögren's syndrome. Diagnostic value of a novel scoring system. Rheumatology. 2005;**44**(6):768-772

[60] Salaffi F, Carotti M, Iagnocco A, Luccioli F, Ramonda R, Sabatini E, et al. Ultrasonography of salivary glands in primary Sjögren's syndrome: A comparison with contrast sialography and scintigraphy. Rheumatology (Oxford, England). 2008;**47**(8): 1244-1249

[61] El Miedany YM, Ahmed I, Mourad HG, Mehanna AN, Aty SA, Gamal HM, et al. Quantitative ultrasonography and magnetic resonance imaging of the parotid gland: Can they replace the histopathologic studies in patients with Sjogren's syndrome? Joint Bone Spine. 2004;**71**(1):29-38

[62] Hellmich B, Agueda A, Monti S, Buttgereit F, De Boysson H, Brouwer E, et al. 2018 update of the EULAR recommendations for the management of large vessel vasculitis. Annals of the Rheumatic Diseases. 2020;**79**(1):19-30

[63] Albayda J, van Alfen N. Diagnostic value of muscle ultrasound for myopathies and myositis. Current Rheumatology Reports. 2020;**22**(11):82

[64] Botar-Jid C, Damian L, Dudea SM, Vasilescu D, Rednic S, Badea R. The contribution of ultrasonography and sonoelastography in assessment of myositis. Medical Ultrasonography. 2010;**12**(2):120-126

Chapter

Perspective Chapter: Recent Advances in Musculo-Skeletal Ultrasound

Felix Okechukwu Erondu

Abstract

Medical imaging specialists continue to explore better ways of demonstrating pathology and anatomy of the musculo-skeletal system. The continuous quest is fuelled by the desire to improve diagnostic yield, perform procedures more quickly and accurately, reduce risks to patient or operator, achieve better cost efficiency and utilize less complex methodologies. In many instances, musculoskeletal ultrasound acts as a screening, diagnostic tool but also guide and monitor therapeutic interventions. The paper outlines the use of ultrasound in the imaging of peripheral nerve disorders, traumatic and atraumatic joint disorders, Doppler techniques such as super micro vascular Imaging and sono-elastography. Refinements in probe technology and application of digital and novel proprietary software, have continued to improve the resolution of ultrasound images and with finer details on a scale not previously possible. With increasing experience and standardization of protocols, Musculoskeletal ultrasound will continue to play a great role in the diagnostic work-up and treatment of related disorders.

Keywords: medical imaging, musculoskeletal, ultrasound, nerve imaging

1. Introduction

Medical imaging specialists continue to explore better ways of demonstrating pathology and anatomy of the musculo-skeletal system. The continuous quest is fuelled by the desire to improve diagnostic yield, perform procedures more quickly and accurately, reduce risks to patient or operator, achieve better cost efficiency and utilize less complex methodologies. The use of ultrasound in diagnosis of musculoskeletal disorders follows the same pattern; becoming an important and effective tool for the diagnosis and follow-up management of various disorders affecting the joints and soft tissues [1, 2].

Ultrasound meets the basic criteria for accuracy, safety, affordability and efficiency. The ability to perform studies in real time and thus possible correlation of physico-clinical features of disease entities are even more pertinent reasons to choose ultrasound. Furthermore, it holds a great potential in providing guide to therapy, allowing effective follow-up to be performed. It has also provided learning opportunities for a variety of practitioners in multiple specialties such as radiology, primary care, orthopedic surgery, podiatry and physiotherapy [3].

For physical therapists in particular, ultrasound provides a unique opportunity to have a real-time assessment of musculoskeletal system to identify changes in

function, isolate pain following an injury and provide guide to useful interventions that can improve outcome [3]. In many climes, it can be argued that MRI is the mainstay modality in the evaluation of musculo-skeletal disorders. Its high cost, unavailability especially in developing and resource limited countries and the degree of sophistication required for its operation, remain reasons to explore ultrasound. Even when an MRI is available, diagnostic Ultrasound findings continue to play a complementary role in the diagnostic work-up.

Thankfully, the capabilities of ultrasound appear to have been enhanced by the presence of improved probe technology, better data acquisition and digital image processing techniques. Ultrasound has great potential for the imaging of tendons, nerves, ligaments, muscle tissue and adjoining joints [3–5].

The chapter is dedicated to reviewing various innovations and techniques of Musculo-skeletal ultrasound and promises to be useful to a wide range of readers.

2. The use of high resolution ultra-high frequency transducers

The improved diagnostic yield from ultrasound studies continues to fuel its utilization in the work up of various disease processes. In Particular, high resolution ultrasound is a requirement for musculo-skeletal imaging. To ensure that these requirements are in place, continuous research and development efforts are geared towards rapid advancements in electronics, computing, and transducer technology. Combined with sophisticated signal processing techniques, ultrasound has acquired the degree of spatial and contrast resolution required for musculo-skeletal imaging. The use of high-frequency transducers in the range of 12–18 MHz has become the mainstay in MSK ultrasound. The improved resolution afforded by this, allows evaluation of subtle changes in nerves, tendons, and ligaments [1, 4, 6]. Improvements in the design of ultrasound transducers has resulted in the development of those with very high frequency in the range of 20–70 MHz. This may have spatial resolution in the range of 50–100 μm, which permit detailed anatomy of the extremities. The higher the frequency, the better the spatial resolution and the less the penetrative ability of the resulting sound waves. Fortunately, deep penetration is not a critical requirement for superficial structures, thus ultra-high-frequency transducers are ideal for evaluating superficial musculoskeletal structures. In principle, what we lack in penetration, we gain in detail and spatial resolution. This sort of detail is invaluable when imaging the nerve fascicles by ultrasound [6–8].

3. Tendon/ligament imaging

Tendons are uniquely positioned to connect muscle tissue to bones. This is due to the high collagen content as well as the arrangement of fibers. Generally, the collagen macro-molecules are grouped into fibrils; an arrangement which is both layered and complex in nature. This in turn are bundled into fibers and fascicles surrounded by vascularized connective tissue endotendon. Each tendon is surrounded by a tendon sheath, made of two layers of synovium. Each tendon is uniquely suited to its function, and explains why the orientation of the fibers change, depending on how much tension it's expected to bear. Sometimes, the collagen is majorly aligned along the long axis of the tendon, as seen in the patella. In other tendons, particularly those with origins from more than one muscle such as the Achilles tendon and quadriceps tendon, the fibers run as discrete bundles. Although, healthy tendon bundles exhibit good tensile strength, repetitive stress may result in trauma to the tendon and tendinopathy. This is common in athletes,

where acute inflammatory response may result in Paratenonitis or tenosynovitis. In contrast, ligaments are important in connecting two bones, and contain more proteoglycan and water, as well as a relatively lower collagen content. Furthermore, the connective tissue structure of ligaments are less uniform and consists of poorly ordered, interlaced and weaving pattern. Injuries to a ligament may cause further restriction of joint movement and therefore is associated with joint derangement. In imaging the ligament, it must be appreciated that the tension of each ligament may be determined by the extent of movement at the adjacent joint. The lesions which result from ligamental injury therefore depends on the position of the joint at the time of injury. The imaging of tendons and ligaments represents one of the best applications of musculoskeletal Ultrasound. It is not only accurate, but the timely diagnosis allows early intervention using conservative measures thereby delaying or reducing the likelihood of surgery) [9].

It is also possible to guide minimally invasive interventional treatments, which improves outcome and reduce the potential for post-intervention complications. In addition to all other advantages of ultrasound, the imaging of tendons is attractive due to a relatively high lesion detection rate [10]. The introduction of high-frequency, high resolution transducers, use of Doppler techniques and increasing information in this area, have improved the ability of ultrasound to detect fine textural abnormalities of these structures as well as to identify a variety of pathological conditions [11]. Ultrasound In tendon imaging, can evaluate the presence of dislocations, degenerative changes and tendon tears, longitudinal splits, partial and complete rupture, inflammatory conditions and tendon tumors. It is also invaluable as a tool to monitor healing after surgery and to identify post-surgical complications.

4. Nerve imaging

Imaging of the nervous and peripheral structures remain a challenge with conventional modalities such as X-rays and Computed tomography. Ultrasound provides an alternative and effective technique for imaging tendons and nerves. Its attraction is due to the fact that it is painless, has no known side effects and can actually be done in real-time examination. Non pathologic nerves are seen as continuous bundles of neuronal fascicle, which are separated from surrounding connective tissue [11, 12]. Ultrasound of the Neuro muscular tissues continue to define the diagnostic and treatment pathways for peripheral neuropathy [12]. The use of Standard transducers, will ensure imaging of a small proportion of nerve fascicles. This is seen as series of multiple hypoechoic parallel linear areas separated by echogenic bands, representing the fascicle and epineurium respectively. The latter is the outermost layer of dense irregular connective tissue surrounding a peripheral nerve. It usually surrounds multiple nerve fascicles as well as blood vessels which supply the nerve. When diseased, there are identifiable changes in the structure of the nerve tissues including disruption of the connective tissue, loss of parallel/linear hypoechoic fascicular architecture and swelling/increase in diameter. Compression of the nerve fascicles may occur with presence of cysts, tumors or aneurysmal dilatation of support vessels [11, 12].

A very common application of this technique is the evaluation of the relationships of median nerve anatomy in carpal tunnel syndrome, which may explain the cause of nerve compression or impingement. Sonographic changes include increase in the cross-sectional area of the nerve just proximal to the site of compression, loss of hyperechoic intensities within nerve as well as a reduction in mobility of the structures which it supplies [13, 14]. Ultrasound information supports clinical and

electrophysiological testing for detection of compressing lesions caused by nerve entrapment in a variety of osteo-fibrous tunnels of the limbs and extremities. It is also possible to evaluate Congenital anomalies, nerve tears, and neurogenic tumors. Generally speaking, ultrasound has many advantages which include dynamic assessment, non-invasiveness, absence of pain and low cost of service. It therefore qualifies as both a screening, diagnostic as well as monitoring tool [12]. MRI provides a wider field of view, with 3- dimensional images when evaluating nerve entrapment, and the use of intravenous contrast, can diagnose persistent median artery. It is however more expensive, complex and time consuming. It may also have less diagnostic yield in children and patients with claustrophobia [12–14].

5. Sono-Elastography

Sono elastography has become increasingly useful in the evaluation of musculoskeletal disorder injuries and provides a non-invasive method of obtaining both qualitative and quantitative information of mechanical and structural properties of tissues [15]. When a tissue is subjected to a force within a defined cross-sectional area, it can experience changes in its structure or deformation. The degree of deformation is a function of how stiff the tissue is. The Tissue stiffness is expressed using a physical property called Young's modulus, or modulus of elasticity. Theoretically, Young's modulus is defined as the ratio of stress (the force per cross-sectional area) for a certain material and the strain (i.e. deformation; in this case, tissue deformation). The study of the elastic properties of tissues using ultrasound is called Sono-elastography. It gives both qualitative and quantitative distribution of biological tissue strains and elasticity, and finds application in various clinical settings. There are two major applications Strain or Quasi-static elastography (QSE): This involves physical compression and displacement of tissues by the sonographer, which in turn induces a slow mechanical stress (strain) on tissues [15].

Both quantitative and qualitative assessment and comparison of the resulting stress is performed for tissues at rest and under compression. In order words the degree of stiffness, which is indicated by the range of tissue displacement is estimated. The degree of stiffness is represented quantitatively by a value and qualitatively in a color scale/mosaic that identifies the "softest" and "hardest" tissue areas. Strain sono-elastography provides a color map of tissue elasticity that is superimposed on the real-time greyscale ultrasound image. The stiffer the tissue, the more likelihood of being malignant. Consequently, in the breast, invasive cancers present as areas of higher stiffness compared to benign or normal tissues. A number of scoring systems have been developed to compare the presence, size and distribution of areas of elasticity within the supposed abnormality seen on a gray-scale image. This method appear to be more effective for superficially located structures such as breast and soft tissue masses. Shear wave elastography: This is a new method which combines the radiation force induced in a tissue by an ultrasonic beam and an ultrafast or supersonic imaging sequence which synchronizes the real- time propagation of the resulting shear waves. Typically, Shear waves cause particulate moves recorded with high-frequency imaging (5000 to 30,000 Hz), from which the system calculates color shades or elastograms in real-time (quantitative analysis).

This shear wave velocity enables the production of a two-dimensional map of shear elasticity. The technique is performed using a conventional linear array or special matrix probes. The effectiveness of shear wave elastography stems from the fact that the radiation force is automatically generated by the probe rather than the strain induced by an operator in conventional sono-elastography. Consequently, shear wave elastography is more reproducible than conventional or quasi-static

elastography. Once an area has been mapped out by the cursor as region of interest (ROI), the values representing the mean and maximum stiffness are produced. The region corresponding to areas of stiffness can thus be mapped in a fairly reproducible, and quantitative manner. Benign lesions tend to be soft, while malignant lesions are generally stiffer. Applications include assessment of the degree of hepatic fibrosis and characterization of liver lesions, kidney, breast masses, prostate cancer detection, thyroid lesions and imaging of tendons.

6. Doppler studies

The application of Doppler principles in ultrasound imaging has a long history. Its use in the demonstration of blood vessels and patterns of flow have been copiously reported. Consequently, Doppler studies finds extensive clinical use in assessment of pregnancies, gynecology, cardio-vascular system, neonatalogy, surgery and small parts. The question of whether flow exists or not in a lesion is an important tool in resolving Dilemmas and recognizing or characterizing disease processes. It must be recognized that the increased use of ultrasound in musculo-skeletal imaging relate to the capability and ease of using real-time Doppler US [15]. The amount of flow in the tissue under investigation can be compared with the normal to make diagnosis easy. Doppler is particularly useful when evaluating tumor masses, inflammatory changes related to the joints, tendinopathies and some forms of neuropathies. It is also important when differentiating a ganglionic lesion from sarcoma, and in synovitis [15, 16]. The need to differentiate between acute synovitis (pannus) and chronic fibrotic synovium, is made possible by the demonstration of increased blood flow in the former. In fact, the presence of increased blood flow which is present in proliferating pannus fairly correlates with active joint destruction and symptom development. Consequently, ultrasound can make valuable judgment about the prognosis of active sinovitis and pathological sequel of aggressive and destructive changes in the joint. The deployment of Superb Microvascular Imaging in current studies has improved the resolution and sensitivity compared to conventional methods such as Power Doppler. It is known that superb microvascular Doppler technology allows the operator to detect low-grade inflammation, which was hitherto impossible with Power Doppler. The consequence of early detection of active inflammation, is the prospect of early intervention and impact on treatment outcomes [17].

7. Ultrafast Doppler ultrasound

There is an increasing interest in studying the function of human brain using neuro-imaging techniques [18]. In particular, ultrasonic waves which are transmitted at extremely high or ultrafast frame rates, have shown promise in detecting blood flow signals in very small vessels such as those that perfuse the brain [18]. This has been experimented in rodents with advantages of high spatial and temporal resolution, improved penetration and ability to detect microvascular changes associated with brain functions [18].

The advantages are further enhanced due to its portability and possibility of bedside use. Over the past one decade, bold attempts at applying the technique in preclinical imaging, creates room for wider possibilities in neonates, during operative surgery, or better still, the development of non-invasive brain machine interfaces [19]. The clinical application of this technique opens a new vista in the understanding of brain hemodynamics, changes following brain insult, and options for preserving neurological function [18, 19].

8. Conclusion

Refinements in technology continue to expand the capabilities and application of medical ultrasound in many clinical frontiers. One of the areas that has received significant acceptance is in its application to musculoskeletal and Neuro vascular disorders. This has further brought together a variety of clinical specialties such as orthopedics, vascular surgery, podiatry and physical therapy and rehabilitation medicine. The improvement in probe technology has allowed the development of ultra-fast high frequencies, with amazing results in spatial resolution, finer details, increased sensitivity and accessibility to obscure locations. The challenges of operator dependence and lack of standardized protocols have gradually been addressed due to increasing experience and applications by imaging experts [20].

Deployment of Doppler techniques such as Super micro vascular imaging, elastography, ultrafast Doppler and skilled maneuvers allow distinctive visualization of tissues such as joint capsular ligaments, tendons retinacula, fasciae and nerves all of which involve tiny mesenchymal structures whose diameters are in fractions of millimeters [11]. One more critical area of application is in the diagnostic evaluation of obscure masses [21]. These are essentially lesions in locations where conventional imaging modalities are less effective due to poor access. Such lesions include the perineum, vulva/labial regions, skin surfaces, abdominal walls and scalp [21]. The result is better diagnosis, improvement in patient navigation, quicker and easier treatment, less hospital stay, lower cost of health care and better prognosis. It is obvious that the future continues to hold better prospect for the ultrasound imaging of musculoskeletal systems.

Author details

Felix Okechukwu Erondu[1,2]

1 Department of Radiography and Radiation Sciences, College of Medicine and Health Sciences, Gregory University, Uturu, Abia State, Nigeria

2 Clinical Imaging, Image Diagnostics, Nigeria

Available from https://dx.doi.org/10.5772/intechopen.101338

References

[1] Lawande AD, Warrier SS, Joshi MS. Role of ultrasound in evaluation of peripheral nerves. Indian Journal of Radiology and Imaging. 2014;**24**(3):254-258. DOI: 10.4103/0971-3026.137037

[2] Walker FO, Cartwright MS, Wiesler ER, Caress J. Ultrasound of nerve and muscle. Clinical Neurophysiology. 2004;**115**(3):495-507

[3] Romero-Morales C, Bravo-Aguilar M, Ruiz-Ruiz B, Almazán-Polo J, López-López D, Blanco-Morales M, et al. Current advances and research in ultrasound imaging to the assessment and management of musculoskeletal disorders. Disease-a-Month. 2021;**67**(3)

[4] Hodgson RJ, O'Connor PJ, Grainger AJ. Tendon and ligament imaging. The British Journal of Radiology. 2012;**85**(1016):1157-1172. DOI: 10.1259/bjr/34786470

[5] Fullerton GD, Rahal A. Collagen structure: the molecular source of the tendon magic angle effect. Journal of Magnetic Resonance Imaging. 2007;**25**:345-361

[6] Bruno F, Palumbo P, Arrigoni F, et al. Advanced diagnostic imaging and intervention in tendon diseases. Acta Biomed. 2020;**91**(8-S):98-106. DOI: 10.23750/abm.v91i8-S.10007

[7] De Filippo M, Pesce A, Barile A, et al. Imaging of postoperative shoulder instability. Musculoskeletal Surgery. 2017;**101**:15-22

[8] Barile A, Bruno F, Arrigoni F, et al. Emergency and trauma of the ankle. Seminars in Musculoskeletal Radiology. 2017;**21**:282-289

[9] Barile A, Bruno F, Mariani S, et al. Follow-up of surgical and minimally invasive treatment of Achilles tendon pathology: A brief diagnostic imaging review. Musculoskeletal Surgery. 2017;**101**:51-61

[10] Di Pietto F, Chianca V, de Ritis R, et al. Postoperative imaging in arthroscopic hip surgery. Musculoskeletal Surgery. 2017;**101**:43-49

[11] van Holsbeeck M, Soliman S, Van Kerkhove F, Craig J. Advanced musculoskeletal ultrasound techniques: What are the applications? American Journal of Roentgenology. 2021;**216**(2):436-445

[12] Carrol AS, Simon NG. Current and future applications of ultrasound imaging in peripheral nerve disorders. World Journal of Radiology. 2020;**12**(6):101-129. DOI: 10.4329/wjr.v12.i6.101

[13] Telleman JA, Grimm A, Goedee S, Visser LH, Zaidman CM. Nerve ultrasound in polyneuropathies. Muscle & Nerve. 2018;**57**:716-728

[14] Borire AA, Visser LH, Padua L, Colebatch JG, Huynh W, Simon NG, et al. Utility of maximum perfusion intensity as an ultrasonographic marker of intraneural blood flow. Muscle & Nerve. 2017;**55**:77-83

[15] Babaei-Ghazani A, Majdalani C-E, Luong DH, Front ABG. Sonoelastography of the shoulder: A narrative review. Frontiers in Rehabilitation Sciences. 2021;**2**(4):25. DOI: 10.3389/fresc.2021.704725

[16] Yokota K, Tsuzuki Wada T, Akiyama Y, Mimura T. Detection of synovial inflammation in rheumatic diseases using superb microvascular imaging: comparison with conventional power Doppler imaging. Modern Rheumatology. 2018;**28**:327-333

[17] Lim AKP, Satchithananda K, Dick EA, Abraham S, Cosgrove DO. Microflow imaging: New Doppler

technology to detect low-grade inflammation in patients with arthritis. European Radiology. 2018;**28**:1046-1053

[18] Demené C, Mairesse J, Baranger J, Tanter M, Baud O. Ultrafast Doppler for neonatal brain imaging. NeuroImage. 2019;**185**:851-856. DOI: 10.1016/j.neuroimage.2018.04.016

[19] Deffieux T, Demené C, Tanter M. Functional ultrasound imaging: A new imaging modality for neuroscience. Neuroscience. 2021;(474):110-121. DOI: 10.1016/j.neuroscience.2021.03.005

[20] Nazarian LN. The top 10 reasons musculoskeletal sonography is an important complementary or alternative technique to MRI. AJR. 2008;**190**: 1621-1626

[21] Erondu OF, Benson S, Ohuegbe I. Ultrasound as a convenient tool in the assessment of masses in obscure locations. Journal of Medicine and Medical Sciences. 2019;**10**(2):98

Chapter

Assessment of Diabetic Foot through the Developmental Stages of Lower Limb Abnormalities Using Ultrasound

Suresh K.S. and Sukesh Kumar A.

Abstract

A diabetic foot is one of the most serious complications of diabetes mellitus. This causes large number of lower leg amputations worldwide. Usually this disease is getting diagnosed in a very later stage. Ankle-arm index, diastolic blood pressure, fasting plasma glucose, hemoglobin A1C, high blood pressure, medial arterial calcification, nerve conduction velocity, peripheral vascular disease, systolic blood pressure, transcutaneous oxygen tension, etc. are some of the major indicators of a diabetic foot. Among these peripheral arterial abnormalities and neuropathy are the most dominant visible factors. Detection and monitoring of diabetic foot help to demonstrate the feet at risk of ulceration positively. This study reveals the various assessment methodologies of lower limb abnormalities leading to diabetic foot using ultrasound. Ultrasound is being used in various cases related to diabetic foot, from the identification of systolic pressure for the ankle brachial pressure index to the velocity analysis of hemodynamic studies. The study analyses the lower limb abnormalities and extracts the features of diabetic foot from the velocity spectrum of ultrasound Doppler scan.

Keywords: diabetic foot, diabetic neuropathy, peripheral arterial disease, diabetes mellitus, early detection, Doppler ultrasound

1. Introduction

Diabetes is a growing global epidemic of the current century. This occurs either when the pancreas does not produce enough insulin or when the body cannot effectively use the produced insulin. According to the International Diabetes Federation, it is estimated that presently 387 million people are being affected by diabetes, and this may increase to 592 million in the coming 20 years [1]. In addition to this, 316 million people are at high risk with impaired glucose tolerance, and a projection shows that in 2035, the count of high-risk people will attain more than 1 billion. According to the recent estimation of the World Health Organization (WHO), diabetes is being suffered by 9% among adults aged 18+ years. Approximately 1.5 million deaths were directly caused by diabetes in 2012, and 80% of this occurred in low- and middle-income countries. Diabetes is estimated to be the seventh leading cause of death in 2030 by the WHO [2]. The statistics of the International Diabetes

Federation reveals that in India there are nearly 65 million diabetes cases [3]. The associated complications of diabetes have also been increased in proportionate to the high rate of diabetes-affected persons.

Among the variety of complications related to diabetes, a diabetic foot stands one of the most threatening one. If the foot exhibits any pathology because of diabetes mellitus or any complications due to the long-term suffering of diabetes. The study reveals various types lower limb abnormalities and analyses the features of diabetic foot from the velocity spectrum of ultrasound Doppler scan.

2. Diabetic foot disease

In diabetic cases, foot problem may develop as a part of damaging nerve and blood vessels. This may cause the infection and ulceration of the leg and finally come to the level of amputation. This is one of the dangerous conditions. Foot diseases are the most probable causes of hospital admissions in the case of diabetes. Considering the total patients suffering from diabetes mellitus, diabetic foot disease probably occurs 15–25% of them. Among the diabetic foot patients, 85% of the cases precede to partial lower leg amputation. Individuals with diabetes are 25 times bound to lose a leg than individuals without the condition.

More than 70% of leg amputations throughout the world are due to diabetes [4]. Every year, around 1 million diabetic people lose a leg because of their diseased condition. The diabetic foot also causes major economic consequences for the patients, their families and the entire society. The International Working Group on the Diabetic Foot estimated that a lower limb is lost to diabetes somewhere in the world in every 20 seconds [5].

Ankle-arm index, diastolic blood pressure, plasma glucose, hemoglobin A1C, high blood pressure, medial arterial calcification, peripheral vascular disease, systolic blood pressure and transcutaneous oxygen tension are the major identified indicators of diabetic foot. Comparing the overall visible symptoms of diabetic foot, peripheral arterial disease and diabetic neuropathy seem to be the most important threatening factors [6, 7].

3. Lower limb abnormalities leading to diabetic foot

Peripheral arterial disease (PAD) is of great clinical significance in diabetic patients. Some of them have high risk of subsequent myocardial infarction or stroke, irrespective of the presence or absence of symptoms of PAD. Lack of proper treatment can lead to functional disability and limb loss. So, regular screening of PAD is very important as a part of proper management to minimize the impact of comorbidities on the diseased person.

The human nervous system is also very much affected with diabetes. The peripheral nerves, the nerves that go to the arms, hands, legs and feet, may get damaged with persistent high glucose level. Usually, the diabetic peripheral neuropathy arises in different places of the human body but very prominently affects the sensations of the toes and feet [8]. This abnormal sensation may lead a feeling of being pricked with pins, throbbing and numbness with sharp pain and tingling and burning sensations.

The risk for foot ulcers and amputation is increased by diabetic peripheral neuropathy. People who are suffering from diabetic peripheral neuropathy mostly do not notice minor cuts, sores or blisters in their foot and toes. This is

because of the loss of sensation in connection with the damage of the nerves in the corresponding areas. Neuropathy affects the sensory, motor and autonomic systems of the human body. The untreated wounds become easily infected and may lead to gangrene, which finally require amputation in that area. If this is diagnosed in the early stages, it is a major opportunity to ameliorate symptoms and prevent the development of the major clinical neuropathic endpoints of the lower limb [9] such as chronic painful foot, the insensate foot, the Charcot foot and the neuropathic ulcer. It is important that physicians and other healthcare providers understand that diabetic neuropathy can occur with no pain or with an insensate foot or may present with pain in the form of dysesthesias and paresthesias.

4. Role of ultrasound

The ultrasound wave is one of the safest and easiest modes of medical diagnosis. This modality of medical imaging helps to identify internal body structures in a noninvasive manner. This has been achieved by computerized analysis of reflected ultrasound waves. Usually frequencies of 1–30 MHz are being used for a diagnostic purpose. The resolution of the image depends on the type of wave used, higher resolution with shorter wavelengths, and the wavelength is inversely proportional to the frequency [10]. However, the use of high frequencies is limited by their greater attenuation in the tissue and thus shorter depth of penetration. The frequencies 2–10 MHz are used for vascular studies.

Doppler ultrasound provides the basis for noninvasive and objective measurements of the spectrum and serially monitors the velocity of flow in the arteries. This Doppler ultrasound has very high potential for monitoring blood flow velocity as it is reliable and noninvasive and provides real-time result. In Doppler analysis, the ultrasound beam has the sum of the instantaneous contributions of each particle crossing that beam. A human observer can interpret it because such mixtures of signals are sorted according to the frequency and weighted with the intensity in the cochlea. The signal needs to endure a similar process of sorting and weighting for visual interpretation. For this process, the Doppler signal has to be translated into the frequency domain, and it is done in real-time computation with fast Fourier transform of successive segments of the Doppler signal. The stationarity of the blood flow may be assumed by shortening the segments.

The power spectrum generated for each segment indicates the velocity distribution of the particles within that beam during the time interval in accordance with the width of the segment. The inverse of the time interval indicates the spectral resolution. Power spectrum point relates to a frequency interval showing a velocity range, whereas the height of each point signifies the power or the quantity of particles in that particular velocity range.

5. Vascular examination

The ankle-brachial pressure index (ABPI) is one of the most common techniques being used for initial diagnosis of foot disease. This is a particular ratio of the recorded highest pressure at the ankle for that leg to the highest brachial pressure measured for both arms. The normal range of ABPI comes below 1. When ABPI < 0.92, it is an indication of arterial disease. The value of ABPI between 0.5 and 0.9 may be connected with claudication, and for these symptoms the patient

should be referred for further examination. If ABPI rate is below 0.5, it is a symptom of severe arterial disease, and this may be associated with gangrene, ischemic ulceration or rest pain, and urgent referral is required for a vascular opinion.
The pressure at the ankle and brachial artery is determined with the ultrasound. Pressure is measured by blood pressure apparatus, but the auscultation is determined by Doppler ultrasound [11]. The state of peripheral circulation can be easily identified with the examination of the legs. Peripheral arterial examination using ultrasound gives a lot of indications related to diabetic foot [12]. Stenosis or occlusions in the segments of the peripheral arteries can be detected in patients who have suspected arterial occlusive disease. The clinical indications such as claudication, ischemic tissue loss, rest pain and suspected arterial embolization may exist in these patients. The sites can be monitored by various percutaneous interventions, including angioplasty, thrombolysis, atherectomy, and stent placements. The examination can also be done by the evaluation of suspected vascular and perivascular abnormalities, such as aneurysms, pseudoaneurysms and arteriovenous fistulas. The presence of significant arterial abnormalities can be identified and confirmed by imaging modalities [13].

One of the indications for peripheral venous ultrasound examinations is the evaluation of possible venous thromboembolic disease or venous obstruction in symptomatic or high-risk asymptomatic individuals. Assessments of venous insufficiency, reflux and varicosities are some of the other indications. The examination is also being done by the evaluation of veins before venous access. Follow-up for patients with known venous thrombosis near the anticipated end of anticoagulation is used in the presence of residual venous thrombosis [14].

The arterial occlusive disease is identified by the evaluation of the arterial segments, such as lower extremity, common femoral artery, proximal superficial femoral artery, mid superficial femoral artery, distal superficial femoral artery, popliteal artery, etc. A focused or limited examination may be appropriate in certain clinical situations. At a minimum, an angle-corrected spectral Doppler waveform with velocity measurements should be obtained from any of the above sites. If clinically appropriate, imaging of the iliac, deep femoral, tibioperoneal and dorsalis pedis arteries can be performed [15].

Figure 1 shows the evaluation of a patient having pain in the left lower limb. The spectral color Doppler ultrasound of the venous system has been done in this case. The color Doppler images analyze the study of veins such as popliteal, left femoral and peroneal veins and anterior-posterior tibial veins.

Usually complete visualization of the veins of the leg is very difficult. Normally it is being done by imaging the upper third and distal third of the anterior, posterior tibial and peroneal veins.

Figure 2 is an ultrasound color Doppler image of the right lower limb showing early indications of diabetic arteriopathy. This is also called as diabetic vasculopathy. The corresponding characteristic features in the color Doppler ultrasound image are:

- In the arterial waveform, there is a spectral broadening from the popliteal artery downwards.
- Slight decrease in the peak systolic velocity below the popliteal artery.
- Early changes of loss of the triphasic spectral waveform are present in the peroneal artery.

The changes mentioned above are typically seen in early diabetic arteriopathy indicating mild stenosis in a diffuse fashion below the popliteal artery.

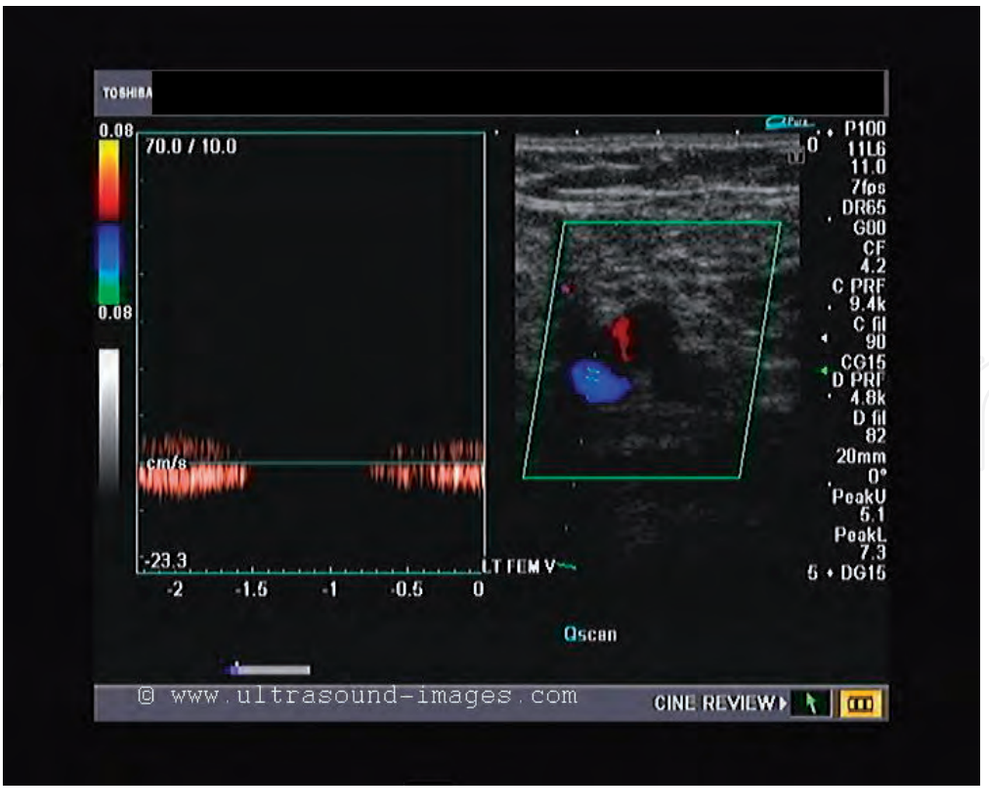

Figure 1.
Venous Doppler of the lower limb: normal case (presented with permission from Dr. Joe's ultrasound).

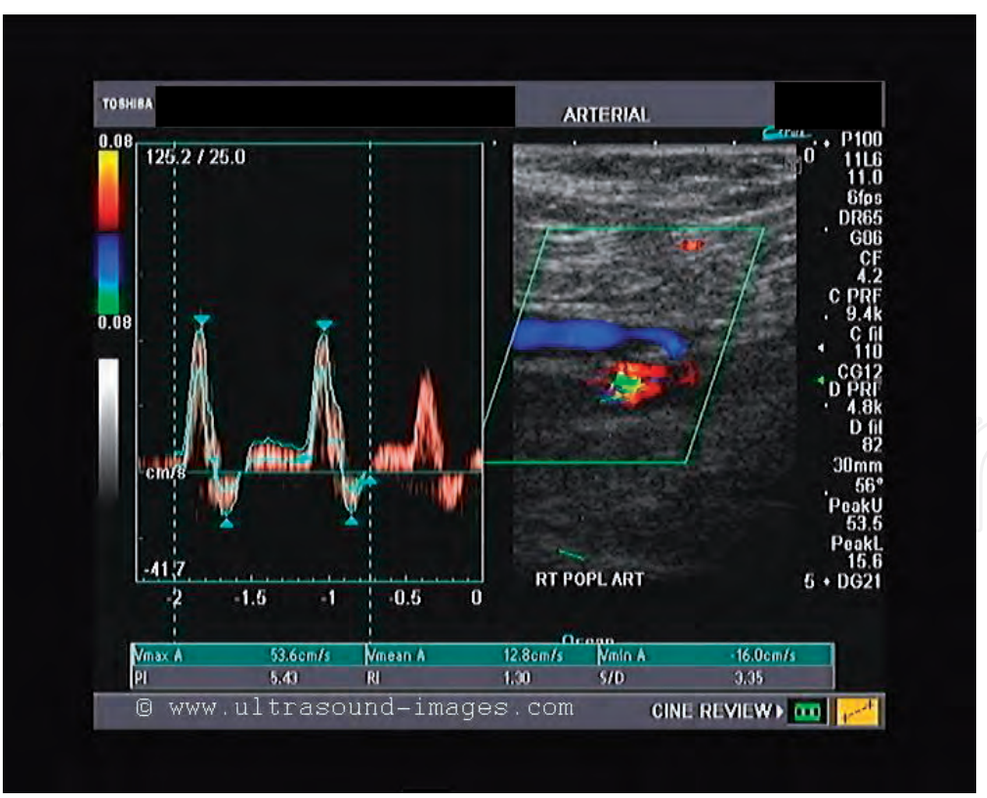

Figure 2.
Mild diabetic arteriopathy of the lower limb (presented with permission from Dr. Joe's ultrasound scan, Cochin).

In Doppler waveform analysis, normal pulsed wave is a clearly defined tracing with narrow Doppler spectrum. In normal cases, the peripheral artery waveform is triphasic. When blood flow becomes turbulent at bifurcations and luminal narrowing, it causes spectral broadening of Doppler waveform.

6. Velocity spectrum

The Doppler arterial waveform images can be analyzed to provide information about blood flow in or out of the gut and related along with the other physiological measurements.

The velocity information perceived from a single location in the blood vessel is displayed in the form of frequency shift-time plot in the case of real-time spectral Doppler analysis. The time along the horizontal axis and frequency shift or identified velocity along the vertical axis will be displayed.

The clinical information attained from the maximum Doppler shift correspond to a spatial maximum in the velocity field. Systematic analysis can be done with spectral Doppler ultrasound velocimetry, an analysis of the spectrum of frequencies by which the Doppler signal is constituted [16].

The Doppler frequency shift happens with backscattering of millions of red blood cells. The resultant shifted signal is the summation of such multiple Doppler frequency shifts.

The processing of Doppler signal is accomplished through various steps. After the initial reception, the next step is amplification. It is demodulated, and the characteristic parameters of flow are identified by further spectral processing methods. The Doppler shift frequency is proportional to the velocity of the blood flow. The power in a particular frequency band of the Doppler spectrum is proportional to the volume of blood, under ideal uniform sampling conditions.

As the blood moving with velocities create frequencies in the particular band, the power Doppler spectrum has the same shape as the velocity distribution plot for the flow in the vessel. The deviation in the shape of the Doppler power spectrum as a function of time is normally denoted in the form of sonograms.

7. Conclusion

The frequency level and patterns of lower limb arterial insufficiency in diabetic patients can be evaluated by Doppler-based techniques. The most prominent case of diabetic foot is the development of vasculopathic changes leading to peripheral vascular insufficiency. This can be detected by analyzing velocity spectrum of blood flow in the lower limb. Angle-corrected spectral Doppler waveforms should be effectively utilized for the recognition procedure. Precise evaluation has to be attained with further analysis.

Acknowledgements

We are very much thankful to Dr. Joe's Ultrasound Scan, Cochin, and Niranjan Ultrasound India (P) Ltd., Calicut, for providing clinical support for this research work.

Author details

Suresh K.S.[1*] and Sukesh Kumar A.[2]

1 Centre for Development of Imaging Technology, Thiruvananthapuram, Kerala, India

2 Rajiv Gandhi Institute of Development Studies, Thiruvananthapuram, India

References

[1] International Diabetes Federation, Annual Report; 2014

[2] World Health Organization. Diabetes Programme. 2015. Available from: http://www.who.int/diabetes/en/

[3] International Diabetes Federation. IDF Diabetes Atlas. 6th ed; 2013. Available from: http://www.idf.org/diabetesatlas

[4] International Diabetes Federation. Diabetes and Foot Care Time to Act; 2005

[5] International Working Group on the Diabetic Foot. Guidance docsuments. 2015. Available from: http://iwgdf.org/guidelines/

[6] Reiber GE, Lemaster JW. Epidemiology and economic impact of foot ulcers and amputations in people with diabetes. In: Levin and O'Neal's the Diabetic Foot. 7th ed. USA: Mosby Elsevier PA; 2008. pp. 3-22

[7] Zimny S, Dessel F, Ehren M, Pfohl M. Helmut Schatz "early detection of microcirculatory impairment in diabetic patients with foot at risk". Diabetes Care. 2001;**24**:1810-1814

[8] Suresh KS, Sukesh Kumar A. An investigation for early stage diagnosis of diabetic foot. International Journal of Enhanced Research In Science Technology & Engineering. 2016;**5**(12):40-43

[9] Suresh KS, Sukesh Kumar A. Clinical need of a diabetic foot infection detector. In: National Conference on Advances in Computational Intelligence & Communication Technologies. 2016. pp. 125-128

[10] World Health Organization. Manual of Diagnostic Ultrasound; 2011

[11] Suresh KS, Sukesh Kumar A. An integrated model for early detection and monitoring of diabetic foot. In: Proceedings of International Conference on Modelling and Simulation, Association for the Advancement of Modelling and Simulation Techniques in Enterprises. 2017

[12] Bessonov N, Sequeira A, Simakov S, Vassilevskii Y, Volpert V. Methods of blood flow modelling. Mathematical Modelling of Natural Phenomena. 2016;**11**(1):1-25

[13] Lingegowda D, Moorthy S, Sreekumar KP, Kannan RR. Imaging in diabetic ischemic foot. International Journal of Diabetes in Developing Countries. 2010;**30**(4):179-184

[14] AIUM Practice Guide Line for the Performance of Peripheral Venous Ultrasound Examinations. American Institute of Ultrasound in Medicine; 2010

[15] AIUM Practice Guide Line for the Performance of Peripheral Arterial Ultrasound Examinations Using Color and Spectral Doppler Imaging. American Institute of Ultrasound in Medicine; 2010

[16] Gerhard-Herman M, Gardin JM, Jaff M, Mohler E, Roman M, Naqvi TZ. Guidelines for noninvasive vascular laboratory testing: A report from the American Society of Echocardiography and the Society of Vascular Medicine and Biology. Journal of the American Society of Echocardiography. 2006;**19**(8):955-972

10

Rheumatoid Arthritis Assessment with Ultrasonography

Thierry Marhadour and Alain Saraux
Rheumatology, CHU and University Hospital,
La Cavale Blanche, Brest
France

1. Introduction

Musculoskeletal ultrasound is a rapidly growing imaging modality used for the investigation and management of musculoskeletal disorders. The first report of musculoskeletal ultrasonography was published in 1958 by K. T. Dussik who measured the acoustic attenuation of articular and periarticular tissues including skin, adipose tissue, muscle, tendon, articular capsule, articular cartilage and bone (Dussik et al., 1958). It was first used in rheumatoid arthritis by Cooperberg in 1978 for the assessment of synovitis in the knee. (Cooperberg et al., 1978). De Flaviis made the first report of ultrasonography in the hand in rheumatoid arthritis in 1988, describing synovitis, tenosynovitis, and erosions (De Flaviis et al., 1988).

The first application of power Doppler in demonstrating soft tissue hyperaemia in musculoskeletal disease was reported in 1994 by J. S. Newman (Newman et al., 1994). Since, power Doppler has started to replace gray-scale ultrasonography as an indicator of inflammatory joint disease.

Ultrasonography has a number of advantages, including good patient tolerability and ability to scan multiple joints in a short period of time. Thanks to smaller high-frequency transducers that were better suited for superficial structures such as the small joints, many reports and studies have been published. However, there are scarce data regarding its validity, reproducibility, and responsiveness to change, making interpretation and comparison of studies difficult. In particular, there are limited data describing standardized scanning methodology and standardized definitions of ultrasonography pathologies.

2. Generalities

2.1 Technique

In contrast to conventional radiography, musculoskeletal ultrasonography can provide multiplanar images of cortical bone, synovium, tendons, muscles, ligaments, and nerves. It is a safe, portable and relatively inexpensive technique. Rheumatoid arthritis is the most studied inflammatory disease in rheumatologic ultrasonography.

Equipment is widely available and comparatively flexible. Examinations can be performed at the bedside. The mean price to acquire a machine is nowadays about 40 000 euros, but costs are decreasing.

In B mode ultrasound, a linear array of transducers simultaneously scans a plane through the body that can be viewed as a two-dimensional image on screen. It allows getting pictures of joints and periarticular structures. The higher the frequency is, the greater both the axial and the lateral resolution of image will be, but at the cost of reduced tissue penetration. Therefore, a higher-frequency transducer is best used for superficial structures, such as the small joints of the hand and feet (e.g. 7–18 MHz), and a low frequency transducer is used for deeper joints, such as the hip (e.g. 3–5 MHz).

Doppler mode makes use of the Doppler effect in measuring and visualizing blood flow. Power Doppler denotes only the amplitude of the Doppler signal, which is determined by the volume of blood present so it is better suited to the assessment of low-velocity flow in small vessels (e.g. synovium). This would be a way to assess joint inflammation.

Learning is quite short: D'agostino evaluated that five hours of theory and three months of practice (around 70 exams) are needed. The concordance between learners and teachers is good, approximately about 80 % (D'agostino et al., 2004).

2.2 Elementary lesions in rheumatoid arthritis

OMERACT stands for Outcome Measures in Rheumatology. It is an informal international network of working groups and gatherings interested in outcome measurement across the spectrum of rheumatology intervention studies. Thanks to Omeract, there is consensus on ultrasonography definitions for common pathological lesions seen in patients with inflammatory arthritis (Wakefield et al., 2006).

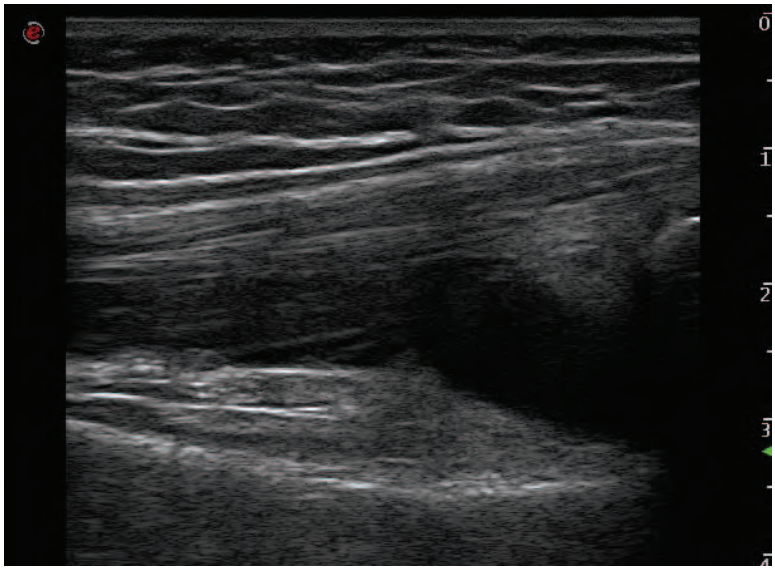

Fig. 1. Effusion of knee

Synovial fluid

Abnormal hypoechoic or anechoic (relative to subdermal fat, but sometimes may be isoechoic or hyperechoic) intraarticular material that is displaceable and compressible, but does not exhibit Doppler signal (Fig. 1).

Synovial hypertrophy

Abnormal hypoechoic (relative to subdermal fat, but sometimes may be isoechoic or hyperechoic) intraarticular tissue that is nondisplaceable and poorly compressible and which may exhibit Doppler signal (Figs. 2, 3).

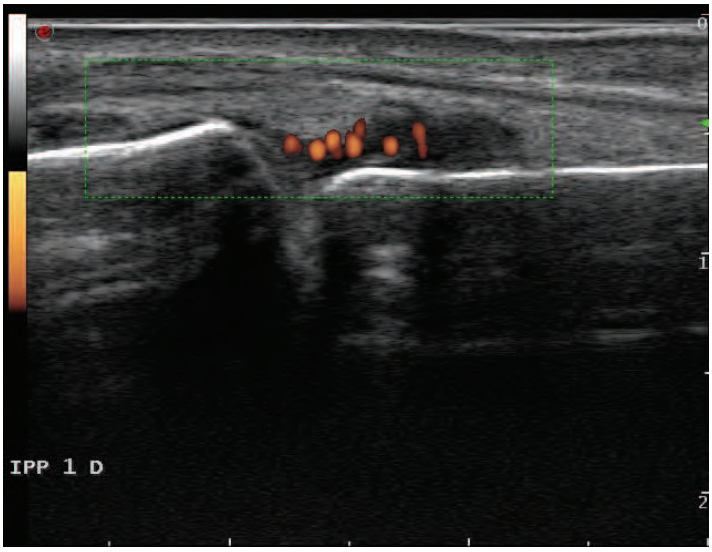

Fig. 2. MCP synovitis with power Doppler signal

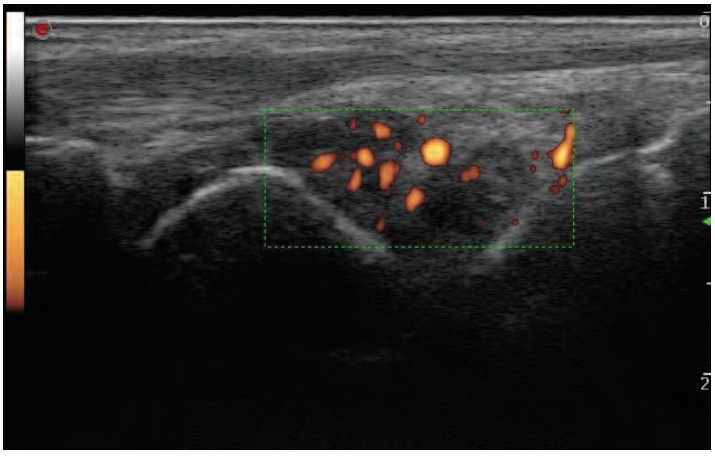

Fig. 3. Arthritis of the wrist

Tenosynovitis

Hypoechoic or anechoic thickened tissue with or without fluid within the tendon sheath, which is seen in 2 perpendicular planes and which may exhibit Doppler Signal (Fig. 4).

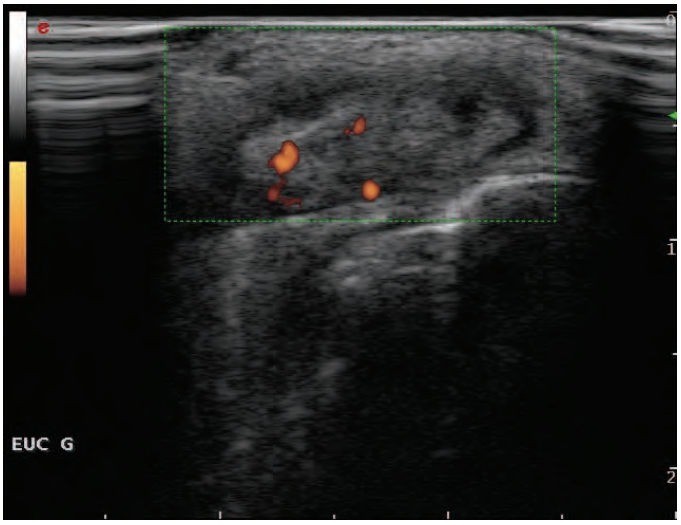

Fig. 4. Tenosynovitis of the left extensor carpi ulnaris tendon with power Doppler signal

Bone erosion

An intraarticular discontinuity of the bone surface that is visible in 2 perpendicular planes (Fig. 5).

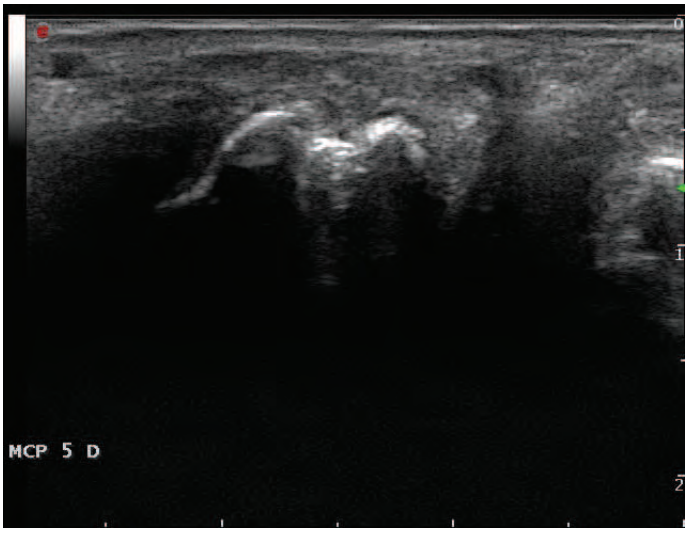

Fig. 5. Bone erosion in the head of the right fifth metacarpal (transversal plane)

2.3 Classification

Joint assessment can be binary (synovitis present or absent) or semi-quantitative. The first one is easily applicable in routine practice whereas the second is mostly used in trials. Szkudlarek described semi-quantitative scales for synovial hypertrophy, effusion Doppler signal and erosions (Szkudlarek et al., 2003).

Joint effusion was defined as a compressible anechoic intracapsular area (0=no effusion, 1=minimal amount of joint effusion, 2=moderate amount of joint effusion [without distension of the joint capsule], 3=extensive amount of joint effusion [with distension of the joint capsule]).

Synovitis was defined as a noncompressible hypoechoic intracapsular area (synovial thickening) (0=no synovial thickening, 1=minimal synovial thickening [filling the angle between the periarticular bones, without bulging over the line linking tops of the bones], 2=synovial thickening bulging over the line linking tops of the periarticular bones but without extension along the bone diaphysis, 3=synovial thickening bulging over the line linking tops of the periarticular bones and with extension to at least one of the bone diaphyses).

Bone erosions were defined as changes in the bone surface of the area adjacent to the joint (0=regular bone surface, 1=irregularity of the bone surface without formation of a defect seen in 2 planes, 2=formation of a defect in the surface of the bone seen in 2 planes, 3=bone defect creating extensive bone destruction).

Power Doppler signal was used to display flow signal in the synovium (0=no flow in the synovium, 1=single vessel signals, 2=confluent vessel signals in less than half of the area of the synovium, 3=vessel signals in more than half of the area of the synovium)

Omeract developed a semi-quantitative scale to assess synovitis in B Mode and power Doppler (Wakefield et al., 2005) (table 1). This score is also based on the assessment of effusion, synovial hypertrophy and Doppler flow.

B Mode	- Grade 0: Normal joint (no synovial hyperthrophy, no joint effusion) - Grade 1: Minimal synovitis (minimal synovial hyperthrophy, with or without minimal joint effusion) - Grade 2: Moderate synovitis (moderate synovial hyperthrophy with or without minimal or moderate joint effusion) - Grade 3: Severe synovitis (severe synovial hypertrophy, with or without severe joint effusion)
Power Doppler	- Grade 0: no vessel in the synovium; - Grade 1: up to 3 single spots signals or 1 confluent spot + up to 2 single spots - Grade 2: vessel signals in less than half of the area of the synovium (< 50%) - Grade 3: vessel signals in more than half of the area of the synovium (> 50%)

Table 1. Omeract semi-quantitative scale for joint assessment

2.4 Scores

For the time being, there is no consensus on ultrasound score. There are comprehensive scores, which integrate the 44 joints of the Disease Activity Score (Wakefield et al., 2005);

there are reduced scores, like the one developed by Backhaus which assess only 7 joints (Backhaus et al., 2009). Actually, Omeract is working on a consensus score, which will be called Gloss (Global Omeract Sonography Scoring). It should be feasible, whereas bringing more information than clinical examination (D'Agostino et al., 2009).

2.5 Artefacts

Some artefacts have to be known:

Anisotropy: This is the effect that makes a tendon appear bright when it runs at 90 degrees to the ultrasound beam, but dark when the angle is changed.

Enhancement: Some structures however allow sound to pass through them more easily than others. The most dramatic example is watery fluid, such as in an effusion, or in a cyst. These are described as being translucent. Because only a minimal amount of energy is absorbed by the fluid, the region that lies behind will receive more sound than the processor expects for that depth. This area will therefore appear uniformly brighter.

Attenuation or **Shadowing** is the reverse effect, where some tissues absorb relatively more of the sound. The area of the image deep to this will appear darker. In the extreme almost no sound is transmitted, leaving a dark shadow behind the structure. This can be caused by a calcification for example.

3. Contribution of ultrasonography in the monitoring of rheumatoid arthritis

3.1 Synovitis

Ultrasound synovitis is not specific of rheumatoid arthritis. Synovial hypertrophy or effusion can be seen in other inflammatory rheumatism, and even in osteoarthritis (Rosenberg et al., 2009). Consequently, the interest for diagnosis of rheumatoid arthritis is poor, but it can help in presence of polyarthralgia. Van de Stadt studied 192 patients with polyarthralgia who had rheumatoid factor and / or CCP antibodies. Subclinical ultrasound anomaly of a joint was predictive of evolution toward authentic arthritis at joint level, but this wasn't true at patient level (Van de Stadt et al., 2010). Nevertheless, the topography of swollen joints and the other signs (like tenosynovitis and obviously erosions) may guide the diagnosis.

Actually, ultrasonography is important for rheumatoid arthritis monitoring. There are several studies that prove that ultrasonography is more sensitive than clinical examination for synovitis assessment. Szkudlarek studied small joints (Metacarpophalangeal MCP 2 and 3, Proximal Interphalangeal PIP 2, and Metatarsophalangeal MTP 1 and 2) in 30 rheumatoid arthritis patients and found approximately 50 % more synovitis with ultrasonography in B mode than with clinical assessment (Szkudlarek et al., 2003).

In other studies, by comparison with MRI, ultrasonography was found to be markedly more sensitive and accurate than clinical examination to search synovitis on the ten MTP joints (sensibility respectively 0.87 versus 0.43) (Szkudlarek et al., 2004) and on the second to fifth MCP and IPP of the dominant hand (sensibility respectively 0.7 versus 0.4) (Szkudlarek et al., 2006).

Ultrasonography is also more sensitive in early rheumatoid arthritis. In 44 patients whose rheumatoid arthritis duration was less than 2 years, Salaffi found a mean swollen joint count of 19.1 (+/-4.1) with ultrasonography and 12.6 (+/-3.6) with clinical examination. Power Doppler signal in the synovium was present in 43 joints, of which 60% showed clinical signs of inflammation (swelling and/or tenderness). Power Doppler signal in the synovium was absent in 107 joints, of which 36% presented clinical signs of inflammation (Salaffi et al., 2008).

Power Doppler permits assessment of low-velocity flow in small vessels and is considered to reflect disease acute inflammatory activity. In the Sea study, the use of Power Doppler dramatically reduced the number of arthritis in rheumatoid arthritis considered as active by clinicians (Marhadour et al., 2010). If the swollen joint count was based on ultrasonography result, disease activity index was lower than if based on clinician assessment.

3.2 Erosions

The detection of radiographic erosions in early disease is associated with a poor outcome (Van der Heijde et al., 1992) and may influence the timing and choice of disease-modifying antirheumatic drug therapy.

Erosion of hand in ultrasonography was first described in 1988, in 20 rheumatoid arthritis patients (De Flaviis et al., 1988) and then Grassi confirmed the ability of ultrasonography to show erosions in a controlled trial with 20 rheumatoid arthritis patients and 20 controls (Grassi et al., 1993).

Ultrasonography is more sensitive than X-Ray to detect erosion in rheumatoid arthritis. In 2000, Wakefield was the first to demonstrate that sonography detects more erosion on the MCP joints of rheumatoid arthritis patients than does conventional radiography, especially in early disease. He compared ultrasonography and X-Ray for erosion detection in the MCP joints of rheumatoid arthritis patients and studied its reliability. There were 100 rheumatoid arthritis patients who were split according to their disease duration. Those with disease duration of less than 12 months with no prior DMARD therapy were classified as having early disease, while those with disease duration of more than 2 months were classified as having late disease. The control group included 20 patients. In the early rheumatoid arthritis group, sonography detected a 6.5-fold increase in the number of erosions detected by sonography over that detected by radiography (P=0.0001), in 7.5-fold the number of patients. In the group with late rheumatoid arthritis, sonography detected a 3.4-fold increase (P=0.0001), in 2.7 fold the number of patients. Sonography detected more erosions than radiography in all MCP joints except the fourth, where it detected fewer (sonography detected proportionately more erosions where the transducer had good access, in particular, the first, second, and fifth joints). Significantly fewer of the small sonographic erosions (less than 2 mm) were visible on radiography (P=0.0001). In this study, MRI was used to validate the additional sonographic lesions not seen on radiography, giving some evidence of their pathologic specificity. Wakefield explained that there were two reasons why sonography detected more erosions than radiography in this study: first, the 3-dimensional capability of sonography allowed joints to be examined in several different planes; second, sonography was able to detect smaller erosions. Erosions were most frequently seen on either the radial or the ulnar aspect of the MCP joint, with relatively few occurring on the volar or dorsal surfaces (Wakefield et al., 2000).

Alasaarela assessed the value of ultrasonography, magnetic resonance imaging, computed tomography (CT) and plain radiography (PR) in detecting bone erosions on the humeral in 26 rheumatoid arthritis patients. MRI depicted humeral erosions in 25 (96%), ultrasonography in 24 (92%), CT in 20 (77%) and PR in 19 (73%) of the 26 shoulders. MRI and ultrasonography were superior to CT in detecting small erosions. Ultrasonography was the most sensitive method to show surface erosions on the greater tuberosity (Alasaarela et al., 1998).

Conventional radiography is based on attenuation of X-rays, and calcified tissues such as bone are readily depicted because of their markedly greater attenuation in comparison with the surrounding soft tissues. Because imaging with ultrasonography does not depend on X-rays, it has been speculated to which extent erosions detected using these modalities reflects true loss of calcified tissue, that is, are true erosions. Therefore, ultrasonography has been compared to computed tomography, which is considered as a gold standard. On 17 rheumatoid arthritis patients, ultrasonography exhibited high specificities (91 %) in detecting bone erosions in MCP joints, even in the radiographically non-erosive joints (92%). Although, sensitivity was moderate (42%) (Døhn et al., 2006).

Nevertheless, a recent study which evaluated bone erosion in 127 healthy subjects matched with a cohort of patients with early arthritis (the ESPOIR cohort) detected bone erosion in 11% of healthy subjects at metacarpo and metatarsophalangeal joint of both hands and feet. However, the combination of power Doppler signal plus bone erosion, on the same joint, was never seen in healthy subjects. A single case of bone erosion or synovial thickening in B-mode is common in healthy subjects. However, more than 1 case of synovial thickening in B-mode or bone erosion is a strong argument for the diagnosis of early inflammatory arthritis (Millot et al., 2010).

4. Outcome assessment validation strategy in rheumatoid arthritis

4.1 Generalities

Scientific rules must be respected when developing a measurement tool. Since ninety's, some consensus are growing in rheumatoid arthritis metrology, especially thanks to OMERACT, which developed a filter of 3 criteria:

1. *Truth*: is the measure truthful, does it measure what it intends to measure? Is the result unbiased and relevant? This criterion captures the issues of face, content, construct and criterion validity.
   Face validity: It is the validity of a test at face value. In other words, a test can be said to have face validity if it "looks like" it is going to measure what it is supposed to measure
   Content validity: Refers to the extent to which a measure represents all facets of a given phenomena.
   Criterion validity: Criterion or concrete validity is the extent to which the measures are demonstrably related to concrete criteria in the "real" world, ie gold standard. For ultrasonography, gold standards are histology or surgical macroscopic findings.
   Construct validity is achieved when measures agree with other measures that evaluate the same phenomenon. For ultrasonography, this can be other imaging techniques or laboratory and clinical data.
2. *Discrimination*: Does the measure discriminate between situations that are of interest? The situations can be states at one time (for classification or prognosis) or states at

different times (to measure change). This criterion captures the issues of reliability and sensitivity to change.

3. *Feasibility*: Can the measure be applied easily, given constraints of time, money, and interpretability? This criterion addresses the pragmatic reality of the use of the measure, one that may be decisive in determining a measure's success.

4.2 Application to ultrasonography

Despite increasing interest in ultrasonography, widespread application has been impeded by a perception that its use is unproven and unreliable. There was limited data describing standardized scanning methodology and standardized definitions of ultrasonography pathologies in addition to how to quantify these abnormalities.

Reliability of a test result is its ability to be reproduced. There are various ways of expressing reliability: Cohen's Kappa (the more the result is near from 1, the best is the agreement), intraclass correlation coefficient (ICC), coefficient of variation, overall agreement, and Kendall's W coefficient. In ultrasonography, it can be divided into the acquisition and the reading phases, as well as the reliability of one observer (intra observer) and multiple observers (interobserver) to reproduce the result. The scanning technique for each joints needs to be standardized, that's why position statements have been developed through consensus meetings (Backhaus, 2001). It is important to test the acquisition reliability of ultrasonography because of its multiplanar capability, and because the sonographer chooses the images he wants to save (even with standard imaging protocols).

Responsiveness is the ability of the tool to demonstrate change. Ultrasonography will be considered sensitive to change if it detects small variation in disease activity. This can be useful to demonstrate the action of a new treatment.

5. Is ultrasonography reliable for the monitoring of rheumatoid arthritis ?

5.1 Synovitis

A first systematic review was performed in 2007 by the Omeract Ultrasound Group on the metric properties of ultrasonography for the detection of synovitis in inflammatory arthritis (the major inflammatory condition studied was rheumatoid arthritis). The major joints assessed were the hand and knee. Few comparisons were done versus histology or surgical findings. Reliability was evaluated with a filter including intra/inter observer acquisition, intra/inter observer reading, sensitivity to change, criterion validity and construct validity. The authors concluded that there were major gaps in the reliability testing, primarily in the assessment of acquisition, and Omeract encouraged rheumatologists to perform more studies on reliability (Joshua et al., 2007).

A way to increase the quality of a reliability study is to multiply the number of examiners. The Sea study was realised in this purpose (Jousse-Joulin et al., 2010). 7 patients with rheumatoid arthritis were examined by 7 clinicians and then 7 sonographers examined each of the 7 patients twice, using B Mode and power Doppler OMERACT grading. The clinical reference standard was the presence of synovitis according to at least 50% of clinical examiners. Different standards were used for sonography (the sonographer with the best reliability, the presence of synovitis according to at least 50% of sonographers) using

different grade to define sonographic abnormalities [at least grade 1 (ALG1) or at least grade 2 (ALG2)]. Agreement was assessed by Cohen's kappa. Concerning intraobserver acquisition reliability for B mode, it was relatively good but varied upon the grade defining synovitis. In ALG1 the results varied to poor (for one sonographer) to fair agreement in 3 sonographers and good for 3 whereas using ALG2, the intraobserver reliability was better with a good agreement for 6:7 sonographers in B mode. The results were slightly lower using power Doppler in both ALG1 and ALG2, as only 2 of 7 sonographers had a good agreement. Interobserver acquisition reliability was also evaluated. The results of the detection of synovitis in B mode with ALG1 showed a fair agreement for 5 of 6 sonographers and only one sonographer has a good agreement. For ALG2, results were better as 4 of 6 sonographers had a good agreement. Using power Doppler with ALG1 we observed a poor agreement for 3 sonographers and a fair agreement for 3. Using ALG2, the power Doppler kappa values were quite similar with one good agreement, 3 fair, and one poor agreement. When we used grade 2 in B mode or in power Doppler, the intra and inter reliability was better. In our study, the reliability was not clearly different between the different sites.

Another systematic review was performed in 2010, focusing exclusively on rheumatoid arthritis (Cheung et al., 2010). 35 studies with a total of 1415 patients were analyzed. Intra and inter observer reliability for still images in B mode and power Doppler was high (k=0.5-1 for intraobserver in B mode; k=0.59-1 for intra observer in power Doppler; k=0.49-1 for inter observer in B mode; k=0.66-1 for inter observer in power Doppler). It appeared that still-image interpretation was more reliable than image acquisition. However, results of acquisition reliability were variable and sometimes poor with kappa values reaching 0.2, and very few studies assessed intraobserver acquisition reliability in either B-mode or power Doppler. Differences in the scanning technique and the lack of familiarity of the ultrasonography machine may also explain the poor results in reliability studies. In this review, few studies looked at the image acquisition reliability. Intraobserver reliability in this domain has been the least studied, and the time interval for retesting was as short as 30 minutes. Power Doppler interobserver reliability was higher than B-mode in still-image interpretation. This may be due to the fact that grading and detection of signal flow on still images would be less liable to variation than identification of hypoechoicstructures. Presence or absence of color signal is also easier to differentiate.

In his 2003's study, Szkudlarek evaluated interobserver agreement between ultrasonography investigators. For the detection of synovitis, the ICC and unweighted kappa estimations for the examined parameters showed a moderate-to-good correlation (0.61–0.81 and 0.48–0.68, respectively) between the ultrasonography investigators. The overall agreement was high (79–91%) (Szkudlarek et al., 2003).

The most important study to evaluate different scoring systems on three main groups of joints (20, 28 and 38) using both a count and a score (comparing the clinical, ultrasonography B mode and ultrasonography power Doppler techniques of acquisition resulting in 18 different global scoring systems) have been published in 2010 (Dougados et al., 2010). A systematic evaluation of the main psychometric/methodological properties in accordance to the OMERACT filter permitted an overview of the performances of these different scoring systems (intra-observer reliability using the intra-class coefficient of correlation, validity on 76 enrolled patients, face validity using the alpha Cronbach test and

external validity using the level of correlation between the scoring system and CRP, sensitivity to change was using the Standardized Response Mean in the 66 patients who completed 4 months of the study and discriminating capacity was using the Standardized Mean Differences in the patients considered by the physician as significantly improved or not at the end of the study). The obtained data suggest that the ultrasonography scoring systems are at least as valid as the conventional clinical ones. Moreover, the ultrasonography acquisition of synovitis appeared to be more objective and can be easily documented. Other studies are required in order to achieve an optimal ultrasonography scoring system endorsed by international societies for monitoring rheumatoid arthritis patients both in clinical trials and in daily practice.

5.2 Erosions

Because of the discrepancy between magnetic resonance and computed tomography concerning erosions, some authors noted that the absolute numbers and sizes of the erosions on the bone surface are not known. To resolve this problem, Koski assessed the ability of ultrasound imaging to detect erosions in a bone phantom model (Koski et al., 2010). 21 bovine lower leg bones were prepared and then were examined by 4 sonographers. The mean correlation coefficient for a correct result in terms of the number of erosions detected was 0.88 (0.75 – 0.75). The overall Cohen's kappa coefficient for interobserver agreement was 0.683 in terms of discrimination between healthy bones and bones with erosions. Ultrasound can be considered as a valid and reliable to detect cortical bone erosions in vitro, when the round erosion is at least 1 mm deep and 1.5 mm wide.

When Wakefield compared ultrasonography to X-rays for the detection of erosion, he assessed intra and inter observer agreement. The intraobserver kappa value for agreement for the detection of cortical bone erosions on the second MCP joint of 55 rheumatoid arthritis patients was 0.75. The interobserver kappa value for agreement between 2 observers for the detection of cortical bone erosions on MCP joints 2–5 in 40 rheumatoid arthritis patients (160 joints) was 0.76. These good results confirmed that ultrasonography is a reliable technique for detecting MCP joint erosions (Wakefield 2000).

Rahmani compared ultrasonography to X-rays and MRI in early rheumatoid arthritis. In 12 patients, 120 first to fifth metacarpophalangeal joints and 96 second to fifth proximal interphalangeal joints were examined. The overall sensitivity and specificity of ultrasonography compared to MRI in detecting bone erosion were 0.63 and 0.98, respectively with a considerable agreement (kappa = 0.68, $p < 0.001$). In patients with more active disease, the sensitivity and specificity were 0.67 and 0.99 (kappa = 0.74, $p < 0.001$) compared to 0.59 and 0.97 (kappa = 0.61, $p < 0.001$) for the rest of patients according to DAS28. Therefore, ultrasonography might be considered as a valuable tool for early detection of bone erosion. (Rahmani et al., 2010).

Not only can ultrasonograpy be seen as reliable for bone erosion, but also for cartilage damage assessment, as Filippucci demonstrated. Two rheumatologists performed ultrasonograpy examination on 80 MCP joints of 20 rheumatoid arthritis patients. There was moderate to good interobserver reproducibility, using a semiquantitative scoring. Unweighted k values were 0.561, 0.366 and 0.766 at dorsal, lateral and volar quadrants respectively (Filippucci et al, 2010).

6. Conclusion

Ultrasonography is a powerful tool to assess rheumatoid arthritis activity. It is widely available, can be performed at the bedside, is not expansive and non ionizing. It is more sensitive than clinical examination to detect synovitis and more sensitive than x-rays to detect erosions. Even though more and more studies have been published to prove its reliability, more consensuses are needed for images acquisition. The next step will be to assess its sensitivity to change, which will expand its use for treatment monitoring.

7. References

Alasaarela E, Suramo I, Tervonen O, Lähde S, Takalo R, & Hakala M. Evaluation of humeral head erosions in rheumatoid arthritis: a comparison of ultrasonography, magnetic resonance imaging, computed tomography and plain radiography. *Br J Rheumatol*. 1998 Nov;37(11):1152-6

Backhaus M, Burmester GR, Gerber T, Grassi W, Machold KP, Swen WA, Wakefield RJ, & Manger B; Working Group for Musculoskeletal Ultrasound in the EULAR Standing Committee on International Clinical Studies including Therapeutic Trials. Guidelines for musculoskeletal ultrasound in rheumatology. *Ann Rheum Dis*. 2001 Jul;60(7):641-9.

Backhaus M, Ohrndorf S, Kellner H, Strunk J, Backhaus TM, Hartung W, Sattler H, Albrecht K, Kaufmann J, Becker K, Sörensen H, Meier L, Burmester GR, & Schmidt WA. Evaluation of a novel 7-joint ultrasound score in daily rheumatologic practice: a pilot project. *Arthritis Rheum*. 2009

Cheung PP, Dougados M, & Gossec L. Reliability of ultrasonography to detect synovitis in rheumatoid arthritis: a systematic literature review of 35 studies (1,415 patients). *Arthritis Care Res* (Hoboken). 2010 Mar;62(3):323-34

Cooperberg PL, Tsang I, Truelove L, & Knickerbocker WJ. Gray scale ultrasound in the evaluation of rheumatoid arthritis of the knee. *Radiology*. 1978 Mar;126(3):759-63

D'Agostino MA, Maillefert JF, Said-Nahal R, Breban M, Ravaud P, & Dougados M. Detection of small joint synovitis by ultrasonography: the learning curve of rheumatologists. *Ann Rheum Dis*. 2004 Oct;63(10):1284-7

D'Agostino MA, Conaghan PG, Naredo E, Aegerter P, Iagnocco A, Freeston JE, Filippucci E, Moller I, Pineda C, Joshua F, Backhaus M, Keen HI, Kaeley G, Ziswiler HR, Schmidt WA, Balint PV, Bruyn GA, Jousse-Joulin S, Kane D, Moller I, Szkudlarek M, Terslev L, & Wakefield RJ. The OMERACT ultrasound task force -- Advances and priorities. J Rheumatol. 2009 Aug;36(8):1829-32. Erratum in: *J Rheumatol*. 2009 Nov;36(11):2625. Zisweiler, Hans-Rudolf [corrected to Ziswiler, Hans-Rudolf]

De Flaviis L, Scaglione P, Nessi R, Ventura R, & Calori G. Ultrasonography of the hand in rheumatoid arthritis. *Acta Radiol*. 1988 Jul-Aug;29(4):457-60

Døhn UM, Ejbjerg BJ, Court-Payen M, Hasselquist M, Narvestad E, Szkudlarek M, Møller JM, Thomsen HS, & Østergaard M. Are bone erosions detected by magnetic resonance imaging and ultrasonography true erosions? A comparison with computed tomography in rheumatoid arthritis metacarpophalangeal joints. *Arthritis Res Ther*. 2006;8(4):R110

Dougados M, Jousse-Joulin S, Mistretta F, d'Agostino MA, Backhaus M, Bentin J, Chalès G, Chary-Valckenaere I, Conaghan P, Etchepare F, Gaudin P, Grassi W, van der

Heijde D, Sellam J, Naredo E, Szkudlarek M, Wakefield R, & Saraux A. Evaluation of several ultrasonography scoring systems for synovitis and comparison to clinical examination: results from a prospective multicentre study of rheumatoid arthritis. *Ann Rheum Dis*. 2010 May;69(5):828-33.

Dussik KT, Fritch DJ, Kyriazidou M, & Sear RS. Measurements of articular tissues with ultrasound. Am J Phys Med. 1958 Jun;37(3):160-5Grassi W, Tittarelli E, Pirani O, Avaltroni D, Cervini C. Ultrasound examination of metacarpophalangeal joints in rheumatoid arthritis. *Scand J Rheumatol*. 1993;22(5):243-7

Filippucci E, da Luz KR, Di Geso L, Salaffi F, Tardella M, Carotti M, Natour J, & Grassi W. Interobserver reliability of ultrasonography in the assessment of cartilage damage in rheumatoid arthritis. *Ann Rheum Dis*. 2010 Oct; 69(10):1845-8.

Joshua F, Lassere M, Bruyn GA, Szkudlarek M, Naredo E, Schmidt WA, Balint P, Filippucci E, Backhaus M, Iagnocco A, Scheel AK, Kane D, Grassi W, Conaghan PG, Wakefield RJ, & D'Agostino MA. Summary findings of a systematic review of the ultrasound assessment of synovitis. *J Rheumatol*. 2007 Apr;34(4):839-47

Jousse-Joulin S, d'Agostino MA, Marhadour T, Albert JD, Bentin J, Chary Valckenaere I, Etchepare F, Gaudin P, Hudry C, Chalès G, Grange L, Hacquard C, Loeuille D, Sellam J, Dougados M, & Saraux A. Reproducibility of joint swelling assessment by sonography in patients with long-lasting rheumatoid arthritis (SEA-Repro study part II). *J Rheumatol*. 2010 May;37(5):938-45

Koski JM, Alasaarela E, Soini I, Kemppainen K, Hakulinen U, Heikkinen JO, Laasanen MS, & Saarakkala S. Ability of ultrasound imaging to detect erosions in a bone phantom model. *Ann Rheum Dis*. 2010 Sep;69(9):1618-22.

Marhadour T, Jousse-Joulin S, Chalès G, Grange L, Hacquard C, Loeuille D, Sellam J, Albert JD, Bentin J, Chary Valckenaere I, d'Agostino MA, Etchepare F, Gaudin P, Hudry C, Dougados M, & Saraux A. Reproducibility of joint swelling assessments in long-lasting rheumatoid arthritis: influence on Disease Activity Score-28 values (SEA-Repro study part I). *J Rheumatol*. 2010 May;37(5):932-7

Millot F, Clavel G, Etchepare F, Gandjbakhch F, Grados F, Saraux A, Rat AC, Fautrel B, Bourgeois P, & Fardellone P; Investigators of the French Early Arthritis Cohort ESPOIR. Musculoskeletal ultrasonography in healthy subjects and ultrasound criteria for early arthritis (the ESPOIR cohort). *J Rheumatol*. 2011 Apr; 38(4):613-20.

Newman JS, Adler RS, Bude RO, & Rubin JM. Detection of soft-tissue hyperemia: value of power Doppler sonography. *AJR Am J Roentgenol*. 1994 Aug;163(2):385-9

Rahmani M, Chegini H, Najafizadeh SR, Azimi M, Habibollahi P, & Shakiba M. Detection of bone erosion in early rheumatoid arthritis: ultrasonography and conventional radiography versus non-contrast magnetic resonance imaging. *Clin Rheumatol*. 2010 Aug;29(8):883-91

Rosenberg C, Arrestier S, Etchepare F, Fautrel B, Rozenberg S, & Bourgeois P. High frequency of ultrasonographic effusion in interphalangeal joints of healthy subjects: a descriptive study. *Joint Bone Spine*. 2009 May;76(3):265-7. Epub 2009 Mar 14.

Salaffi F, Filippucci E, Carotti M, Naredo E, Meenagh G, Ciapetti A, Savic V, & Grassi W. Inter-observer agreement of standard joint counts in early rheumatoid arthritis: a comparison with grey scale ultrasonography--a preliminary study. *Rheumatology* (Oxford). 2008 Jan;47(1):54-8

Szkudlarek M, Court-Payen M, Jacobsen S, Klarlund M, Thomsen HS, & Østergaard M. Interobserver agreement in ultrasonography of the finger and toe joints in rheumatoid arthritis. *Arthritis Rheum*. 2003 Apr;48(4):955-62

Szkudlarek M, Narvestad E, Klarlund M, Court-Payen M, Thomsen HS, & Østergaard M. Ultrasonography of the metatarsophalangeal joints in rheumatoid arthritis: comparison with magnetic resonance imaging, conventional radiography, and clinical examination. *Arthritis Rheum*. 2004 Jul;50(7):2103-12

Szkudlarek M, Klarlund M, Narvestad E, Court-Payen M, Strandberg C, Jensen KE, Thomsen HS, & Østergaard M. Ultrasonography of the metacarpophalangeal and proximal interphalangeal joints in rheumatoid arthritis: a comparison with magnetic resonance imaging, conventional radiography and clinical examination. *Arthritis Res Ther*. 2006;8(2):R52

Van der Heijde DM, van Leeuwen MA, van Riel PL, Koster AM, van 't Hof MA, van Rijswijk MH, & van de Putte LB. Biannual radiographic assessments of hands and feet in a three-year prospective followup of patients with early rheumatoid arthritis. *Arthritis Rheum*. 1992 Jan;35(1):26-34

van de Stadt LA, Bos WH, Meursinge Reynders M, Wieringa H, Turkstra F, van der Laken CJ, & van Schaardenburg D. The value of ultrasonography in predicting arthritis in auto-antibody positive arthralgia patients: a prospective cohort study. *Arthritis Res Ther*. 2010;12(3):R98

Wakefield RJ, Gibbon WW, Conaghan PG, O'Connor P, McGonagle D, Pease C, Green MJ, Veale DJ, Isaacs JD, & Emery P. The value of sonography in the detection of bone erosions in patients with rheumatoid arthritis: a comparison with conventional radiography. *Arthritis Rheum*. 2000 Dec;43(12):2762-70

Wakefield RJ, Balint PV, Szkudlarek M, Filippucci E, Backhaus M, D'Agostino MA, Sanchez EN, Iagnocco A, Schmidt WA, Bruyn GA, Kane D, O'Connor PJ, Manger B, Joshua F, Koski J, Grassi W, Lassere MN, Swen N, Kainberger F, Klauser A, Ostergaard M, Brown AK, Machold KP, & Conaghan PG; OMERACT 7 Special Interest Group. Musculoskeletal ultrasound including definitions for ultrasonographic pathology. J Rheumatol. 2005 Dec;32(12):2485-7. Erratum in: *J Rheumatol*. 2006 Feb;33(2):440.

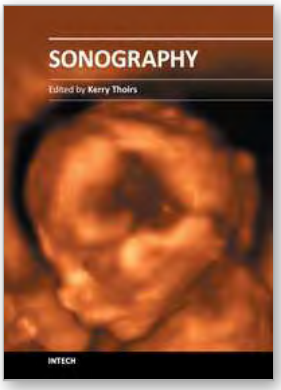

Sonography

Edited by Dr. Kerry Thoirs

ISBN 978-953-307-947-9
Hard cover, 346 pages
Publisher InTech
Published online 03, February, 2012
Published in print edition February, 2012

Medical sonography is a medical imaging modality used across many medical disciplines. Its use is growing, probably due to its relative low cost and easy accessibility. There are now many high quality ultrasound imaging systems available that are easily transportable, making it a diagnostic tool amenable for bedside and office scanning. This book includes applications of sonography that can be used across a number of medical disciplines including radiology, thoracic medicine, urology, rheumatology, obstetrics and fetal medicine and neurology. The book revisits established applications in medical sonography such as biliary, testicular and breast sonography and sonography in early pregnancy, and also outlines some interesting new and advanced applications of sonography.

INTECH
open science | open minds

InTech Europe
University Campus STeP Ri
Slavka Krautzeka 83/A
51000 Rijeka, Croatia
Phone: +385 (51) 770 447
Fax: +385 (51) 686 166
www.intechopen.com

InTech China
Unit 405, Office Block, Hotel Equatorial Shanghai
No.65, Yan An Road (West), Shanghai, 200040, China
中国上海市延安西路65号上海国际贵都大饭店办公楼405单元
Phone: +86-21-62489820
Fax: +86-21-62489821

17

Dynamic Tissue Perfusion Measurement – Basics and Applications

Thomas Scholbach
Chemnitz Clinics, Chemnitz
Germany

1. Introduction

1.1 Rationale

Perfusion is a fundamental prerequisite for all living tissues to meet their needs in terms of supply of oxygen, nutrients, hormones, messenger substances and other necessary dilutes. Dynamic Tissue Perfusion Measurement (DTPM) was developed to quantify the perfusion of tissues and organs by means of colour Doppler sonography. Perfusion is perceived as a certain amount of blood passing through a defined region of interest (ROI) in a certain time.

Colour Doppler sonography is universally used to visualize blood flow inside tissues. The velocity of moving red blood cells is depicted as coloured pixels on the background of uncoloured, black and white pixels, which describe parts of tissues without detectable blood flow. The colouration differs according to the velocity and direction of flow. A colour scale within each image shows the spectrum of reddish and bluish colours used to differentiate the direction (reddish hues describe flow which is reversely directed to bluish flow, in most cases the machine is set to depict flow towards the transducer in red). In both directions, lighter shades describe higher velocities than darker shades. A wall filter is used to exclude extremely low velocity signals from imaging, which mostly emanate from vessel wall vibrations and do not add to real blood flow. The colour scale or colour bar thus gives a visual clue to assign velocity signals from zero to a maximum value to certain vessels inside a tissue. At both ends of the colour scale, the maximum flow velocities for red and blue colour are depicted. These values are determined by the actual pulse repetition frequency and the applied ultrasound frequency. They correspond to the outermost hue on each side of the colour bar whereas the minimum flow is determined by the hue next to the black line (indicating the wall filter) separating blue and red hues from each other.

To calculate perfusion in a certain ROI two parameters must be known:

1. The flow velocity in all vessels within the ROI
2. The area of all vessel transsections in this ROI

Both parameters change during the heart cycle. A third prerequisite is thus to take into account these rhythmic changes and to refer them to their basic rhythm which is a full heart cycle.

DTPM makes use of the data offered by any colour Doppler machine, namely the real time depiction of rhythmically changing coloured pixels and the colour scale to gauge them. To achieve this each hue at the scale is assigned a specific velocity value. This value is calculated by the DTPM-software (PixelFlux, Chameleon-Software, Germany [1]) from a linear correlation of all colours from zero (the lower end of the scale) to the actual maximum value (which is depicted numerically at the outer end of the scale and corresponds to the lightest reddish and bluish shades of the scale). The PixelFlux-software also calculates the area of all coloured pixels inside the ROI. Thus, each coloured pixel is evaluated by assigning a specific velocity and area to it. This is possible only after calibrating the image.

Distance calibration is also done automatically by use of the DICOM data, which are delivered along with the image by the ultrasound machine. A so-called DICOM- header file accompanying each image contains non-visible data such as the type of the ultrasound machine, the transducer, the preset information, the patient data and the distance calibration among many other data.

The mean flow intensity (Q) inside a ROI with the area (A_{ROI}) is then automatically calculated by assigning each colour pixel a velocity (v) and area (A) value according to the following equation:

$$Q\ [cm/s] = v\ [cm/s]^* A\ [cm^2]/A_{ROI}\ [cm^2]$$

2. Standardized video acquisition

An indispensable precondition for reliable measurements is the use of comparable videos in terms of the imaging conditions applied to the investigated tissue. Only by keeping the fundamental circumstances of data acquisition constant, it is possible to compare the measurement results. Such parameters which need to be held constant are colour Doppler frequency and gain, type and software of the ultrasound machine, transducer type, persistence, wall filter, smoothing, type of the colour scale, preference for spatial versus time-resolution and others, depending on the actual configuration of the ultrasound machine. These parameters are summarized and stored as a certain preset of the machine and must be recalled at the beginning of an ultrasound investigation. This step is a widely used practice in order to maintain optimum imaging conditions also in examinations, where a measurement of image data is not a priori planned. The prepared preset is then re-instituted before recording videos for DTPM.

3. Setting the region of interest (ROI) and Doppler angle correction

The ROI is that area inside an ultrasound image, where tissue perfusion measurement is scheduled. The selection of the ROI depends on the type of tissue, structure of the organ and aim of the investigation. The following principles and physical restrictions should be kept in mind in defining the ROI.

In 2D-images, vessels are encoded in colour depending on the angle, which they have with the ultrasound wave. This propagation line of waves is oriented perpendicular to the transducer surface. The colouration represents the exact velocity value only in vessels running straight towards the transducer, i.e. parallel to the course of the sound wave propagation line. All other vessels are encoded with colour hues representing velocity

values (v) which are a product of the cosine of the Doppler angle (α) and the true velocity (v_t), according to the Doppler principle:

$$fd = 2* fo * v_t/c *\cos \alpha$$

with: fd: Doppler shift, fo: insonation frequency, c: sound velocity

This means that in many cases the tissue microvasculature colouration shows velocity values which are smaller than real. To overcome this, an angle correction for each vessel would be necessary. This cannot be done yet in two-dimensional images. With 3D imaging, such a correction is already feasible (see below in section "foetus"). In 2D images, thus an error occurs with DTPM, which must be kept constant to allow comparisons between investigations. This can be achieved under following circumstances:

1. A chaotic vessel architecture without predominant vessel diameters and Doppler angles (type tumour perfusion) (fig. 1)
2. A regular vessel architecture, which can be reliably retrieved (kidney type).

In the latter case, the orientation on anatomical landmarks offers a sufficient framework to find the vascular patterns, which are typical for a certain organ (fig. 2). An example how to choose relevant landmarks is given for the kidney below.

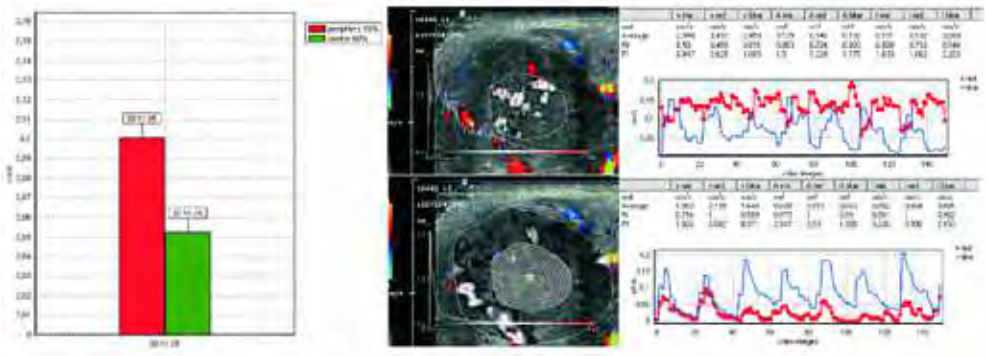

Fig. 1. Example of tumor perfusion measurement. Two concentric ROIs are separately investigated. The vessel architecture is irregular or chaotic (center). No specific prevailing vessel size or orientation can be stated. Left: comparisons of perfusion intensities in the periphery (red column) and the center (green column). Center: Display of the ROIs and false color maps with perfusion intensity curves. Right: time course of the relevant perfusion parameters (from [2])

In both cases, the inevitable error of impossible individual Doppler angle correction for each vessel is held constant. Comparisons of different examinations thus become possible.

For all these considerations, it is crucial to achieve comparable conditions for depicting the vessels in a certain ROI. In the kidney the ROI should be placed inside the outer cortex, in a layer stretching from the outer border of the medullary pyramids to the renal surface and laterally from the watershed of two neighbouring segments to the opposite watershed (see chapter: kidney). In the lymph node and thyroid lobes, a longitudinal section trough the

centre of the ovoid shaped organ should be used as definite transsection plane. In the bowel wall, a longitudinal cut perpendicular to the proximal wall is the best. Tumours should be cut centrally in two perpendicular planes.

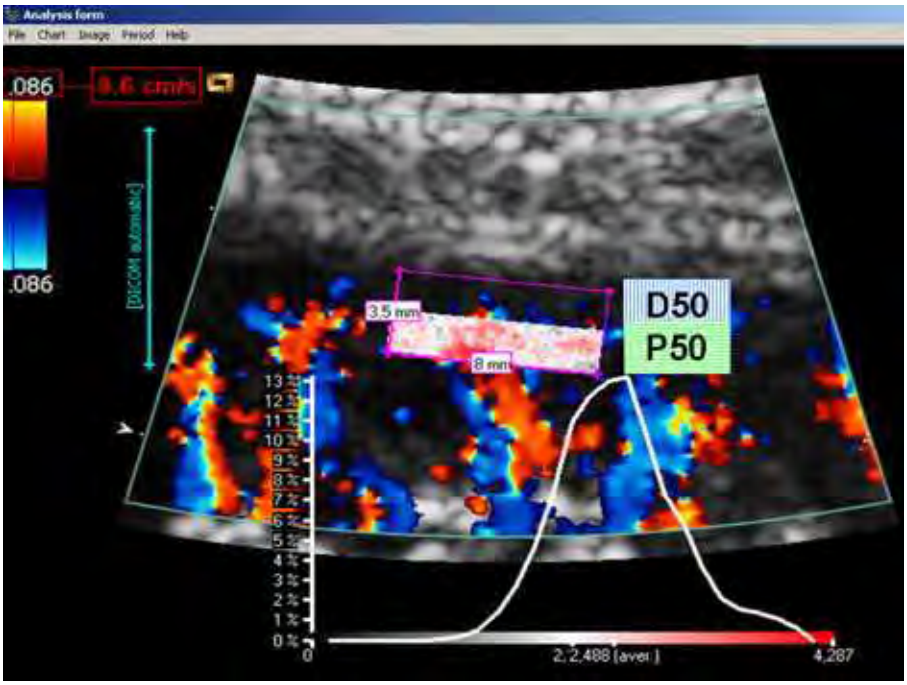

Fig. 2. Example for regular vessel architecture in a renal transplant – see also figure 3. The sub-ROIs are highlighted: P50 – proximal 50% of the outer cortex. D50- distal 50% of the outer cortex. False color map and distribution curve of perfusion intensities are displayed

4. Reading the results

Figure 3 gives an overview of the most important output features in a typical DTPM measurement. In DTPM all data are derived from the basic parameters mean flow velocity, mean perfused area and their change during the heart beat with reference to the entire ROI [2, 3]. In three-dimensional images, the spatial angle correction adds to the primary 2D measurement inside the horizontal plane.

In addition to mean perfusion intensity, calculation parameters are generated to describe the dynamics of perfusion. Examples are Tissue Resistance Index (TRI) and Tissue Pulsatility Index (TPI). TRI and TPI may refer to velocity, intensity and perfused area according to the following formulas:

TRI(velocity *or intensity or area*) = maximum mean velocity *or* intensity *or* area of the ROI during one heart cycle – minimum mean velocity *or intensity or area* of the ROI during one heart cycle divided by maximum mean velocity *or intensity or area* of the ROI during one heart cycle

TPI(velocity *or intensity or area*) = maximum mean velocity *or* intensity *or* area of the ROI during one heart cycle – minimum mean velocity *or intensity or area* of the ROI during one heart cycle divided by mean mean velocity *or intensity or area* of the ROI during one heart cycle divided by mean mean velocity *or intensity or area* of the ROI during one heart cycle

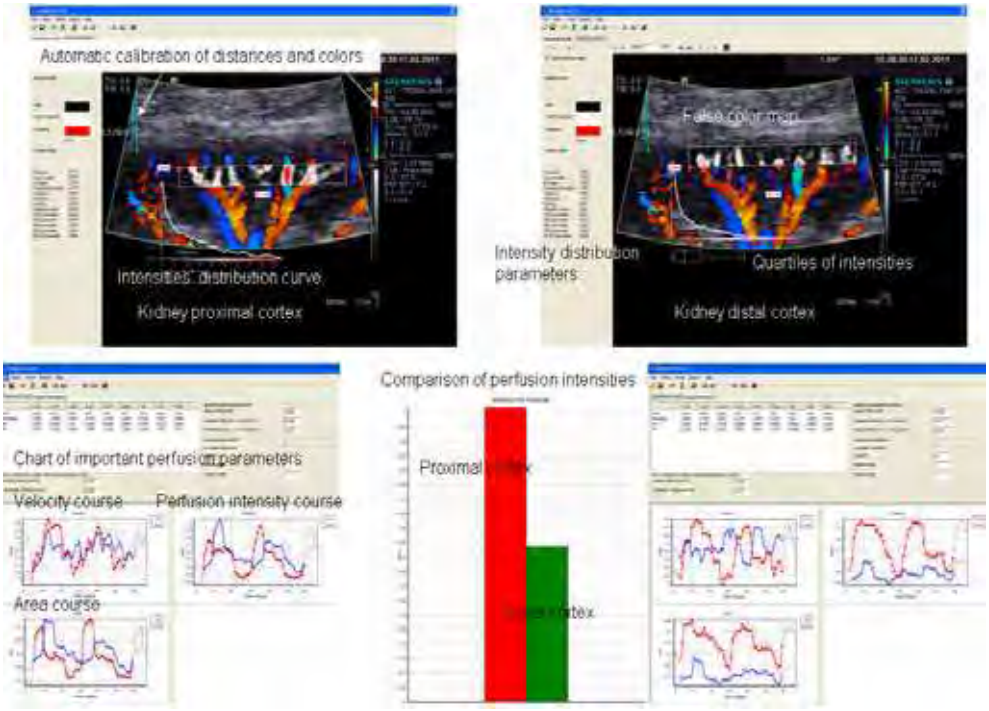

Fig. 3. Example of DTPM output. Overview of the most important output features of a DTPM measurement. Comparison of the proximal and distal cortical ROIs. False color maps (areas shaded in white, red and grey hues), perfusion intensities' distribution curves and additional parameters (upper line). Time curves of the basic perfusion parameters and perfusion intensities (below). Comparison of the overall perfusion intensities in both sub-ROIs (lower line center)

A dynamic perfusion map is generated to pinpoint the local perfusion in a sub-millimetre graded fashion numerically with false colours (fig. 2 and 13). Moreover, the distribution of perfusion intensities according to the whole spectrum of occurring intensities, which are assigned to one of 33 intensity classes, is calculated and diagrammatically displayed. Thus, tissues may be compared according to their content of stronger or weaker perfused areas and vessels (fig. 2, fig. 11). This allows insights into the microarchitecture of a tissue's vascular tree and its changes over time, which is helpful in chronic diseases and tumours. These intensity distribution curves are further described mathematically with the parameters kurtosis and skewness according to their bulging and asymmetry.

Altogether more than 50 parameters are calculated to describe the tissue perfusion numerically. The most important is perfusion intensity to give a general measure of tissue

perfusion. Very instructive too is the distribution curve, outlined below the false colour map (fig. 11). Here shifts within the microvessel population can be reviewed at a glance. This is further underlined with the distribution parameters skewness and kurtosis, which describe the shape of this curve numerically. Statistical comparison of microvessel arrangement thus becomes feasible, permitting the follow up of slight changes of an organ's chronic vascular changes, which begin in the periphery. Another important feature is the false colour map. This map stains the ROI according to the local perfusion intensities over the entire length of the colour Doppler sonographic video clip. The information added to the anatomical structures displayed by the ultrasound image can be helpful in differentiating parts of the tissue with respect to their vascular structures. The flow of the hepatic artery can be separated from the same coloured flow of the portal vein in this way, which might be welcome in the follow up of liver transplants. Another possible application might be the differentiation of local tissue disturbances, as caused by tumour infiltration or scarring or inflammation. To perform an automatic angle correction of all vessels 3D images are used. Here the spatial angel is calculated from both the angle in the frontal and in the sagittal plane. This angle then is applied to calculate true spatially angle corrected flow velocities and vessel diameters. Both are distorted in the original frontal view and can be corrected for 3D flow calculations in so doing. Another important feature is the use of predefined relational sub-ROIs to describe the blood flow on its way through the tissue. Gradients of perfusion can be used to quantify the dampening of perfusion in the depth of a vascular tree. This can be used to detect the very early loss of the tiniest vessels in a tissue, which are often the first to be damaged due to their small lumen. So a chronic pathological process can be discovered in the very beginning and treatment can be started preventing further damage in stages, where the organ's compensatory capacity is still strong enough to recover.

5. Differences to existing methods of sonographic perfusion evaluation

Today RI and PI calculations are the most widely used techniques to quantify flow velocity changes [4-10]. They do not allow conclusions as for the perfusion intensity or volume since the perfused area of the vessel under investigation is not included in the calculation. Even the exact velocities of flow do not need to be measured since the formula refers to two (RI) or three (PI) velocities only which are related to each other to define the velocity change throughout the heart cycle instead of exact velocities. RI = peak systolic velocity - end diastolic velocity / peak systolic velocity and PI = peak systolic velocity - end diastolic velocity / mean velocity of the entire heart cycle.

Contrast enhanced ultrasound (CEUS) can describe the perfusion of larger regions inside organs and thus deliver precise images of typical perfusion patterns of e.g. liver tumours or renal transplant cortical perfusion [11-13]. External influences are relevant concerning the reproducible influx of the contrast enhancer from the injection site to the ROI [14, 15]. The perfusion in CEUS is calculated as the velocity of contrast saturation. The pulsatility of perfusion is not depicted. CEUS thus delivers two parameters to measure: level of saturation and the velocity to reach this level.

The advantages of dynamic tissue perfusion measurement over conventional resistance index measurements and contrast-enhanced sonography (CEUS) are summarized below:

Dynamic tissue perfusion measurement	RI measurement	Contrast enhanced sonography
Measurement of perfusion intensity in all vessels of a larger ROI	Single point measurement in colored vessels	Measurement of contrast enhancement in a larger ROI
Measurement of flow velocities of all pixels in all vessels' transsection	Measurement of flow velocities only in some pixels of a vessel (sample volume)	No flow velocity measurement
Appreciation of heart beat specific flow dynamics	Appreciation of heart beat specific flow dynamics	Loss of heart beat dynamics – saturation curves are calculated
All relevant raw data (i.e. velocities and areas of perfusion) are measured directly during complete heart cycles	Only systolic and enddiastolic velocities are measured	Perfusion intensity is evaluated indirectly from contrast enhancer influx curves (steepness of influx and level of saturation)
Use of unmodified flow data	Use of unmodified flow data	Contrast enhancer as additional source of error
Non-invasive	Non-invasive	Injection necessary
No side effects	No side effects	Rarely side effects
No running costs	No running costs	Additional costs for contrast enhancer (about 92 € per vial)
No age limitation	No age limitation	Not universally licensed for paediatric use

6. Comparison to RI measurements

Resistance index (RI) measurements are widely used to extract a handy quantitative measure from PW (pulsed wave) – Doppler investigations by using to velocity measurements, peak systolic (vs) and enddiastolic velocity (vd) from a single site inside a vessel according to the equation: RI = vs-vd/vs. Despite its broad use the theoretical basis for perfusion quantification remains weak and not surprisingly leads to misleading conclusions. A high RI is commonly linked to a high downstream resistance against flow – often raising the suspicion of a suppressed perfusion while normal RI measurements are referred to as a sign of normal perfusion. Figure 4 clearly demonstrates that this fundamental theoretical misconception also might have obvious practical implications. In the upper line spectral analysis of three peripheral arterial branches of a renal transplant with a stark reduction of peripheral cortical microvessels are shown – averaging to a RI of 0.66. The same value is calculated in the lower line, which stems from another transplant with much better function (serum creatinine 70 vs. 231 µmol/l in the upper line) and abundant vascular signals in the outer cortical periphery. A decision based on RI would attest both transplants a normal "perfusion". DTPM brings out the difference clearly (fig. 5): Perfusion intensity is eight times higher in the proximal cortex in the transplant with a normal function. The insufficient transplant has no peripheral perfusion at all.

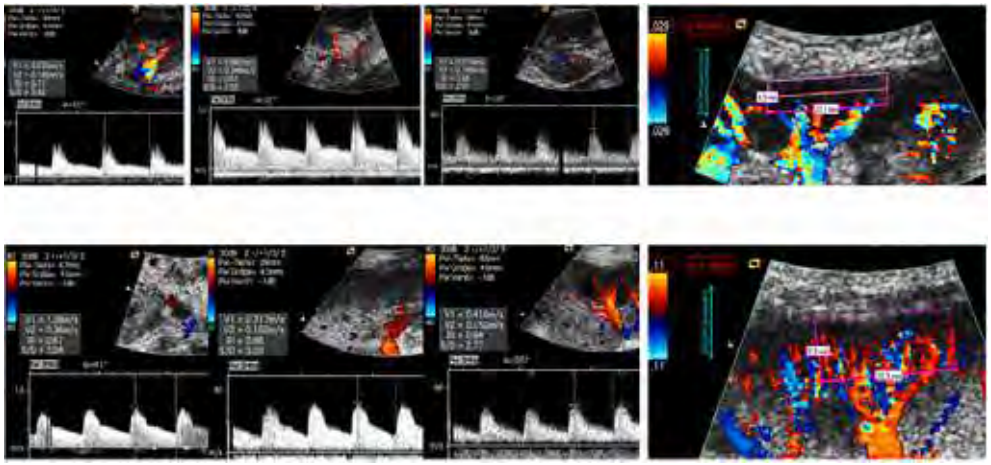

Fig. 4. Two renal transplants compared: upper line insufficient kidney with serum creatinine of 231 µmol/l and normal kidney with a serum creatinine of 70 µmol/l in the lower line. Left: RI measurement in three cortical arteries. Right: Color Doppler sonograms. Insufficient kidney displays a pronounced loss of peripheral perfusion despite more sensible color Doppler setting compared to the kidney below. RI mean values are 0,66 for both transplants

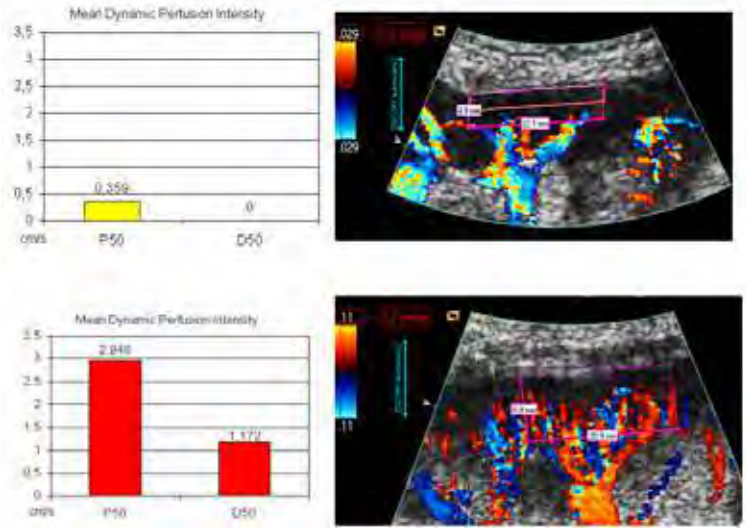

Fig. 5. Same transplants as in fig. 3. DTPM is able to demonstrate a massive difference of tissue perfusion in contrary to RI measurements

Another example for the low power of RI evaluations is figure 6. In a child with acute renal insufficiency due to a hemolytic-uraemic syndrome (HUS), two neighbouring cortical arteries demonstrate vastly different RIs. Depending on which arteries the investigator selects, contradictory conclusions must be drawn from such evaluations. Another seldom-

considered drawback of RI measurements inside tissues is that thin arteries can only be located to interrogate the flow as long as the vessel is still coloured. If perfusion drops significantly, colour signals become weak and disappear at all. These vessels, the most affected, are excluded from evaluation by RI altogether. This must distort the overall evaluation of tissue perfusion if RI measurements are its basis.

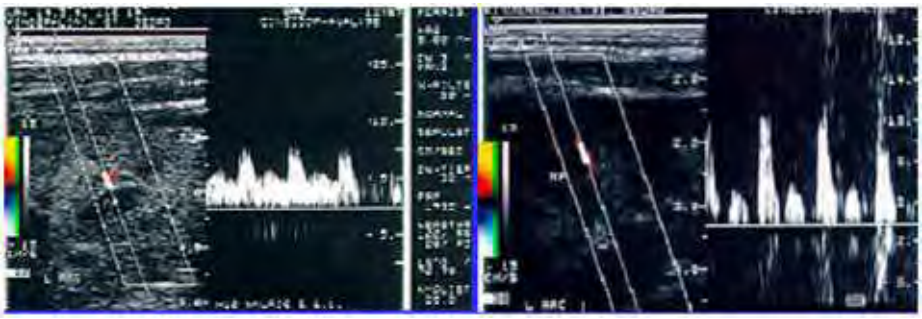

Fig. 6. Misleading RI measurements in a kidney af a child affected by haemolytic-ureamic syndrome. During the same investigation strikingly different RIs are found in intimate neighborhood

The only way out of this dilemma is a method that takes into account simultaneously all flow signals in all vessels inside a larger ROI instead of single vessels, which also takes into account non-perfused areas. These are the fundamentals of DTPM, referring all flow signals inside an entire ROI thus reflecting properly vessel and flow intensity loss in chronic disease. It is just in chronic disease where remaining vessels amidst fibrosed tissue try to compensate the loss of neighbouring vessels by dilatation to feed the "thirsting" periphery and thus exhibit a lower RI than under normal conditions (fig. 5).

7. Phantom flow measurements

A phantom was built to measure the volume flow under externally controlled conditions consisting of a Teflon tube with an internal diameter of 2.0 mm that was placed into a water basin and fixed in a way that the tube was running straight in a steep angle towards the ultrasound transducer that was fixed to a tripod. The tube was perfused with a watery homogeneous rice starch solution.

Colour Doppler videos were recorded under standardized imaging conditions (ultrasound device: S2000, Siemens, Germany, linear transducer, colour Doppler frequency 4 MHz, the angle of the tube towards the ultrasound propagation line was 36°). The pump rate was changed; repeated colour Doppler recordings were made and measured by DTPM.

Two separate investigators independently performed these PixelFlux-measurements from 87 datasets (mean values based on altogether 191 recordings) at 22 different pump rates.

Phantom flow measurements showed an excellent correlation to pump rates (fig. 7) with a Pearson correlation coefficient of pump rate and investigator 1 of 0,987 and 0,991 for investigator 2. Both investigators measurements correlated with 0,997.

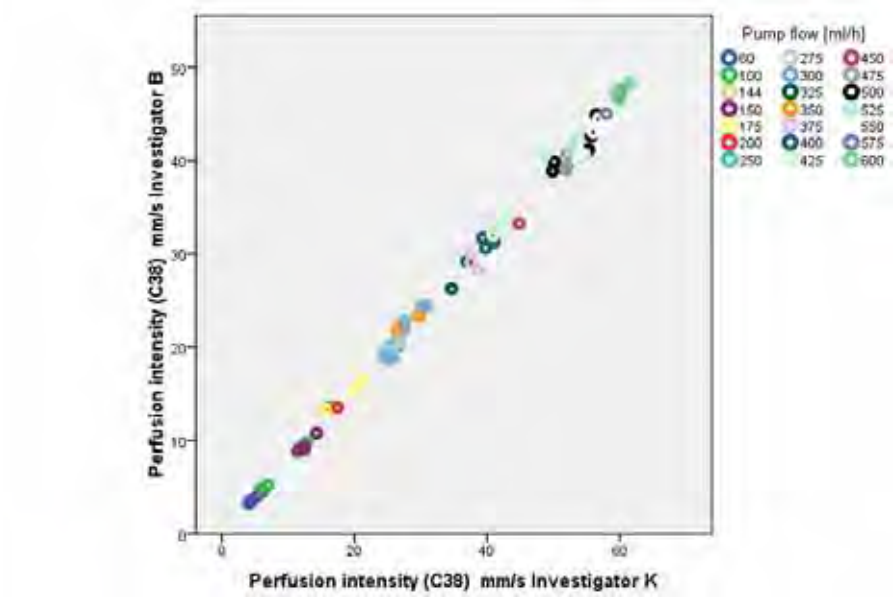

Fig. 7. In a perfusion phantom* DTPM measurements of two investigators were compared. An excellent correlation in-between both investigators and of both investigators to the externally measured flow rate was found. * Homogenized rice starch solution pumped by a precision laboratory pump, Flow volumes measured constantly by a laboratory balance

8. Dynamic tissue perfusion measurement – Applications

8.1 Kidneys

Kidneys are abundantly perfused and are second only to the brain with respect to their blood supply in the systemic circulation [16, 17]. Perfusion measurement is important to detect changes, which precede function loss – the so-called creatinine blind stage of renal insufficiency [18]. For reliable kidney perfusion measurements, it is necessary to adjust the ROI to the typical anatomical pattern of the renal microvessel architecture. The kidney consists of segments, each with an individual blood supply via an interlobar artery. This vessel is crossing the inner parenchyma in-between two neighbouring medullary pyramids to branch off symmetrically into arcuate arteries from which in a brush-like manner interlobular arteries emanate. Such a segment is chosen as the ROI in a way that the feeding interlobar artery runs straight towards the transducer.

The ROI itself is a parallelogram adjusted to the individual kidney's anatomical landmarks, which are as follows: the left upper corner of the parallelogram lies at the renal surface on the watershed line between two segments (i.e. where the interlobular arteries from two neighbouring segments seem to touch each other). The right upper corner then is fixed at the right border of the segment under investigation with the same premises as the first corner. The right lower corner then lies on the right watershed line, which is extended to the surface of the medullary pyramid and ends at the centre of the outer edge of the pyramid. From

there the lower border of the ROI extends to the left pyramid to reach its centre point on its outer border. This is the left lower corner of the parallelogram. This way a symmetric distribution pattern of all branches of this vascular segment is achieved [19]. This parallelogram is divided into horizontal layers (e.g. p50 and d50) encompassing the proximal 50% (p50) or distal 50% (d50) of the ROI's height. Any other layer thickness can be chosen to meet the needs of the investigation (for instance 10 layers with the thickness of 1/10 of the ROI (fig. 13)). These layers thus have a thickness that refers to the overall dimensions of the ROI and are therefore relational layers. In thicker cortices, the layers are thicker than in thinner cortices. Nevertheless, the layers of different kidneys are comparable to each other since they comprise the comparable level of the cortical vascular tree (fig. 8).

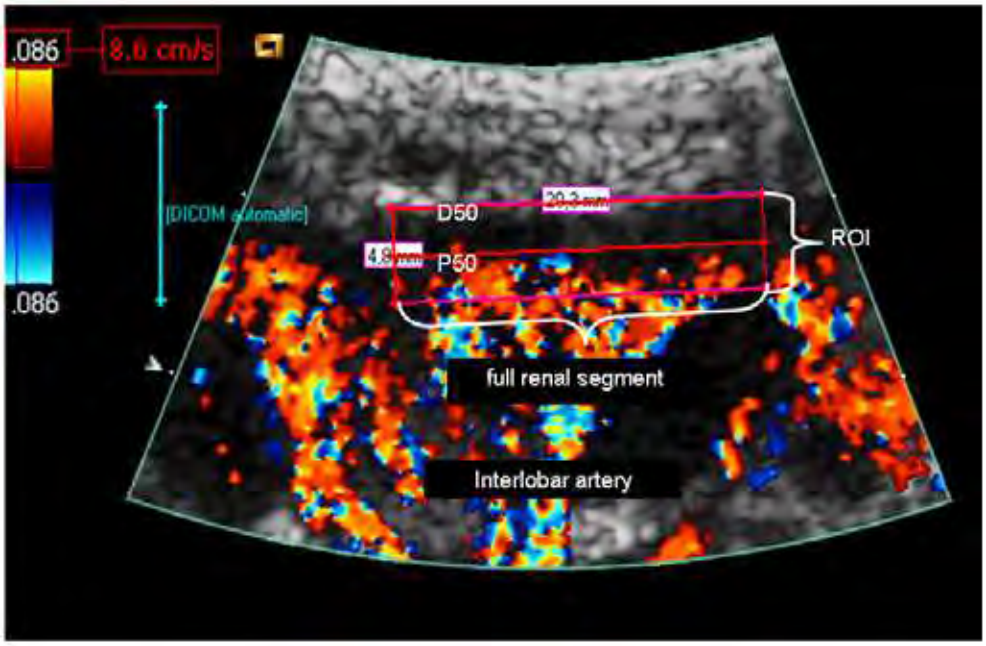

Fig. 8. Example of placing of a ROI in a kidney with indication of the anatomical landmarks to guide the setting

Own investigations yielded a decline of renal cortical perfusion with compromised creatinine clearance (fig. 9). Normal kidneys display a decline of cortical perfusion intensity from central to peripheral cortex (fig. 10) [19]. Inflammation causes a strong hyperperfusion (fig. 11). DTPM can help to differentiate the affection of either right or left kidney – helpful in children and non-communicating patients. Moreover, the different effects of hydronephrotic perfusion loss even in a state of general hyperperfusion due to inflammation can be demonstrated (fig. 11). In kidneys with vesico-ureteral reflux, we found a decline of perfusion inside the peripheral cortical layers, which corresponded to the reflux degree (low grade vs. high-grade reflux) (fig. 12).

In nutcracker phenomenon, a frequent anatomical variant of the course of the left renal vein with sharp narrowing of the vessel between the superior mesenteric artery and the

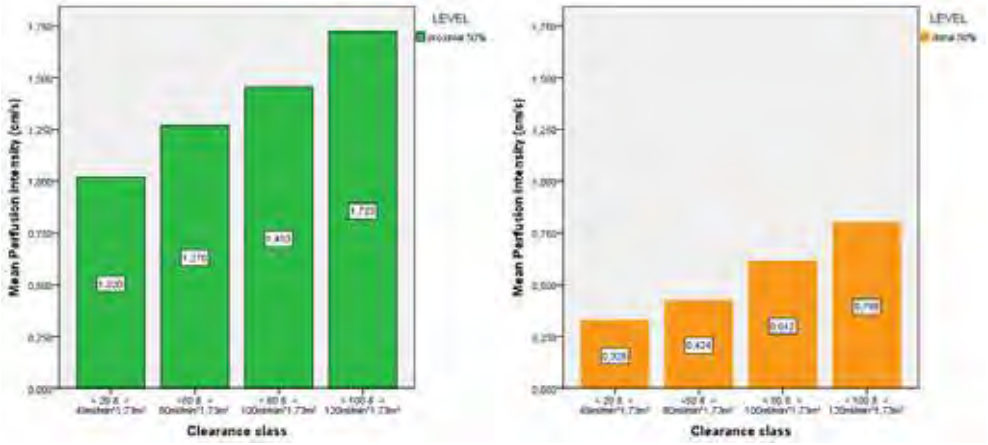

Fig. 9. Constant decline of cortical perfusion with progression of renal insufficiency. Left: proximal cortex. Right: distal cortex

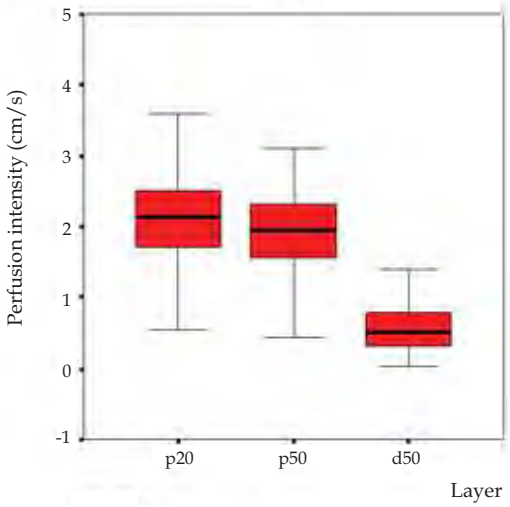

Fig. 10. Decline of renal cortical perfusion from the inner to the outer cortex

abdominal aorta, a venous congestion of the left kidney ensues. Its consequences are often misinterpreted from conventional imaging alone but are nonetheless often disabling for the affected ones. Many patients suffer from chronic and exacerbating abdominal fits of cramping pain. The congested kidney is often swollen and less perfused than the right one. This can be easily demonstrated by DTPM (fig. 13). Perfusion diminution is a signal of insufficient collateral pathways to drain the renal blood from the left side. A treatment with aspirin can either alleviate or often abolish pain and functional disturbances of the congested organs, which have to deal with the massive venous overflow from the left renal vein. Simultaneously with the clinical improvement, a significant increase of left kidney's perfusion can also be measures by DTPM (fig. 14) [20].

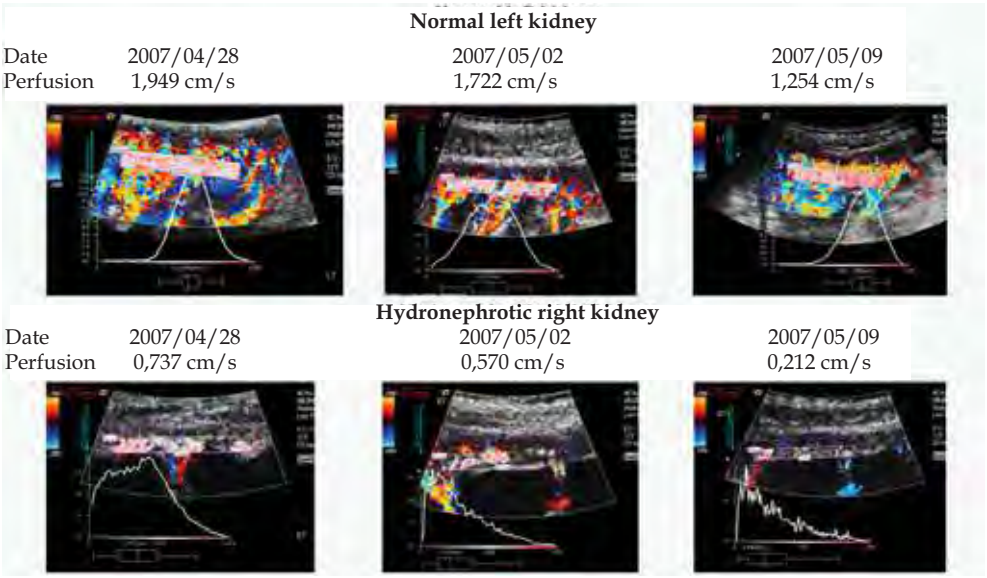

Fig. 11. Differing response of both kidneys towards an bacterial infection in a patient with a right sided hydronephrosis Perfusion intensity in the proximal cortex. MAG3 scintigraphy right kidney: 30% of both kidneys' function. Renal perfusion in a child with a normal kidney on the left and a hydronephritc kidney on the other side. Inflammation due to bacterial infection causes an initial perfusion increase (2007/04/28). With recovery perfusion drops in both kidneys (from 2007/05/02 to 2007/05/09). The decline is more pronounced in the hydronephrotic kidney. Perfusion intensity distribution curves differ markedly between both kidneys pointing to the damage of the microvasculature in the hydronephrotic kidney and a compensatory hyperperfusion trough dilated microvasculature on the left side

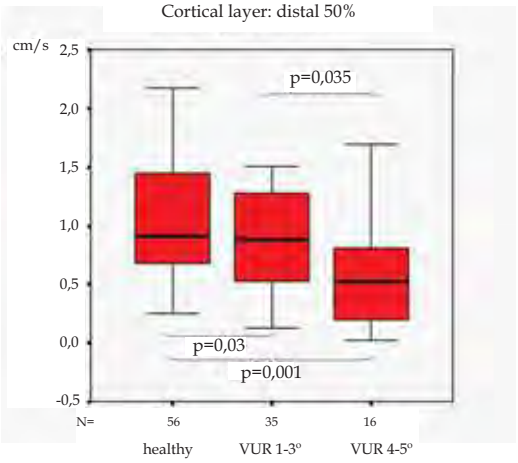

Fig. 12. Diminished perfusion of kidney in vesico-ureteral reflux compared to healthy ones. Compromise of perfusion dependent on degree of reflux

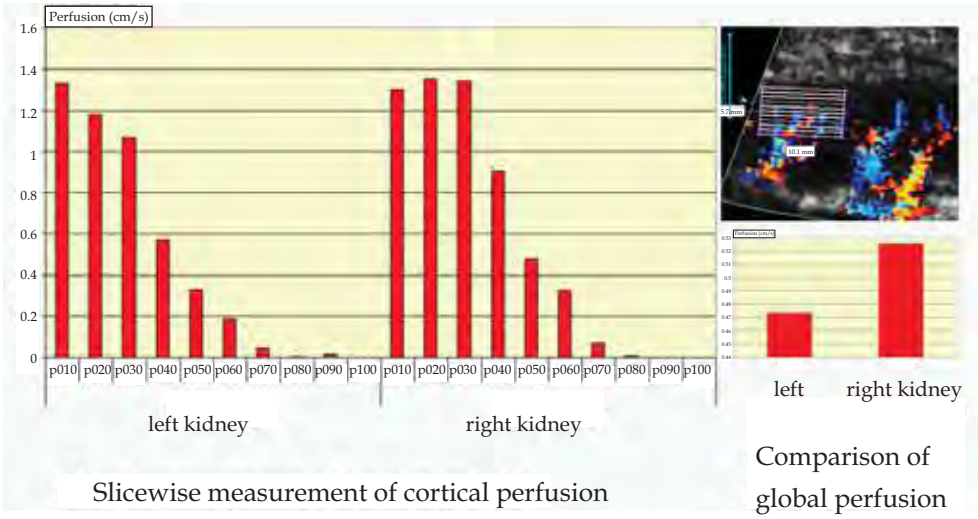

Fig. 13. The nutcracker phenomenon of the left kidney often causes depression of left renal perfusion. Left: Sub-millimeter layers show very precisely the potential of DTPM to describe microvascular perfusion in an unprecedented subtlety. Right: Heavily depressed perfusion of the left kidney in nutcracker phenomenon

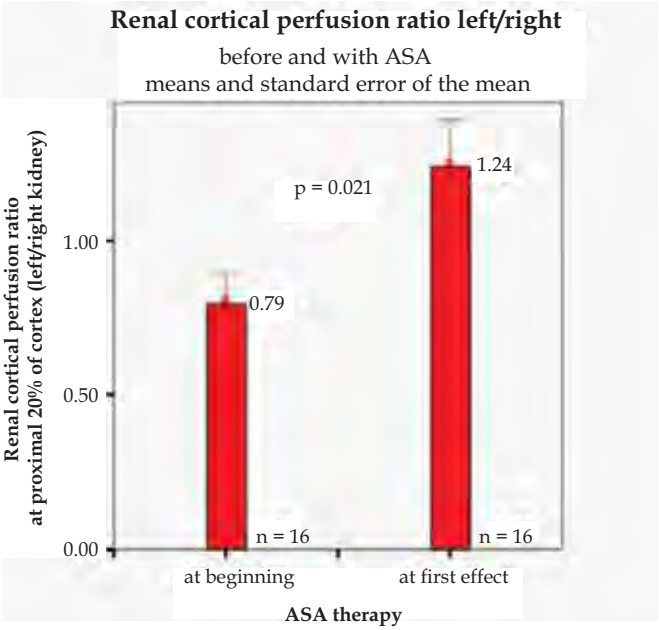

Fig. 14. Effect of aspirin (acetylsalicylic acid: ASA) onto the perfusion of the left kidney. The ratio of left to right kidney perfusion is displayed. After aspirin treatment a significant increase of this ratio can be stated. From [21]

In a preliminary study, we compared kidneys from children with juvenile diabetes of varying duration of disease to kidneys from healthy children with respect to the perfusion drop from central to peripheral cortical layers. Even in an early stage of disease, (no child had microalbuminuria) a highly significant peripheral perfusion loss could be demonstrated in diabetic kidneys (fig. 15).

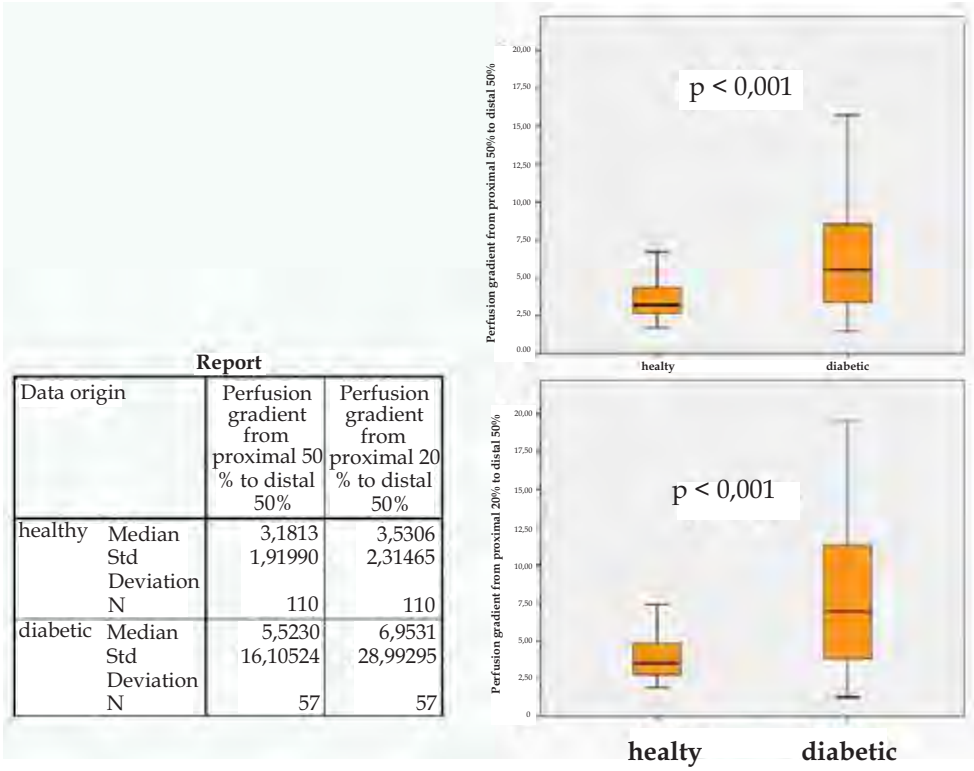

Report

Data origin		Perfusion gradient from proximal 50 % to distal 50%	Perfusion gradient from proximal 20 % to distal 50%
healthy	Median	3,1813	3,5306
	Std Deviation	1,91990	2,31465
	N	110	110
diabetic	Median	5,5230	6,9531
	Std Deviation	16,10524	28,99295
	N	57	57

Fig. 15. DTPM discloses a significant reduction of peripheral to central cortical perfusion in diabetic children compared to healthy ones. The effect is more pronounced when comparing the proximal 20%/distal 50%-ratio (lower diagram) then in proximal 50%/distal 50%-ratio (upper diagram)

9. Renal transplants

Renal transplants are subject to chronic immunological attacks as well as toxic effects of immunosuppressive treatment. Repeated biopsies are today the only way to clarify the creeping changes within the renal parenchyma. We conducted a study on 75 renal transplant recipients, which had a DTPM immediately before their biopsy. Banff criteria were correlated to DTPM results. Some of the very important histological features correlated significantly with perfusion changes [21], pointing to the potential of DTPM for renal transplant long term follow up. RI values were much less instructive (insignificant differences) than DTPM measurements (significant differences) to discriminate varying

stages of peritubular inflammation. Varying grades of transplant Polyomavirus infection were marked with significant increases of cortical tissue perfusion [21]. In another study, we found in children a marked decline of cortical perfusion in allograft cortices beginning already one year after transplantation [22] while the pulsatility of cortical perfusion rose significantly [23]. Recently, it was shown, that intrinsic donor-derived factors are associated with GFR and cortical parenchymal perfusion intensity, measured by DTPM, but not the RI of segmental arteries in renal allografts [24].

10. Bowel

A main area of interest for DTPM is chronic inflammatory bowel diseases. In Crohn disease as well as in ulcerative colitis inflammatory hyperperfusion of the bowel wall could be demonstrated.

Patients with Crohn disease irrespective of disease activity had higher blood flow intensity compared to healthy probands. Mean small bowel wall perfusion intensity was 0.025 cm/s in healthy probands whereas in patients with Crohn disease 0.095 cm/s was found [25]. Large bowel wall perfusion intensity in healthy probands was distinctively less than in patients with Crohn disease (0.012 cm/s vs. 0.082 cm/s, $p < 0.001$) [25]. Conventional evaluation of disease activity by means of activity indices did not clearly distinguish patients with high from those with less pronounced inflammatory hyperperfusion. The correlation of bowel wall perfusion and PCDAI-values was weak albeit significant ($r = 0.349$, $p = 0.001$) [25]. The individual effect of TNF-alpha antibody treatment can be closely followed and treatment regimes can be tailored according to DTPM. Inflammatory activity in fistulas can be measured even after closure of the cutaneous orifice. DTPM can also be used to locate the focus of an abdominal inflammatory process by comparing the perfusion of different structures, which may be involved, but in different extent and activity. So lymph nodes, vermiform appendix, cecum and terminal ileum can be evaluated separately and clear decisions on the main source of complaints can be made. Unnecessary appendectomies can be avoided based on an imaging and perfusion measurements guided approach.

In ulcerative colitis, 14 histological criteria (changes of crypt architecture, depletion of goblet cells, Paneth cells distal of the left colon flexure, lymphocyte infiltration, plasma cells, eosinophils, unspecific inflammatory infiltrates, granulocytes in the lamina propria and lamina epithelialis, crypt abscesses, oedema, erosions or ulcerations, regenerative epithelium , fibrosis, increased cryptal distance to muscularis mucosae) of disease activity were compared to the local perfusion state of the bowel wall. Scores of neutrophil as well as lymphocytic invasion of the wall, crypt abscesses and wall oedema were significantly correlated (in oedema inversely) to the local wall perfusion (fig. 16) [26]. DTPM can add more differentiated and important numerical data, which make imaging data comparable and thus a tool for decision making in a clinical setting. Figure 17 compares histological images, colonoscopic photographs, colour Doppler sonographic images and the results of DTPM at the site where the images stem from. A convincing differentiation of these three bowel segments can be demonstrated by the different perfusion intensities.

Faingold et al. found a trend to decreased intestinal wall perfusion (0.040±0.015 cm/s vs. 0.052±0.029 cm/s) in neonates that died due to hypoxic ischemic injury [27].

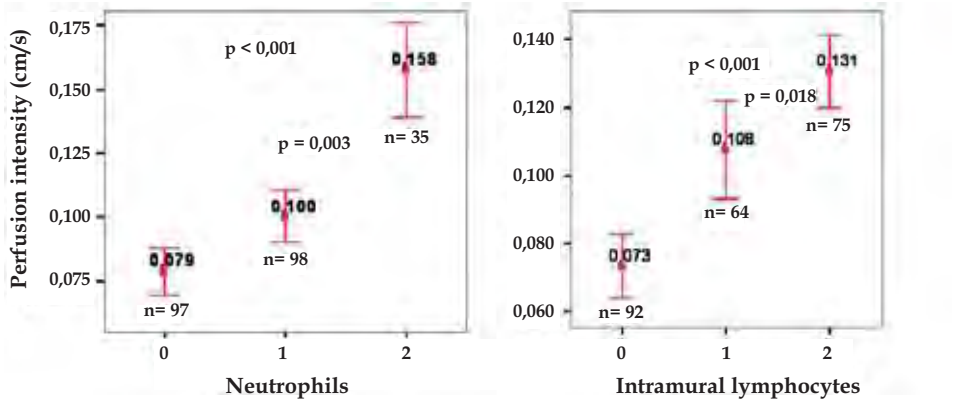

Fig. 16. Large bowel wall perfusion in ulcerative colitis. In ulcerative colitis an increasing score of granulocytic (left) and lymphocytic (right) wall infiltration is reflected by significant increase in wall perfusion

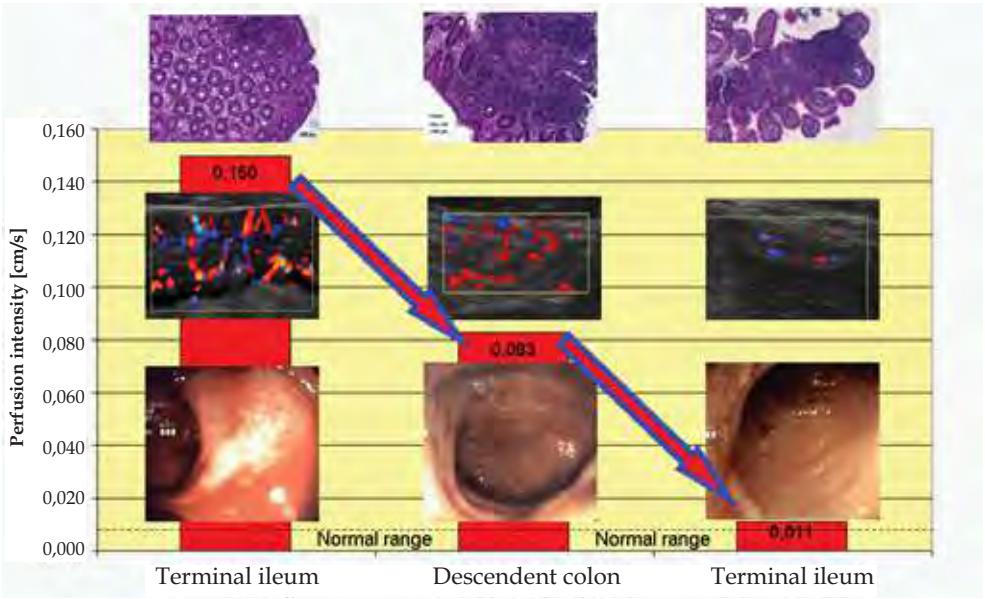

Fig. 17. Synopsis of DTPM measurements (red columns) histological images, color Doppler sonograms and colonoscopic images from three IBD patients and different sites. DTPM differentiates better than all other methods between acutely inflamed and resting bowel segments in IBD patients

11. Lymph nodes

Lymph node perfusion measurement helps to tell inflammatory changes and can provide insight into the dynamics of progression or retreat of the underlying process. Normal lymph

nodes in the neck have a minute but always detectable perfusion, which can be measured accurately. In upper airway infections, lymph nodes do not react with a hyperperfusion whereas lymphotropic EBV infection resulted in a marked increase of perfusion (fig. 18) [28].

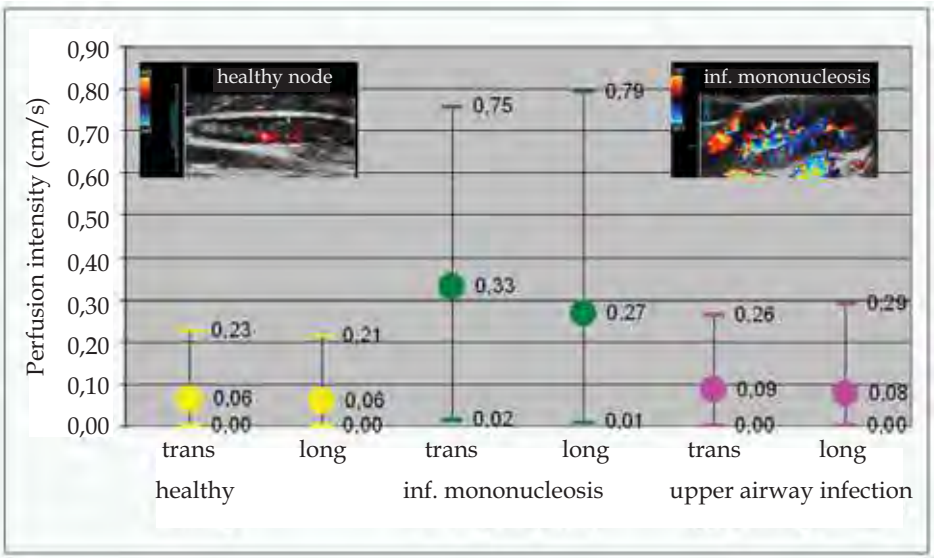

Fig. 18. Lymph node perfusion as seen in DTPM: no differences exist between longitudinal (long) and transverse (trans) sections of the nodes. Infectious mononucleosis raises cervical node perfusion significantly (green symbols) compared to nodes from healthy probands (yellow) in contrast to nodes in acute upper airway infections (pink). Insets: left: normal node in color Doppler Right: Node in infectious mononucleosis (EBV-infection)

12. Muscle

A muscle perfusion measurement is feasible with the demonstration of a marked increase during exercise and steep decline afterwards in athletes (fig. 19). The perfusion was measured in the M. rectus femoris in a horizontal section before during and after exercise along with the measurement of serum lactate and a self-estimation of subjective workload (fig. 20).

In aged patients, an increase of muscle perfusion of the M. biceps brachii was demonstrated during an exercise program to foster rehabilitation.

13. Thyroid

Reproducibility of thyroid DTPM between two investigators is significant (fig. 21).

Thyroid perfusion is strongly increased in thyreoiditis (fig. 22). It is not yet clear however, if the amount of perfusion is paralleled by conventional laboratory parameters or clinical symptoms.

Thyroid nodules differed with respect to their distribution of perfusion according to their biological behaviour. Comparison of perfusion intensities obtained from peripheral and central parts of the nodules revealed that, in non-neoplastic nodules the peripheral flow was more intense than the central flow and, on the contrary central flow was more prominent than the peripheral flow in neoplastic nodules ($p<0.005$) [29].

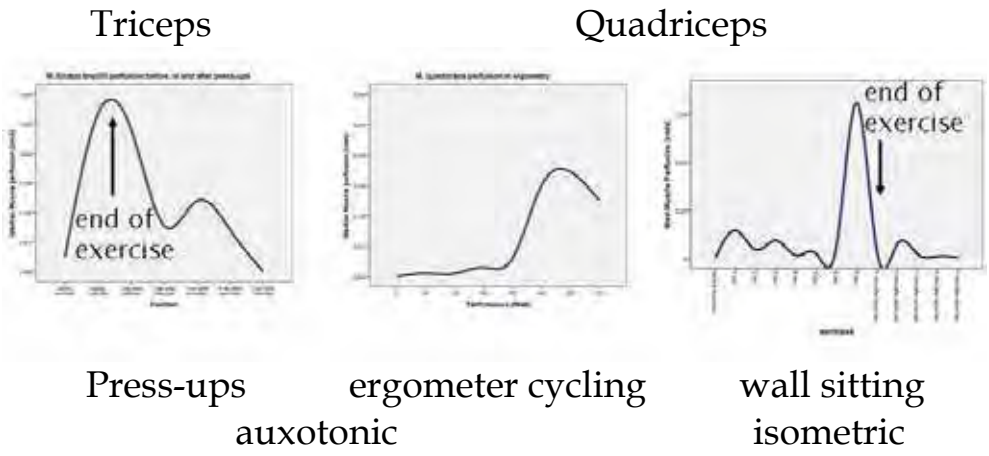

Fig. 19. Significant muscle perfusion increase in 13 athletes – maximal exercise. DTPM reflects the perfusion in muscles before, during and after physical exercise in various settings. Auxotonic as well as isometric exercises cause a strong perfusion increase. After exercise perfusion drops sharply

		Duration of exercise	Heart rate
Muscle Perfusion	Spearman corr. Coeff.	**,535**	**,469**
	Sig. (2-tailed)	**,000**	**,000**
	N	61	61

Fig. 20. Correlation of quadriceps perfusion during ergometer cycling. Exercise induced muscle perfusion correlates significantly to duration of exercise and heart rate

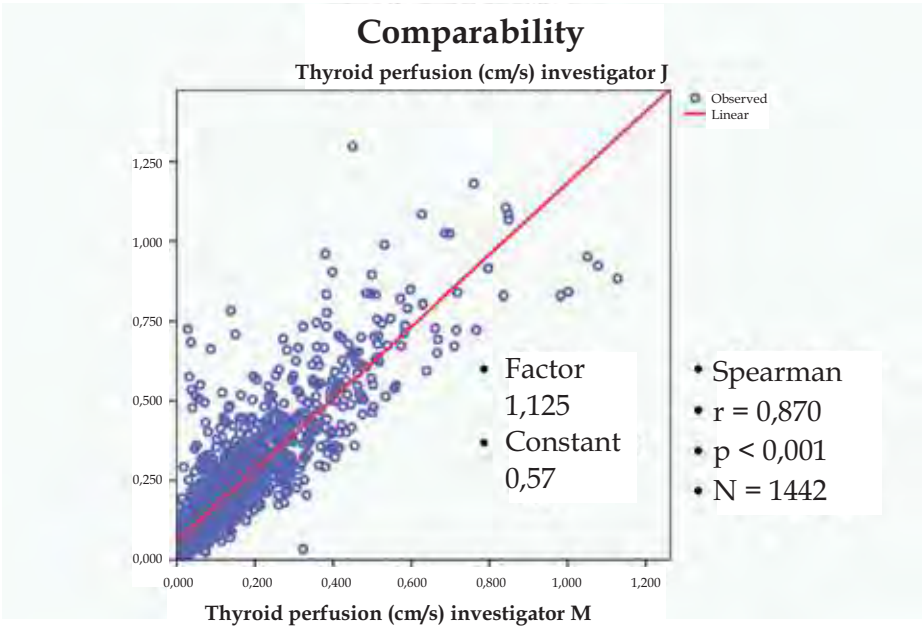

Fig. 21. Thyroid perfusion in 1142 measurements – low interobserver variation and highly significant correlation between both investigators

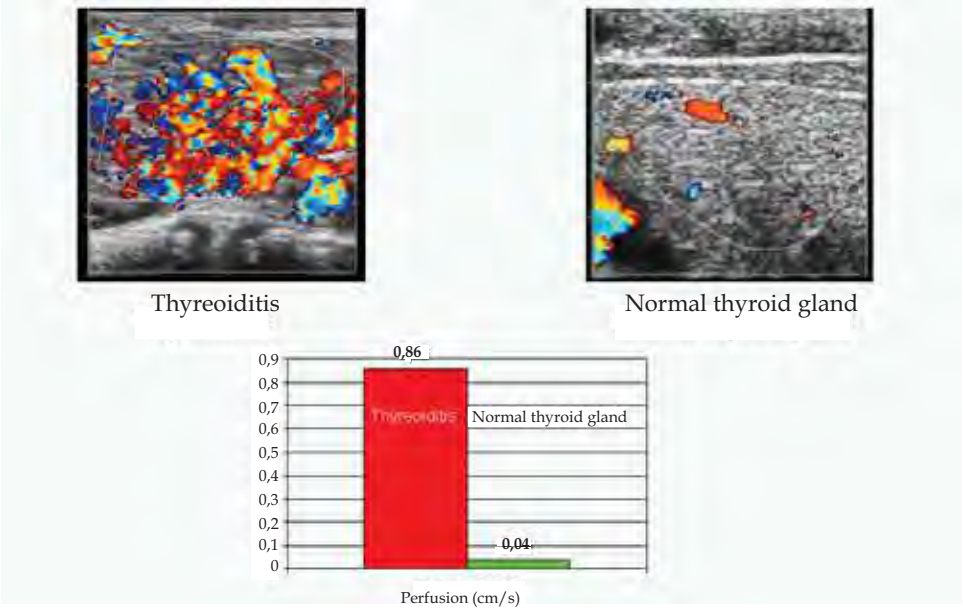

Fig. 22. Example of ample perfusion increase in thyroiditis – color Doppler sonograms and corresponding DTPM values are displayed

14. Tumours

Tumour perfusion evaluation by DTPM is also feasible and defined regions such as tumour core and periphery, whose size can be predefined, e.g. as concentric regions. This can uncover central tumour necrosis or ischemia, which might be relevant for treatment decisions. Hypoxia due to ischemia is a factor of chemo- and radioresistance of tumours [30-32]. Therefore, it might be useful to monitor tumour perfusion in separated shells.

In a series of metastatic tumours of the neck, a direct correlation of tumour perfusion measured by means of DTPM and directly measured tumour oxygenation could be demonstrated (fig. 23) [33]. In hypoxic tumours perfusion was significantly lower compared to normally oxygenated ones (fig. 24). Moreover, the pulsatility of tumour perfusion differed significantly between groups with different stages of metastasis (fig. 25) [33]. These results may be interpreted as a change of tumour stroma. The more densely packed the stroma is the higher the pulsatility is, since the distension of small vessels is influenced by the pressure change during a heart cycle on the one hand but on the other hand by the resistance against the widening of a vessel by the surrounding structures and their stiffness.

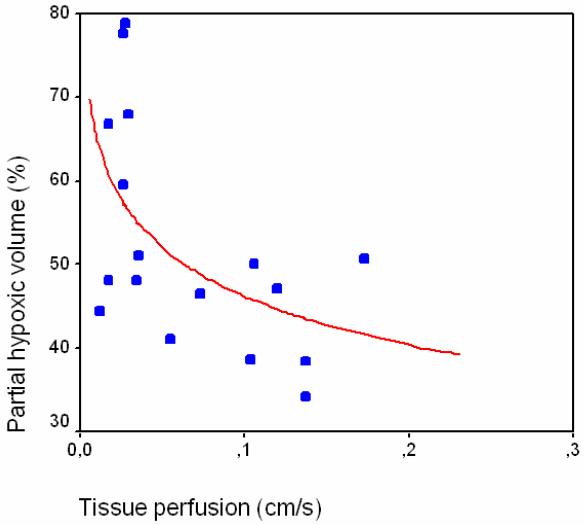

Fig. 23. Significant correlation between directly measured hypoxic volumes in metastatic lymph node tumors of the neck (Eppendorf histiograph) and DTPM (from [2])

15. Foetus

The foetal perfusion has to meet the needs of the rapidly growing organism, to deliver oxygen and nutrients in order to permit a normal intrauterine growth. Among other causes placental insufficiency is an important reason for disturbed intrauterine growth, resulting in intrauterine growth retardation (IUGR) and postnatal complications. The evaluation of foetal perfusion today is based in daily practice on the calculation of RI and PI in large arteries, mainly the umbilical, the cerebral arteries and the aorta, sometimes supplemented by flow pattern evaluations in the venous duct [34, 35]. In the eighties of the last century, first

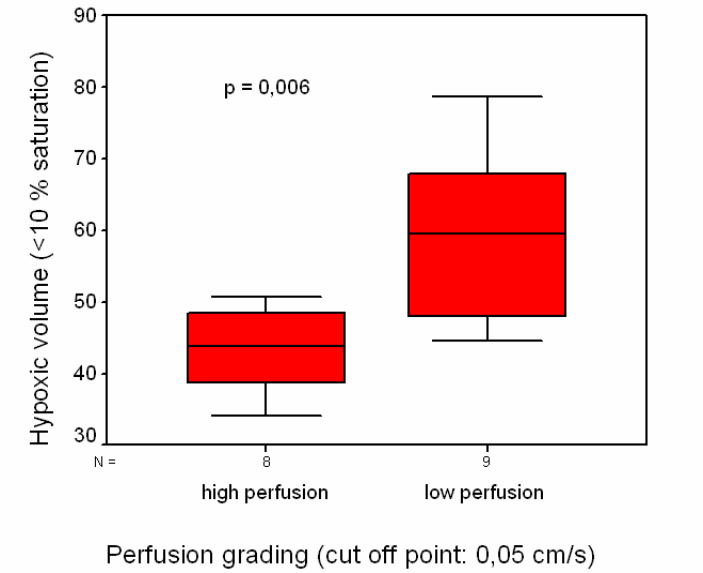

Fig. 24. Oxygenation differences in relation to tumor perfusion. Less perfused metastatic lymph nodes in the neck (cut off in DTPM: 0,05 cm/s) have a significantly higher hypoxic volume than well perfused nodes (from [2])

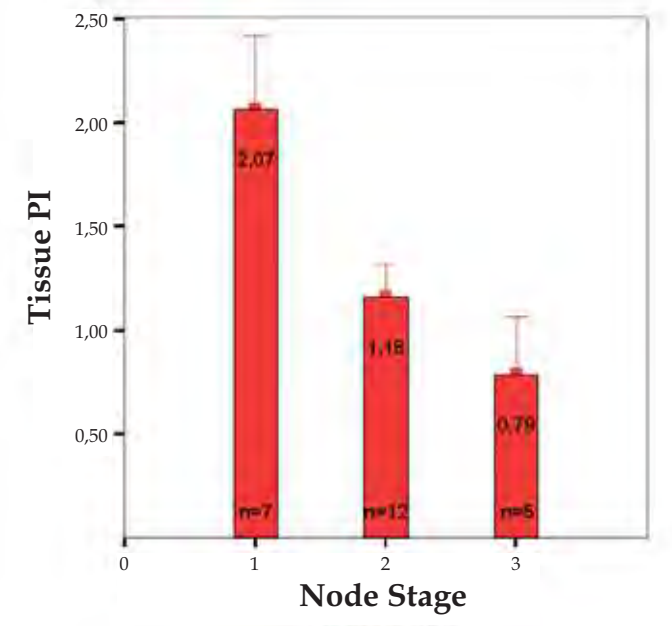

Fig. 25. The Tissue Perfusion Pulsatility Index (TPI) falls significantly with increasing N-stages of the nodes (from [2])

attempts tried to quantify the umbilical venous flow volume with the aim to evaluate the foetal perfusion in quantitative terms [36, 37]. These studies were not continued because of limited reproducibility [38]. Nevertheless, these studies targeted at a parameter – volume flow –, which has a much better rationale than the popular and easy to measure RI and PI. The early studies were flawed mainly by two limitations, which could not be overcome with two-dimensional sonographic techniques. First the angle correction of flow velocity in space and second the non-circular shape of the transsection of the umbilical vein (UV).

Spatial angle correction is but pivotal in this setting, because the UV is continuously winding around the umbilical arteries and the whole cord is irregularly bent within the amniotic cavity. Two-dimensional images thus may allow an angle correction within the frontal plane but this can be vastly misleading. Depending on the sagittal angle the true and only relevant spatial angle can differ substantially thus leading to unpredictable errors of the volume flow calculation, when unknown. The second source of error was the universal assumption, that the UV is a round tube. The investigators tried to depict a straight running venous segment with parallel borders to apply the formula for circular area calculation in order to multiply this area with the mean flow velocity which was traced with a pulsed-wave- Doppler instrument in the centre of the vein.

These sources of error combined in an unpredictable manner and caused the refusal of this approach.

The technique of DTPM combined with the modern three-dimensional imaging techniques can resolve all of these imponderabilities. We developed the three-dimensional, spatial angle corrected umbilical vein flow volume measurement, which is outlined below.

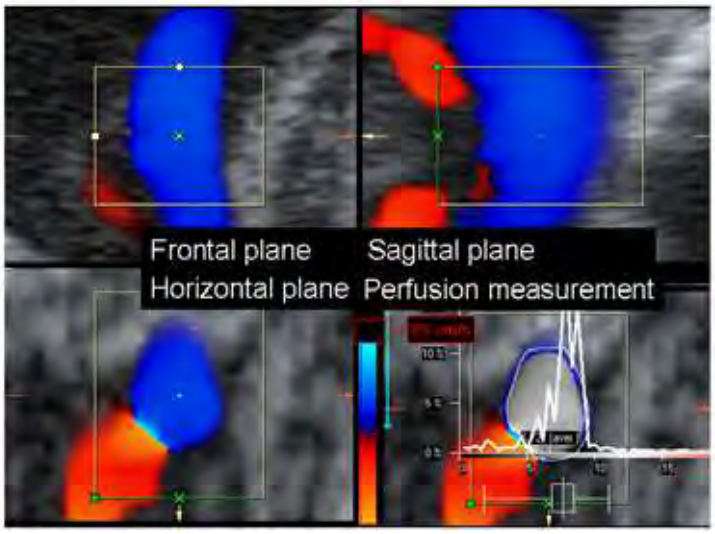

Fig. 26. Example of a spatially angle corrected fetal volume flow measurement in the umbilical vein. A 3D-dataset is shown displaying three perpendicular imaging planes. The horizontal plane is used for DTPM (right lower quarter): False color map of the venous flow. From these data the flow volume is directly calculated by the PixelFlux-software

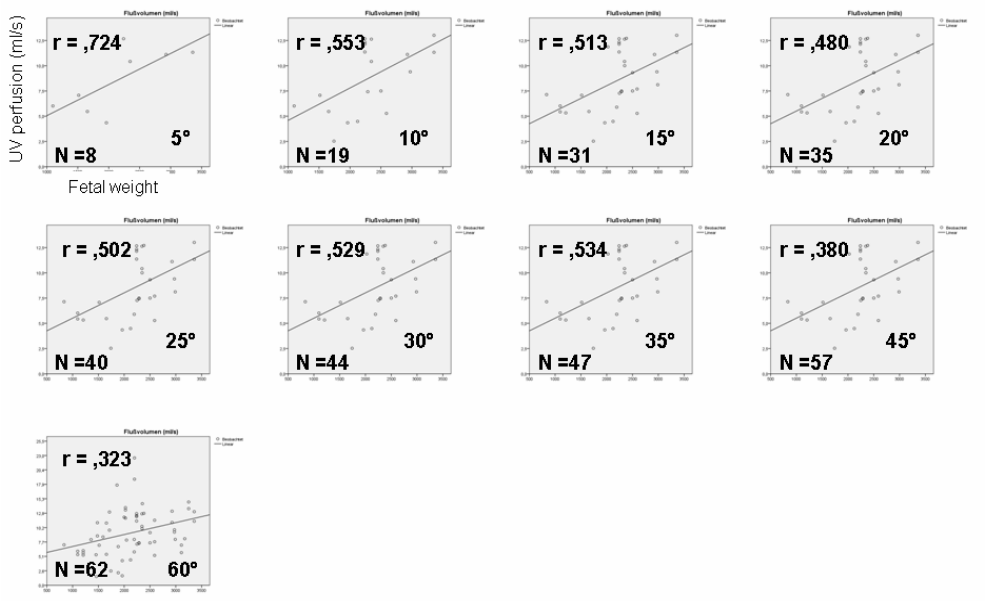

Fig. 27. DTPM reveals a significant correlation of fetal volume flow and fetal weight. This correlation improves significantly with reduction of the spatial angle (specified within each diagram)

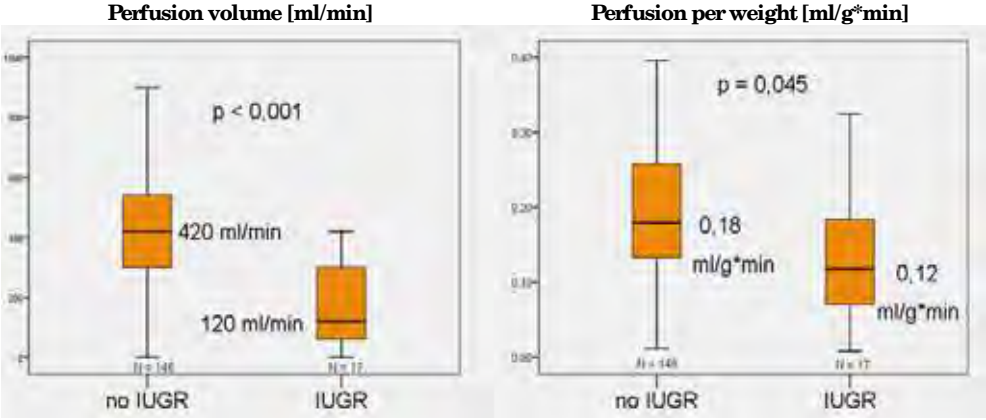

Fig. 28. A significant reduction of fetal perfusion per gram fetal weight could be demonstrated by DTPM in fetuses with intrauterine growth retardation (IUGR) compared to normal children

To achieve best results the umbilical cord should be recorded in a 3D-colour Doppler sweep so that the vein is running in a steep angle towards the transducer. The data block is then scanned with a 3D-manipulation software (4Dview, GE) by parallel shifts of the frontal and sagittal images to search for a transsection of the UV in the horizontal plane, which is clearly cut, has distinct borders and is not taken from a segment of the vein with strong bending (fig.

26). In this plane both velocity as displayed by a certain colour hue and shape of the vessel's cross section are distorted by a stretching factor which is equal to the cosine of the spatial angle between vessel's course and the ultrasound waves' propagation line – the so called Doppler angle α. While the area is stretched by the reciprocal of cos α the velocity is virtually reduced by the by multiplication with cos α (proof see chapter 18. Addendum on page 27). Therefore, direct calculation of true flow volumes directly from measurements within the horizontal plane is possible. This is accomplished by the DTPM software PixelFlux. The reproducibility of these measurements in a clinical situation lies in the range of around 6 % and less, if exclusively data with steep spatial Doppler angles are allowed (own unpublished data).

A significant correlation of such volume flow measurements with fetal weight could be demonstrated (fig. 27) [41] that was the better the steeper the spatial angle could be arranged. Moreover, in a preliminary study a significantly diminished flow volume per gram fetal weight could be shown (fig. 28).

16. Miscellaneous

In animal models, numerous reports underscore the interest in DTPM, especially in the field of theriogenology. The functional status of the bovine ovary (evaluated by the plasma progesterone concentration during the oestrous cycle) could be better correlated to luteal blood flow than to luteal size ([39]. The course of luteal perfusion mirrored progesterone levels much more readily than the sheer size of the corpus luteum. The perfusion measurement of the ovary in cows could differentiate between varying courses of progesterone plasma levels [41]. Perfusion measurements of the follicle, the corpus luteum and the uterus yielded differing responses in cows undergoing synchronization of ovulation [42]. They helped to explain the effect of human chorionic gonadotropin onto the progesterone synthesis and luteal blood flow [43], were useful in monitoring luteal perfusion during pregnancy and after embryonic loss [44] and could be used to tackle a variety of interactions between hormone production, luteal blood flow and gene expressions in luteal tissue [45].

In another study on the regulation of follicular development in cows DTPM demonstrated significant correlation with the follicular NO concentration and Estradiol (E2)/Progesterone (P4) ratio in those follicles, which developed to the dominant follicle in the ovary [46].

In milking of cows, a significant increase of utter perfusion was measured after 15 – 30 min to settle down after 45 min to the basic, pre-milking values. These basic values but differed considerably among the animals [47].

DTPM helped to describe the periurethral vascularity in women [3], was used to estimate the effect of periprostatic vascularity on the effect of HIFU in prostate cancer [48], proved to be more sensitive than computer assisted B-mode image analysis in testicular torsion and showed clearly a perfusion decline within two hours after torsion [49].

Perfusion measurements of the basal ganglia using DTPM in neonates with hypoxic ischemic encephalopathy (HIE) treated with therapeutic hypothermia demonstrated significantly higher perfusion values in neonates that died compared to the survivors (0.226± 0.221 cm/s vs. 0.111±0.082 cm/sec; p=0.02) (fig. 29). DTPM values also were higher

in nine neonates with MRI showing moderate to severe injury (0.142±0.070 cm/s vs. 0.072±0.080 cm/s; p=0.04). DTPM opens a window to better understand reperfusion injury in HIE [49].

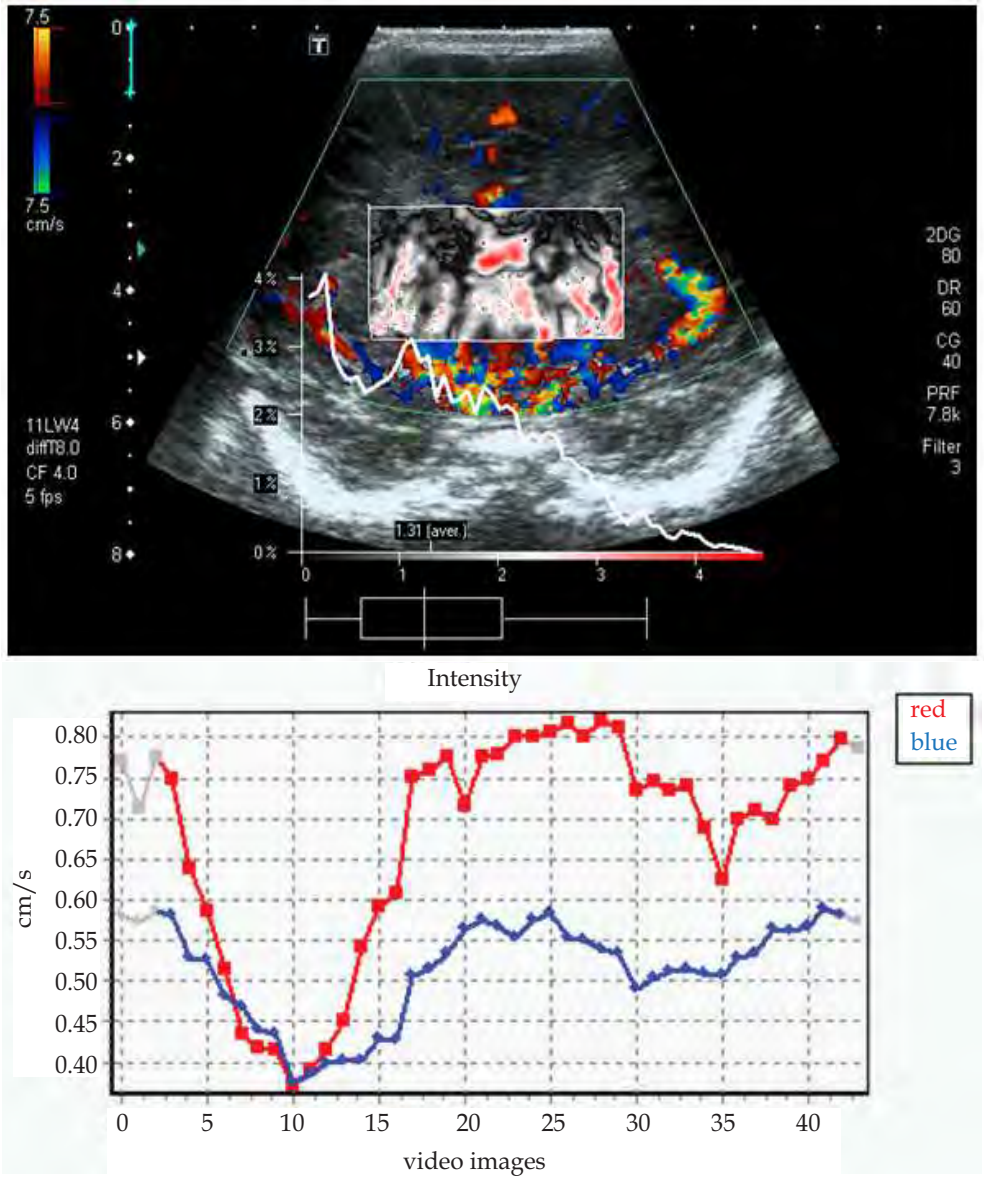

Fig. 29. Example of a DTPM of basal ganglia in a newborn. Upper part: false color map of the basal ganglia and distribution curve. Lower part: Perfusion intensity course during one examination. (Image and measurement courtesy of Dr. Ricardo Faingold, Montreal)

17. Summary

DTPM offers a universally applicable approach to tissue perfusion measurement as far as sonographic depiction of tissues is possible. So far, inaccessible details of perfusion intensity, perfusion distribution, perfusion gradients within a certain vasculature open a widow to an individualized evaluation of the specific pathophysiological situation. Treatment efforts can be evaluated according to their effect on perfusion. Besides these intrinsic advantages, the technique requires no additional hardware, is non-invasive, needs no specific preparation of the patient and thus can be recommended for a broad array of clinical applications.

18. Addendum: Proof of the congruence of the true flow volume and the flow volume calculated from the horizontally projected velocity and area of any vessel

True volume flow calculation becomes feasible with three-dimensional colour Doppler data.

True volume flow calculation means the exact calculation of the blood flow volume running through any vessel which is cut perpendicularly.

Our method of true volume perfusion measurement in vessels cut by the horizontal plane in any spatial angle is described and proven below.

The spatial angle, which is the angle between the vessel and the ultrasound propagation line, influences simultaneously the stretching of the shape of the vessels' cross-sectional area as well as the change of the recorded flow velocity. Figure 30 displays the respective situation schematically. The blood vessel (yellow rectangle) runs with the Doppler angle α towards the ultrasound propagation line (blue line). The horizontal imaging plane, which is calculated during the three-dimensional ultrasound imaging, cuts the vessel. Line a' is the stretched vessel's diameter as it can be seen in the horizontal plane. Vector b is the original flow velocity within the vessel. Due to the Doppler angle α the recorded velocity is displayed with the value for vector b'. This means, the color hue of b' is darker, representing a lower velocity as if vector b would be displayed in its appropriate color. This is the well known Doppler effect $\left(fd = 2 * fo * v_t / c * \cos\alpha\right)$, which reduces the recorded velocity according to the cosine of α.

The real flow volume per time (V) of a circular vessel is calculated as

$$V/t = \pi/4 * a * a * \vec{b} \tag{1}$$

// $\pi/4 * a * a$ calculates the circular area of the perpendicularly cut vessel

The oblique transsection of a round vessel, a vessel running not perpendicularly towards the horizontal plane, results in stretching of the circular vessel's round cross-sectional area in the direction of the projection vector of the spatial angle of this vessel with the horizontal plane. This results in an ellipse which longer axis is represented by a', the stretched projection of a onto the horizontal plane (Fig. 30). The shorter axis is equal to the original diameter of the vessel. It remains unstretched since no angulation occurs.

It is therefore possible to consider the change of diameter a towards a', the long axis of the ellipse in order to describe the change of the horizontally projected cross-sectional area of

the vessel. The change of the circular area towards the elliptical area is thus equal to the stretching factor a'/a.

The other relevant change is the reduction of the displayed flow velocity compared to the original velocity b, the reduction factor is b'/b.

It is now claimed, that the flow volume V′ per time, which is passing through the horizontal plane in direction of the vessel, calculated by multiplying the elliptical area $(A = \pi/4 * a * a')$ with the flow velocity b′ of the vessel in the horizontal plane is equal to V per time, the flow volume passing through the perpendicularly cut vessel in the same time.

Claim:

$$V' = V \tag{2}$$

Proof:

$$V'/t = \pi/4 * a * a' * \vec{b}' \tag{3}$$

// $\pi/4 * a * a'$ calculates the elliptic area of the horizontally cut vessel
a: short axis of the ellipse
a': long axis of the ellipse

The depiction of the horizontally cut vessel shows the velocity $\vec{b}'$ and a stretched vessel diameter a'.

The triangle ABC is rectangular, since the blood vessel is a rectangle, a perpendicularly cut circular straight vessel. Doppler angle α is complemented to 90° by the angles DAB and FAC since the ultrasound propagation line (blue line running through F) runs perpendicular to the transducer's surface and thus the horizontal imaging plane. Both angles are thus equal and named β. Angles FAC and CAB add to 90° since again the ultrasound propagation line runs perpendicular to the horizontal imaging plane. Thus angle CAB is α again, the Doppler angle.

$$a' = a/\cos\alpha \tag{4}$$

$$\vec{b}' = \vec{b} * \cos\alpha \tag{5}$$

by inserting (3) and (4) into (2) results (5)

$$V' = \pi/4 * a * a/\cos\alpha * \vec{b} * \cos\alpha \tag{6}$$

which is (6) after cancelling cos α

$$V' = \pi/4 * a * a * \vec{b} = V \text{ see (1)} \tag{7}$$

thus

$$V' = V \tag{8}$$

q.e.d.

This means, that it is possible to calculate the true flow volume of all vessels cut horizontally from the depicted flow velocities[1] and the pixelwise calculated cross-sectional areas[2] directly, thus compensating any spatial angle. Both measurements ([1] and [2]), are carried out automatically by the PixelFlux-software, which delivers thus true flow volumes of all vessels in any tissue section cut horizontally in three-dimensional color Doppler ultrasound data.

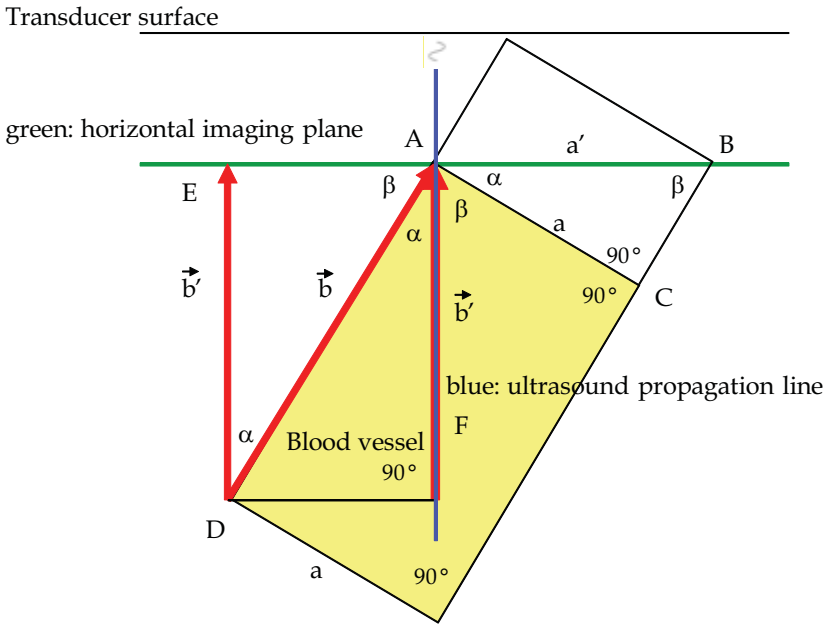

Fig. 30. Schematical depiction of a horizontally cut vessel in a 3D-color Doppler sonographic dataset

19. References

[1] Chameleon-Software, *PixelFlux*. 2011. http://www.chameleon-software.de/index-de.html.

[2] Scholbach T., DiMartino E., Scholbach J. "Dynamic color Doppler sonographic tissue perfusion measurement in tumors" in Cancer imaging (2 volumes) (Elsevier/ Academic Press, 2008) ed by M.A. Hayat

[3] Scholbach, T. and J. Scholbach, Can We Measure Renal Tissue Perfusion by Ultrasound? *Journal of Medical Ultrasound*, 2009. 17(1): p. 9-16.

[4] Wieczorek, A., et al., The assessment of normal female urethral vascularity with Color Doppler endovaginal ultrasonography: preliminary report. *Pelviperineology* 2009. 28: p. 59-61.

[5] Masulli, M., et al., Measurement of the intrarenal arterial resistance index for the identification and prediction of diabetic nephropathy. *Nutr Metab Cardiovasc Dis*, 2009. 19(5): p. 358-64.

[6] Radermacher, J., et al., The renal arterial resistance index and renal allograft survival. *N Engl JMed*, 2003. 349(2): p. 115-24.

[7] Ozelsancak, R., et al., Relationship between renal resistive index and inflammation in untreated hypertensive patients. *Int Heart J*, 2009. 50(6): p. 753-61.
[8] Crutchley, T.A., et al., Clinical utility of the resistive index in atherosclerotic renovascular disease. *JVasc Surg*, 2009. 49(1): p. 148-55, 155 e1-3; discussion 155.
[9] Soria Galvez, F., et al., [Usefulness of renal resistive index in the diagnosis and evolution of the obstructive uropathy. Experimental study]. *Actas Urol Esp*, 2007. 31(1): p. 38-42.
[10] Onur, M.R., et al., Role of resistive index in renal colic. *Urol Res*, 2007. 35(6): p. 307-12.
[11] Krumme, B. and M. Hollenbeck, Doppler sonography in renal artery stenosis--does the Resistive Index predict the success of intervention? *Nephrol Dial Transplant*, 2007. 22(3): p. 692-6.
[12] Braun, B., Focal liver processes: "better is the enemy of good": CEUS in the fast lane. *Ultraschall Med*, 2009. 30(4): p. 329-32.
[13] D'Onofrio, M., et al., Focal liver lesions: sinusoidal phase of CEUS. *Abdom Imaging*, 2006. 31(5): p. 529-36.
[14] Trojan, J., et al., Contrast-enhanced ultrasound in the diagnosis of malignant mesenchymal liver tumors. *JClin Ultrasound*. 38(5): p. 227-31.
[15] Dietrich, C.F., et al., Pitfalls and artefacts using contrast enhanced ultrasound. *Z Gastroenterol*. 49(3): p. 350-6.
[16] Hocke, M., et al., Contrast-enhanced endoscopic ultrasound in discrimination between benign and malignant mediastinal and abdominal lymph nodes. *J Cancer Res Clin* Oncol, 2008. 134(4): p. 473-80.
[17] O'Connor, P.M., Renal oxygen delivery: matching delivery to metabolic demand. *Clin Exp Pharmacol Physiol*, 2006. 33(10): p. 961-7.
[18] Wolff, C.B., Normal cardiac output, oxygen delivery and oxygen extraction. *Adv Exp Med Biol*, 2007. 599: p. 169 - 82.
[19] Ikee, R., et al., Correlation between the resistive index by Doppler ultrasound and kidney function and histology. *Am JKidney Dis*, 2005. 46(4): p. 603-9.
[20] Scholbach, T., I. Dimos, and J. Scholbach, A new method of color Doppler perfusion measurement via dynamic sonographic signal quantification in renal parenchyma. *Nephron Physiol*, 2004. 96(4): p. p99-104.
[21] Scholbach, T., From the nutcracker-phenomenon of the left renal vein to the midline congestion syndrome as a cause of migraine, headache, back and abdominal pain and functional disorders of pelvic organs. *Med Hypotheses*, 2007. 68(6): p. 1318-27.
[22] Scholbach, T., et al., Correlation of histopathology and dynamic tissue perfusion measurement (DTPM) in renal transplants. http://www.postersessiononline.com/173580348_eu/congresos/48era/aula/poster_43104.pdf, 2011(ERA-EDTA Congress 2011).
[23] Scholbach, T., E. Girelli, and J. Scholbach, Dynamic tissue perfusion measurement: a novel tool in follow-up of renal transplants. *Transplantation*, 2005. 79(12): p. 1711-6.
[24] Scholbach, T., E. Girelli, and J. Scholbach, Tissue pulsatility index: a new parameter to evaluate renal transplant perfusion. *Transplantatio*n, 2006. 81(5): p. 751-5.
[25] Marti, E., et al., Donor effect on cortical perfusion intensity in renal allograft recipients: a paired kidney analysis. *Am JNephrol*. 33(6): p. 530-6.
[26] Scholbach, T., I. Herrero, and J. Scholbach, Dynamic color Doppler sonography of intestinal wall in patients with Crohn disease compared with healthy subjects. *JPediatr Gastroenterol Nutr*, 2004. 39(5): p. 524-8.

[27] Scholbach, T., J. Hormann, and J. Scholbach, Dynamic tissue perfusion measurement of the intestinal wall - correlation to histology in ulcerative colitis. *Journal of Medical Ultrasound* 2010. 18(2): p. 62-70.

[28] Cassia, G., et al., Hypoxic ischemic injury: intestinal appearances and perfusion measurements using ultrasound and dynamic color Doppler sonography in neonates submitted to therapeutic hypothermia. *Pediatr Radiol*, 2011. 41(Suppl 1): p. S250-S310 FN-9.

[29] Schäfer, M., Dynamische farbduplexsonografische Gewebeperfusionsmessung an cervicalen Lymphknoten (Dissertationsschrift). Katalog der Deutschen Nationalbibliothek, 2009: p. http://d-nb.info/1002591465

[30] Oktar, S., et al., Quantitative Color Doppler Evaluation of Perfusion in the Differential Diagnosis of Benign and Malignant Thyroid Nodules Using a Dedicated Software Program. http://rsna2007.rsna.org/rsna2007/v2007/conference/event_display.cfm?am_id=3&em_id=5008569, 2007.

[31] Vaupel, P., et al., Hypoxia in breast cancer: role of blood flow, oxygen diffusion distances, and anemia in the development of oxygen depletion. *Adv Exp Med Biol*, 2005. 566: p. 333-42.

[32] Vaupel, P. and A. Mayer, Hypoxia and anemia: effects on tumor biology and treatment resistance. *Transfus Clin Biol*, 2005. 12(1): p. 5-10.

[33] Vaupel, P., Prognostic potential of the pre-therapeutic tumor oxygenation status. *Adv Exp Med Biol*, 2009. 645: p. 241-6.

[34] Scholbach, T., et al., New method of dynamic color doppler signal quantification in metastatic lymph nodes compared to direct polarographic measurements of tissue oxygenation. *Int JCancer*, 2005. 114(6): p. 957-62.

[35] Ebrashy, A., et al., Middle cerebral/umbilical artery resistance index ratio as sensitive parameter for fetal well-being and neonatal outcome in patients with preeclampsia: case-control study. *Croat Med J*, 2005. 46(5): p. 821-5.

[36] Figueras, F., et al., Umbilical artery pulsatility index: reliability at different sampling sites. *JPerinat Med*, 2006. 34(5): p. 409-13.

[37] Eik-Nes, S.H., K. Marsal, and K. Kristoffersen, Methodology and basic problems related to blood flow studies in the human fetus. *Ultrasound Med Biol*, 1984. 10(3): p. 329-37.

[38] Gill, R.W., et al., Umbilical venous flow in normal and complicated pregnancy. *Ultrasound Med Biol*, 1984. 10(3): p. 349-63.

[39] Erskine, R.L. and J.W. Ritchie, Quantitative measurement of fetal blood flow using Doppler ultrasound. *Br JObstet Gynaecol*, 1985. 92(6): p. 600-4.

[40] Scholbach T., Stolle J., Scholbach J. Three dimensional volumetric spatially angle corrected pixelwise fetal flow volume measurement. *Eur J Ultrasound* (2011 accepted for publication)

[41] Herzog, K., et al., Luteal blood flow is a more appropriate indicator for luteal function during the bovine estrous cycle than luteal size. *Theriogenology*. 73(5): p. 691-7.

[42] Luttgenau, J., et al., Low plasma progesterone concentrations are accompanied by reduced luteal blood flow and increased size of the dominant follicle in dairy cows. *Theriogenology*. 76(1): p. 12-22.

[43] Bollwein, H., et al., Effects of a shortened preovulatory follicular phase on genital blood flow and endometrial hormone receptor concentrations in Holstein-Friesian cows. *Theriogenology*. 73(2): p. 242-9.
[44] Beindorff, N., et al., Effects of human chorionic gonadotropin on luteal blood flow and progesterone secretion in cows and in vitro-microdialyzed corpora lutea. *Theriogenology*, 2009. 72(4): p. 528-34.
[45] Herzog, K., et al., Luteal blood flow increases during the first three weeks of pregnancy in lactating dairy cows. *Theriogenology*. 75(3): p. 549-54.
[46] Luttgenau, J., et al., Plasma progesterone concentrations in the mid-luteal phase are dependent on luteal size, but independent of luteal blood flow and gene expression in lactating dairy cows. *Anim Reprod Sci*. 125(1-4): p. 20-9.
[47] Pancarcı, Ş.M., et al., Changes in follicular blood flow and nitric oxide levels in follicular fluid during follicular deviation in cows. *Animal Reproduction Science*, 2011. 123 (3-4): p. 149-156.
[48] Kuchler, K., et al., Measuring the blood flow of teats of dairy cows by using Color-Angiography. *Reproduction in Domestic Animals*, 2011. 46(S1): p. 25 http://onlinelibrary.wiley.com/doi/10.1111/j.1439-0531.2011.01755.x/pdf.
[49] Rouviere, O., et al., Can color doppler predict the uniformity of HIFU-induced prostate tissue destruction? *Prostate*. 2004 60(4): p. 289-97.
[50] Aslan, M., et al., Quantitative Analysis of Ultrasonographic Textures with Software in Experimental Testicular Torsion. *Turkish Association of Pediatric Surgeons*, 2011. http://www.tccd.org.tr/abstract/yayinlanan_bildiri.php?bid=77.
[51] Faingold, R., et al., Cerebral perfusion measurements using dynamic color Doppler sonography in neonates with hypoxic ischemic encephalopathy (HIE) treated with therapeutic hypothermia. *Pediatr Radiol* 2011. 41(Suppl 1): p. S250-S310 NE2-3.

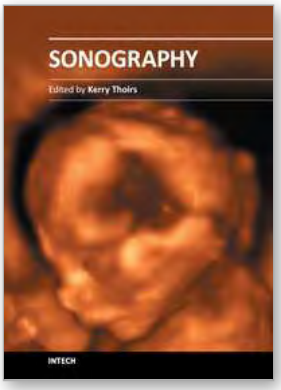

Sonography
Edited by Dr. Kerry Thoirs

ISBN 978-953-307-947-9
Hard cover, 346 pages
Publisher InTech
Published online 03, February, 2012
Published in print edition February, 2012

Medical sonography is a medical imaging modality used across many medical disciplines. Its use is growing, probably due to its relative low cost and easy accessibility. There are now many high quality ultrasound imaging systems available that are easily transportable, making it a diagnostic tool amenable for bedside and office scanning. This book includes applications of sonography that can be used across a number of medical disciplines including radiology, thoracic medicine, urology, rheumatology, obstetrics and fetal medicine and neurology. The book revisits established applications in medical sonography such as biliary, testicular and breast sonography and sonography in early pregnancy, and also outlines some interesting new and advanced applications of sonography.

INTECH
open science | open minds

InTech Europe
University Campus STeP Ri
Slavka Krautzeka 83/A
51000 Rijeka, Croatia
Phone: +385 (51) 770 447
Fax: +385 (51) 686 166
www.intechopen.com

InTech China
Unit 405, Office Block, Hotel Equatorial Shanghai
No.65, Yan An Road (West), Shanghai, 200040, China
中国上海市延安西路65号上海国际贵都大饭店办公楼405单元
Phone: +86-21-62489820
Fax: +86-21-62489821

Chapter 5

Ultrasound-Guided Peripheral Nerve Block Anesthesia with Emphasis on the Interscalene Approach to Brachial Plexus Blockade

James C. Krakowski and Steven L. Orebaugh

Additional information is available at the end of the chapter

http://dx.doi.org/10.5772/56645

1. Introduction

Epidemiologic data has revealed a progressive rise in the aggregate number of patient surgical visits with an increasing number occurring within the ambulatory setting [1]. Accompanying this rise has been a growing need for adequate, efficient patient anesthesia and analgesia [2]. With a significant proportion of procedures involving focal orthopedic interventions of the knee and shoulder, peripheral nerve blockade has become an increasing trend in anesthetic practice while neuraxial blockade use has decreased [2]. The popularity of peripheral nerve blockade may stem from its demonstrated effectiveness with studies showing improved analgesia and recovery during the postoperative period versus opioids [3] or general anesthetic [4]. In this chapter, we will review ultrasonography and its application to a commonly employed peripheral nerve block, namely, the interscalene block.

2. Ultrasound guidance for peripheral nerve blockade

2.1. A brief history

The first published account of ultrasound use with peripheral nerve blockade occurred in 1978 when Doppler sonography assisted blood flow detection during supraclavicular brachial plexus block [5]. Although the initial technology did not allow for direct nerve visualization, this was later rectified in 1994, when advancements in technology allowed the first documented use of ultrasound to visually facilitate supraclavicular brachial plexus block [5]. Since this time, ultrasound use for regional anesthesia has shown increasing popularity, and ultrasound

technology has mirrored practitioner demand with machines possessing greater portability, simplicity, and image resolution [5]. Literature regarding the utility of ultrasound for a variety of peripheral nerve blocks continues to emerge.

2.2. Advantages

The rising popularity of ultrasound guidance for peripheral nerve blockade (PNB) stems from numerous described advantages supporting its use [6], [7], [5]. Perhaps the principal benefit of ultrasound resides in the technology's inherent ability to directly visualize peripheral nerves and tissue planes in real-time, allowing for optimal injectate or catheter placement with the ultimate goal of optimizing neural blockade [7]. Today's ultrasound machines are equipped with high-frequency probes capable of imaging the majority of nerves necessary for a wide array of regional blocks, and also their oblique course as they traverse the body [7]. This imaging modality permits the identification of relatively diminutive 2 mm diameter digital nerves [7], as well as differentiation of complex neurovascular nuances as found within the brachial plexus [8]. Additional benefit is conveyed in the ability to reposition one's needle in assessing for adequate local anesthetic spread, fascial plane movement, or lack thereof with intravascular injection [7]. The idea of preemptively scanning patient anatomy for neurovascular variations or abnormalities has been suggested as a means of improving patient safety by preventing block complication [9].

A number of objective evaluations have supported the efficacy of ultrasound guidance during PNB. When compared with performance via peripheral nerve stimulation (PNS), PNB executed using ultrasound guidance has been shown to require less time to perform, possesses more rapid onset and longer duration of anesthesia, and is more likely to be successful (less block failure) [6]. The use of ultrasound rather than PNS has also been shown to decrease the risk of vascular puncture [6], [10], and demonstrate improved quality of sensory block [11]. The use of ultrasonography does not exclude the use of PNS for PNB, and the combination for brachial plexus block was shown to have decreased risk of central nervous system toxicity secondary to local anesthetic versus a PNS-landmark technique [12]. Another study demonstrated high rates of success with axillary brachial plexus block using sonography regardless of concurrent PNS use [13]. Compared with PNS for femoral nerve block, ultrasound guidance also provides a reduction in the minimum effective anesthetic volume (MEAV50) [14], and has allowed reduced dosing for many blocks, with a potential impact on local anesthetic systemic toxicity and therefore patient safety [15]. Lastly, given the steady rise in yearly surgical procedures [1], findings such as decreased time to perform PNB [6], [7] and recent demonstration of cost-effectiveness in clinical practice [5] will likely support the role of ultrasound guidance in regional anesthesia's future.

2.3. Disadvantages

Despite many reported advantages to ultrasound guidance during PNB, several barriers to implementation and training have been described. One such limitation arises from peripheral nerve anatomical variation leading to difficulty in regional pattern recognition [16]. Difficulty to trainees may arise from the necessary knowledge of cross-sectional anatomy, terminology,

appropriate local anesthetic spread, as well as an understanding of novel probe operating mechanics and regular needle tip visualization [7], [17], [18]. As a result, images may appear ambiguous to the novice operator [19], and identifying the intricate neurovascular anatomy of a common PNB structure as the brachial plexus may prove formidable [20]. Inexperience leading to inability to recognize common on-screen artifacts stemming from image processing may also skew interpretation [21]. In contrast to a definitive motor response end-point elicited with nerve stimulator, the optimal pattern of local anesthetic deposition and distribution continues to be investigated [22], [18].

Ultrasonography may also prove challenging as a result of current technological limitations. For example, discriminating neuronal tissue and its epineurium from that of connective tissue or tendons may prove difficult due to the similar hyperechoicity, or echotexture [7], [20]. Furthermore, ultrasound imaging has been shown to underrepresent the total number of neuronal fascicles as compared to light microscopy, and the possibility of intraneural injection (a topic of controversy with respect to morbidity) exists [23], [20].

3. The interscalene brachial plexus block

3.1. Block description

Upper extremity peripheral nerve blocks account for the majority of performed regional anesthesia techniques in most anesthesia practices [24]. Of the upper extremity PNBs, the interscalene block (ISB) is the most commonly applied block for patients undergoing shoulder surgery [25], [26], [8], imparting both anesthesia and analgesia with adequate coverage of the shoulder, lateral arm, and lateral forearm [27]. The ISB was first described in 1970 by Winnie, who noted based on anatomic and radiographic imaging that the interscalene space allowed for a novel, percutaneous approach to anesthetizing the proximal brachial plexus [28]. This approach allowed for brachial plexus anesthesia of similar quality to that of thoracic epidural anesthesia [28]. Compared to the previously described axillary and subclavian approaches prior to this time, the ISB was quickly favored for its ease of execution due to readily palpable landmarks in patients with large body habitus, no requirement for unique upper extremity positioning, and ability to readily repeat the block during protracted surgical procedures [28]. Both single-shot and continuous catheter placement have been successfully performed with ISB via landmark-paresthesia, nerve stimulator, or ultrasound-guided technique [8].

3.2. Anatomy

With the exception of the supraclavicular nerves, the brachial plexus is responsible for all motor and sensory innervation to the shoulder area [8]. The brachial plexus is an intricate neuronal network originating as ventral rami from cervical nerve roots, C5-8, and initial thoracic nerve root, T1 [24]. Together, these roots within the neck further subdivide into trunks, divisions, cords, and, ultimately, peripheral branches traveling distally into the upper arm [29]. After exiting the vertebral column, the roots become trunks as they traverse through the apposition of the anterior and middle scalene muscles, or interscalene groove [24]. Beyond the distal first

rib, the trunks divide into divisions. At the distal clavicle and latter portion of the axillary artery, the divisions combine to form cords, which further subdivide into terminal branches at the level of the humerus [24].

Winnie described three anatomical spaces comprising the fascial sheath-enveloped area, cradling the neurovasculature of the brachial plexus along its course from the proximal, cervical vertebral bodies distally toward the axilla [28]. These regions included the axillary, subclavian, and interscalene spaces [28]. The interscalene space describes the contiguous area enveloped posteriorly by the fascial sheath covering of the middle scalene muscle and anteriorly by that of the anterior scalene fascia [28]. The interscalene space was noted to be continuous with both the axillary and subclavian spaces, thereby allowing appropriate peripheral nerve blockade introduction at this site [28].

In order to provide effective analgesia for shoulder surgery, one must anesthetize the nerves supplying all of the muscle, ligamentous, and osseous tissues of the shoulder joint and surrounding area [8]. Properly performed interscalene blockade provides anesthesia to the superior and middle trunks of the brachial plexus with C5-7 coverage, while also blocking the supraclavicular nerves arising from C3-4 [26]. The C3-4 blockade of the superficial cervical plexus is both fortunate and necessary as this innervation lies outside of the brachial plexus while supplying cutaneous sensation to the rostral shoulder [24].

3.3. Indications

Since its initial description, the interscalene block has been met with widespread acceptance, demonstrating effective [30], [31], [26], [8] and reliable perioperative analgesia for shoulder surgery [27], [26]. The interscalene block is suitable for a wide array of surgical procedures involving the shoulder with coverage including the shoulder joint, proximal humerus, as well as distal clavicle [8].

ISB offers several advantages afforded by regional anesthesia [8]. ISB may be used as an adjuvant to general anesthesia or as solitary anesthetic technique for shoulder surgery [8]. As a primary anesthetic, ISB may thereby reduce the risk of adverse events associated with general anesthesia, including time to ambulation secondary to impaired motor function, postoperative nausea and vomiting, and prolonged length of stay [4]. ISB also allows for a reduction in opioid analgesics and their consequential ill-effects [27], [8]. Additionally, ISB may prove more cost-effective as solitary anesthetic when compared to general anesthesia [8].

Although ISB has proved well-suited for shoulder surgery, it lacks coverage of C8 and T1 distribution, and so it has not been routinely used for surgeries involving the hand or elbow without supplying additional peripheral nerve block technique [30].

3.4. Landmark and nerve stimulator techniques

Prior to the advent of ultrasound imaging guidance, the primary methods for performing brachial plexus blockade included landmark and peripheral nerve stimulator (PNS) techniques [32], [33]. Both methods of nerve localization involve non-visualization of internal

http://dx.doi.org/10.5772/56645

structures, and instead rely on either paresthesias or muscle twitch responses for landmark and PNS, respectively [32]. Originally described by Winnie in 1970, the ISB landmark technique entails localizing the interscalene groove lateral to the cricoid cartilage at approximate C6 level, needle advancement until elicitation of paresthesias along the shoulder and upper arm distribution, and completion with deposition of local anesthetic [28].

After its introduction in performing regional anesthesia, PNS later overcame landmark/paresthesia technique as the method of choice for performing ISB [6], [34]. A common method for performing PNS guidance involves applying a current, ranging from 0.2 to 0.5 mA, at a frequency of 2 Hz while observing for muscle twitch with needle advancement [35]. Specifically, a contraction of the biceps or triceps may be appreciated, corresponding to cervical nerve stimulation at levels C5-6 and C6-8, respectively, at which point local anesthetic is deposited [35]. Of note, PNS may hold limited effectiveness in diabetic patients complicated by neuropathy, as motor response may not be elicited despite application of a standard stimulus [36]. Despite a theoretical advantage in determining needle tip proximity to neuronal tissue with greater precision using PNS as compared to paresthesia elicitation, both techniques have shown similar efficacy for peripheral nerve blockade [24]. In addition, ultrasound studies have revealed that the 0.2 to 0.5 mA range of current has limitations in predicting the accuracy of needle tip placement [37].

3.5. Ultrasonography for interscalene block

In contrast to prior methods of nerve localization, ultrasound guidance provides visualization of the block needle, neurovascular structures and their anatomical course, and the spread of local anesthetic injectate in real-time [38], [7], [5], [24], [39], [8]. Ultrasound guidance has been implemented both with and without concomitant nerve stimulator for the performance of regional anesthesia [10], although no added benefit has been proven with the addition of PNS [24], [40].

Typical sonoanatomy seen while performing the interscalene block has been described. Application of an ultrasound probe in the vicinity of interscalene groove allows for direct visualization of the C5-7 nerve roots exiting their corresponding intervertebral foramina and subsequently passing between the anterior and middle scalene muscles [20]. One may reliably differentiate the seventh cervical nerve root, as the C7 transverse process possesses no anterior tubercle [24]. Elements of the brachial plexus appear characteristically as a cluster of hypoechoic, or comparably dark, bodies on ultrasound imaging, while surrounding fascial layers appear hyperechoic, or comparably white [20]. Of note, numerous variations of the brachial plexus have been characterized, and these subtle deviations may be appreciated with ultrasonography [24].

Reliable brachial plexus blockade via ISB and ultrasonography has been described using a consistent method [38], [41] (Table 1). Patients undergoing ISB should have routine monitoring and supplemental oxygen in place prior to beginning the PNB, with low dose anxiolytic premedication administered when appropriate. Head positioning away from the intended block site may facilitate probe placement (Figure 1). Antiseptic technique including cleansing solution, drape, transducer dressing, gel, and standard practitioner barriers should be

implemented. In order to assist avoidance of initial vascular trauma or injection, the subclavian artery is first visualized in cross-sectional view within the supraclavicular region. Color Doppler mode may assist in identifying additional vasculature surrounding the plexus [9]; [42]. Translation of the transducer probe medially reveals the characteristic hypoechoic cluster of brachial plexus fascicles located between the anterior and middle scalene muscle bellies [38] (Figure 2).

Figure 1. Typical ultrasound probe placement on a patient's neck while performing the interscalene block. Note positioning of the patient's head to the contralateral side of the intended nerve block may facilitate ultrasound probe placement and visualization of brachial plexus anatomy.

Subcutaneous local anesthetic is often administered for patient comfort prior to block needle insertion. Optimally, the entire length of block needle is maintained on-screen during advancement, with particular emphasis on visualizing its tip [7] (Figure 3).

Direct needle tip visualization in relation to neuronal structures allows for repositioning prior to injection while also permitting monitoring of live local anesthetic spread within the interscalene groove [30] (Figure 4). The desired volume of local anesthetic is deposited in 5 cc or less increments following aspiration with each injection [15].

The block needle may be equipped with a PNS for further confirmation of appropriate plexus proximity before deposition of local anesthetic [38]. For example, stimulating with settings of 0.7 to 0.8 mA for 0.1 ms at 2 Hz while approaching the plexus allows for monitoring of desired motor twitch response, which includes contraction of the ipsilateral pectoralis, deltoid, biceps, and triceps muscle groups. These responses indicate adequate proximity to the brachial plexus

http://dx.doi.org/10.5772/56645

1. Apply routine patient monitors and supplemental oxygen
2. Adjust patient bed to comfortable height for block placement
3. Position ultrasound machine with screen readily visible and probe accessible to practitioner
4. Position patient head away from intended block site to facilitate block placement (Figure 1)
5. Provide anxiolytic and/or sedative premedication as necessary
6. Verify patient monitors and vital signs
7. Choose ultrasound probe[1]
8. Prepare ultrasound probe in sterile fashion
9. Prepare patient's skin with antiseptic solution
10. Verify block needle is of appropriate type[2] and primed with selected local anesthetic[3]
11. Verify patient and procedure
12. Verify probe anatomical orientation on patient matches orientation displayed on ultrasound screen
13. Adjust ultrasound machine depth and gain parameters to enhance displayed image
14. Identify subclavian artery at the supraclavicular area
15. Identify brachial plexus lateral/dorsal to subclavian artery
16. Scan with probe to interscalene groove in order to identify optimal local anesthetic injection site (consider ultrasound Doppler function to scan for vessels at chosen injection site)
17. Warn patient of local anesthetic skin infiltration and provide skin wheel
18. Warn patient of needle insertion and insert block needle
19. Visualize block needle tip prior to advancing to desired position within interscalene groove
20. Instruct assistant to provide negative-pressure syringe aspiration to rule out intravascular needle placement
21. Warn patient of possible discomfort and instruct assistant to inject local anesthetic in small (3 – 5 ml) increments (aspirate prior to injecting each aliquot)
22. Assess local anesthetic spread on ultrasound screen for adequacy and reposition block needle if necessary
23. Remove block needle and clean patient's skin at site of insertion
24. Follow-up block adequacy via patient physical exam assessment

[1]Typical ultrasound probe selection for the performance of interscalene block includes a straight, linear array probe due to its higher operating frequencies (5 - 13 MHz), providing increased resolution at the expense of decreased penetration. This probe type facilitates superficial imaging optimal for visualizing the brachial plexus.

[2]Typical block needle selection may include a 22 gauge, beveled needle 5 cm or greater in length. Greater length may allow for superior ultrasound needle visualization due to its ability to provide a less acute angle of approach and thus increased right-angle ultrasound beam reflection.

[3]Local anesthetic choice is typically dependent on desired anesthetic duration. For example, 10 – 12 h of shoulder anesthesia may be elicited when 20 cc of ropivicaine 0.75% is administered via ultrasound-guided interscalene blockade.

Table 1. Routine clinical procedure in performance of the single shot, ultrasound-guided interscalene block

Figure 2. Ultrasound view of the interscalene region demonstrating hypoechoic nerve cross sections of the brachial plexus (N), lying between the middle scalene (MS) and anterior scalene (AS) muscle bellies.

prior to local anesthetic delivery, if consistent with appropriate deposition of local anesthetic solution in the interscalene groove as visualized with real-time ultrasound imaging [41].

Physical examination is used to evaluate for brachial plexus block success. Just as Winnie noted maximal anesthetic effect within 15 min of landmark ISB technique [28], physical examination to assess for appropriate motor and sensory block after ultrasound-guided ISB should be conducted after this timeframe. Examination may include the patient's ability to abduct the arm, assessing deltoid function; flex at the elbow, assessing biceps function; as well as discrimination of pain by prick and temperature by alcohol swab of the shoulder and arm surfaces, or C4 and C5, respectively [38], [30], [41].

http://dx.doi.org/10.5772/56645

Figure 3. Ultrasound view demonstrating typical lateral approach of a peripheral nerve block needle within the interscale groove. N: nerve cross sections of the brachial plexus; MS: middle scalene muscle belly; AS: anterior scalene muscle belly.

3.6. Efficacy of ultrasound guidance for interscalene block

The successful implementation of ultrasonography for interscalene block has been well-documented with a variety of studies citing its efficacy [6]. Regarding imaging sensitivity, Muhly et al compared ultrasound imaging with cadaveric dissections of ISB anatomy and found that ultrasound was successfully able to detect vasculature branching as well as its course closely bordering nerves of the brachial plexus [42]. Due to individual variation in the neurovasculature surrounding the brachial plexus, one may appreciate the utility of directly visualizing such discrepancies from typical anatomy that might otherwise remain undetected using prior forms of PNB guidance [42].

Several studies have examined the effect of ultrasound with respect to quality of ISB anesthesia. Kapral et al compared performance of ISB using ultrasound versus peripheral nerve stimulation in a randomized trial, finding a significantly greater motor, sensory, and extent of brachial

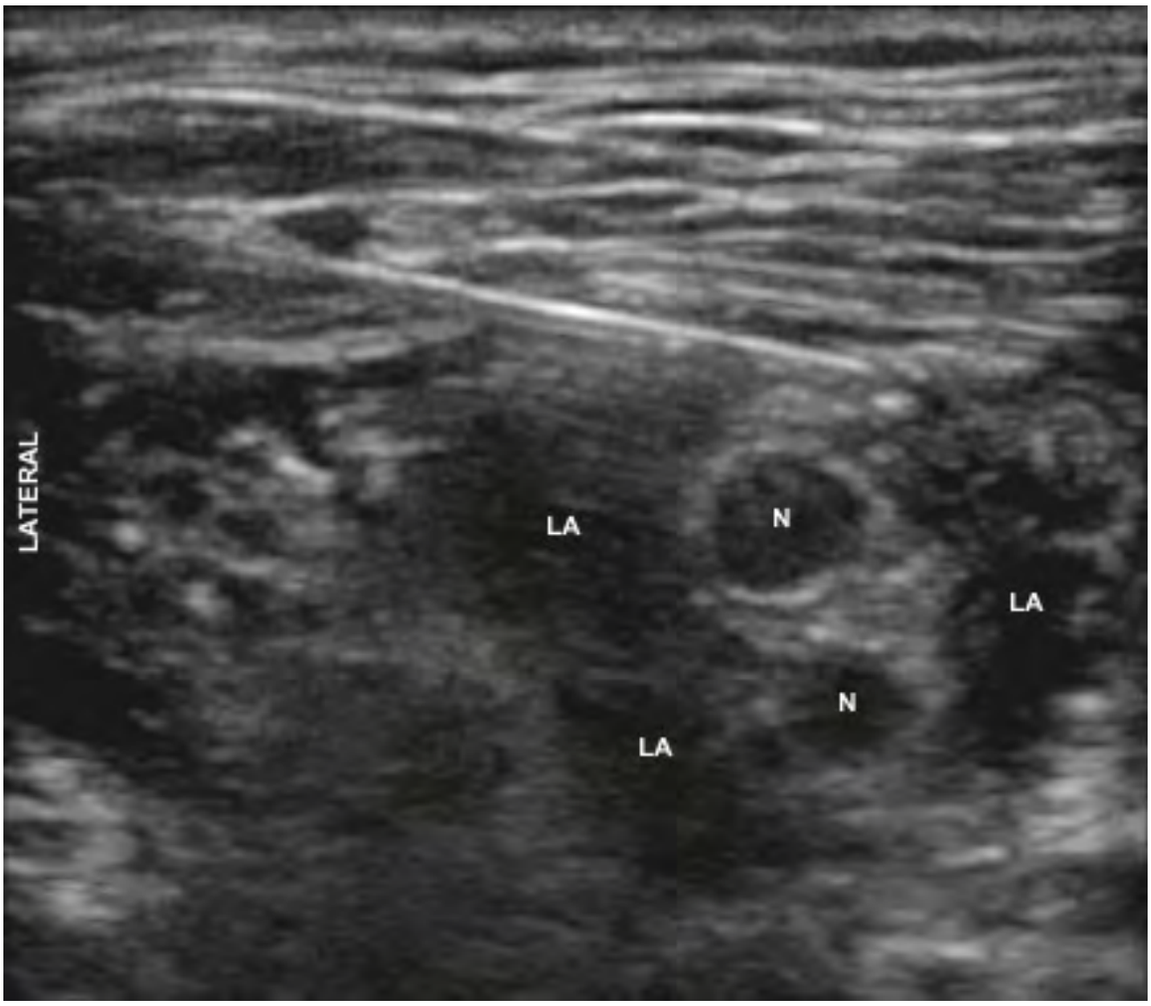

Figure 4. Ultrasound view of areas of local anesthetic (LA) volume deposition surrounding the brachial plexus at the level of the interscalene groove. Note the circumferential enhancement of the brachial plexus nerves (N) after local anesthetic deposition. The peripheral block needle is seen here as a hyperechoic linear structure positioned above the brachial plexus.

plexus blockade while using ultrasound [30]. Similarly, a randomized study by Liu et al, examining ultrasound versus nerve stimulator for ISB in randomized patients, revealed increased motor blockade assessed after five minutes as well as a decreased number of needle attempts for the ultrasound group [25]. McNaught et al also noted decreased needle attempts using ultrasound for ISB, while showing a significant decrease in the minimum effective analgesic volume (MEAV) of local anesthetic, and decreased pain 30 min postoperatively when compared to a nerve stimulator group [27]. When examining ultrasound placement versus nerve stimulator placement of ISB catheters in randomized patients, Fredrickson et al demonstrated greater effectiveness in the ultrasound group, requiring less local anesthetic boluses and tramadol use in addition to fewer needle attempts [43]. Additionally, examination of ISB performance among supervised resident trainees at a large academic center has shown a significant decrease in needle attempts, time required for block completion, and incidence of needle perforation of vasculature [44].

3.7. Revelations with ultrasound and interscalene block

Unexpected findings have been revealed when utilizing ultrasound guidance for interscalene block since the technique's initial application. One such revelation includes the cervical level of block performance. Plante et al carried out a study comparing ultrasound-guided ISB performed at the C5 versus C6 anatomical level in randomized patients undergoing shoulder surgery [39]. This study revealed ISB performed at both levels possessing similar efficacy, however the C6 level resulted in significantly greater block success of the distal brachial plexus, including the ulnar, radial, and medial nerves [39].

Needle proximity and neuronal tissue microanatomy with regard to ISB have also been examined. Spence et al sought to determine the ideal location of local anesthetic deposition for ISB [18]. When comparing needle tip and injection superficial to the brachial plexus sheath versus penetration deep to this plexus covering in randomized patients, both positions showed comparable times to block onset, yet the deeper injection resulted in longer mean block duration [18]. In examining ultrasound-guided needle tip placement relative to the nerve roots of the brachial plexus epineurium in the interscalene groove, using india ink staining in a cadaveric study, it was demonstrated that subepineural injection occurred more often than anticipated despite ultrasound guidance [45].

Although the middle scalene muscle itself was largely thought devoid of neuronal structures, the continued use of ultrasound guidance in performance of the interscalene block has indeed proven useful in both identifying and localizing brachial plexus nerves within this area. In conducting an observational study in 50 adult patients receiving ultrasound-guided, posterior approach interscalene block prior to shoulder surgery, Hanson and Auyong identified the dorsal scapular nerve and/or long thoracic nerve in 90% of these patients (verified with peripheral nerve stimulator twitch monitoring). These nerves were found to occur at a depth approximating the C6 nerve root level and less than 1 cm posterior to the larger brachial plexus with the dorsal scapular nerve identified more commonly than the long thoracic nerve (77% versus 23%, respectively) [46]

Local anesthetic volume and concentration necessary for successful ISB have also been studied. Riazi et al compared the use of 5 ml versus 20 ml ropivicaine 0.5% with ultrasound-guided ISB for randomized patients receiving shoulder surgery [26]. The lower volume group was shown to provide equivalent analgesia to the 20 ml group while resulting in a significant decrease in respiratory complications, including diaphragmatic or phrenic nerve paralysis, declines in oxygen saturation, and reduced function on spirometry testing [26]. A later study by Renes et al examined the minimum effective volume (MEV) of ropivicaine 0.75% necessary to provide successful analgesia for elective shoulder surgery when deposited at the C7 level via ultrasonography [31]. This study revealed the MEV to be 2.9 ml and 3.6 ml for 50% and 95% of patients, respectively [31]. Fredrickson et al compared varying ISB bolus ropivicaine concentrations and volumes for preoperative PNB in randomized patients undergoing shoulder surgery and also receiving postoperative 0.2% ropivicaine infusions [47]. The larger volume, 30 ml of 0.5% ropivicaine demonstrated no significant increase in anesthesia duration as compared to 20 ml of

ropivicaine 0.375% [47]. Of note, local anesthetic concentration was shown to be the principle determinant of motor blockade [47].

Goebel et al conducted a randomized trial examining the use of ultrasound-placed ISB catheters in managing postoperative pain for major shoulder surgery [48]. Patient controlled infusions of ropivicaine 0.2% resulted in less concomitant pain medication administration in the first 24 h postoperatively as compared to catheter infusions of normal saline [48].

3.8. Adverse effects with interscalene block

With the performance of interscalene block over the past four decades, notable adverse effects have been established. Perhaps most notable, phrenic nerve (C3-5) paralysis occurs in nearly all patients receiving ISB that may lead to significant decline respiratory function, particularly in patients with underlying pulmonary disease [26], [31]. One ultrasound study found the anatomical separation between the brachial plexus and phrenic nerve lateral to the cricoid cartilage to be as little as 2 mm [49]. Other undesirable effects of regional anesthesia at this site may include blockade of the recurrent laryngeal nerve causing hoarseness, stellate ganglion causing Horner's syndrome, and increased local anesthetic spread rarely causing elements of epidural or spinal quality anesthesia [27]. Inadvertent needle placement during ISB performance may lead to vasculature puncture and direct nerve injury, including reported cases of spinal cord injury [50]. As with other forms of regional anesthesia, systemic local anesthetic toxicity as well as block failure may occur [51]. Failure to anesthetize the distribution of the ulnar nerve is of particular propensity with ISB, as the lower trunk is often spared [24].

3.9. Impact of ultrasound on adverse effects

With the inclusion of ultrasound guidance for interscalene block, several studies have demonstrated an impact on previously reported adverse effects. Renes et al conducted a randomized trial in patients undergoing shoulder surgery, comparing general anesthesia combined with ISB performed with 10 ml ropivacaine deposited via ultrasound versus peripheral nerve stimulator technique [35]. The ultrasound group showed a significantly decreased incidence of diaphragmatic hemiparesis [35]. In addition, the use of ultrasound technique has allowed ISB studies that have revealed decreased incidence of phrenic nerve blockade and respiratory complications based on level of block performance (C7) and reduced volume of local anesthetic [27], [26]. Abrahams et al conducted a systematic review and meta-analysis of randomized trials for a variety of peripheral nerve blocks [6]. When comparing ultrasound guidance versus peripheral nerve stimulation, ultrasound guided blocks were shown to have significantly less risk of vascular puncture [6]. Despite direct visualization when using ultrasound-guidance for PNB, no significant difference in the incidence of neuronal injury or neurologic symptoms postoperatively has been shown [25], [24]. With regard to failure to anesthetize the brachial plexus inferior trunk with ISB, Kapral et al demonstrated improved ulnar nerve and median nerve blockade 30 min post-block when compared to PNS guidance [30].

http://dx.doi.org/10.5772/56645

Perhaps the most important impact of ultrasound guidance during performance of peripheral nerve blockade to date has been related to an increase in patient safety via a decrease in local anesthetic systemic toxicity (LAST). Over a hundred cases of severe toxicity have been described in the medical literature, including some that have resulted in fatality, though the incidence of actual cases are likely much more numerous [15]. Most such cases involve toxicity to the central nervous system, including loss of consciousness, agitation, or, most commonly, seizure. Fifty percent of reported cases showed some evidence of cardiovascular toxicity, for which resuscitation may prove quite challenging [15]. Several studies have recently been published which strongly support the idea that ultrasound imaging has reduced the incidence of serious LAST. Sites, et al, reported over 12,000 cases of ultrasound-guided nerve blocks, with only one case of LAST [52], which compares quite favorably to reports of this complication during the era of nerve stimulator guidance, with rates of 1/1000 to 1/3000. In another large database report from a single site summarizing experience at a single teaching institution, Orebaugh, et al, reported a significant reduction in LAST episodes over a six-year period as the practice transitioned from nerve stimulator to ultrasound guidance-there were no such complications in over 9000 cases in which ultrasound was utilized [53]. Finally, Barrington, et al, reported from a large, multicenter, international database on complications related to peripheral nerve blockade, that the risk of LAST was significantly lowered when ultrasound guidance was utilized (relative risk 0.25-0.31), compared to blocks guided by nerve stimulation alone [54]. These reports have allowed the regional anesthesiologist, using ultrasound guidance, to approach his/her patients with greater certainty, confidence and safety.

4. Conclusions

Peripheral nerve blockade has become an ever-increasing tool in providing analgesia for patients undergoing focal surgical interventions. Advancements in ultrasound guidance for performance of these peripheral nerve blocks have allowed a parallel increase in this technology's utilization. The interscalene approach to brachial plexus blockade is a commonly employed peripheral nerve block that has demonstrated effectiveness in providing perioperative analgesia for patients undergoing shoulder surgery. The use of ultrasound guidance in performing the interscalene block has been shown to be effective in providing postoperative analgesia while decreasing specific respiratory side-effects [26], [27], [35], vascular puncture [6], and local anesthetic toxicity [53] as compared to non-ultrasongraphic, blind techniques. These benefits likely stem from the direct visualization of anatomical structures afforded by ultrasound implementation during block performance. Ultrasound guidance for peripheral nerve blockade remains an exciting advancement in caring for patients during the perioperative period, and this technology will likely continue to become commonplace with an increasing patient population and demonstrated effectiveness.

Author details

James C. Krakowski and Steven L. Orebaugh
Dept. of Anesthesiology, University of Pittsburgh Medical Center, Pittsburgh, PA, USA

Available from https://dx.doi.org/10.5772/56645

References

[1] Cullen KA, Hall MJ, Golosinskiy A. Ambulatory surgery in the United States, 2006. Natl Health Stat Report 2009 Jan 28;(11)(11):1-25.

[2] Memtsoudis SG, Kuo C, Ma Y, Edwards A, Mazumdar M, Liguori G. Changes in anesthesia-related factors in ambulatory knee and shoulder surgery: United States 1996-2006. Reg Anesth Pain Med 2011 Jul-Aug;36(4):327-331.

[3] Hadzic A, Arliss J, Kerimoglu B, Karaca PE, Yufa M, Claudio RE, et al. A comparison of infraclavicular nerve block versus general anesthesia for hand and wrist day-case surgeries. Anesthesiology 2004 Jul;101(1):127-132.

[4] Hadzic A, Williams BA, Karaca PE, Hobeika P, Unis G, Dermksian J, et al. For outpatient rotator cuff surgery, nerve block anesthesia provides superior same-day recovery over general anesthesia. Anesthesiology 2005 May;102(5):1001-1007.

[5] Marhofer P, Harrop-Griffiths W, Kettner SC, Kirchmair L. Fifteen years of ultrasound guidance in regional anaesthesia: part 1. Br J Anaesth 2010 May;104(5):538-547.

[6] Abrahams MS, Aziz MF, Fu RF, Horn JL. Ultrasound guidance compared with electrical neurostimulation for peripheral nerve block: a systematic review and meta-analysis of randomized controlled trials. Br J Anaesth 2009 Mar;102(3):408-417.

[7] Gray AT. Ultrasound-guided regional anesthesia: current state of the art. Anesthesiology 2006 Feb;104(2):368-73, discussion 5A.

[8] Sripada R, Bowens C,Jr. Regional anesthesia procedures for shoulder and upper arm surgery upper extremity update--2005 to present. Int Anesthesiol Clin 2012 Winter; 50(1):26-47.

[9] Manickam BP, Perlas A, Chan VW, Brull R. The role of a preprocedure systematic sonographic survey in ultrasound-guided regional anesthesia. Reg Anesth Pain Med 2008 Nov-Dec;33(6):566-570.

[10] Barrington MJ, Watts SA, Gledhill SR, Thomas RD, Said SA, Snyder GL, et al. Preliminary results of the Australasian Regional Anaesthesia Collaboration: a prospective audit of more than 7000 peripheral nerve and plexus blocks for neurologic and other complications. Reg Anesth Pain Med 2009 Nov-Dec;34(6):534-541.

[11] Marhofer P, Schrogendorfer K, Koinig H, Kapral S, Weinstabl C, Mayer N. Ultrasonographic guidance improves sensory block and onset time of three-in-one blocks. Anesth Analg 1997 Oct;85(4):854-857.

[12] Orebaugh SL, Williams BA, Vallejo M, Kentor ML. Adverse outcomes associated with stimulator-based peripheral nerve blocks with versus without ultrasound visualization. Reg Anesth Pain Med 2009 May-Jun;34(3):251-255.

[13] Swenson JD, Bay N, Loose E, Bankhead B, Davis J, Beals TC, et al. Outpatient management of continuous peripheral nerve catheters placed using ultrasound guidance: an experience in 620 patients. Anesth Analg 2006 Dec;103(6):1436-1443.

[14] Casati A, Baciarello M, Di Cianni S, Danelli G, De Marco G, Leone S, et al. Effects of ultrasound guidance on the minimum effective anaesthetic volume required to block the femoral nerve. Br J Anaesth 2007 Jun;98(6):823-827.

[15] Neal JM, Bernards CM, Butterworth JF,4th, Di Gregorio G, Drasner K, Hejtmanek MR, et al. ASRA practice advisory on local anesthetic systemic toxicity. Reg Anesth Pain Med 2010 Mar-Apr;35(2):152-161.

[16] Orebaugh SL, Pennington S. Variant location of the musculocutaneous nerve during axillary nerve block. J Clin Anesth 2006 Nov;18(7):541-544.

[17] Sites BD, Spence BC, Gallagher JD, Wiley CW, Bertrand ML, Blike GT. Characterizing novice behavior associated with learning ultrasound-guided peripheral regional anesthesia. Reg Anesth Pain Med 2007 Mar-Apr;32(2):107-115.

[18] Spence BC, Beach ML, Gallagher JD, Sites BD. Ultrasound-guided interscalene blocks: understanding where to inject the local anaesthetic. Anaesthesia 2011 Jun;66(6): 509-514.

[19] Sites BD, Beach ML, Spence BC, Wiley CW, Shiffrin J, Hartman GS, et al. Ultrasound guidance improves the success rate of a perivascular axillary plexus block. Acta Anaesthesiol Scand 2006 Jul;50(6):678-684.

[20] Van Geffen GJ, Moayeri N, Bruhn J, Scheffer GJ, Chan VW, Groen GJ. Correlation between ultrasound imaging, cross-sectional anatomy, and histology of the brachial plexus: a review. Reg Anesth Pain Med 2009 Sep-Oct;34(5):490-497.

[21] Antonakakis JG, Sites B. The 5 most common ultrasound artifacts encountered during ultrasound-guided regional anesthesia. Int Anesthesiol Clin 2011 Fall;49(4):52-66.

[22] Brull R, Macfarlane AJ, Parrington SJ, Koshkin A, Chan VW. Is circumferential injection advantageous for ultrasound-guided popliteal sciatic nerve block?: A proof-of-concept study. Reg Anesth Pain Med 2011 May-Jun;36(3):266-270.

[23] Silvestri E, Martinoli C, Derchi LE, Bertolotto M, Chiaramondia M, Rosenberg I. Echotexture of peripheral nerves: correlation between US and histologic findings and criteria to differentiate tendons. Radiology 1995 Oct;197(1):291-296.

[24] Neal JM, Gerancher JC, Hebl JR, Ilfeld BM, McCartney CJ, Franco CD, et al. Upper extremity regional anesthesia: essentials of our current understanding, 2008. Reg Anesth Pain Med 2009 Mar-Apr;34(2):134-170.

[25] Liu SS, Zayas VM, Gordon MA, Beathe JC, Maalouf DB, Paroli L, et al. A prospective, randomized, controlled trial comparing ultrasound versus nerve stimulator guidance for interscalene block for ambulatory shoulder surgery for postoperative neurological symptoms. Anesth Analg 2009 Jul;109(1):265-271.

[26] Riazi S, Carmichael N, Awad I, Holtby RM, McCartney CJ. Effect of local anaesthetic volume (20 vs 5 ml) on the efficacy and respiratory consequences of ultrasound-guided interscalene brachial plexus block. Br J Anaesth 2008 Oct;101(4):549-556.

[27] McNaught A, Shastri U, Carmichael N, Awad IT, Columb M, Cheung J, et al. Ultrasound reduces the minimum effective local anaesthetic volume compared with peripheral nerve stimulation for interscalene block. Br J Anaesth 2011 Jan;106(1): 124-130.

[28] Winnie AP. Interscalene brachial plexus block. Anesth Analg 1970 May-Jun;49(3): 455-476.

[29] Yang WT, Chui PT, Metreweli C. Anatomy of the normal brachial plexus revealed by sonography and the role of sonographic guidance in anesthesia of the brachial plexus. AJR Am J Roentgenol 1998 Dec;171(6):1631-1636.

[30] Kapral S, Greher M, Huber G, Willschke H, Kettner S, Kdolsky R, et al. Ultrasonographic guidance improves the success rate of interscalene brachial plexus blockade. Reg Anesth Pain Med 2008 May-Jun;33(3):253-258.

[31] Renes SH, van Geffen GJ, Rettig HC, Gielen MJ, Scheffer GJ. Minimum effective volume of local anesthetic for shoulder analgesia by ultrasound-guided block at root C7 with assessment of pulmonary function. Reg Anesth Pain Med 2010 Nov-Dec;35(6):529-534.

[32] Chan VW, Perlas A, Rawson R, Odukoya O. Ultrasound-guided supraclavicular brachial plexus block. Anesth Analg 2003 Nov;97(5):1514-1517.

[33] Perlas A, Chan VW, Simons M. Brachial plexus examination and localization using ultrasound and electrical stimulation: a volunteer study. Anesthesiology 2003 Aug; 99(2):429-435.

[34] Tsui B, Hadzic A. Peripheral nerve stimulators and electrophysiology of nerve stimulation. In: Hadzic A, editor. Textbook of Regional Anesthesia and Acute Pain Management New York: McGraw-Hill; 2007. p. 93-104.

[35] Renes SH, Rettig HC, Gielen MJ, Wilder-Smith OH, van Geffen GJ. Ultrasound-guided low-dose interscalene brachial plexus block reduces the incidence of hemidiaphragmatic paresis. Reg Anesth Pain Med 2009 Sep-Oct;34(5):498-502.

[36] Byrne K, Tsui BC. Practical concepts in nerve stimulation: impedance and other recent advances. Int Anesthesiol Clin 2011 Fall;49(4):81-90.

[37] Bigeleisen PE, Moayeri N, Groen GJ. Extraneural versus intraneural stimulation thresholds during ultrasound-guided supraclavicular block. Anesthesiology 2009 Jun; 110(6):1235-1243.

[38] Chan VW. Applying ultrasound imaging to interscalene brachial plexus block. Reg Anesth Pain Med 2003 Jul-Aug;28(4):340-343.

[39] Plante T, Rontes O, Bloc S, Delbos A. Spread of local anesthetic during an ultrasound-guided interscalene block: does the injection site influence diffusion? Acta Anaesthesiol Scand 2011 Jul;55(6):664-669.

[40] Sites BD, Beach ML, Chinn CD, Redborg KE, Gallagher JD. A comparison of sensory and motor loss after a femoral nerve block conducted with ultrasound versus ultrasound and nerve stimulation. Reg Anesth Pain Med 2009 Sep-Oct;34(5):508-513.

[41] Orebaugh SL, Williams BA, Kentor ML, Bolland MA, Mosier SK, Nowak TP. Interscalene block using ultrasound guidance: impact of experience on resident performance. Acta Anaesthesiol Scand 2009 Nov;53(10):1268-1274.

[42] Muhly WT, Orebaugh SL. Sonoanatomy of the vasculature at the supraclavicular and interscalene regions relevant for brachial plexus block. Acta Anaesthesiol Scand 2011 Nov;55(10):1247-1253.

[43] Fredrickson MJ, Ball CM, Dalgleish AJ. A prospective randomized comparison of ultrasound guidance versus neurostimulation for interscalene catheter placement. Reg Anesth Pain Med 2009 Nov-Dec;34(6):590-594.

[44] Orebaugh SL, Williams BA, Kentor ML. Ultrasound guidance with nerve stimulation reduces the time necessary for resident peripheral nerve blockade. Reg Anesth Pain Med 2007 Sep-Oct;32(5):448-454.

[45] Orebaugh SL, McFadden K, Skorupan H, Bigeleisen PE. Subepineurial injection in ultrasound-guided interscalene needle tip placement. Reg Anesth Pain Med 2010 Sep-Oct;35(5):450-454.

[46] Hanson NA, Auyong DB. Systematic ultrasound identification of the dorsal scapular and long thoracic nerves during interscalene block. Reg Anesth Pain Med. 2013 Jan-Feb;38(1):54-7.

[47] Fredrickson MJ, Smith KR, Wong AC. Importance of volume and concentration for ropivacaine interscalene block in preventing recovery room pain and minimizing motor block after shoulder surgery. Anesthesiology 2010 Jun;112(6):1374-1381.

[48] Goebel S, Stehle J, Schwemmer U, Reppenhagen S, Rath B, Gohlke F. Interscalene brachial plexus block for open-shoulder surgery: a randomized, double-blind, placebo-controlled trial between single-shot anesthesia and patient-controlled catheter system. Arch Orthop Trauma Surg 2010 Apr;130(4):533-540.

[49] Kessler J, Schafhalter-Zoppoth I, Gray AT. An ultrasound study of the phrenic nerve in the posterior cervical triangle: implications for the interscalene brachial plexus block. Reg Anesth Pain Med 2008 Nov-Dec;33(6):545-550.

[50] Benumof JL. Permanent loss of cervical spinal cord function associated with interscalene block performed under general anesthesia. Anesthesiology 2000 Dec;93(6): 1541-1544.

[51] Neal JM, Brull R, Chan VW, Grant SA, Horn JL, Liu SS, et al. The ASRA evidence-based medicine assessment of ultrasound-guided regional anesthesia and pain medicine: Executive summary. Reg Anesth Pain Med 2010 Mar-Apr;35(2 Suppl):S1-9.

[52] Sites BD, Taenzer AH, Herrick MD, Gilloon C, Antonakakis J, Richins J, et al. Incidence of local anesthetic systemic toxicity and postoperative neurologic symptoms associated with 12,668 ultrasound-guided nerve blocks: An analysis from a prospective clinical registry. Reg Anesth Pain Med. 2012 Sep-Oct;37(5):478-82.

[53] Orebaugh SL, Kentor ML, Williams BA. Adverse Outcomes Associated with Nerve Stimulator-Guided and Ultrasound-Guided Peripheral Nerve Blocks by Supervised Trainees: Update of a Single-Site Database. Reg Anesth Pain Med 2012 (in press).

[54] Barrington MJ, Kluger R. Use of ultrasound guidance for peripheral nerve blockade is associated with a reduced incidence of local anesthetic systemic toxicity [abstract]. American Society of Anesthesiologists Annual Meeting. October 16, 2012. BOC12.

Journal of
Clinical Medicine

MDPI

Article

What Is the Diagnosis in Patients with Type 2 Diabetes Who Have a Painful Shoulder? Results from a Prospective Cross-Sectional Study

Login Ahmed S. Alabdali [1,2,*], Jasmien Jaeken [3], Nens van Alfen [4], Geert-Jan Dinant [1], Rob A. P. Borghans [5] and Ramon P. G. Ottenheijm [1]

[1] Department of Family Medicine, CAPHRI Care and Public Health Research Institute, Maastricht University, P.O. Box 616, 6200 MD Maastricht, The Netherlands;

[2] Ministry of Education, Riyadh 12435, Saudi Arabia
[3] Department of Public Health and Primary Care, Catholic University of Leuven, Kapucijnenvoer 33, B-3000 Leuven, Belgium;

[4] Department of Neurology and Clinical Neurophysiology, Radboud University Medical Center, Donders Institute for Brain Cognition and Behaviour, 6500 HB Nijmegen, The Netherlands;

[5] Department of Radiology, Zuyderland Medical Centre, 6162 BG Sittard-Geleen, The Netherlands;

Received: 24 November 2020; Accepted: 15 December 2020; Published: 18 December 2020

Abstract: Background: Patients with diabetes mellitus have higher risk of developing shoulder pathology. However, only adhesive capsulitis is addressed in shoulder pain guidelines as a disorder associated with diabetes. Yet, patients with diabetes are at risk of having several other shoulder disorders, including focal neuropathy. Our aim was to quantify the presence of shoulder disorders using physical examination and ultrasound imaging in patients with type 2 diabetes (T2DM) suffering from shoulder pain in general practice. Methods: In this prospective cross-sectional study, patients with T2DM who had had a painful shoulder for at least four weeks were included. Patients filled out a questionnaire and underwent a physical examination of the shoulders and feet and ultrasound imaging of the shoulder. Results: A total of 66 patients were included, of whom 40.9% (n = 27) had bilateral complaints resulting in 93 symptomatic shoulders. Subacromial pain syndrome was most frequently diagnosed by physical examination (66.6%, 95% CI 51.6–72.0%; $p < 0.0001$), while ultrasound imaging showed that subacromial disorders were statistically significantly the most prevalent (90.3%, 95% CI 81.9–95.2%). Only two patients (3%) were diagnosed with neuropathic shoulder pain. Conclusion: When choosing treatment, general practitioners should be aware that in patients with T2DM the subacromial region is most frequently affected.

Keywords: type 2 diabetes; physical examination; diagnosis; ultrasound; shoulder pain; adhesive capsulitis; subacromial pain syndrome

1. Introduction

Patients with type 2 diabetes mellitus (T2DM) are at increased risk for shoulder disorders, such as adhesive capsulitis and rotator cuff disorders (e.g., tears). The prevalence of adhesive capsulitis ranges from 4 to 30% in patients with diabetes, compared to up to 10% in patients without diabetes [1–4], while rotator cuff tears are also more frequently observed in patients with diabetes [5–8]. Lesser known is that adhesive capsulitis is also associated with diabetic neuropathy [9].

The exact pathophysiology of the increased risk of shoulder disorders in patients with diabetes remains uncertain, but there is evidence that the shoulder can be affected through two pathophysiological pathways: connective tissue damage to the rotator cuff tendons and joint capsule, and peripheral or autonomic neuropathy. Connective tissue damage seems to be caused by abnormal collagen disposition in the periarticular connective tissues, due to the formation of advanced glycosylation end-products. This alters the structural matrix and the mechanical properties of these tissues. Additionally, it is hypothesized that the altered glucose metabolism in patients with diabetes causes functional as well as structural changes to the peripheral nerve system, which ultimately leads to neuropathy [5,10]. About 50% of patients with diabetes mellitus develop diabetic neuropathy [11,12], which can be classified as generalized symmetrical polyneuropathy or (multi)focal asymmetrical neuropathy [11,13]. If patients with subclinical levels of neuropathy are included, the prevalence might exceed 90% [14,15]. However, in patients with diabetes, shoulder involvement has been described in case studies, but is currently regarded as rare [16–18].

While rotator cuff disorders (also named subacromial pain syndrome, abbreviated to SAPS [19,20]) are widely considered the most common cause of shoulder pain in general practice [21–23], diabetes mellitus is currently only associated with adhesive capsulitis in shoulder pain guidelines, while neuropathy is not addressed at all [20,24,25]. However, to ensure optimal treatment outcomes, it is important to identify the underlying disorder in patients with diabetes to prevent the development of chronic shoulder pain. For example, patients with SAPS and neuropathic pain might benefit more from treatment targeted to the neuropathic pain [26]. This seems important especially in patients with T2DM, as shoulder pain might negatively influence physical activity, which is considered to be the cornerstone of diabetes treatment. Therefore, inadequate treatment of shoulder pain might negatively influence diabetes treatment, eventually leading to a vicious circle [27,28].

To our knowledge, no studies have been conducted to establish the frequency of underlying shoulder disorders in patients with T2DM suffering from shoulder pain. In order to prevent the development of chronic shoulder pain in patients with diabetes, more insight is needed into which specific types of shoulder pathology are prevalent in T2DM. Given the complex nature of shoulder pain, the primary aim of this study was to quantify the presence of specific shoulder disorders using physical examination and musculoskeletal ultrasound imaging in patients with type 2 diabetes mellitus (T2DM) in general practice. Secondarily, we sought to examine the relationship of the specific disorders with the presence of a diabetic neuropathy. With this information, we can increase general practitioners (GP) awareness of this specific problem in T2DM.

2. Methods

2.1. Participants and Study Design

This was a prospective cross-sectional study of patients with T2DM suffering from shoulder pain in general practice. Patients were invited to this study while participating in a questionnaire study assessing the prevalence of upper extremity musculoskeletal disorders (manuscript under review). During their annual check-ups in general practice, they had been asked to participate in a questionnaire study, which also included an invitation for the current study that was only intended for patients who had shoulder pain. All eligible participants from the questionnaire study were invited to participate. To increase recruitment, a flyer announcing this study was sent out to physiotherapy and general practices in the Sittard-Geleen area in the Netherlands. During our inclusion period, for which we had a time frame of nine months (March 2018 to November 2018), we included all eligible patients. Inclusion criteria were being aged between 30 and 70 years, and having shoulder pain that had lasted longer than 4 weeks. Exclusion criteria were inability to complete the assessments, and inability to give informed consent. After providing informed consent, patients underwent the following assessments: a questionnaire addressing shoulder pain including co-morbidity and diabetes-related questions, standardized physical examination of the shoulder, neurological examination of the feet, and ultrasound

imaging of the shoulder (see below). All examinations were carried out in the Meditta Medical Center in Echt, a diagnostic center, between March 2018 and November 2018. This study was approved by the Medical Ethics Committee of Zuyderland Medical Centre (METC-Z 17-N-165).

2.2. Questionnaire

The following demographic and shoulder-specific information was collected: an 11-point Numerical Rating Scale, affected side and dominant arm, pain onset (sudden or gradual), neck pain involvement, and if there was a history of rheumatoid arthritis, osteoarthritis, and any other joint inflammation. Additionally, we collected information about the most recent HBA1c value, the current body mass index (BMI), and year of their diabetes diagnosis.

2.3. Ultrasound Imaging

Ultrasound examination of the shoulder was the first examination participants underwent, and was performed by one of the three participating, experienced radiologists, using a Phillips EPIQ 7G (Philips Healthcare, Eindhoven, the Netherlands) with a high-resolution, multi-frequency 4–18 MHz linear transducer. A standardized protocol was performed following the technical guidelines of the European Society of Musculoskeletal Radiology for shoulder scanning [29]. In patients with diabetes, both shoulders were assessed. The following structures were assessed: the tendon of the supraspinatus, infraspinatus, subscapularis, and the long head of biceps, as well as the subacromial-subdeltoid bursa, rotator interval, glenohumeral recess, and acromioclavicular joint (AC joint). We used standardized criteria for subacromial pathology previously defined by us, and added criteria for adhesive capsulitis (see Supplement Table S1) [30–32]. The following disorders were recorded: dislocation of the long head of biceps tendon, biceps tenosynovitis, (calcific) tendinopathy, any kind of tendon tear, bursitis, adhesive capsulitis, paralabral cyst, and acromioclavicular osteoarthritis. Next, they were categorized by their anatomical location as subacromial, glenohumeral, or other disorders, by following a detailed standard operating procedure (see Supplement Table S1 for full details).

2.4. Physical Examination

One trained medical doctor of our study team (LA), blinded to the ultrasound imaging results, carried out a structured physical examination of both shoulders, hands, and a neurological examination of the feet.

Shoulders were examined according to the shoulder pain guidelines of the Dutch College of General Practitioners prevailing at the time of conducting the study [33]. One year later (2019), these guidelines were revised. Therefore, we used the revised version for subsequent classification of the shoulder disorders [20]. Shoulders were inspected for muscle wasting and scapular winging. Active and passive abduction and passive external rotation were carried out to assess for pain and range of motion was visually estimated. Additionally, the Hawkins–Kennedy test and the Neer impingement test were carried out [34,35]. The 10-item Douleur Neuropathique questionnaire was performed to assess neuropathic shoulder pain; a commonly used questionnaire including physical examination for screening and diagnosing neuropathic pain in patients with neurological complaints, valid for the Dutch population, and validated in diabetes patients [36–38]. In the Dutch population, the cut-off score for neuropathic pain is considered ≥5 (out of 10 points) [39]. Physical examination findings were used to diagnose the following disorders: SAPS, a glenohumeral or an "other disorder", and categorized using a mutually exclusive method leading to a single diagnosis (Figure 1) [20]. Glenohumeral disorders were defined by an external rotation range of motion of less than 45 degrees, while SAPS was defined by either a painful abduction (including a painful arc) with or without a limited range of motion during abduction, or a positive Hawkins–Kennedy and Neer test. An "other disorder" was defined as not having any of the two previous disorders.

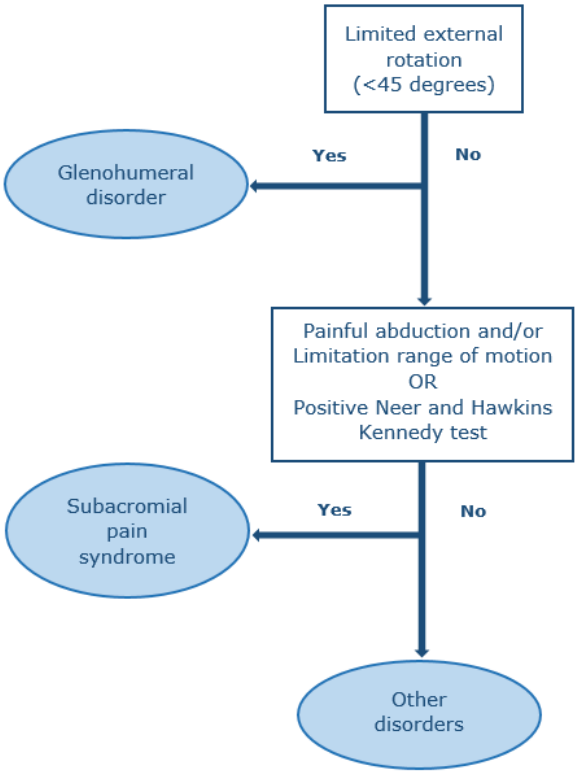

Figure 1. Diagnosis based on physical examination by a mutually excluding method.

Examination of the feet consisted of two parts: an interview part to evaluate neuropathic symptoms, and a neurological examination to evaluate signs. Participants were asked if they had a burning, tingling, or numbness sensation, and whether they felt like they were walking on cotton wool. The neurological examination included inspection for distal muscle weakness or atrophy, ankle reflexes, touch sensation, and vibration sense. The diagnosis of clinical polyneuropathy was based on a combination of symptoms and signs: presence of at least one symptom in combination with decreased or absent ankle reflexes, and decreased or absent distal sensation (vibration sense and/or touch sensation) with or without distal muscle weakness. For subclinical polyneuropathy, the abovementioned signs had to be present in the absence of symptoms. All examinations including criteria for pathology are presented in the Supplement (see Supplement Table S2) [40–46]. Finally, the hands were examined for the presence of a positive tabletop sign or prayer sign as a manifestation of stiff hand syndrome (see Supplement Table S3) [47–49].

2.5. Statistical Analysis

Continuous variables were tested for normal distribution. Descriptive statistics are presented for continuous variables as means with standard deviations, and categorical variables data are presented as absolute frequencies and percentages. Statistical differences for physical-examination-diagnosed shoulder disorders were calculated using the Chi-square test to compare between the three diagnostic groups. All statistical analysis were performed using IBM SPSS Statistics for Windows (version 25.0, Armonk, NY, USA).

3. Results

Table 1 presents the demographic and shoulder pain characteristics, as well as the results of the neurological and hand examination. A total of 66 patients with T2DM suffering from shoulder pain could be included during the study period. In total, 39 were recruited via the questionnaire study, and 27 via the flyers. The mean age was 63.0 years and 28.8% ($n = 19$) was female. Bilateral complaints were present in 41% of the patients ($n = 27$), resulting in 93 symptomatic shoulders and 39 asymptomatic shoulders.

Table 1. Physical-examination-diagnosed shoulder disorders with the comparison of the demographic and clinical variables in patients with type 2 diabetes mellitus (T2DM), on both patient and shoulder level.

	Total Number of Patients with Shoulder Pain $n = 66$	**Symptomatic Shoulders, $n = 93$**		
		GH	**SAPS**	**Other Disorder**
		$n = 17$ (18.2%, 95% CI: 11.3–27.9) [#]	**$n = 58$ (66.6%, 95% CI: 51.6–72.0) [#]**	**$n = 18$ (16.1%, 95% CI: 12.1–29.1) [#]**
Age mean ± SD IQR range (years)	 63.0 ± 6.9 38–70	 58.8 ± 5.8 48–70	 61.5 ± 7.0 38–70	 61.5 ± 7.6 52–70
Female sex	19 (28.8)	5 (31.3)	11 (25.0)	3 (42.9)
BMI (kg/m^2) mean ± SD range	 28.5 ± 4.2 16–41.5	 28.1 ± 3.7 23.9–35.9	 28.4 ± 4.5 16–41.5	 29.7 ± 3.5 25.4–34.0
Bilateral shoulder pain	27 (40.9)	8 (50)	15 (34.1)	4 (57.1)
Dominant shoulder affected	26 (39.3)	13 (81.3)	36 (81.8)	7 (100)
NRS mean ± SD range	 5.3 ± 2.1 1–9	 6.25 ± 1.9 3–9	 5.2 ± 2.06 1–8	 4.0 ± 2.6 1–8
Pain onset sudden gradual	 13 (19.7) 51 (79.7)	 2 (11.7) 15 (88.3)	 13 (20.9) 44 (70.9)	 2 [a] (11.1) 10 (12.5)
Neck pain	9 (13.6)	2 (12.5)	5 (11.4)	2 (11.1)
Duration of diabetes mean ± SD range (years)	 9.0 ± 5.5 1–27	 8.2 ± 4.3 [a] 1–14	 9.4 ± 5.8 [b] 1–27	 8.2 ± 5.8 2–19
HbA1C (mmol/mol) mean ± SD range	 55.7 ± 7.7 43–75	 55.6 ± 6.2 [a] 44–64	 55.8 ± 8.03 [b] 43–75	 53.6 ± 10.1 [c] 43–70
Rheumatoid arthritis [a]	8 (12.5)	3 (18.8)	4 [a] (10.3)	1 (14.3)
Osteoarthritis [a]	33 (51.6)	9 (56.3)	22 [a] (52.4)	3 (33.3)
Stiff hand syndrome (%)	28 (42.4)	9 (56.3)	17 (38.6)	2 (28.6)
Neuropathic shoulder pain by DN4 (score ≥ 5)	2 (3.0)	0	1 (1.6)	1 (5.2)
Polyneuropathy Clinical Subclinical	 19 (28.8) 37 (56.1)	 5 (29.4) 11 (64.7)	 11 (19.2) 22 (38.5)	 3 (15.7) 4 (21.1)

Values are presented as absolute numbers and percentages unless otherwise stated; SAPS: subacromial pain syndrome; GH: glenohumeral disorder; IQR: interquartile range; BMI: body mass index; SD: standard deviation; NRS: numerical rating scale; DN4: Douleur Neuropathique 4 questionnaire; [a] 2 are missing; [b] 4 are missing; [c] 1 is missing. [#] Statistical comparison between GH vs. SAPS: p-value < 0.0001, SAPS vs. Other disorder: p-value < 0.0001, GH vs. Other disorder: p-value 0.072.

3.1. Physical-Examination-Diagnosed Symptomatic Shoulder Disorders

The results of the shoulder diagnosis based on physical examination are presented in Table 1. SAPS was statistically the most frequently observed disorder in symptomatic shoulders (66.6%, 95% CI 51.6–72.0%), followed by glenohumeral disorders (18.2%, 95% CI 11.3–27.9%; $p < 0.0001$ versus SAPS), and then "other disorder" (16.1%, 95% CI 12.1–29.1%; $p < 0.0001$ versus SAPS). Neuropathic shoulder

pain was observed in two patients (3.2%); one patient was diagnosed with SAPS, the other with an "other disorder".

3.2. Polyneuropathy

Clinical polyneuropathy of the feet was observed in 28.8% (n = 19), while subclinical polyneuropathy was present in 56.1% (n = 37). In patients with a glenohumeral disorder, polyneuropathy was most commonly observed (29.4%, n = 5).

3.3. Ultrasound-Diagnosed Shoulder Disorders

Table 2 presents the results of the ultrasound findings in both symptomatic and asymptomatic shoulders. Subacromial disorders were most frequently diagnosed in both symptomatic and asymptomatic shoulders (90.3% (n = 84) and 76.9% (n = 30), respectively) with rotator cuff disorders being most prevalent. This was followed by osteoarthritis of the AC joint (59.1% (n = 55) and 43.5% (n = 17), respectively) and then glenohumeral disorders (8.6%, n = 8) in symptomatic shoulders, while these were not observed in asymptomatic shoulders. Of the rotator cuff disorders, the most frequently observed specific disorder was calcific tendinopathy in both symptomatic and asymptomatic shoulders (80.6% (n = 75), 95% CI 70.8–87.8% and 66.7% (n = 26), 95%CI 49.7–80.4%, respectively), while rotator cuff tears were least commonly observed (38.7% (n = 36), 95% CI 28.9–49.4% and 20.5% (n = 8), 95% CI 9.8–36.9%, respectively) (these results are not shown in Table 2). Of the eight patients with a glenohumeral disorder, adhesive capsulitis was present in four cases.

When we matched the results of the physical examination and ultrasound diagnosis, in 97% (56/58) of the patients diagnosed with SAPS, a subacromial disorder was observed by ultrasound imaging. Only two out of 17 patients (12%) diagnosed with a glenohumeral disorder showed ultrasound findings matching this diagnosis.

Table 2. Ultrasound-diagnosed disorders in symptomatic and asymptomatic shoulders in patients with T2DM (n = 132).

Ultrasound-Diagnosed Disorders	All 66 Patients with 132 Shoulders					
	Symptomatic Shoulders (n = 93)			Asymptomatic Shoulders (n = 39)		
	n	%	95% CI	n	%	95% CI
Subacromial pain disorders	84	90.3	81.9–95.2	30	76.9	60.2–88.2
Subacromial bursitis	13	14.0	7.9–23.1	3	7.7	2.0–21.9
Rotator cuff disorder	84	90.3	81.9–95.2	30	76.9	60.2–88.2
LHBT disorder	10	10.7	5.5–19.3	3	7.6	2.01–21.9
Dynamic impingement	14	15.1	8.7–24.3	3	7.6	2.0–21.9
Glenohumeral disorders	8	8.6	4.1–16.7	0	0	0
Adhesive capsulitis	4	4.3	1.3–11.2	0	0	0
GH effusion only	4	4.3	1.3–11.2	0	0	0
Other disorders						
Acromioclavicular OA	55	59.1	48.4–69.1	17	43.5	28.1–60.2
No disorders	0	0	0	0	0	0

LHBT: Long head of biceps tendon; OA: osteoarthritis; GH: glenohumeral.

4. Discussion

In this study, using physical examination and ultrasound imaging, we found that the subacromial region is the most frequently affected region in patients with T2DM suffering from shoulder pain. Of these subacromial structures, ultrasound imaging shows that the rotator cuff tendons are most frequently affected, with calcific tendinopathy by far the most common specific disorder. Interestingly,

we found that adhesive capsulitis, believed to be frequently diagnosed in patients with T2DM suffering from shoulder pain, was present only in a minority of patients. Moreover, neuropathic shoulder pain can be considered rare as it was present in only two patients.

4.1. Diagnosis by Physical Examination and Ultrasound Imaging

Currently, shoulder pain guidelines only associate diabetes with adhesive capsulitis [20,24,25], while we showed that subacromial disorders are by far the most common in this population. In the absence of prevalence studies, a possible explanation for the current misperception might be that adhesive capsulitis is more prevalent among patients with T2DM compared with patients without diabetes [1–4], but this does not mean that it is the most prevalent shoulder disorder in patients with diabetes.

In line with previous studies conducted in patients with shoulder pain in unselected populations [21–23], we also observed that overall, SAPS is the most common cause of shoulder pain in diabetics. The rotator cuff tendons and subacromial-subdeltoid bursa are considered to be the key sources of pathology in this syndrome [50].

SAPS is a generic term, and incorporates all disorders related to subacromial structures including tendinopathy (tendon degeneration), where calcific tendinopathy is seen as a separate diagnosis, tendon tears, and bursitis. From this spectrum of disorders, calcific tendinopathy was the most common specific disorder in our cohort (81%), which echoes the results of previous studies conducted in general practice [51–53]. However, in these previous ultrasound studies, the frequency did not exceed 50%, but it is known that diabetes is associated with calcific tendinopathy [54]. Additionally, other rotator cuff tendon disorders were more frequently present in our study. These differences might be explained in pathophysiological terms, and although the exact pathophysiology of tendon disorders in patients with diabetes remains uncertain, there is evidence that abnormal tendon collagen disposition alters the structural matrix and the mechanical properties of the tendons [6]. Through this process, the continuum of tendon pathology might be initiated, where a normal tendon changes into a degenerative tendon (called tendinopathy, different stages are described), and ultimately can tear [55]. Part of this process seems reversible through healing responses, but in patients with diabetes and other endocrine disorders, this healing process can fail; calcium deposits then arise due to a mechanism not yet elucidated [54].

In our study, the large majority of our patients clinically diagnosed with SAPS showed ultrasound findings matching SAPS. In clinical practice, ultrasound findings should always be interpreted together with the clinical findings to determine the cause of symptoms. Several shoulder imaging studies have shown that asymptomatic pathology findings are present, for example supraspinatus tears and osteoarthritis of the AC joint [56,57], and these asymptomatic findings are likely to become symptomatic over time [57]. Surprisingly, we also found ultrasound abnormalities of subacromial pathology in 16 out of 17 patients with a clinical glenohumeral disorder, while only 2 out of these 17 patients had ultrasound evidence of glenohumeral pathology. It might be that ultrasound misses the presence of osteoarthritis of the glenohumeral joint, something we did not assess radiographically in this study. The diagnostic accuracy of ultrasound imaging for osteoarthritis of the glenohumeral joint is unknown, but is likely to be suboptimal.

We also observed that 41% of the patients has bilateral complaints. This is in line with previous studies [58,59], and might be explained in the light of the above and systemic effects of diabetes.

4.2. Neuropathy

Although neuropathy is a well-known complication of diabetes, any type of neuropathy of the shoulder is currently regarded as rare [16–18]. In line with this observation, we diagnosed only two patients with neuropathic shoulder pain: both these patients were diagnosed with clinical polyneuropathy, but did not have a glenohumeral disorder on physical examination, or adhesive capsulitis on ultrasound imaging. Overall, polyneuropathy on a clinical and subclinical level was present in 39% and 56% of the patients, respectively. This is broadly consistent with a study showing

that 38% of patients with T2DM and musculoskeletal disorders had polyneuropathy [9]. We do know that diabetic neuropathy increases the risk of developing adhesive capsulitis of the shoulder, a glenohumeral disorder [9]. In our study, any form of polyneuropathy was most prevalent in patients diagnosed with a glenohumeral disorder.

4.3. Strengths and Limitations

Our study had several strengths. We were able to investigate the frequency of the shoulder-diagnosed disorders by two measurements: physical examination and ultrasound imaging. Both indicate that the subacromial region is the most frequently affected structure. The medical doctor who performed the physical examination was blinded to the ultrasound results, which avoided bias for the results of the physical examination.

Our study also had limitations. First, the sample size is small. A larger sample size would have resulted in narrower 95% confidence intervals. Second, we did not include palpation of the AC joint in our protocol, because it was not included in the shoulder pain guidelines of the Dutch College of General Practitioners prevailing at the time of conducting this study. If we had incorporated this in our study, this would also have allowed us to diagnose AC disorders, usually osteoarthritis. In our approach, this disorder is included in the "other disorder" group [33]. It is worth noting that palpation of the AC joint is included in the revised version [20]. Third, neuropathic shoulder pain was diagnosed only by physical examination, while if we had used additional tests, e.g., nerve conducting studies or muscle ultrasound (qualitative or quantitative), it might have increased the number of patients diagnosed with neuropathic shoulder pain. Fourth, the ultrasound diagnostic criteria for glenohumeral disorders such as adhesive capsulitis are debatable as more features are described in the literature, e.g., thickening of the coracohumeral ligament and restriction of external rotation on dynamic scanning [31]. These features are not detected during scanning according to the standardized protocol of the European Society of Musculoskeletal Radiology. For practical purposes, we did not incorporate additional scanning positions necessary to detect these features. This may have introduced an underestimation of the presence of adhesive capsulitis.

4.4. Implications for Practice and Future Research

General practitioners and other healthcare professional involved in the care for patients with shoulder pain should be aware that in patients with T2DM suffering from shoulder pain, the subacromial region is the most frequently affected structure. This knowledge can help make a more accurate diagnosis and can influence treatment decisions. When physical examination is not conclusive enough to establish a diagnosis, GPs may consider ultrasound imaging. This seems to be becoming more usual, as GPs increasingly rely on ultrasound imaging [60,61]. Although we showed that polyneuropathy is frequently present, neuropathic shoulder pain seems rare. However, this finding is based only on physical examination results of the shoulder. To assess whether shoulder pain in T2DM might be caused by neuropathy, studies are needed that use techniques to detect neurological denervation, e.g., nerve conducting studies of qualitative or quantitative muscle ultrasound.

Supplementary Materials: The following are available online at http://www.mdpi.com/2077-0383/9/12/4097/s1, Table S1: Criteria for ultrasound-diagnosed disorders groups, Table S2: Neurological feet examination procedures with diagnostic criteria, Table S3: Diagnostic criteria for stiff hand syndrome.

Author Contributions: Conceptualization, R.P.G.O., G.-J.D., L.A.S.A., and N.v.A.; Methodology, R.P.G.O., G.-J.D., L.A.S.A., N.v.A., and R.A.P.B.; Formal Analysis, L.A.S.A. and J.J.; Clinical investigation, L.A.S.A.; Data curation, L.A.S.A.; Writing the original draft preparation, L.A.S.A.; Writing—review and editing, R.P.G.O., G.-J.D., L.A.S.A., N.v.A., and R.A.P.B.; supervision, R.P.G.O. and G.-J.D.; All authors have read and agreed to the published version of the manuscript.

Funding: L.A.S.A. is funded by the Ministry of Education of the Kingdom of Saudi Arabia.

Acknowledgments: Funding was completely provided by the Ministry of Education of the Kingdom of Saudi Arabia. This funding body was not involved in the design of the study, or writing the manuscript.

Conflicts of Interest: The authors declare no conflict of interest.

References

1. Smith, L.L.; Burnet, S.P.; McNeil, J.D. Musculoskeletal manifestations of diabetes mellitus. *Br. J. Sports Med.* **2003**, *37*, 30–35. [CrossRef] [PubMed]
2. Cagliero, E.; Apruzzese, W.; Perlmutter, G.S.; Nathan, D.M. Musculoskeletal disorders of the hand and shoulder in patients with diabetes mellitus. *Am. J. Med.* **2002**, *112*, 487–490. [CrossRef]
3. Thomas, S.J.; McDougall, C.; Brown, I.D.; Jaberoo, M.C.; Stearns, A.; Ashraf, R.; Fisher, M.; Kelly, I.G. Prevalence of symptoms and signs of shoulder problems in people with diabetes mellitus. *J. Shoulder Elb. Surg.* **2007**, *16*, 748–751. [CrossRef] [PubMed]
4. Kidwai, S.S.; Wahid, L.; Siddiqi, S.A.; Khan, R.M.; Ghauri, I.; Sheikh, I. Upper limb musculoskeletal abnormalities in type 2 diabetic patients in low socioeconomic strata in Pakistan. *BMC Res. Notes* **2013**, *6*, 16. [CrossRef]
5. Abate, M.; Schiavone, C.; Salini, V.; Andia, I. Management of limited joint mobility in diabetic patients. *Diabetes Metab. Syndr. Obes.* **2013**, *6*, 197–207. [CrossRef]
6. Lebiedz-Odrobina, D.; Kay, J. Rheumatic manifestations of diabetes mellitus. *Rheum. Dis. Clin. N. Am.* **2010**, *36*, 681–699. [CrossRef]
7. Bhat, T.A.; Dhar, S.A.; Dar, T.A.; Naikoo, M.A.; Naqqash, M.A.; Bhat, A.; Butt, M.F. The Musculoskeletal Manifestations of Type 2 Diabetes Mellitus in a Kashmiri Population. *Int. J. Health Sci. (Qassim)* **2016**, *10*, 57–68. [CrossRef]
8. Abate, M.; Schiavone, C.; Salini, V. Sonographic evaluation of the shoulder in asymptomatic elderly subjects with diabetes. *BMC Musculoskelet. Disord.* **2010**, *11*, 278. [CrossRef]
9. Abourazzak, F.E.; Akasbi, N.; Houssaini, G.S.; Bazouti, S.; Bensbaa, S.; Hachimi, H.; Ajdi, F.; Harzy, T. Articular and abarticular manifestations in type 2 diabetes mellitus. *Eur. J. Rheumatol.* **2014**, *1*, 132–134. [CrossRef]
10. Arkkila, P.E.; Gautier, J.F. Musculoskeletal disorders in diabetes mellitus: An update. *Best Pract. Res. Clin. Rheumatol.* **2003**, *17*, 945–970. [CrossRef]
11. Boulton, A.J. Diabetic neuropathy: Classification, measurement and treatment. *Curr. Opin. Endocrinol. Diabetes Obes.* **2007**, *14*, 141–145. [CrossRef] [PubMed]
12. Dyck, P.J.; Overland, C.J.; Low, P.A.; Litchy, W.J.; Davies, J.L.; Dyck, P.J.; O'Brien, P.C.; Albers, J.W.; Andersen, H.; Bolton, C.F.; et al. Signs and symptoms versus nerve conduction studies to diagnose diabetic sensorimotor polyneuropathy: Cl vs. NPhys trial. *Muscle Nerve* **2010**, *42*, 157–164. [CrossRef] [PubMed]
13. Tesfaye, S.; Boulton, A.J.; Dyck, P.J.; Freeman, R.; Horowitz, M.; Kempler, P.; Lauria, G.; Malik, R.A.; Spallone, V.; Vinik, A.; et al. Diabetic neuropathies: Update on definitions, diagnostic criteria, estimation of severity, and treatments. *Diabetes Care* **2010**, *33*, 2285–2293. [CrossRef] [PubMed]
14. Association, A.D. Standards of Medical Care in Diabetesd2017. *J. Clin. Appl. Res. Educ.* **2017**, *40*, 142.
15. Yagihashi, S.; Mizukami, H.; Sugimoto, K. Mechanism of diabetic neuropathy: Where are we now and where to go? *J. Diabetes Investig.* **2011**, *2*, 18–32. [CrossRef] [PubMed]
16. Pica, E.C.; Verma, K.K. Bilateral brachial plexopathy as an initial presentation in a newly-diagnosed, uncontrolled case of diabetes mellitus. *Singap. Med. J.* **2008**, *49*, e29–e32.
17. Ogawa, K.; Sasaki, H.; Kishi, Y.; Yamasaki, H.; Okamoto, K.; Yamamoto, N.; Hanabusa, T.; Nakao, T.; Nishi, M.; Nanjo, K. A suspected case of proximal diabetic neuropathy predominantly presenting with scapulohumeral muscle weakness and deep aching pain. *Diabetes Res. Clin. Pract.* **2001**, *54*, 57–64. [CrossRef]
18. Wada, Y.; Yanagihara, C.; Nishimura, Y.; Oka, N. A case of diabetic amyotrophy with severe atrophy and weakness of shoulder girdle muscles showing good response to intravenous immune globulin. *Diabetes Res. Clin. Pract.* **2007**, *75*, 107–110. [CrossRef]
19. Diercks, R.; Bron, C.; Dorrestijn, O.; Meskers, C.; Naber, R.; de Ruiter, T.; Willems, J.; Winters, J.; van der Woude, H.J. Guideline for diagnosis and treatment of subacromial pain syndrome: A multidisciplinary review by the Dutch Orthopaedic Association. *Acta Orthop.* **2014**, *85*, 314–322. [CrossRef]
20. Nederlands Huisartsen Genootschap. NHG-Standaard Schouderklachten (Dutch College of General Practitioners Guidelines of Shoulder Complaints). Available online: https://www.nhg.org/standaarden/samenvatting/schouderklachten (accessed on 20 March 2020).

21. Littlewood, C.; May, S.; Walters, S. Epidemiology of Rotator Cuff Tendinopathy: A Systematic Review. *Shoulder Elb.* **2013**, *5*, 256–265. [CrossRef]
22. Littlewood, C.; Bateman, M.; Connor, C.; Gibson, J.; Horsley, I.; Jaggi, A.; Jones, V.; Meakins, A.; Scott, M. Physiotherapists' recommendations for examination and treatment of rotator cuff related shoulder pain: A consensus exercise. *Physiother. Pract. Res.* **2019**, *40*, 87–94. [CrossRef]
23. Van der Windt, D.A.; Koes, B.W.; de Jong, B.A.; Bouter, L.M. Shoulder disorders in general practice: Incidence, patient characteristics, and management. *Ann. Rheum. Dis.* **1995**, *54*, 959–964. [CrossRef]
24. CKS. Shoulder Pain Guideline. Available online: http://www.cks.nhs.uk/shoulder_pain (accessed on 20 March 2020).
25. New Zealand Guidelines Group. The Diagnosis and Management of Soft Tissue Shoulder Injuries and Related Disorders 2020. Available online: https://cdn.ymaws.com/www.alaskachiropracticsociety.com/resource/resmgr/imported/shoulder.pdf (accessed on 20 March 2020).
26. Boer, B.C.; Boetje, J.; Stevens, M.; van den Akker-Scheek, I.; van Raay, J. Adaptation, validity and reliability of the modified painDETECT questionnaire for patients with subacromial pain syndrome. *PLoS ONE* **2019**, *14*, e0211880. [CrossRef] [PubMed]
27. Molsted, S.; Tribler, J.; Snorgaard, O. Musculoskeletal pain in patients with type 2 diabetes. *Diabetes Res. Clin. Pract.* **2012**, *96*, 135–140. [CrossRef] [PubMed]
28. Miksch, A.; Hermann, K.; Rolz, A.; Joos, S.; Szecsenyi, J.; Ose, D.; Rosemann, T. Additional impact of concomitant hypertension and osteoarthritis on quality of life among patients with type 2 diabetes in primary care in Germany—A cross-sectional survey. *Health Qual. Life Outcomes* **2009**, *7*, 19. [CrossRef] [PubMed]
29. ESSR. Ultrasound Shoulder Protocol of the ESSR. 2016. Available online: https://essr.org/content-essr/uploads/2016/10/shoulder.pdf (accessed on 20 March 2020).
30. Lee, J.C.; Sykes, C.; Saifuddin, A.; Connell, D. Adhesive capsulitis: Sonographic changes in the rotator cuff interval with arthroscopic correlation. *Skelet. Radiol.* **2005**, *34*, 522–527. [CrossRef]
31. Tandon, A.; Dewan, S.; Bhatt, S.; Jain, A.K.; Kumari, R. Sonography in diagnosis of adhesive capsulitis of the shoulder: A case-control study. *J. Ultrasound* **2017**, *20*, 227–236. [CrossRef]
32. Ottenheijm, R.P.; Joore, M.A.; Walenkamp, G.H.; Weijers, R.E.; Winkens, B.; Cals, J.W.; de Bie, R.A.; Dinant, G.J. The Maastricht Ultrasound Shoulder pain trial (MUST): Ultrasound imaging as a diagnostic triage tool to improve management of patients with non-chronic shoulder pain in primary care. *BMC Musculoskelet. Disord.* **2011**, *12*, 154. [CrossRef]
33. Geraets, J.J.; de Jongh, A.C.; Boeke, A.J.; Buis, P.A.; Spinnewijn, W.E.; Geijer, R.M.; Goudswaard, A.N. Summary of the practice guideline for shoulder complaints from the Dutch College of General Practitioners. *Ned. Tijdschr. Geneeskd.* **2009**, *153*, A164.
34. Hegedus, E.J.; Goode, A.P.; Cook, C.E.; Michener, L.; Myer, C.A.; Myer, D.M.; Wright, A.A. Which physical examination tests provide clinicians with the most value when examining the shoulder? Update of a systematic review with meta-analysis of individual tests. *Br. J. Sports Med.* **2012**, *46*, 964–978. [CrossRef]
35. Gismervik, S.; Drogset, J.O.; Granviken, F.; Rø, M.; Leivseth, G. Physical examination tests of the shoulder: A systematic review and meta-analysis of diagnostic test performance. *BMC Musculoskelet. Disord.* **2017**, *18*, 41. [CrossRef] [PubMed]
36. Van Seventer, R.; Vos, C.; Giezeman, M.; Meerding, W.J.; Arnould, B.; Regnault, A.; van Eerd, M.; Martin, C.; Huygen, F. Validation of the Dutch version of the DN4 diagnostic questionnaire for neuropathic pain. *Pain Pract. Off. J. World Inst. Pain* **2013**, *13*, 390–398. [CrossRef] [PubMed]
37. Van Seventer, R.; Vos, C.; Meerding, W.; Mear, I.; Le Gal, M.; Bouhassira, D.; Huygen, F.J. Linguistic validation of the DN4 for use in international studies. *Eur. J. Pain* **2010**, *14*, 58–63. [CrossRef] [PubMed]
38. Spallone, V.; Morganti, R.; D'Amato, C.; Greco, C.; Cacciotti, L.; Marfia, G.A. Validation of DN4 as a screening tool for neuropathic pain in painful diabetic polyneuropathy. *Diabet. Med.* **2012**, *29*, 578–585. [CrossRef] [PubMed]
39. Bouhassira, D.; Attal, N.; Alchaar, H.; Boureau, F.; Brochet, B.; Bruxelle, J.; Cunin, G.; Fermanian, J.; Ginies, P.; Grun-Overdyking, A.; et al. Comparison of pain syndromes associated with nervous or somatic lesions and development of a new neuropathic pain diagnostic questionnaire (DN4). *Pain* **2005**, *114*, 29–36. [CrossRef]

40. England, J.D.; Gronseth, G.S.; Franklin, G.; Miller, R.G.; Asbury, A.K.; Carter, G.T.; Cohen, J.A.; Fisher, M.A.; Howard, J.F.; Kinsella, L.J.; et al. Distal symmetric polyneuropathy: A definition for clinical research: Report of the American Academy of Neurology, the American Association of Electrodiagnostic Medicine, and the American Academy of Physical Medicine and Rehabilitation. *Neurology* **2005**, *64*, 199–207. [CrossRef]
41. Alport, A.R.; Sander, H.W. Clinical approach to peripheral neuropathy: Anatomic localization and diagnostic testing. *Continuum* **2012**, *18*, 13–38. [CrossRef]
42. Yang, Z.; Zhang, Y.; Chen, R.; Huang, Y.; Ji, L.; Sun, F.; Hong, T.; Zhan, S. Simple tests to screen for diabetic peripheral neuropathy. *Cochrane Database Syst. Rev.* **2014**. [CrossRef]
43. Feng, Y.; Schlösser, F.J.; Sumpio, B.E. The Semmes Weinstein monofilament examination as a screening tool for diabetic peripheral neuropathy. *J. Vasc. Surg.* **2009**, *50*, 675–682. [CrossRef]
44. Smieja, M.; Hunt, D.L.; Edelman, D.; Etchells, E.; Cornuz, J.; Simel, D.L. Clinical examination for the detection of protective sensation in the feet of diabetic patients. International Cooperative Group for Clinical Examination Research. *J. Gen. Intern. Med.* **1999**, *14*, 418–424. [CrossRef]
45. Kästenbauer, T.; Sauseng, S.; Brath, H.; Abrahamian, H.; Irsigler, K. The value of the Rydel-Seiffer tuning fork as a predictor of diabetic polyneuropathy compared with a neurothesiometer. *Diabet. Med.* **2004**, *21*, 563–567. [CrossRef] [PubMed]
46. Liniger, C.; Albeanu, A.; Bloise, D.; Assal, J.P. The tuning fork revisited. *Diabet. Med.* **1990**, *7*, 859–864. [CrossRef] [PubMed]
47. Fisher, L.; Kurtz, A.; Shipley, M. Association between cheiroarthropathy and frozen shoulder in patients with insulin-dependent diabetes mellitus. *Br. J. Rheumatol.* **1986**, *25*, 141–146. [CrossRef] [PubMed]
48. Hill, N.E.; Roscoe, D.; Stacey, M.J.; Chew, S. Cheiroarthropathy and tendinopathy in diabetes. *Diabet. Med.* **2019**, *36*, 939–947. [CrossRef] [PubMed]
49. Gokcen, N.; Cetinkaya Altuntas, S.; Coskun Benlidayi, I.; Sert, M.; Nazlican, E.; Sarpel, T. An overlooked rheumatologic manifestation of diabetes: Diabetic cheiroarthropathy. *Clin. Rheumatol.* **2019**, *38*, 927–932. [CrossRef]
50. Lewis, J. Rotator cuff related shoulder pain: Assessment, management and uncertainties. *Manual Ther.* **2016**, *23*, 57–68. [CrossRef]
51. Ottenheijm, R.P.; Cals, J.W.; Weijers, R.; Vanderdood, K.; de Bie, R.A.; Dinant, G.J. Ultrasound imaging for tailored treatment of patients with acute shoulder pain. *Ann. Fam. Med.* **2015**, *13*, 53–55. [CrossRef]
52. Cadogan, A.; Laslett, M.; Hing, W.A.; McNair, P.J.; Coates, M.H. A prospective study of shoulder pain in primary care: Prevalence of imaged pathology and response to guided diagnostic blocks. *BMC Musculoskelet. Disord.* **2011**, *12*, 119. [CrossRef]
53. Ottenheijm, R.P.; van't Klooster, I.G.; Starmans, L.M.; Vanderdood, K.; de Bie, R.A.; Dinant, G.J.; Cals, J.W. Ultrasound-diagnosed disorders in shoulder patients in daily general practice: A retrospective observational study. *BMC Fam. Pract.* **2014**, *15*, 115. [CrossRef]
54. Oliva, F.; Via, A.G.; Maffulli, N. Physiopathology of intratendinous calcific deposition. *BMC Med.* **2012**, *10*, 95. [CrossRef]
55. Cook, J.L.; Purdam, C.R. Is tendon pathology a continuum? A pathology model to explain the clinical presentation of load-induced tendinopathy. *Br. J. Sports Med.* **2009**, *43*, 409–416. [CrossRef] [PubMed]
56. Girish, G.; Lobo, L.G.; Jacobson, J.A.; Morag, Y.; Miller, B.; Jamadar, D.A. Ultrasound of the shoulder: Asymptomatic findings in men. *AJR Am. J. Roentgenol.* **2011**, *197*, W713–W719. [CrossRef] [PubMed]
57. Lawrence, R.L.; Moutzouros, V.; Bey, M.J. Asymptomatic Rotator Cuff Tears. *JBJS Rev.* **2019**, *7*, e9. [CrossRef] [PubMed]
58. Arkkila, P.E.; Kantola, I.M.; Viikari, J.S.; Ronnemaa, T. Shoulder capsulitis in type I and II diabetic patients: Association with diabetic complications and related diseases. *Ann. Rheum Dis.* **1996**, *55*, 907–914. [CrossRef] [PubMed]
59. Noël, E.; Thomas, T.; Schaeverbeke, T.; Thomas, P.; Bonjean, M.; Revel, M. Frozen shoulder. *Joint Bone Spine* **2000**, *67*, 393–400. [PubMed]
60. Naunton, J.; Harrison, C.; Britt, H.; Haines, T.; Malliaras, P. General practice management of rotator cuff related shoulder pain: A reliance on ultrasound and injection guided care. *PLoS ONE* **2020**, *15*, e0227688. [CrossRef]

61. Ottenheijm, R.P.; Hesselmans, N.J.; Kemper, A.; Moser, A.; de Bie, R.A.; Dinant, G.J.; Cals, J.W. GPs' perspectives on the diagnostic work-up in patients with shoulder pain: A qualitative study. *J. Eval. Clin. Pract.* **2014**, *20*, 239–245. [CrossRef]

Journal of
Clinical Medicine

MDPI

Article

Electrodiagnostic Testing and Nerve Ultrasound of the Carpal Tunnel in Patients with Type 2 Diabetes

Bianka Heiling [1,2,*], Leonie I. E. E. Wiedfeld [1], Nicolle Müller [3], Niklas J. Kobler [1], Alexander Grimm [4], Christof Kloos [3] and Hubertus Axer [1]

[1] Department of Neurology, Jena University Hospital, Friedrich Schiller University, 07747 Jena, Germany;
[2] Clinician Scientist Program OrganAge, Jena University Hospital, 07747 Jena, Germany
[3] Department of Internal Medicine III, Jena University Hospital, Friedrich Schiller University, 07747 Jena, Germany;
[4] Department of Neurology, Tuebingen University Hospital, 72076 Tuebingen, Germany;

Abstract: In diabetic patients, controversies still exist about the validity of electrodiagnostic and nerve ultrasound diagnosis for carpal tunnel syndrome (CTS). We analyzed 69 patients with type 2 diabetes. Nerve conduction studies and peripheral nerve ultrasound of the median nerve over the carpal tunnel were performed. CTS symptoms were assessed using the Boston Carpal Tunnel Questionnaire. Polyneuropathy was assessed using the Neuropathy Symptom Score and the Neuropathy Disability Score. Although 19 patients reported predominantly mild CTS symptoms, 37 patients met the electrophysiological diagnosis criteria for CTS, and six patients were classified as severe or extremely severe. The sonographic cross-sectional area (CSA) of the median nerve at the wrist was larger than 12 mm^2 in 45 patients (65.2%), and the wrist-to-forearm-ratio was larger than 1.4 in 61 patients (88.4%). Receiver operating characteristic analysis showed that neither the distal motor latency, the median nerve CSA, nor the wrist-to-forearm-ratio could distinguish between patients with and without CTS symptoms. Diagnosis of CTS in diabetic patients should primarily be based upon typical clinical symptoms and signs. Results of electrodiagnostic testing and nerve ultrasound have to be interpreted with caution and additional factors have to be considered especially polyneuropathy, but also body mass index and hyperglycemia.

Keywords: carpal tunnel syndrome; diabetes mellitus; nerve conduction study; peripheral nerve ultrasound

Citation: Heiling, B.; Wiedfeld, L.I.E.E.; Müller, N.; Kobler, N.J.; Grimm, A.; Kloos, C.; Axer, H. Electrodiagnostic Testing and Nerve Ultrasound of the Carpal Tunnel in Patients with Type 2 Diabetes. *J. Clin. Med.* **2022**, *11*, 3374. https://doi.org/10.3390/jcm11123374

Academic Editor: Jorma Ryhänen

Received: 18 May 2022
Accepted: 10 June 2022
Published: 13 June 2022

1. Introduction

Carpal tunnel syndrome (CTS) is the most common entrapment neuropathy in the general population [1]. Risk factors for CTS are diabetes mellitus, obesity, metabolic syndrome, thyroid dysfunction, rheumatic diseases, and others [2,3]. It has been shown that the incidence of CTS is increased in diabetic patients [4]. Typical symptoms are numbness, predominantly nocturnal par- and dysesthesias, and/or neuropathic pain, which are associated with localized compression of the median nerve at the wrist, and weakness and atrophy of the thenar muscle later in the course of the disease [5,6].

Nerve conduction studies are the technical gold standard for diagnosis [7]. CTS typically shows an elongation of the distal motor latency (DML) and a decrease in sensory nerve conduction velocity (CV) measured over the wrist. Principally, sensory changes occur before motor changes and changes in latencies and CV precedes changes in the amplitudes of compound motor action potentials (CMAP) and sensory nerve action potentials (SNAP). It is recommended that nerve conduction studies for the diagnosis of CTS be performed in patients with clinical manifestations of CTS [8].

Recently, peripheral nerve ultrasound was revealed to give valuable additional information; so, it has been advised to perform nerve ultrasound in addition to electrodiagnostic testing [9]. Sonographic diagnosis is based on a swelling of the median nerve at the inlet of the carpal tunnel (at the level of the pisiform bone), where an increase in the cross-sectional area (CSA) of the median nerve can be measured [10,11]. In addition, the wrist-to-forearm-ratio (WFR) compares the median nerve CSA at the wrist to the CSA 12 cm proximal at the forearm and shows a high sensitivity to detect CTS if the ratio is larger than 1.4 [12].

However, in diabetic patients, still controversies and uncertainties exist as to how far the diagnosis criteria for CTS may be valid for electrodiagnostic testing [13,14] and nerve ultrasound as well [15]. A major factor is generally seen in the coexistence of diabetic neuropathy, which also influences carpal tunnel measurements [16]. Most of the studies evaluated diabetic patients with the clinical diagnosis of CTS.

The clinical question here is how to interpret electrodiagnostic testing and ultrasound results for suspected CTS in patients with type 2 diabetes. Therefore, the aim of this study is to analyze patients with type 2 diabetes independent from the medical history of CTS or diabetic neuropathy in order to compare CTS symptoms (measured by the Boston Carpal Tunnel Questionnaire), diabetic neuropathy, nerve conduction studies, and peripheral nerve ultrasound of the median nerve.

2. Materials and Methods

2.1. Patients

We analyzed a database of patients with type 2 diabetes mellitus who participated in the still-ongoing SELECT study (Sonographic and electrophysiological characterization of peripheral nerves in patients with type 2 diabetes, German Clinical Trials Register DRKS00023026). All patients presented in the tertiary care outpatient clinic for diabetology at Jena University Hospital. The data were collected prospectively between September 2020 and April 2022. All participants gave written informed consent. The study was approved by the local ethics committee (number 2019-1416-BO).

Inclusion criteria were patients with type 2 diabetes, age between 40 and 85 years, willing to fill out questionnaires, and willing to undergo nerve conduction studies and peripheral nerve ultrasound. Exclusion criteria were known other etiologies for polyneuropathy (such as alcohol abuse, inflammatory polyneuropathies, etc.), rheumatic disease, peripheral arterial occlusive disease, active malignant tumor disease, and history of chemotherapy and CTS surgery.

2.2. Assessments

Several baseline parameters were collected: age, gender, duration of diabetes in years, body mass index (kg/m^2), HbA_{1c} (mmol/mol), and glomerular filtration rate (mL/min). HbA_{1c} was measured using high-performance liquid chromatography (TOSOH-Glykohaemoglobin-Analyzer HLC-723 GhbV, Tosoh Corporation, Tokyo, Japan).

Symptoms and deficits due to CTS were inquired using the Boston Carpal Tunnel Questionnaire (BCTQ) [17], which consisted of two parts: the Symptom Severity Scale (SSS) and the Functional Status Scale (FSS). The SSS included eleven questions and the answers ranged from 1 (no pain or difficulties) to 5 (severe/permanent pain or difficulties). The score (ranging from 11 to 55) discerns five degrees of severity (0 = asymptomatic to 4 = severely affected). The SSS is performed for each hand separately. The FSS includes eight activities in daily life, which are scored from 1 (no difficulties) to 5 (not feasible). The score (ranging from 8 to 40) also discerns five degrees of severity (0 = asymptomatic to 4 = severely affected). The German version of the BCTQ has been shown to have sufficient internal consistency, reliability, and validity to assess the health status in CTS [18].

Subjective symptoms due to diabetic polyneuropathy were evaluated using the Neuropathy Symptom Score (NSS) and the severity of sensory deficits using the Neuropathy Disability Score (NDS) [19]. NSS asks for sensory symptoms in the legs (burning, numbness, tingling, fatigue, cramping), the localization, time of appearance, and improvements.

Scores of 3–4 imply mild, 5–6 moderate, and 7–10 severe symptoms. The NDS checks ankle reflexes, vibration perception threshold (tuning fork), pain sensitivity (pin-prick), and temperature sensitivity. Scores of 3–5 imply mild, 6–8 moderate, and 9–10 severe deficits. Based on NSS and NDS scores, diabetic polyneuropathy can be diagnosed; if the NDS is between 6 and 8 or NDS is between 3 and 5 and NSS is between 5 and 6 [20].

Principally, the right median nerve was measured with nerve conduction studies (NCS) and peripheral nerve ultrasound, except if there was a pathology at the right wrist (such as complex regional pain syndrome, amputation, status after surgery, fractures, and others). In this exception, the left median nerve was measured (in 11 patients). The examiner was blinded with respect to the existence of CTS symptoms.

Nerve conduction studies (NCS) of the median nerve were performed by an experienced neurologist using a Medelec Synergy device (Synergy 15.0; Viasys Healthcare, Natus Europe GmbH, Planegg, Germany). Measurements were carried out on the median nerve (on the same side as the ultrasound measurements). Here, we measured the distal motor latency (DML), the amplitude of compound muscle action potential (CMAP) of the abductor pollicis brevis muscle, the sensory nerve conduction velocity (CV), and the amplitude of the sensory nerve action potential (SNAP) measured at the second finger (Figure 1A–C). The distance over the wrist between stimulation and recording electrode for motor NCS was kept constant at 7 to 8 cm. Skin temperature was controlled to be between 32 and 34 °C. Cut-off values in our laboratory for the median nerve are (according to [21]) DML 4.2 ms, CMAP amplitude 5.0 mV, sensory CV 45 m/s, and SNAP amplitude 6.9 µV.

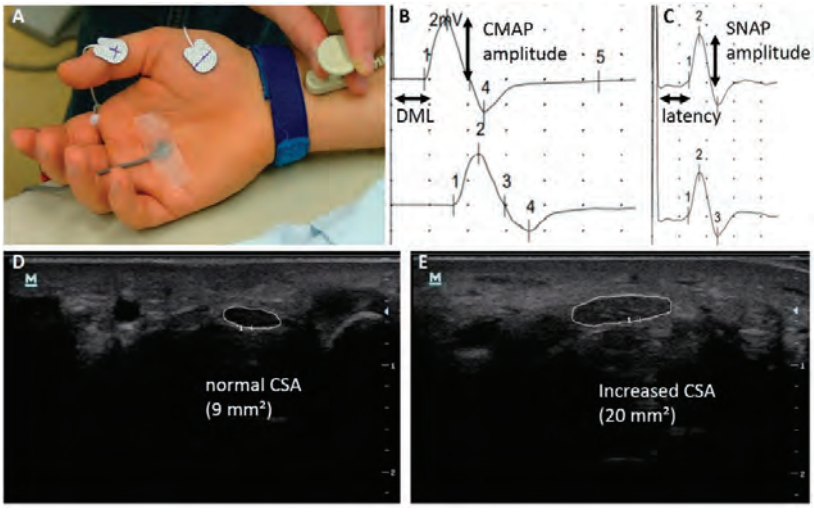

Figure 1. Nerve conduction studies and peripheral nerve ultrasound of the median nerve at the wrist. (**A**) Placement of electrodes. (**B**) Motor nerve conduction study. (**C**) Sensory nerve conduction study. (**D**) Normal cross-sectional area (CSA) of the median nerve. (**E**) Increased CSA of the median nerve. Abbreviations: CMAP, compound motor action potential; CSA, cross-sectional area; DML, distal motor latency; SNAP, sensory nerve action potential.

Sonographic examinations were performed by an experienced neurologist using a high-resolution ultrasound device (Mindray M7, Medical Australia Ltd., Ultrasound systems, Darmstadt, Germany) with a 14 MHz linear-array transducer. The median nerve was measured at the inlet of the carpal tunnel (at the level of the pisiform bone) and 12 cm proximal of the wrist at the forearm. We measured the CSA using direct-tracing technique around the inner margin of the hyperechoic epineural sheath (Figure 1B,D) and calculated the wrist-to-forearm-ratio. For the CSA of the median nerve at the level of the pisiforme

bone, a cut-off value of 10 mm^2 showed good diagnostic utility and a wrist-to-forearm-ratio of $\geq$1.4 showed a high sensitivity in the general population [22].

2.3. Statistics

All data were analyzed with the Statistical Package for the Social Sciences software (SPSS version 25.0; IBM Corporation, Armonk, NY, USA). The values were presented as mean and standard deviation (SD) or as numbers and percentages. First, we described the cohort using descriptive statistics.

Spearman correlations were used to analyze correlations between nerve conduction studies and peripheral nerve ultrasound. Unpaired t-test was used to analyze differences of measurements between patients with and without CTS symptoms and between patients with and without diabetic polyneuropathy. Linear regression was used to evaluate potential influences of clinical parameters on electrodiagnostic measurements and sonographic measurements. Finally, receiver operating characteristic (ROC) analysis was used to evaluate the potential of these measurements to differentiate between patients with and without CTS symptoms. For all analyses, a p value < 0.05 was considered statistically significant.

3. Results

3.1. Patients

At the time point of analysis, 88 patients were included in the SELECT cohort and were screened for eligibility for this study. Nine patients had CTS surgery before and 10 patients did not answer the BCTQ. Therefore, 19 patients had to be excluded from analysis. Thus, 69 patients with type 2 diabetes (26 female and 43 male) were finally included into this study. Tables 1 and 2 show the baseline characteristics of the patients. Fifty patients reported no CTS typical symptoms at the analyzed hand (BCTQ SSS = 0) and 19 patients only reported predominantly mild CTS symptoms. In contrast, 49 patients were diagnosed having typical signs of diabetic polyneuropathy (when NDS was between 6 and 8 or NDS was between 3 and 5 and NSS was between 5 and 6, according to [20]).

Table 1. Baseline characteristics of the patients (n = 69), categorical variables.

Variable		n	%
Sex	Female	26	37.7
	Male	43	62.3
BCTQ SSS at the measured hand	0	50	72.5
	1	17	24.6
	2	1	1.4
	3	1	1.4
BCTQ SSS right hand	0	50	72.5
	1	17	24.6
	2	1	1.4
	3	1	1.4
BCTQ SSS left hand	0	51	73.9
	1	16	23.2
	2	1	1.4
	3	1	1.4
BCTQ FSS	0	50	72.5
	1	18	26.1
	4	1	1.4
Polyneuropathy if NDS > 5 or (NDS > 2 and NSS > 4)	Yes	49	71.0
	No	20	29.0

Table 1. *Cont.*

Variable		n	%
NSS	No symptoms (0–2)	27	39.1
	Mild symptoms (3–4)	10	14.5
	Moderate symptoms (5–6)	16	23.2
	Severe symptoms (7–10)	17	24.6
NDS	No deficits (0–2)	9	13.2
	Mild deficits (3–5)	18	26.5
	Moderate deficits (6–8)	26	38.2
	Severe deficits (9–10)	15	22.1
CTS symptoms and diabetic polyneuropathy	Asymptomatic + no neuropathy	18	26.1
	CTS symptoms only	2	0.3
	Diabetic neuropathy only	32	46.4
	CTS symptoms and neuropathy	17	24.6

Abbreviations: BCTQ, Boston Carpal Tunnel Questionnaire; FSS, Functional Status Scale; NDS, Neuropathy Disability Score; NSS, Neuropathy Symptom Score; SSS, Symptom Severity Scale.

Table 2. Baseline characteristics of the patients (n = 69), metric variables.

Variable	Mean	SD	Minimum	Maximum
Age (years)	66.77	9.72	44	82
Duration of diabetes (years)	14.72	8.95	0.63	38
Body mass index (kg/m^2)	32.42	6.17	20.1	48.0
HbA_{1c} (mmol/mol)	59.08	10.94	27.98	82.51
Glomerular filtration rate (mL/min)	71.79	20.64	27.92	107.25
CSA median nerve at wrist (mm^2)	13.53	4.74	5.00	37.00
CSA median nerve at forearm (mm^2)	7.03	2.09	4.00	15.00
Wrist-to-forearm-ratio	2.05	0.76	0.33	4.75
Distal motor latency median nerve (ms)	4.42	0.67	3.50	6.15
CMAP amplitude median nerve (mV)	10.12	4.39	0	22.30
Sensory nerve CV median nerve (m/s)	43.26	7.84	29.0	63.6
SNAP amplitude median nerve (µV)	13.31	9.64	0	48.9
NSS (0–10 points)	3.84	3.23	0	9
NDS (0–10 points)	6.10	2.75	0	10

Abbreviations: CMAP, compound motor action potential; CSA, cross-sectional area; CV, conduction velocity; NDS, Neuropathy Disability Score; NSS, Neuropathy Symptom Score; SNAP, sensory nerve action potential.

3.2. Nerve Conduction Studies

Distal motor latencies of the right median nerve larger than 4.2 ms were found in 34 patients, and in two patients, no CMAP could be measured. Thirty-four patients showed sensory nerve conduction velocities slower than 45 m/s and five patients had no SNAPs. Figure 2 shows the measurements of nerve conduction studies. As expected, there was a correlation between DML and sensory conduction velocity (Spearman correlation coefficient of -0.532, $p < 0.001$). Using the Bland classification of neurophysiological severity of CTS [23], nine patients showed mild, twenty-two moderate, four severe, and two extremely severe neurophysiological measurements.

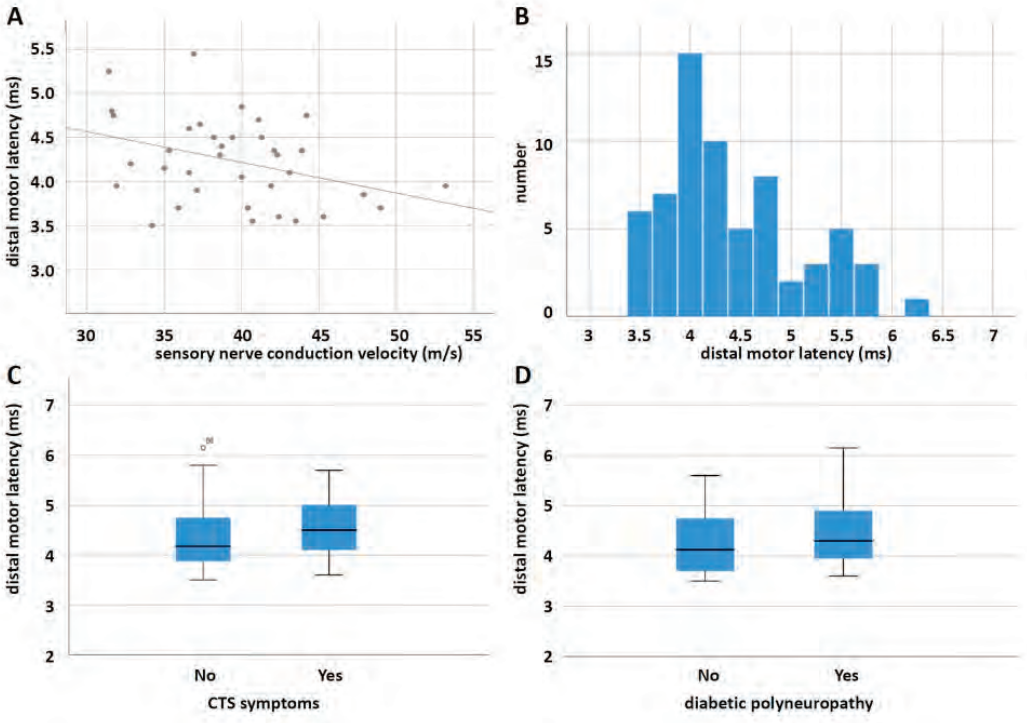

Figure 2. Nerve conduction studies of the median nerve. (**A**) Scatter plot of sensory nerve conduction velocity and distal motor latency. (**B**) Histogram of distal motor latencies. (**C**) Box plots of distal motor latencies in patients with and without CTS symptoms. (**D**) Box plots of distal motor latencies in patients with and without diabetic polyneuropathy.

DML did not show statistically significant differences between patients with and without CTS symptoms (Figure 2C, *t*-test: T = 1.151, $p = 0.254$) and between patients with and without diabetic polyneuropathy (Figure 2D, *t*-test: T = 1.465, $p = 0.148$).

3.3. Peripheral Nerve Ultrasound

Median nerve CSA at the wrist was between 10 and 12 mm^2 in 16 patients, between 12 and 15 mm^2 in 24 patients, and larger than 15 mm^2 in 21 patients. Sixty-one patients had a WFR $\geq$ 1.4. Figure 3 shows the ultrasound measurements of the median nerve.

Median nerve CSA at the wrist and wrist-to-forearm-ratio did not show any statistically significant differences between patients with and without CTS symptoms (Figure 3C, CSA: *t*-test, T = 0.621, $p = 0.537$; wrist-to-forearm-ratio: *t*-test, T = 0.161, $p = 0.873$) nor between patients with and without diabetic polyneuropathy (Figure 3D, CSA: *t*-test, T = 1.273, $p = 0.207$; wrist-to-forearm-ratio: *t*-test, T = 0.120, $p = 0.905$).

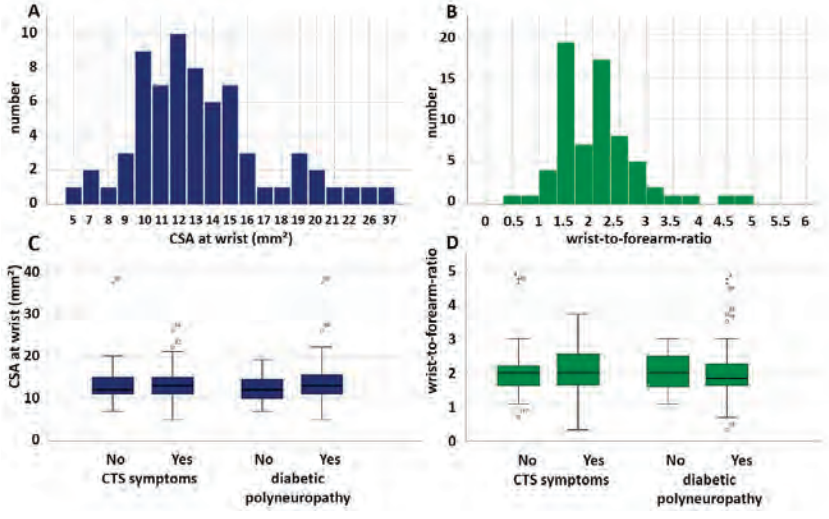

Figure 3. Peripheral nerve ultrasound measurements of the median nerve at the wrist. (**A**) Histogram of the CSA at the wrist. (**B**) Histogram of the wrist-to-forearm-ratio. (**C**) Box plots of median nerve CSA at the wrist in patients with and without CTS symptoms and patients with and without diabetic polyneuropathy. (**D**) Box plots of wrist-to-forearm-ratio in patients with and without CTS symptoms and patients with and without diabetic polyneuropathy.

3.4. Interactions

A correlation (Figure 4) between DML and median nerve CSA at the wrist (Spearman correlation coefficient of 0.406, $p = 0.001$) and between DML and wrist-to-forearm-ratio (Spearman correlation coefficient of 0.324, $p = 0.009$) could be found.

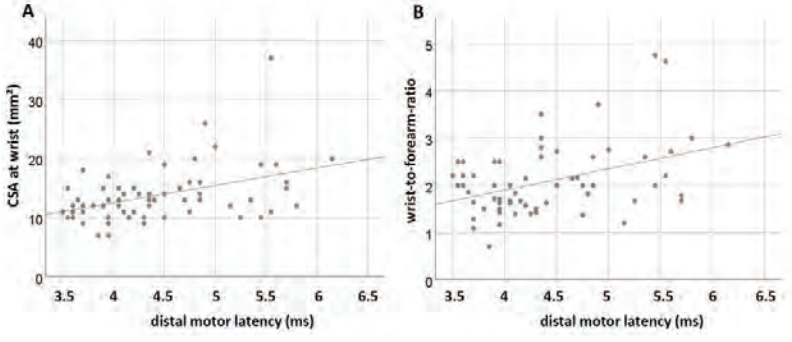

Figure 4. Scatterplots of distal motor latencies and peripheral nerve ultrasound measurements. (**A**) Distal motor latencies and median nerve CSA at the wrist. (**B**) Distal motor latencies and wrist-to-forearm-ratio.

Linear regression showed body mass index being a predictive variable for median nerve CSA and HbA_{1c} being a predictive variable for wrist-to-forearm-ratio (Table 3), although both had small R^2 (0.065 and 0.068, respectively).

Table 3. Linear regression.

Variable	Coefficient	Standard Error	*p*	Beta
Model1 with median nerve CSA as dependent variable (R^2 = 0.065)				
Constant	7.269	8.375	0.027	
Body mass index	0.197	0.102	0.047	0.255
Model2 with wrist-to-forearm-ration as dependent variable (R^2 = 0.068)				
Constant	1.036	3.206	0.052	
HbA_{1c}	0.018	0.097	0.043	0.260

Receiver operating characteristic (ROC) analysis showed that neither distal motor latency, cross-sectional area of the median nerve at the wrist, nor the wrist-to-forearm-ratio were able to distinguish between diabetic patients with and without symptoms for CTS (Figure 5). Area under the curve was 0.632 for the distal motor latency, 0.473 for the median nerve CSA, and 0.546 for the wrist-to-forearm-ratio.

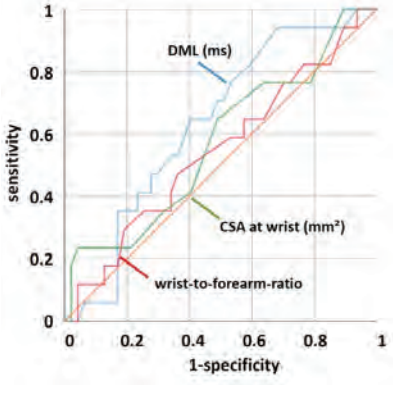

Figure 5. ROC curve analysis shows that DML, median nerve CSA at the wrist, and wrist-to-forearm-ratio were not suited to distinguish between diabetic patients with and without symptoms for CTS.

4. Discussion

Symptoms characteristic of CTS such as pain, numbness, and/or tingling in the median nerve distribution in the hands have been shown to have a prevalence of 14.4% in the general population, while CTS typical changes in nerve conduction studies of the median nerve have a prevalence of 4.9% [24]. According to the clinical diagnosis of CTS, the prevalence of CTS was 2% in the general population, 14% in diabetic patients without neuropathy, and 30% in patients with diabetic neuropathy [13].

In our study, patients with type 2 diabetes were examined regardless of having CTS or not. In this cohort, 50 patients did not report typical symptoms of CTS (according to the BCTQ), and the other 19 patients predominantly complained about mild symptoms. In contrast, 49 patients showed typical clinical signs of diabetic polyneuropathy (due to the NSS and NDS).

Electrodiagnostic testing is the technical gold standard to evaluate CTS [7]. It has been shown that approximately one quarter of diabetic patients had an electrophysiological, but clinically asymptomatic CTS while only 7.7% also had CTS symptoms [25]. A more recent study [14] found about 6.8% of persons with diabetes showing typical electrophysiological signs of CTS being clinically asymptomatic. Thus, it was suggested that asymptomatic CTS constellation in nerve conduction studies in diabetic patients are related to increased vulnerability of peripheral nerves at entrapment sites [14].

In our study, half of the patients showed a pathological increase in DML according to the cut-off values in our lab. Referring to the Bland classification [23] of electrophysiological severity of CTS, 37 patients met the diagnosis criteria for CTS and six patients were classified as severe or extremely severe. Thus, many more patients met the electrophysiological criteria for CTS diagnosis, while considerably fewer patients reported typical symptoms. The major hallmark of our study was that nerve conduction study was not able to differentiate between diabetic patients with CTS symptoms from diabetic patients without.

However, we did not use additional nerve conduction studies to increase sensitivity such as comparison studies of sensory-latency difference between the 2nd and 5th digit, between the median and ulnar part of the 4th digit, or between the median and radial thumb [26], which may be of additional value in diabetic patients.

Considering the results of peripheral nerve ultrasound in our study, the median nerve CSA at the wrist was larger than 12 mm^2 in 45 patients, and the wrist-to-forearm-ratio was larger than 1.4 in 61 patients.

It has been suggested before that sonographic assessment for the diagnosis of CTS requires a different cut-off value for diabetic patients [27]. A cut-off value for CSA of the median nerve at the wrist to diagnose coexisting CTS and diabetic polyneuropathy of 11.6 mm^2 was suggested (in contrast to the cut-off used for the diagnosis of CTS in nondiabetic patients of 9.2 mm^2) [28]. Others suggested a cut-off value of CSA at the wrist for CTS confirmation of more than 13 mm^2 in both diabetic and nondiabetic patients [29]. Overall, the cut-off values for CSA abnormality in CTS vary considerably in different studies and no consensus exists on a specific optimum cut-off value [9].

Nevertheless, ultrasound measurements in our study were not able to differentiate between patients with CTS symptoms and patients without, and even not between patients with polyneuropathy and those without.

A recent meta-analysis [15] of CSAs of the median nerve at the wrist level described larger CSA measurements in patient groups with both CTS and diabetes than in patients with CTS only and patients with diabetes only, and the smallest CSAs in normal controls. The wrist-to-forearm-ratio in CTS patients with diabetes was significantly lower than in nondiabetic patients, and no difference between the wrist-to-forearm-ratio could be demonstrated between diabetics with and without CTS [30]. It was suggested that an increase in median nerve CSA without change in the wrist-to-forearm-ratio might be an indicator of diabetic polyneuropathy [31]. However, this assumption could not be verified in our study.

In a study of patients with typical clinical symptoms of CTS, patients with diabetes tended to have a longer latency, smaller amplitude, and lower conduction velocity in nerve conduction studies compared to patients without diabetes mellitus, but the ultrasound CSA values did not differ significantly [32]. In contrast, it was found in a comparison between diabetic patients with symptomatic and asymptomatic CTS that the symptoms of CTS in patients with diabetes are related to CSA of the median nerve [33].

In a small percentage of patients with median nerve entrapment at the carpal tunnel, the CSA is abnormal at the outlet rather than the inlet of the carpal tunnel. However, we measured the CSA at the inlet only. CSA measurements at the outlet had possibly shown other results. In addition, other promising ultrasound techniques were not used in this study—particularly, the evaluation of echogenicity, the intraneural blood flow using Doppler ultrasound [9], or ultrasound elastography—to assess changes in stiffness of the nerve [34,35]. These techniques may provide additional information for CTS diagnosis but need more clinical evaluation.

Polyneuropathy is a common complication in diabetes mellitus [20]. In our study population, 49 (out of 69) patients had polyneuropathic symptoms. However, diabetic polyneuropathy causes alterations in nerve conduction studies [36,37] and in peripheral nerve ultrasound as well [27,38,39]. Generally, diabetic polyneuropathy leads to an enlargement of peripheral nerve CSAs with particular nerve enlargement at entrapment

sites [27,40]. These sonographic alterations are explicitly less pronounced than those found in demyelinating polyneuropathies [41,42].

The presence of diabetic polyneuropathy has been shown to be associated with an increase in CSA of the median nerve at the carpal tunnel [16,31]. In contrast, others found median nerve CSA at the wrist significantly smaller in patients with CTS and diabetic polyneuropathy compared with diabetic patients with CTS only [15,43].

We found a correlation between distal motor latency and median nerve CSA at the wrist and also between distal motor latency and wrist-to-forearm-ratio, which shows that sonographically enlarged nerves also have slower conduction velocities. This was already shown generally in polyneuropathy [42,44] but also in CTS measurements in patients with diabetic neuropathy [45]. Moreover, it demonstrates that the measurements in our study show the same physiological relationship as those found in other studies and, therefore, seem conclusive. Nevertheless, NCS is generally seen to be superior to ultrasound for the identification of superimposed CTS in diabetic polyneuropathy [45,46].

Besides the existence of polyneuropathy, there may be additional factors able to influence carpal tunnel measurements. In our cohort, we found a small but significant influence of body mass index on median nerve CSA and HbA_{1c} on wrist-to-forearm-ratio. It has been shown that CTS was significantly associated with high body mass index in diabetic patients [47] and generally in the normal population also [48,49]. In addition, higher levels of HbA_{1c} and plasma glucose levels were shown to be associated with an increased risk for CTS in diabetic patients [50]. This shows that the quality of long-term blood glucose control (measured by HbA_{1c}) has an impact on CTS ultrasound measurements and, therefore, should be taken into account. It has to be noted that body mass index and HbA_{1c} also have a strong correlation to each other [51,52].

Limitations of the study are the relatively small sample size and the single-center character of the study. All patients were cared for in a tertiary care outpatient clinic for diabetology, which may introduce some selection bias towards patients with potentially more complicated diabetes mellitus. In addition, the study was not primarily designed to study CTS in diabetes. If electrodiagnostic testing and ultrasound had been conducted on the most symptomatic wrist, the results would possibly have been different. However, BCTQ scores were not strikingly different between the left and right hand. Nevertheless, strengths of the study are the use of standardized scores for CTS and diabetic neuropathy in addition to standardized electrophysiological and ultrasound measurements.

5. Conclusions

In conclusion, the major finding of our study was that neither the distal motor latency of the median nerve, the cross-sectional area of the median nerve at the wrist, nor the wrist-to-forearm-ratio were able to distinguish between diabetic patients with and without CTS symptoms. This may especially be caused as electrodiagnostic testing and peripheral nerve ultrasound of the carpal tunnel in diabetic patients may significantly be altered due to the existence of additional factors such as diabetic neuropathy, but also body mass index, hyperglycemia, and others. Therefore, it is advisable to primarily rely upon typical symptoms and clinical signs of CTS in diabetic patients. Results of electrodiagnostic testing and peripheral nerve ultrasound have to be interpreted with caution and additional factors have to be considered, especially the existence of diabetic polyneuropathy.

Author Contributions: Conceptualization, B.H., N.M., C.K. and H.A.; methodology, B.H. and H.A.; validation, H.A. and A.G.; formal analysis, H.A. and B.H.; investigation, B.H., L.I.E.E.W. and N.J.K.; resources, B.H.; data curation, B.H.; writing—original draft preparation, H.A. and B.H.; writing—review and editing, A.G., N.M., C.K., L.I.E.E.W. and N.J.K.; visualization, H.A.; project administration, B.H. and H.A. All authors have read and agreed to the published version of the manuscript.

Funding: This work was funded by the Deutsche Forschungsgemeinschaft (DFG, German Research Foundation) Clinician Scientist Program OrganAge funding number 413668513 and by the Interdisciplinary Center of Clinical Research of the Medical Faculty Jena.

Institutional Review Board Statement: This study was carried out in accordance with the Declaration of Helsinki. The study was approved by the local ethics committee (ethics committee of the Friedrich-Schiller-University Jena, number 2019-1416-BO).

Informed Consent Statement: All participants gave written informed consent.

Data Availability Statement: The data used to support the findings of this study are available from the corresponding author upon request.

Conflicts of Interest: The authors declare no conflict of interest. The funders had no role in the design of the study; in the collection, analyses, or interpretation of data; in the writing of the manuscript, or in the decision to publish the results.

References

1. Zimmerman, M.; Gottsäter, A.; Dahlin, L.B. Carpal Tunnel Syndrome and Diabetes—A Comprehensive Review. *J. Clin. Med.* **2022**, *11*, 1674. [CrossRef] [PubMed]
2. De Krom, M.C.; Kester, A.D.; Knipschild, P.G.; Spaans, F. Risk Factors for Carpal Tunnel Syndrome. *Am. J. Epidemiol.* **1990**, *132*, 1102–1110. [CrossRef] [PubMed]
3. Gül Yurdakul, F.; Bodur, H.; Öztop Çakmak, Ö.; Ateş, C.; Sivas, F.; Eser, F.; Yılmaz Taşdelen, Ö. On the Severity of Carpal Tunnel Syndrome: Diabetes or Metabolic Syndrome. *J. Clin. Neurol.* **2015**, *11*, 234–240. [CrossRef] [PubMed]
4. Chen, L.-H.; Li, C.-Y.; Kuo, L.-C.; Wang, L.-Y.; Kuo, K.N.; Jou, I.-M.; Hou, W.-H. Risk of Hand Syndromes in Patients with Diabetes Mellitus: A Population-Based Cohort Study in Taiwan. *Medicine* **2015**, *94*, e1575. [CrossRef] [PubMed]
5. Doughty, C.T.; Bowley, M.P. Entrapment Neuropathies of the Upper Extremity. *Med. Clin. N. Am.* **2019**, *103*, 357–370. [CrossRef]
6. Padua, L.; Coraci, D.; Erra, C.; Pazzaglia, C.; Paolasso, I.; Loreti, C.; Caliandro, P.; Hobson-Webb, L.D. Carpal Tunnel Syndrome: Clinical Features, Diagnosis, and Management. *Lancet Neurol.* **2016**, *15*, 1273–1284. [CrossRef]
7. Sasaki, T.; Koyama, T.; Kuroiwa, T.; Nimura, A.; Okawa, A.; Wakabayashi, Y.; Fujita, K. Evaluation of the Existing Electrophysiological Severity Classifications in Carpal Tunnel Syndrome. *J. Clin. Med.* **2022**, *11*, 1685. [CrossRef]
8. Pugdahl, K.; Tankisi, H.; Fuglsang-Frederiksen, A. Electrodiagnostic Testing of Entrapment Neuropathies: A Review of Existing Guidelines. *J. Clin. Neurophysiol.* **2020**, *37*, 299–305. [CrossRef]
9. Pelosi, L.; Arányi, Z.; Beekman, R.; Bland, J.; Coraci, D.; Hobson-Webb, L.D.; Padua, L.; Podnar, S.; Simon, N.; van Alfen, N.; et al. Expert Consensus on the Combined Investigation of Carpal Tunnel Syndrome with Electrodiagnostic Tests and Neuromuscular Ultrasound. *Clin. Neurophysiol.* **2022**, *135*, 107–116. [CrossRef]
10. Cartwright, M.S.; Hobson-Webb, L.D.; Boon, A.J.; Alter, K.E.; Hunt, C.H.; Flores, V.H.; Werner, R.A.; Shook, S.J.; Thomas, T.D.; Primack, S.J.; et al. Evidence-Based Guideline: Neuromuscular Ultrasound for the Diagnosis of Carpal Tunnel Syndrome. *Muscle Nerve* **2012**, *46*, 287–293. [CrossRef]
11. Walker, F.O.; Cartwright, M.S.; Alter, K.E.; Visser, L.H.; Hobson-Webb, L.D.; Padua, L.; Strakowski, J.A.; Preston, D.C.; Boon, A.J.; Axer, H.; et al. Indications for Neuromuscular Ultrasound: Expert Opinion and Review of the Literature. *Clin. Neurophysiol.* **2018**, *129*, 2658–2679. [CrossRef] [PubMed]
12. Hobson-Webb, L.D.; Massey, J.M.; Juel, V.C.; Sanders, D.B. The Ultrasonographic Wrist-to-Forearm Median Nerve Area Ratio in Carpal Tunnel Syndrome. *Clin. Neurophysiol.* **2008**, *119*, 1353–1357. [CrossRef] [PubMed]
13. Perkins, B.A.; Olaleye, D.; Bril, V. Carpal Tunnel Syndrome in Patients with Diabetic Polyneuropathy. *Diabetes Care* **2002**, *25*, 565–569. [CrossRef] [PubMed]
14. Kim, W.K.; Kwon, S.H.; Lee, S.H.; Sunwoo, I.N. Asymptomatic Electrophysiologic Carpal Tunnel Syndrome in Diabetics: Entrapment or Polyneuropathy. *Yonsei Med. J.* **2000**, *41*, 123–127. [CrossRef]
15. Chen, I.-J.; Chang, K.-V.; Lou, Y.-M.; Wu, W.-T.; Özçakar, L. Can Ultrasound Imaging Be Used for the Diagnosis of Carpal Tunnel Syndrome in Diabetic Patients? A Systemic Review and Network Meta-Analysis. *J. Neurol.* **2020**, *267*, 1887–1895. [CrossRef]
16. Attah, F.A.; Asaleye, C.M.; Omisore, A.D.; Kolawole, B.A.; Aderibigbe, A.S.; Alo, M. Relationship between Sonographically Measured Median Nerve Cross-Sectional Area and Presence of Peripheral Neuropathy in Diabetic Subjects. *World J. Diabetes* **2019**, *10*, 47–56. [CrossRef]
17. Levine, D.W.; Simmons, B.P.; Koris, M.J.; Daltroy, L.H.; Hohl, G.G.; Fossel, A.H.; Katz, J.N. A Self-Administered Questionnaire for the Assessment of Severity of Symptoms and Functional Status in Carpal Tunnel Syndrome. *J. Bone Joint Surg. Am.* **1993**, *75*, 1585–1592. [CrossRef]
18. Keilani, M.Y.; Pernicka, E.; Paternostro-Sluga, T.; Sycha, T.; Schett, G.; Pieber, K.; Fialka-Moser, V.; Crevenna, R. Übersetzung und Validierung des "Boston Carpal Tunnel Syndrome Questionnaire" zum Einsatz bei deutschsprachigen Patienten. *Phys. Med. Rehab. Kurortmed.* **2008**, *18*, 136–144. [CrossRef]
19. Young, M.J.; Boulton, A.J.; MacLeod, A.F.; Williams, D.R.; Sonksen, P.H. A Multicentre Study of the Prevalence of Diabetic Peripheral Neuropathy in the United Kingdom Hospital Clinic Population. *Diabetologia* **1993**, *36*, 150–154. [CrossRef]
20. Ziegler, D.; Keller, J.; Maier, C.; Pannek, J. Diabetic Neuropathy. *Exp. Clin. Endocrinol. Diabetes* **2021**, *129*, S70–S81. [CrossRef]
21. Stöhr, M.; Pfister, R. *Klinische Elektromyographie und Neurographie—Lehrbuch und Atlas*, 6th ed.; Kohlhammer: Stuttgart, Germany, 2014; pp. 397–399.

22. Linehan, C.; Childs, J.; Quinton, A.E.; Aziz, A. Ultrasound Parameters to Identify and Diagnose Carpal Tunnel Syndrome. A Review of the Literature. *Australas. J. Ultrasound Med.* **2020**, *23*, 194–206. [CrossRef] [PubMed]
23. Bland, J.D. A Neurophysiological Grading Scale for Carpal Tunnel Syndrome. *Muscle Nerve* **2000**, *23*, 1280–1283. [CrossRef]
24. Atroshi, I.; Gummesson, C.; Johnsson, R.; Ornstein, E.; Ranstam, J.; Rosén, I. Prevalence of Carpal Tunnel Syndrome in a General Population. *JAMA* **1999**, *282*, 153–158. [CrossRef]
25. Dyck, P.J.; Kratz, K.M.; Karnes, J.L.; Litchy, W.J.; Klein, R.; Pach, J.M.; Wilson, D.M.; O'Brien, P.C.; Melton, L.J.; Service, F.J. The Prevalence by Staged Severity of Various Types of Diabetic Neuropathy, Retinopathy, and Nephropathy in a Population-Based Cohort: The Rochester Diabetic Neuropathy Study. *Neurology* **1993**, *43*, 817–824. [CrossRef]
26. Alanazy, M.H. Clinical and Electrophysiological Evaluation of Carpal Tunnel Syndrome: Approach and Pitfalls. *Neurosciences* **2017**, *22*, 169–180. [CrossRef]
27. Kang, S.; Kim, S.H.; Yang, S.N.; Yoon, J.S. Sonographic Features of Peripheral Nerves at Multiple Sites in Patients with Diabetic Polyneuropathy. *J. Diabetes Complic.* **2016**, *30*, 518–523. [CrossRef] [PubMed]
28. Kim, L.-N.; Kwon, H.-K.; Moon, H.-I.; Pyun, S.-B.; Lee, H.-J. Sonography of the Median Nerve in Carpal Tunnel Syndrome with Diabetic Neuropathy. *Am. J. Phys. Med. Rehabil.* **2014**, *93*, 897–907. [CrossRef] [PubMed]
29. Tsai, N.-W.; Lee, L.-H.; Huang, C.-R.; Chang, W.-N.; Wang, H.-C.; Lin, Y.-J.; Lin, W.-C.; Lin, T.-K.; Cheng, B.-C.; Su, Y.-J.; et al. The Diagnostic Value of Ultrasonography in Carpal Tunnel Syndrome: A Comparison between Diabetic and Non-Diabetic Patients. *BMC Neurol.* **2013**, *13*, 65. [CrossRef]
30. Steinkohl, F.; Loizides, A.; Gruber, L.; Karpf, M.; Mörsdorf, G.; Gruber, I.; Glodny, B.; Löscher, W.; Gruber, H. Ultrasonography for the Diagnosis of Carpal Tunnel Syndrome in Diabetic Patients: Missing the Mark? *Rofo* **2019**, *191*, 117–121. [CrossRef]
31. Moon, H.I.; Kwon, H.K.; Kim, L.; Lee, H.J.; Lee, H.J. Ultrasonography of Palm to Elbow Segment of Median Nerve in Different Degrees of Diabetic Polyneuropathy. *Clin. Neurophysiol.* **2014**, *125*, 844–848. [CrossRef]
32. Kim, Y.H.; Yang, K.S.; Kim, H.; Seok, H.Y.; Lee, J.H.; Son, M.H.; Kim, B.J. Does Diabetes Mellitus Influence Carpal Tunnel Syndrome? *J. Clin. Neurol.* **2017**, *13*, 243–249. [CrossRef] [PubMed]
33. Han, H.Y.; Kim, H.M.; Park, S.Y.; Kim, M.-W.; Kim, J.M.; Jang, D.-H. Clinical Findings of Asymptomatic Carpal Tunnel Syndrome in Patients with Diabetes Mellitus. *Ann. Rehabil. Med.* **2016**, *40*, 489–495. [CrossRef] [PubMed]
34. Sung, J.H.; Kwon, Y.J.; Baek, S.-H.; Son, M.H.; Lee, J.H.; Kim, B.-J. Utility of Shear Wave Elastography and High-Definition Color for Diagnosing Carpal Tunnel Syndrome. *Clin. Neurophysiol.* **2022**, *135*, 179–187. [CrossRef]
35. Liu, F.; Li, D.; Xin, Y.; Liu, F.; Li, W.; Zhu, J. Quantification of Nerve Viscosity Using Shear Wave Dispersion Imaging in Diabetic Rats: A Novel Technique for Evaluating Diabetic Neuropathy. *Korean J. Radiol.* **2022**, *23*, 237–245. [CrossRef] [PubMed]
36. Padua, L.; Saponara, C.; Ghirlanda, G.; Padua, R.; Aprile, I.; Caliandro, P.; Tonali, P. Lower Limb Nerve Impairment in Diabetic Patients: Multiperspective Assessment. *Eur. J. Neurol.* **2002**, *9*, 69–73. [CrossRef]
37. Dunnigan, S.K.; Ebadi, H.; Breiner, A.; Katzberg, H.D.; Lovblom, L.E.; Perkins, B.A.; Bril, V. Conduction Slowing in Diabetic Sensorimotor Polyneuropathy. *Diabetes Care* **2013**, *36*, 3684–3690. [CrossRef]
38. Agirman, M.; Yagci, I.; Leblebicier, M.A.; Ozturk, D.; Akyuz, G.D. Is Ultrasonography Useful in the Diagnosis of the Polyneuropathy in Diabetic Patients? *J. Phys. Ther. Sci.* **2016**, *28*, 2620–2624. [CrossRef]
39. Watanabe, T.; Ito, H.; Sekine, A.; Katano, Y.; Nishimura, T.; Kato, Y.; Takeda, J.; Seishima, M.; Matsuoka, T. Sonographic Evaluation of the Peripheral Nerve in Diabetic Patients: The Relationship between Nerve Conduction Studies, Echo Intensity, and Cross-Sectional Area. *J. Ultrasound Med.* **2010**, *29*, 697–708. [CrossRef]
40. Ma, X.; Li, T.; Du, L.; Liu, G.; Sun, T.; Han, T. Applicability of High-Frequency Ultrasound to the Early Diagnosis of Diabetic Peripheral Neuropathy. *Biomed Res. Int.* **2021**, *2021*, 5529063. [CrossRef]
41. Grimm, A.; Vittore, D.; Schubert, V.; Rasenack, M.; Décard, B.F.; Heiling, B.; Hammer, N.; Axer, H. Ultrasound Aspects in Therapy-Naive CIDP Compared to Long-Term Treated CIDP. *J. Neurol.* **2016**, *263*, 1074–1082. [CrossRef]
42. Grimm, A.; Heiling, B.; Schumacher, U.; Witte, O.W.; Axer, H. Ultrasound Differentiation of Axonal and Demyelinating Neuropathies. *Muscle Nerve* **2014**, *50*, 976–983. [CrossRef] [PubMed]
43. Kotb, M.A.; Bedewi, M.A.; Aldossary, N.M.; Mahmoud, G.; Naguib, M.F. Sonographic Assessment of Carpal Tunnel Syndrome in Diabetic Patients with and without Polyneuropathy. *Medicine* **2018**, *97*, e11104. [CrossRef] [PubMed]
44. Di Pasquale, A.; Morino, S.; Loreti, S.; Bucci, E.; Vanacore, N.; Antonini, G. Peripheral Nerve Ultrasound Changes in CIDP and Correlations with Nerve Conduction Velocity. *Neurology* **2015**, *84*, 803–809. [CrossRef]
45. Drăghici, N.C.; Tămaș, M.M.; Leucuța, D.C.; Lupescu, T.D.; Strilciuc, Ș.; Rednic, S.; Mureșanu, D.F. Diagnosis Accuracy of Carpal Tunnel Syndrome in Diabetic Neuropathy. *Medicina* **2020**, *56*, 279. [CrossRef]
46. Hassan, A.; Leep Hunderfund, A.N.; Watson, J.; Boon, A.J.; Sorenson, E.J. Median Nerve Ultrasound in Diabetic Peripheral Neuropathy with and without Carpal Tunnel Syndrome. *Muscle Nerve* **2013**, *47*, 437–439. [CrossRef]
47. Bekele, A.; Abebe, G.; Hailu, T.; Fekadu, T.; Gebremickael, A.; Getachew, T.; Churko, C.; Alelign, D.; Wassihun, B.; Teshome, D.; et al. Prevalence and Associated Factors of Carpal Tunnel Syndrome Among Diabetic Patients in Arba Minch General Hospital, South West Ethiopia, 2021. *Diabetes Metab. Syndr. Obes.* **2022**, *15*, 983–993. [CrossRef] [PubMed]
48. Lampainen, K.; Shiri, R.; Auvinen, J.; Karppinen, J.; Ryhänen, J.; Hulkkonen, S. Weight-Related and Personal Risk Factors of Carpal Tunnel Syndrome in the Northern Finland Birth Cohort 1966. *J. Clin. Med.* **2022**, *11*, 1510. [CrossRef]

49. Wiberg, A.; Smillie, R.W.; Dupré, S.; Schmid, A.B.; Bennett, D.L.; Furniss, D. Replication of Epidemiological Associations of Carpal Tunnel Syndrome in a UK Population-Based Cohort of over 400,000 People. *J. Plast. Reconstr. Aesthet. Surg.* **2022**, *75*, 1034–1040. [CrossRef] [PubMed]
50. Rydberg, M.; Zimmerman, M.; Gottsäter, A.; Nilsson, P.M.; Melander, O.; Dahlin, L.B. Diabetes Mellitus as a Risk Factor for Compression Neuropathy: A Longitudinal Cohort Study from Southern Sweden. *BMJ Open Diabetes Res. Care* **2020**, *8*, e001298. [CrossRef]
51. Boye, K.S.; Lage, M.J.; Thieu, V.; Shinde, S.; Dhamija, S.; Bae, J.P. Obesity and Glycemic Control among People with Type 2 Diabetes in the United States: A Retrospective Cohort Study Using Insurance Claims Data. *J. Diabetes Complic.* **2021**, *35*, 107975. [CrossRef]
52. Ngiam, K.Y.; Lee, W.-J.; Lee, Y.-C.; Cheng, A. Efficacy of Metabolic Surgery on HbA1c Decrease in Type 2 Diabetes Mellitus Patients with BMI < 35 kg/m^2—A Review. *Obes. Surg.* **2014**, *24*, 148–158. [CrossRef] [PubMed]

Ultrasonography: Sports Injuries

16

Gina M. Allen and Jon A. Jacobson

Learning Objectives

- To understand the value of ultrasound in the examination of sports injuries.
- To be familiar with common sport-related disease of the upper extremity.
- To be familiar with common sport-related disease of the lower extremity.

16.1 Upper Extremity

16.1.1 Introduction

Ultrasound is an effective imaging method for evaluation of upper extremity sports injuries. For evaluation of the shoulder, ultrasound is ideal in assessment of the rotator cuff, the biceps brachii tendon and the subacromial-subdeltoid bursa. Evaluation of the cartilaginous structures of the shoulder is significantly limited, and therefore MRI and preferably MR arthrography are considered in this scenario. An algorithm based on patient age is often used, where patients over the age of 40 years often are evaluated with ultrasound and patients under 40 years are evaluated with MRI or MR arthrography. This algorithm is used as patients under the age of 40 years will often have articular-sided partial-thickness rotator cuff tears and concomitant labral pathology, both of which are ideally seen with MRI [1]. Beyond the shoulder, ultrasound is most accurate when the indication for imaging is targeted and the structure imaged is superficial. Last, ultrasound complements MRI given its ability to dynamically assess pathology of the upper extremity. Given the superficial location of soft tissue abnormalities, a linear transducer of greater than 12 MHz is preferred, and a small footprint probe is used for the most distal aspects of the upper extremity.

16.1.2 Shoulder

The rotator cuff is the most commonly imaged tendon group using ultrasound, where its accuracy in the diagnosis of cuff pathology is equal to MRI. Unlike the distal aspects of the upper extremity, a protocol-based evaluation with ultrasound is recommended as symptoms do not always directly correlate with pathology, and symptoms may also be multifactorial in aetiology [2]. Each individual rotator cuff tendon (supraspinatus, infraspinatus, subscapularis, teres minor) is imaged in short and long axis. Given the curvature of the humeral head and the overlying supraspinatus, care must be taken not to misinterpret artefactual hypoechogenicity from anisotropy as tendon abnormality. Pathology of the rotator cuff, similar to other tendons, include tendinosis and tendon tear. The term tendinosis is used rather than tendinitis as inflammation diminishes after the first week after a tendon injury [3]. Tendinosis refers to mucoid degeneration and chondroid metaplasia of the involved tendon [4, 5]. At ultrasound, tendinosis will appear as abnormal hypoechogenicity with possible increased in tendon thickness [6]. Tendon tear will appear as a well-defined hypoechoic or anechoic defect in the normal hyperechoic fibrillar tendon architecture. Such tendon tears may be partial-thickness and only involve the articular surface, bursal surface or may be intrasubstance (or interstitial) not contacting either the articular (Fig. 16.1) or bursal surface of the tendon, although isolated greater tuberosity extension is common. A full-thickness tear will extend from the articular to bursal surface of the tendon. Of note, most supraspinatus tendon tears extend to the greater tuberosity footprint, which creates the cortical irregularity as a

G. M. Allen
St Luke's Radiology Oxford Ltd, Oxford, Oxfordshire, UK

J. A. Jacobson (✉)
Radiology, University of Michigan, Ann Arbor, MI, USA

J. Hodler et al. (eds.), *Musculoskeletal Diseases 2021–2024*, IDKD Springer Series,
https://doi.org/10.1007/978-3-030-71281-5_16

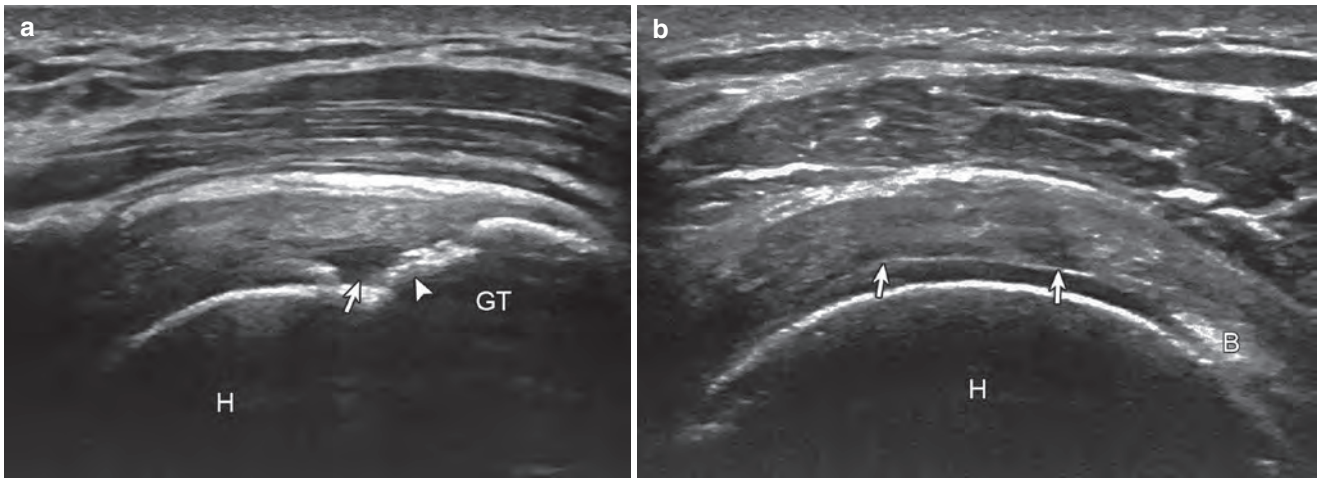

Fig. 16.1 Supraspinatus tear: articular side partial-thickness. Ultrasound images long axis (**a**) and short axis (**b**) to supraspinatus tendon show hypoechoic tendon tear (arrows) extending to the articular surface of the humeral head (H). Note cortical irregularity (arrowhead) of greater tuberosity (GT). *B* Biceps brachii long head tendon in rotator interval

very important indirect sign in such tears in patients over the age of 40 years [6, 7]. Once a tear is identified, the short- and long-axis dimensions, as well as per cent tear depth (in the case of partial-thickness tears), are measured and included in the imaging report. Chronic and large full-thickness tears, especially those involving the anterior aspect of the supraspinatus, are associated with tendon retraction and subsequent infraspinatus and supraspinatus fatty infiltration and possible muscle atrophy [8]. This information should be included in the imaging report as muscle atrophy is associated with poor outcomes after surgical repair of a rotator cuff tear [9].

Another structure commonly imaged with ultrasound is the biceps brachii long head tendon. While the most proximal aspect of the biceps brachii long head tendon at the labrum is not visible with ultrasound, the segment in the bicipital groove and more proximally into the glenohumeral joint are well seen, with the latter best seen with the shoulder in the modified Crass position. Fluid distention of the biceps brachii long head tendon sheath is most commonly from extension of a glenohumeral joint effusion. Heterogeneous or focal distention with hyperemia and focal symptoms would suggest true tenosynovitis. Tendinosis will appear as abnormal hypoechogenicity and possible increased tendon thickness, partial-thickness tears will appear as surface irregularity and hypoechoic or anechoic clefts, and a full-thickness tear will show complete tendon discontinuity [10]. The thin hyperechoic aponeurotic expansion of the supraspinatus should not be confused with a longitudinal split of the biceps brachii [11]. Unlike a longitudinal split, the aponeurotic expansion characteristically is located anterior the tendon and blends into the supraspinatus tendon when imaging proximally. Ultrasound may also be used to dynamically assess for biceps brachii tendon subluxation and dislocation and guide percutaneous tendon sheath injection [12].

Another common structure that is abnormal with overuse injuries is the subacromial-subdeltoid bursa. This composite bursa is quite extensive located deep to the deltoid and covering portions of the supraspinatus, infraspinatus, subscapularis, biceps brachii long head and proximal humerus. Distention of the bursa may range from anechoic fluid to hypoechoic or hyperechoic synovial hypertrophy [13]. To diagnose subacromial impingement with ultrasound, the arm is abducted, and ultrasound will reveal gradual distention of the subacromial-subdeltoid bursa at the edge of the acromion; however, this finding may be found in asymptomatic individuals, and clinical correlation is required [14]. Ultrasound may also be used to guide percutaneous bursal injection.

Key Points

- Cortical irregularity of the greater tuberosity is a helpful secondary sign of a supraspinatus tear.
- Fluid surrounding the biceps brachii long head tendon is most commonly due to a communicating glenohumeral joint effusion.
- Subacromial-subdeltoid bursal distention can range from anechoic fluid to hyperechoic synovial hypertrophy.

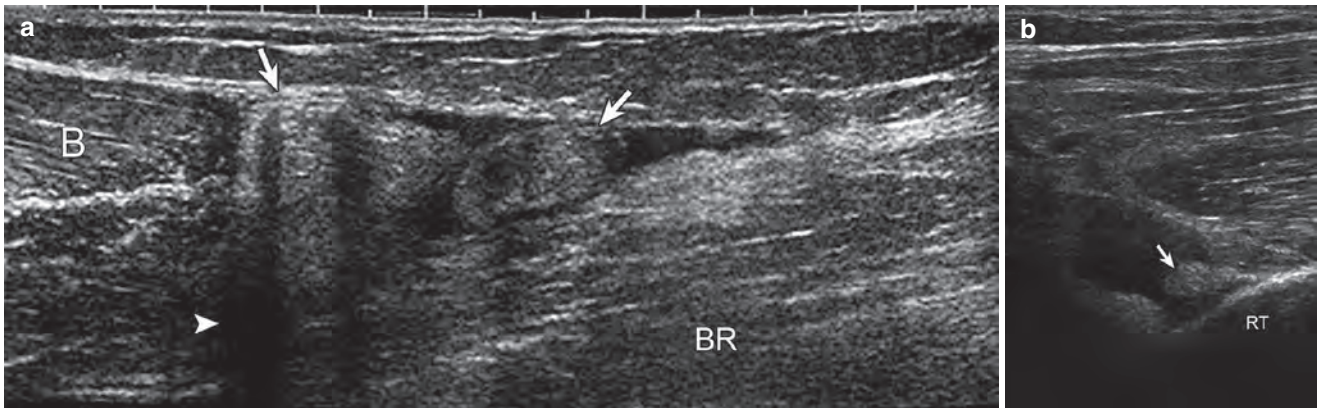

Fig. 16.2 Biceps brachii: full-thickness tear. Ultrasound images show (**a**) proximal and (**b**) distal stumps of the torn and retracted biceps brachii (arrows). Note refractions shadowing (arrowhead) deep to recoiled proximal stump in (**a**). *B* biceps brachii muscle, *BR* brachialis muscle, *RT* radial tuberosity

16.1.3 Elbow

The distal biceps brachii tendon may show findings of tendinosis (hypoechoic enlargement), partial-thickness tear (anechoic clefts) and full-thickness tear (complete tendon discontinuity) (Fig. 16.2) associated with sports injuries [15]. Ultrasound imaging of the distal biceps brachii tendon is often difficult given the oblique course of the distal tendon and resulting anisotropy. Imaging the biceps tendon from a medial or pronator window approach, with possible elbow flexion, is often helpful [16]. Partial-thickness biceps tears may involve one of the two heads, commonly the more superficial short head, which can create refraction shadowing artefact possibly obscuring the deeper long head tendon. In differentiating partial-thickness from a full-thickness tendon tear, the use of dynamic evaluation is helpful, either imaging from a medial or lateral approach [17]. With supination and pronation, lack of tendon movement to the same degree as radial tuberosity rotation is indirect evidence of a full-thickness tear. Often full-thickness distal biceps brachii tendon tears will be associated with significant tendon retraction.

Distal triceps brachii tendon tear are also effectively assessed with ultrasound. Partial-thickness tears often involve the superficial combined long and lateral heads, associated with an avulsed enthesophyte bone fragment (Fig. 16.3) [18]. The deeper medial head is often intact but may be erroneously interpreted as torn given that the medial head tendon is very short. Tendinosis may uncommonly involve the distal triceps brachii tendon, as well as distention of the overlying olecranon bursa.

Epicondylitis may also be diagnosed with ultrasound. With lateral (tennis elbow) more common than medial (golfer's elbow), the term "epicondylitis" is a misnomer in that it is not a primary epicondyle problem and is not actively inflamed [19]. The underlying pathology, similar to other tendons, represents tendinosis, interstitial tear or uncommonly full-thickness tear (Fig. 16.4). The presence of hyperemia on colour Doppler imaging correlates with symptoms and represents neovascularity rather than an indirect sign of inflammation.

The ulnar collateral ligament is evaluated dynamically with ultrasound and complements MR arthrography where the accuracy in diagnosis of tear is highest when both imaging methods are used [20]. With the elbow flexed at least 30°, valgus stress is placed across the elbow. Asymmetric widening of the medial joint space between the humerus and ulna with valgus stress can indicate ligament tear [20]. The ulnar nerve can also be imaged by dynamic ultrasound to assess for injury or subluxation.

Key Points

- Evaluating the biceps brachii tendon medially and laterally complements anterior evaluation.
- Triceps brachii partial tears most commonly involve the superficial layer with avulsion of an enthesophyte.
- Hyperemia of the common extensor tendon represents neovascularity and not inflammation.
- Dynamic evaluation of the ulnar collateral ligament with valgus stress assesses joint space gapping to indicate tear.

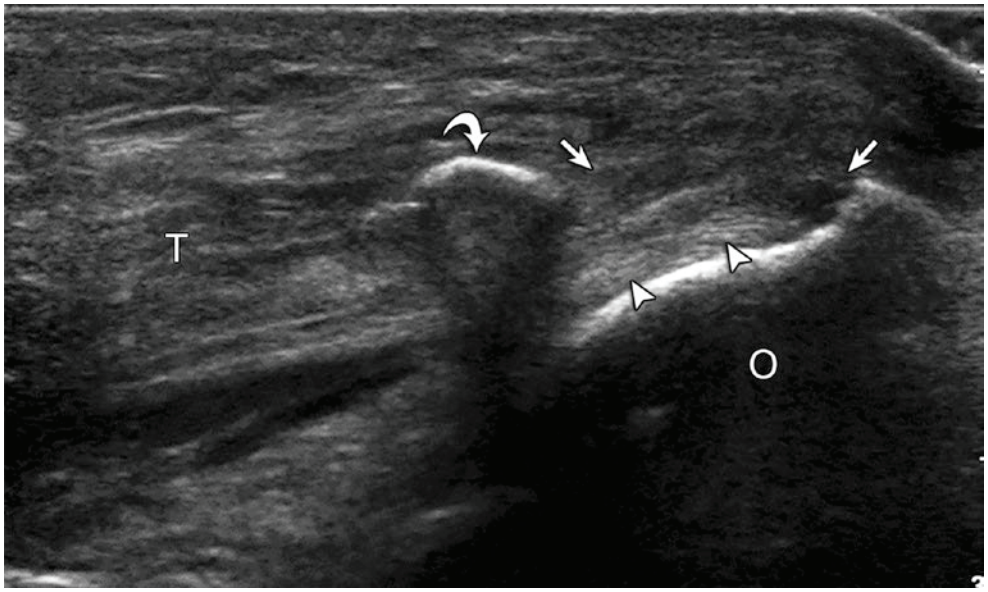

Fig. 16.3 Triceps brachii: partial-thickness tear. Ultrasound image long axis to triceps brachii (T) shows retracted tear of superficial combined lateral and long head tendons (between arrows) with hyperechoic and shadowing enthesophyte avulsion fragment (curved arrow). Note intact deep medial head of triceps brachii (arrowheads). *O* olecranon process

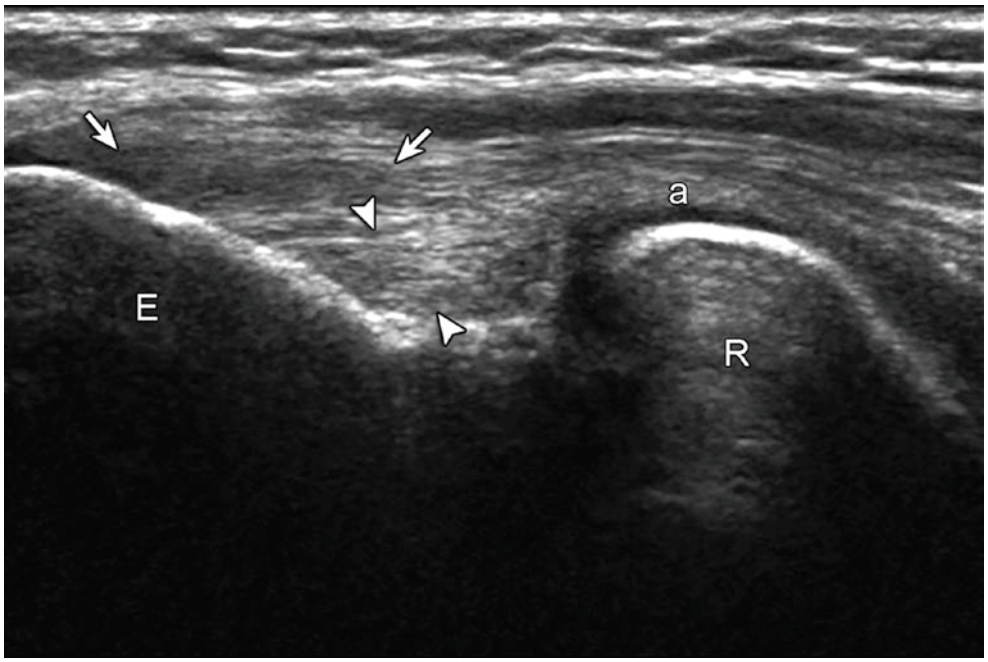

Fig. 16.4 Common extensor tendon abnormality (lateral epicondylitis). Ultrasound image long axis to common extensor tendon shows hypoechoic tendinosis (arrows). Note radial collateral ligament proper (arrowheads). *E* lateral epicondyle, *R* radial head, *a* annular ligament

16.1.4 Wrist and Hand

Sports injuries of the hand and wrist are often ligamentous or related to the triangular fibrocartilage complex, which are best evaluated with MR or preferably MR arthrography; however, ultrasound can be used to evaluate focal tendon abnormalities. For example, intersection syndrome will appear as asymmetric hypoechoic swelling, oedema and possible hyperemia where the first extensor wrist compartment muscles (extensor pollicis longus and abductor pollicis brevis) cross over the second extensor wrist compartment (extensor carpi radialis longus and brevis) [21]. This can be very subtle and a very light pressure on the transducer is needed to see fluid in these cases. Full-thickness tendon tears are often associated with tendon retraction. Related to the extensor tendons, sagittal band injury at the level of the metacarpophalangeal joints is diagnosed when abnormal hypoechogenicity is seen with asymmetric location of the extensor tendon, best seen dynamically with flexion at the metacarpophalangeal joints, termed Boxer's knuckle [22]. Related to the flexor tendons of the fingers, ultrasound is effective in evaluation of the pulleys of the digits. Non-

visualisation of a pulley can indicate injury; however, the finding of tendon bowstringing is an important indirect sign of pulley injury, which appears as an abnormal position of the flexor tendon not approximated to the phalanx (Fig. 16.5). Bowstringing is evaluated dynamically with active finger flexion against resistance where a distance between the flexor tendon and phalanx greater than 1 mm indicates pulley injury; a distance greater than 3 mm indicates a complete A2 pulley tear; and a distance of 5 mm indicates a combined complete tears of A2 and A4 pulleys [23].

One ligament that is ideally assessed with ultrasound is the ulnar collateral ligament of the thumb [24]. Injury to this ligament, termed skier's or gamekeeper's thumb, can range from sprain (hypoechoic swelling), partial tear (partial anechoic defect) and complete tear (discontinuous ligament), with the latter either being non-displaced or displaced [25]. A displaced ulnar collateral ligament tear with an interposed adductor aponeurosis is termed a Stener lesion. Ultrasound is able to diagnose a Stener lesion with 100% accuracy [24]. Key to evaluation is correct placement of the transducer in the coronal plane relative to the thumb with visualisation of the characteristic bone contours at the expected attachments of the ulnar collateral ligament. The adductor aponeurosis is identified as a thin hypoechoic structure that normally overlies the intact ulnar collateral ligament, where flexion and extension at the interphalangeal joint cause isolated movement of the aponeurosis, which aides in its identification. The distal aspect of the displaced ulnar collateral ligament is identified as a hypoechoic round abnormality proximal to the metacarpal joint (Fig. 16.6), with a possible hyperechoic and shadowing avulsion bone fragment. The end of the torn ligament may be seen superficial to the adductor aponeurosis or may be seen along the distal metacarpal shaft with the ligament coursing proximal.

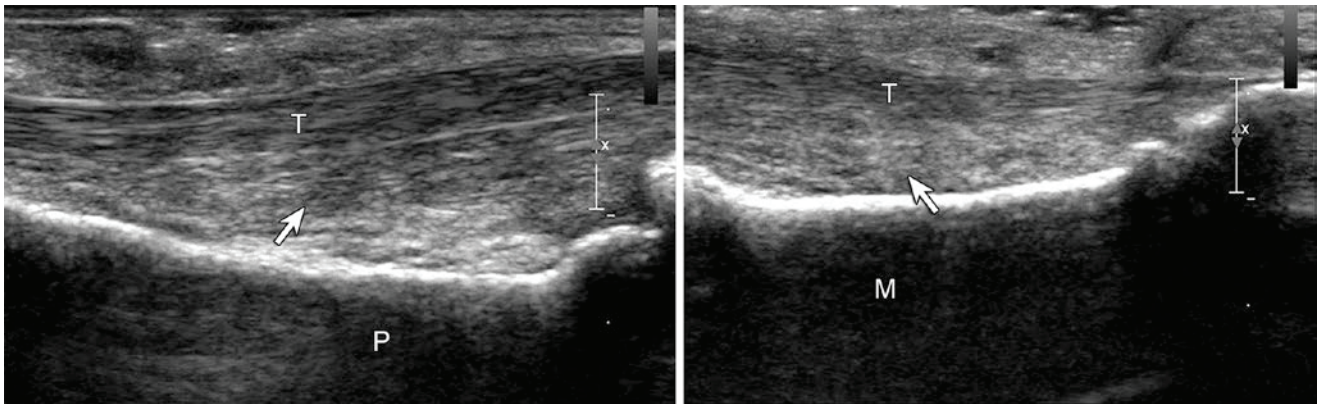

Fig. 16.5 Pulley injury. Ultrasound image long axis to the flexor tendons (T) of the finger shows abnormal volar displacement or bowstringing of the tendons (arrows) opposite the proximal (P) and middle (M) phalanges indicating A2 and A4 pulley tears, respectively

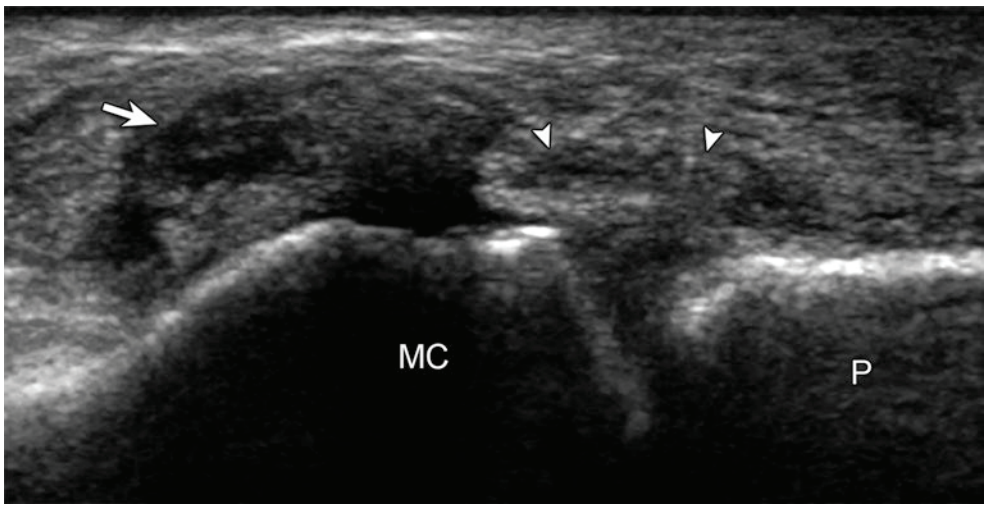

Fig. 16.6 Ulnar collateral ligament tear of the thumb (skier's thumb). Ultrasound image long axis to the ulnar collateral ligament of the thumb shows torn and proximally displaced ligament (arrow) with interposed, hypoechoic and thickened adductor aponeurosis (arrowheads). *MC* metacarpal, *P* proximal phalanx

Key Points
- Tendon retraction indicates full-thickness tear.
- Flexor tendon bowstringing indicates pulley injury.
- Ultrasound can diagnose a Stener lesion with very high accuracy.

16.2 Lower Extremity

16.2.1 Introduction

For athletic injuries, diagnostic ultrasound is used daily as a "stethoscope" to confirm injury and guide treatment. It is not only performed by radiologists but also by sports physicians, physiotherapists and orthopaedic surgeons, to name a few [26].

Ultrasound examination is very important in the assessment of lower limb injuries because of its dynamic capabilities and excellent line pair resolution. Vascularity can be demonstrated within a structure without the need for intravenous contrast agent by pressing a button. Recently microvascular imaging allows us to observe subtle vascularity. Vascular supply is important in determining the nature and the time course of an injury. If increased, it indicates that an injury is in the acute or subacute phases, while its absence means that the injury is old. It is also be used to date tendinopathy. There may be some correlation with a painful tendon, but it is particularly useful in determining resolution after treatment.

In our practice diagnostic ultrasound is the first-line investigation for tendon, ligament and nerve-related disorders. It is also useful in detecting effusions and synovitis within joints. Ultrasound can reliably demonstrate small avulsion fractures at the site of ligamentous attachment which are difficult to see on conventional radiography and MRI. Dynamic stress across a ligament or tendon in the context of injury can determine and emphasise the degree of separation of the injured fibres. With high-resolution ultrasound probes, normal or diseased nerves can be directly seen. When metal work is present ultrasound will demonstrate structures that would be obscured by artefact on other imaging. The presence of intermittent impingement of a tendon, ligament or nerve can be assessed dynamically and precisely. Ultrasound examination is often the only imaging that will demonstrate this important phenomenon.

16.2.2 Pelvis

16.2.2.1 Groin Pain

To examine the groin, you will need a probe that has a range of frequencies demonstrating superficial to deep structures.

Ultrasound is a very useful technique in the diagnosis of groin pain as it can cover many areas that can cause pain [27, 28]. Dynamic assessment for hernias is important (Fig. 16.7). In a study of groin pain, 89% of symptomatic athletes had inguinal hernias compared to 12% asymptomatic controls. Most of the athletes returned to normal sporting activity after surgery [29].

With diagnostic ultrasound, you can assess the exact site of the pain as demonstrated by the patient and examine the nearby joint, tendon insertions and muscles.

16.2.3 Hip

Ultrasound examination of the hip needs a probe covering the 12–8 MHz range due to the joint's depth. Imaging should start obliquely along the line of the femoral neck.

Diagnostic ultrasound can detect an effusion, synovitis within the hip joint and sometimes labral tears especially if they are associated with paralabral cysts. The technique has greater sensitivity for cysts than MRI but less sensitivity for labral tears than MRI arthrography. The presence of synovi-

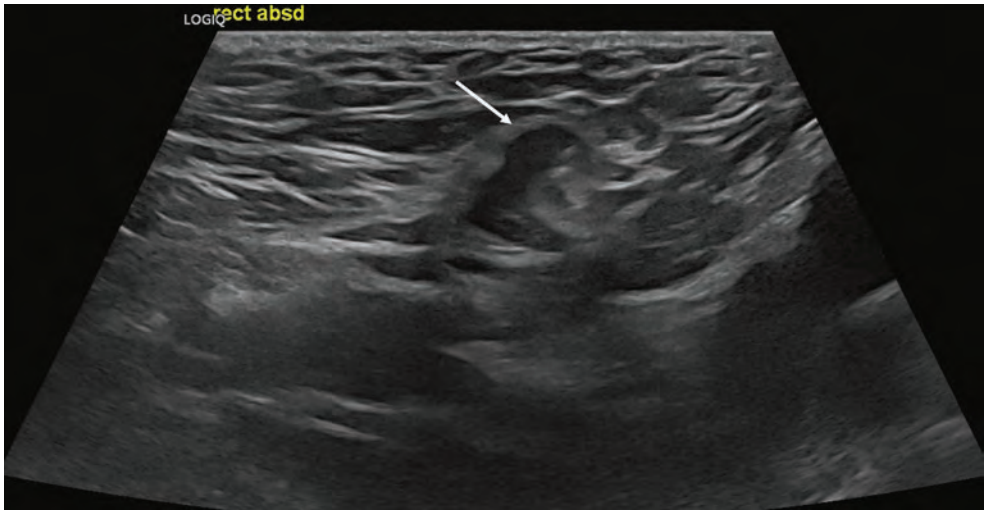

Fig. 16.7 Direct inguinal hernia. Soccer player with groin pain but no clinical evidence of a hernia. The hernia is best appreciated on the dynamic assessment. You can see a loop of bowel moving forward on Valsalva. Static view is provided in this article

tis with its higher echogenicity, neovascularity and frondlike appearance against the anechoic fluid of an effusion is seen with standard ultrasound. MRI would require intravenous contrast agent enhancement and a longer examination to achieve similar results. A substantial benefit of diagnostic ultrasound is that it clearly differentiates cystic versus solid mass lesions. This is often difficult using MRI.

In younger athletes the most injured areas are the joint and the labrum. These are best seen with MR arthrography, but ultrasound can be used to guide the arthrography injection and guide pain-relieving injections such as steroid and sodium hyaluronic acid in the treatment of conditions that do not need surgery.

Key Points

- Groin pain can be due to hernias which can be reliably identified by dynamic ultrasound examination.
- To detect a hip effusion, the probe is best placed obliquely along the line of the femoral neck.

16.2.4 Insertional Tendinosis (Traction Enthesopathy)

Diagnostic ultrasound is useful in the athlete in detecting tendinopathies around the hip.

Age determines the weakest area of the tendon. Before apophyseal closure, the apophyseal attachment is the weakest, and avulsion injuries usually pull off a fragment of bone. These fragments may be very difficult to identify using MRI but are obvious when using ultrasound as they cast an acoustic shadow and a sharp margin [30]. In adults with repetitive stress, the tendon insertion may be injured. The appearances on ultrasound of an abnormal tendon are identical to that described in the upper limb, with reduction in echogenicity, often neovascularisation and irregularity of the bone cortex due to enthesopathy.

In the adolescent, the pelvis is a common area for apophyseal injuries. Without the need for radiation, comparing both sides, the area of tendon insertion can be imaged by diagnostic ultrasound. The injuries occur before the age of 20. The most common apophyseal injuries occur at the insertion of the hamstrings, rectus femoris, sartorius and iliopsoas at the ischial tuberosity (54%), anterior inferior iliac spine (22%), anterior superior iliac spine (19%) and the lesser tuberosity of the femur, respectively. Less common sites are the adductor tubercle and the iliac crest [31].

In adult athletes the hamstring insertion is a common site of injury. This can be seen in runners, soccer players and cross-country skiers. Rectus femoris injuries are also seen (Fig. 16.8). Soccer players also acquire adductor insertional injuries and injuries at the insertion of the rectus abdominis muscle.

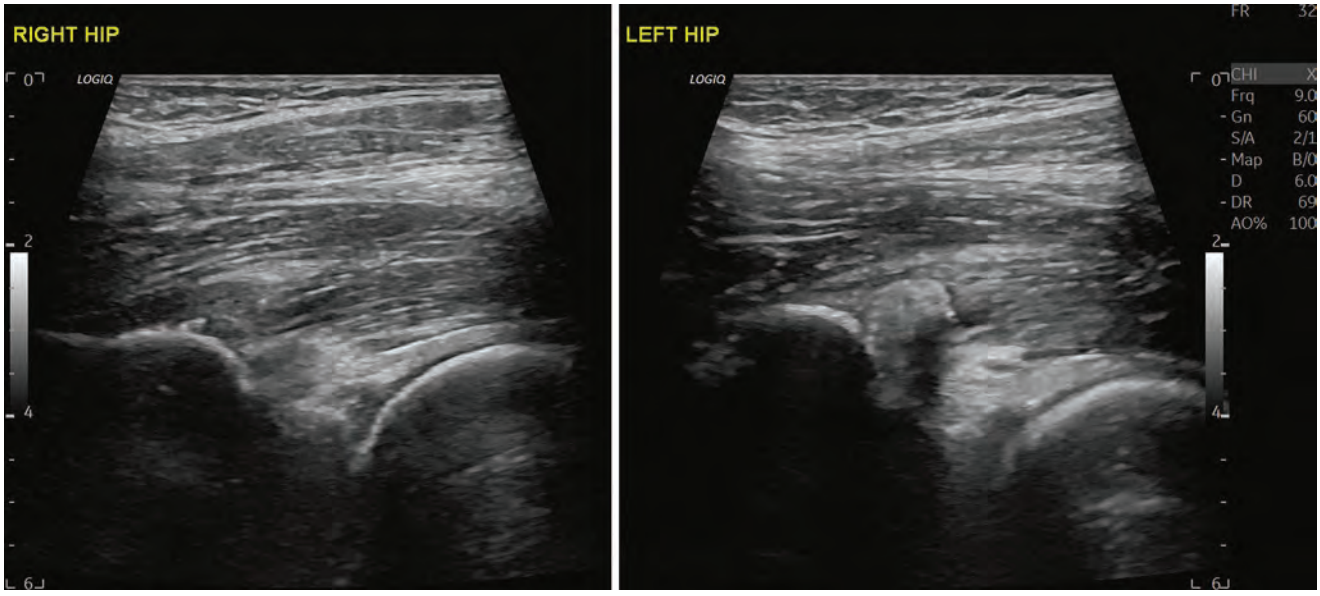

Fig. 16.8 Rectus femoris insertional injury. Horse rider. Left anterior groin pain after gym session 3 weeks before. Clinically thought to be a labral tear. Note the calcification in the insertion of the direct tendon as it joins the anterior inferior Iliac spine compared to the asymptomatic normal right side. Side-by-side comparison is very useful in these cases

Key Points

- Apophyseal injuries in the adolescent can be detected more accurately by ultrasound than by radiographs or MRI by looking for detached fragments of bone that cause acoustic shadowing.
- Insertional tendinosis or enthesopathy shows reduction of the tendon echogenicity, neovascularity and irregularity of the bone cortex at the insertion.

16.2.5 Knee

Most knee injuries are best assessed by MRI to determine both bony and ligamentous injury; however, diagnostic ultrasound is a very useful technique, if there is an area of pinpoint pain or swelling. It can detect effusions and synovitis within the joint and is useful in the assessment and treatment of patellar and quadriceps tendinosis. Collateral ligament injuries and other tendinosis can also be accurately detected and assessed dynamically by ultrasound examination.

The proximal patella tendon is most affected by traction tendinosis. At the insertion into the patella, it becomes thickened and lower in echogenicity and contains neovascularisation (Fig. 16.9). In young athletes, there is also the possibility of an apophyseal injury of both the inferior pole of the patella in Sinding-Larsen syndrome and the tibial tuberosity in Osgood-Schlatter's disease. In its early appearance, these disorders may only show fluid surrounding the tendon with-

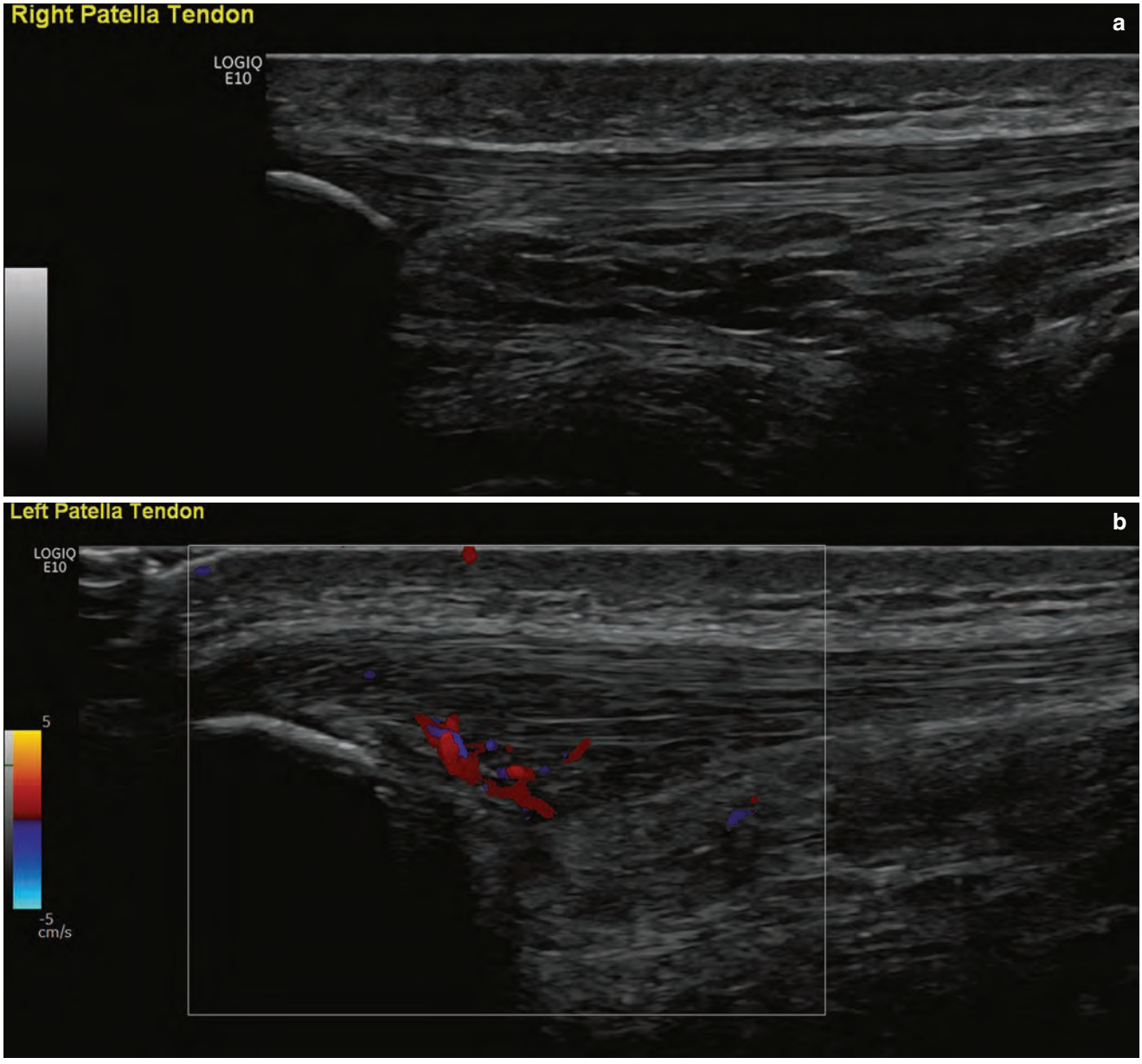

Fig. 16.9 A 22-year-old ballet dancer. (**a**) Normal right patellar tendon. (**b**) Insertional patellar tendinosis. Note the thickened proximal tendon with reduced echogenicity and neovascularisation

out the bony fragmentation as seen in more established cases. These disorders are a traction apophysitis for which offloading is the primary treatment.

Rupture of the patella tendon or quadriceps tendon may occur in the older age group of athletes and can be seen by ultrasound. Here there is a discontinuity of the tendons, and dynamic assessment allows the differentiation of partial- and full-thickness tears. In this last role, diagnostic ultrasound is a much more accurate technique than MRI whether severity and extent of the injuries are difficult to judge.

Key Points

- Knee effusions are best seen in the suprapatellar region using ultrasound.
- Collateral ligament injuries are easily and accurately assessed by ultrasound, but the other internal knee injuries can only be fully appreciated by MRI.
- Proximal patellar tendinosis is identified by thickening of the tendon with reduced echogenicity and neovascularisation.

16.2.6 Ankle

Perhaps the most important area in sports imaging is the ankle. It is important to use a large amount of coupling gel and light touch around this area as pressure over the bones of the ankle can be very painful and you can compress fluid around joints and tendons.

The Achilles tendon is commonly affected in athletes, especially runners. It is best seen by lying the patient prone with the foot dangling off the end of the couch so that movement of the foot can be performed. An 18 MHz probe is the most useful with a larger footplate. Midsubstance tendinosis and insertional tendinosis can be assessed in detail using diagnostic ultrasound. In midsubstance tendinosis, there is a fusiform swelling of the tendon with reduction in echogenicity and neovascularisation. In insertional tendinosis, there is thickening of the tendon, reduction in echogenicity, neovascularisation and often an enthesopathy involving the calcaneal insertion (Fig. 16.10). The presence of a plantaris tendon can also easily be identified. This can be involved in Achilles tendinosis as well or have an isolated tendinosis of its own. The plantaris tendon is important as it may be the

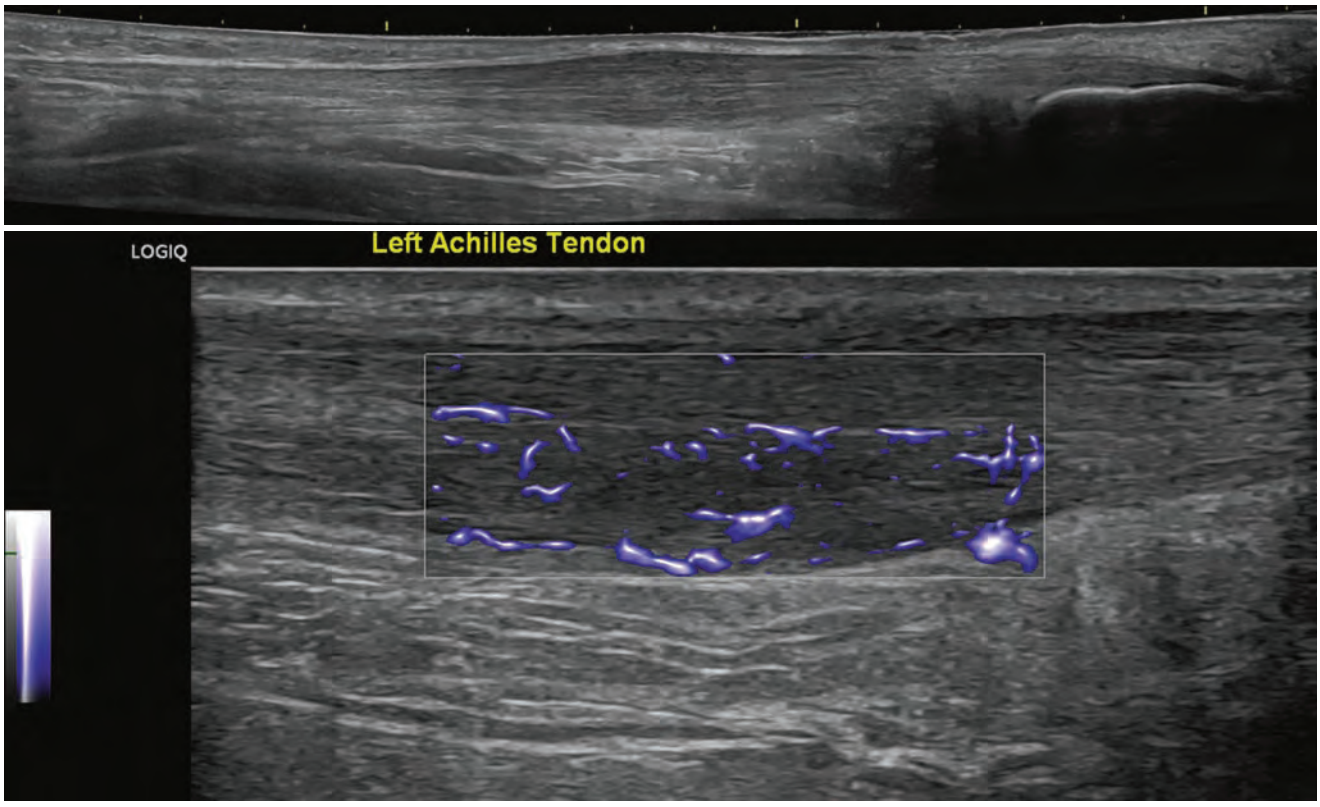

Fig. 16.10 Marathon Runner with Achilles tendinosis. Fusiform swelling of the Achilles tendon with reduction in echogenicity on this extended field of view US image and neovascularity

reason the patient with Achilles tendinosis is not responding to physiotherapy. Sometimes surgical excision can aid recovery in these cases.

Achilles rupture can occur in athletes. A complete rupture can be identified on diagnostic ultrasound by discordant movement at the site of injury when the tendon ends move in different directions producing a gap in the tendon that increases with dorsiflexion. Ultrasound can precisely locate the area of rupture which allows for measurements to be made and allows the possibility of small incisions to repair the tendon surgically. In the acute injury, it is fortunate that the only movement required is a very minor movement of the foot; if the examination is performed gently and carefully, it should not cause pain even on the day of the injury. The presence of an intact plantaris tendon spanning the Achilles tendon can falsely reassure the clinician that the Achilles tendon is intact as compression of the calf muscles will still cause movement of the foot even though the Achilles tendon itself is fully separated.

Ligamentous rupture is the most common abnormality in athletes. Ankle sprains commonly cause injury to the anterior talofibular ligament in 86%. This can either be a sprain to the ligament or a full rupture. The other lateral ligaments can also be assessed by ultrasound including the anterior tibiofibular ligament which can be injured in association with the anterior talofibular ligament or on its own. In isolation this injury often occurs when an athlete wears high boots such as ski boots or large walking boots. Injury to the calcaneofibular ligament occurs in approximately 30% of ankle sprains and is a much more significant injury with relatively poor outcome (Fig. 16.11). The posterior tibiofibular and talofibular ligament can also be injured and assessed by ultrasound. Deltoid ligament injury is also common (in 50% of lateral ligament injuries) [32]. Dynamic assessment of all the ankle ligaments is possible with ultrasound including the posterior ligaments best seen using a small footprint. High-frequency probe with dynamic assessment is especially useful in assessing a syndesmotic injury to the distal tibiofibular joint. On moving the foot in dorsiflexion and plantar flexion, the tibia and fibula should remain at an equal distance apart and in the same location. If there is any dynamic separation of the bones, then this is the diagnosis. This is often missed on any other imaging because you cannot dynamically stress this area on MRI or CT unless you have the facility to perform standing MRI or CT for comparison with supine examination!

Damage to the peroneal retinacula can also occur. The retinacula can become thickened in a chronic injury (Fig. 16.12). If the superior retinaculum is ruptured, this may lead to sublux-

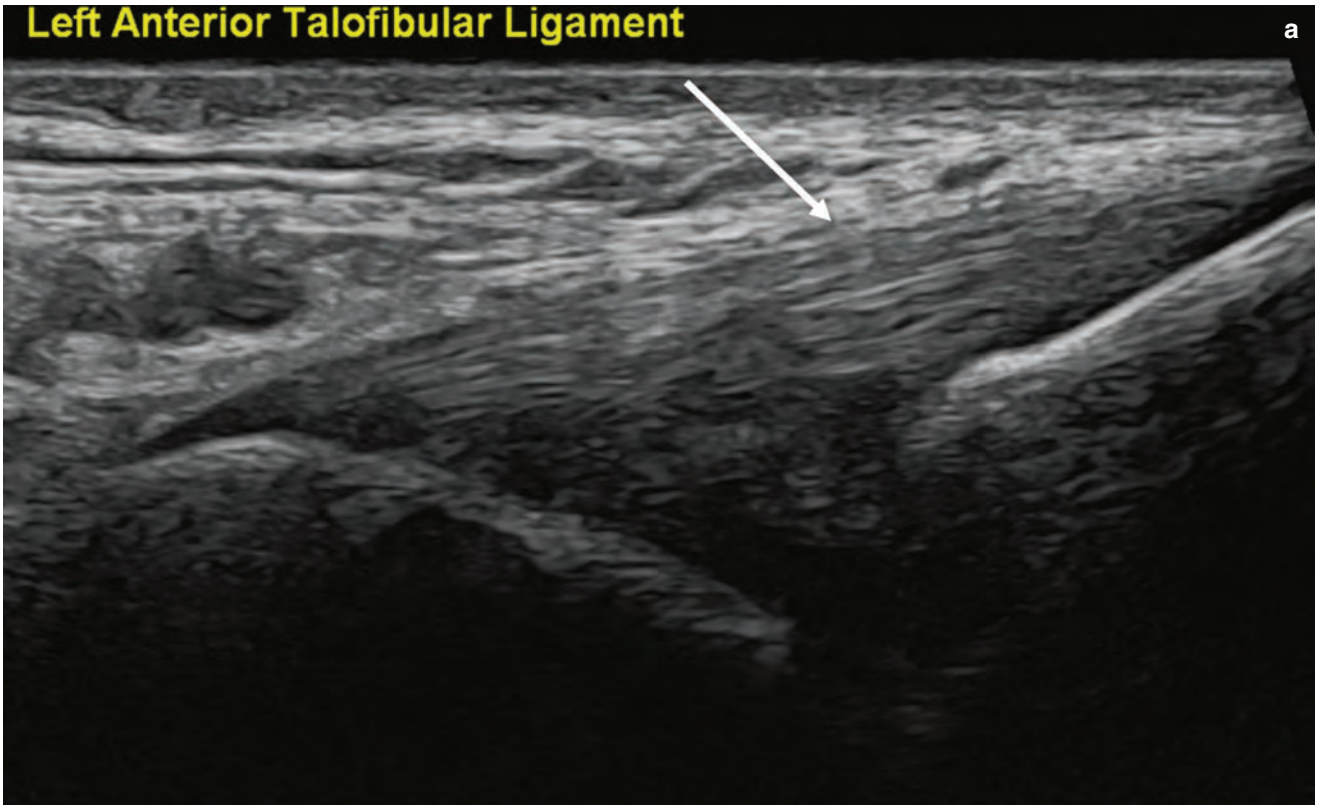

Fig. 16.11 Ruptured anterior talofibular ligament. A 19-year-old soccer player. (**a**) Normal left anterior talofibular ligament. (**b**) Torn right anterior talofibular ligament. (**c**) Injured right calcaneofibular ligament. (**d**) Right ankle effusion

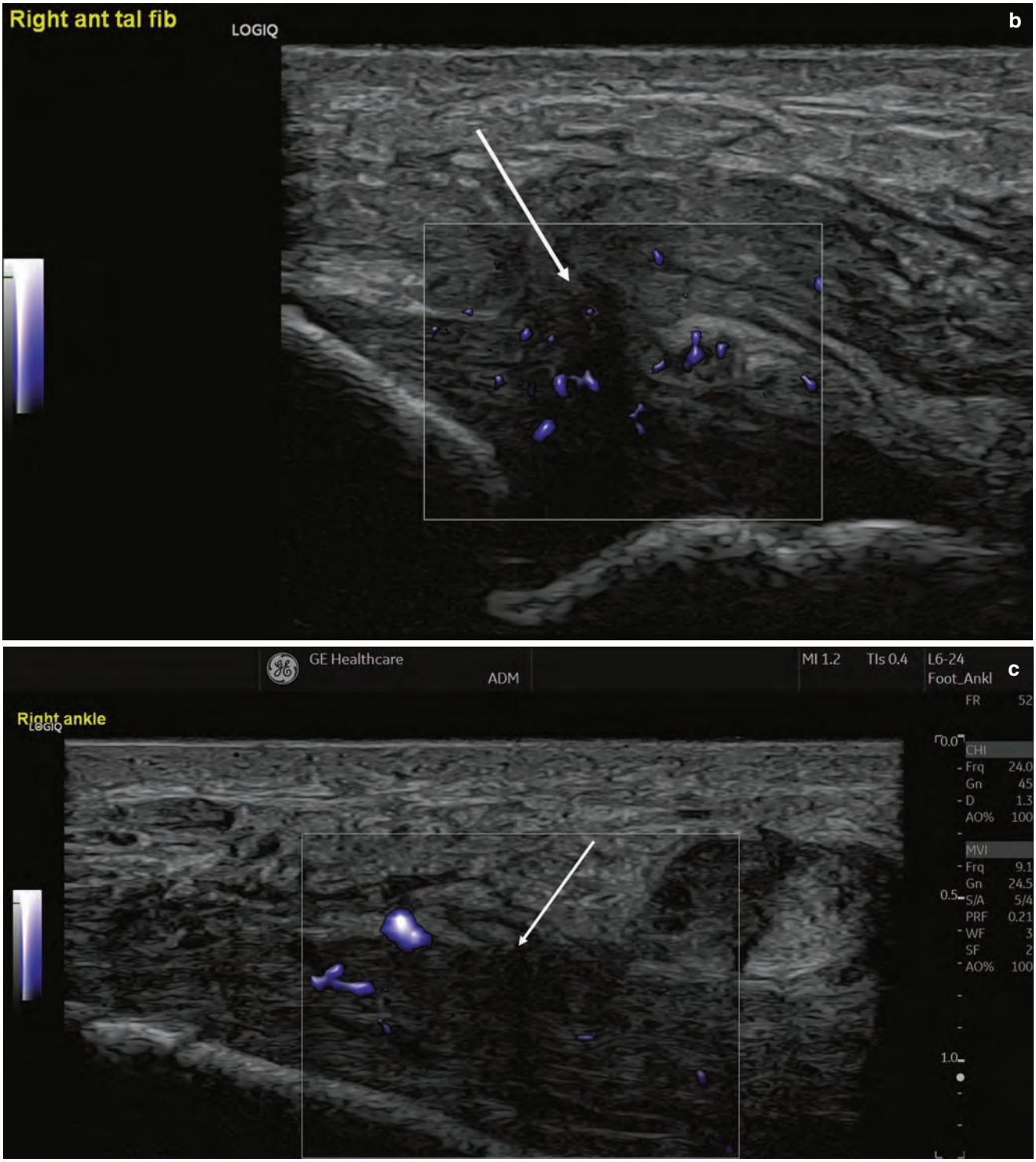

Fig. 16.11 (continued)

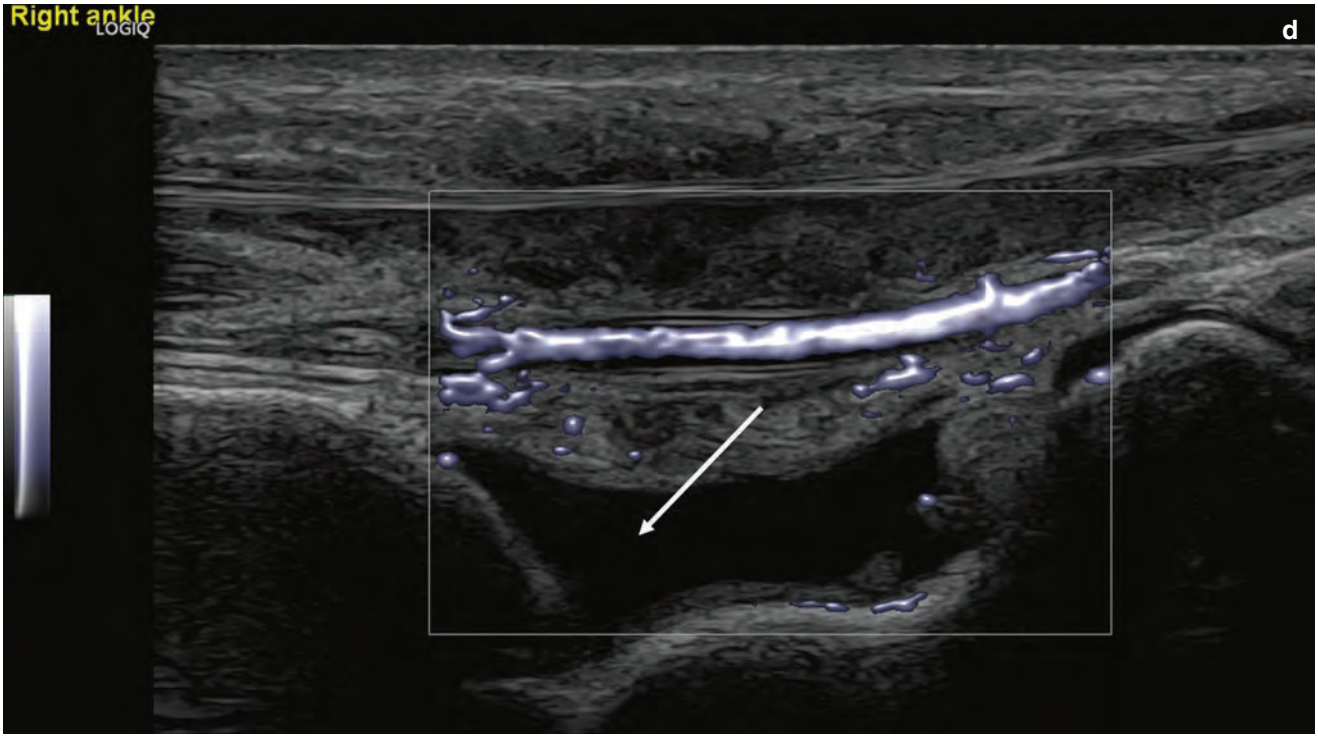

Fig. 16.11 (continued)

ation of the peroneal tendons. Injury in this region can also lead to pseudo-subluxation of the peroneal tendons when there is an abnormal movement of the peroneus brevis tendon against the peroneal longus. Both of these abnormalities can be a cause of clicking of the tendons in this region [33]. Dynamic assessment of tendon movement and retinaculum function is only available with diagnostic ultrasound. Intermittent or transient symptoms are often not identified using MRI or CT.

Ballet dancers suffer problems with the flexor hallucis longus tendon due to dancing on pointe over many years. This tendon is naturally larger than the other tendons in these dancers. Active tendinopathy with neovascularisation is easily demonstrated using diagnostic ultrasound.

Key Points

- Complete Achilles rupture is best assessed by ultrasound due to dynamic movement of the tendon showing the tendon ends moving in different directions. This technique has greater precision than MRI.
- Clicking of the peroneal tendons can either be due to pseudo subluxation or true subluxation which can be dynamically demonstrated using ultrasound.
- Ligamentous injury in the ankle is best seen by ultrasound due to the different obliquities of the ligaments; integrity of the ligament may be judged stressing the ligament while scanning.

16.2.7 Foot

The scanning technique is similar to that of the ankle using a large amount of coupling gel, and light touch around this area as pressure over the bones of the ankle can be very painful and you can compress fluid around joints and tendons.

The tibialis anterior tendon is affected in fell walkers. This is usually due to an insertional tendinosis.

The tibialis posterior tendon can rupture or develop tendinopathy. As this tendon forms part of the arch of the foot, these abnormalities can both cause a new flat foot deformity. The spring ligament can also be injured causing an acute flatfoot. These conditions are readily diagnosed using diagnostic ultrasound with high-resolution probes and good-quality Doppler imaging.

Ligamentous injury of the small ligaments of the foot can be identified using diagnostic ultrasound, especially if they are superficial. Injury to the talonavicular ligament can occur in isolation or in association with lateral ligamentous injury [34]. This destabilises the midfoot allowing movement across the talonavicular joint which is vital in the normal windlass mechanism of walking; this is the dynamic tightening of the arch of the foot by long and short stabilisers prior to pushing off from the ball of the foot. Deficiency in the strength of the arch prevents this movement and is associated with premature osteoarthritis of the midfoot.

Nerve damage can occur in athletes due to poor fitting shoes or the constant agitation of the deep peroneal nerve on

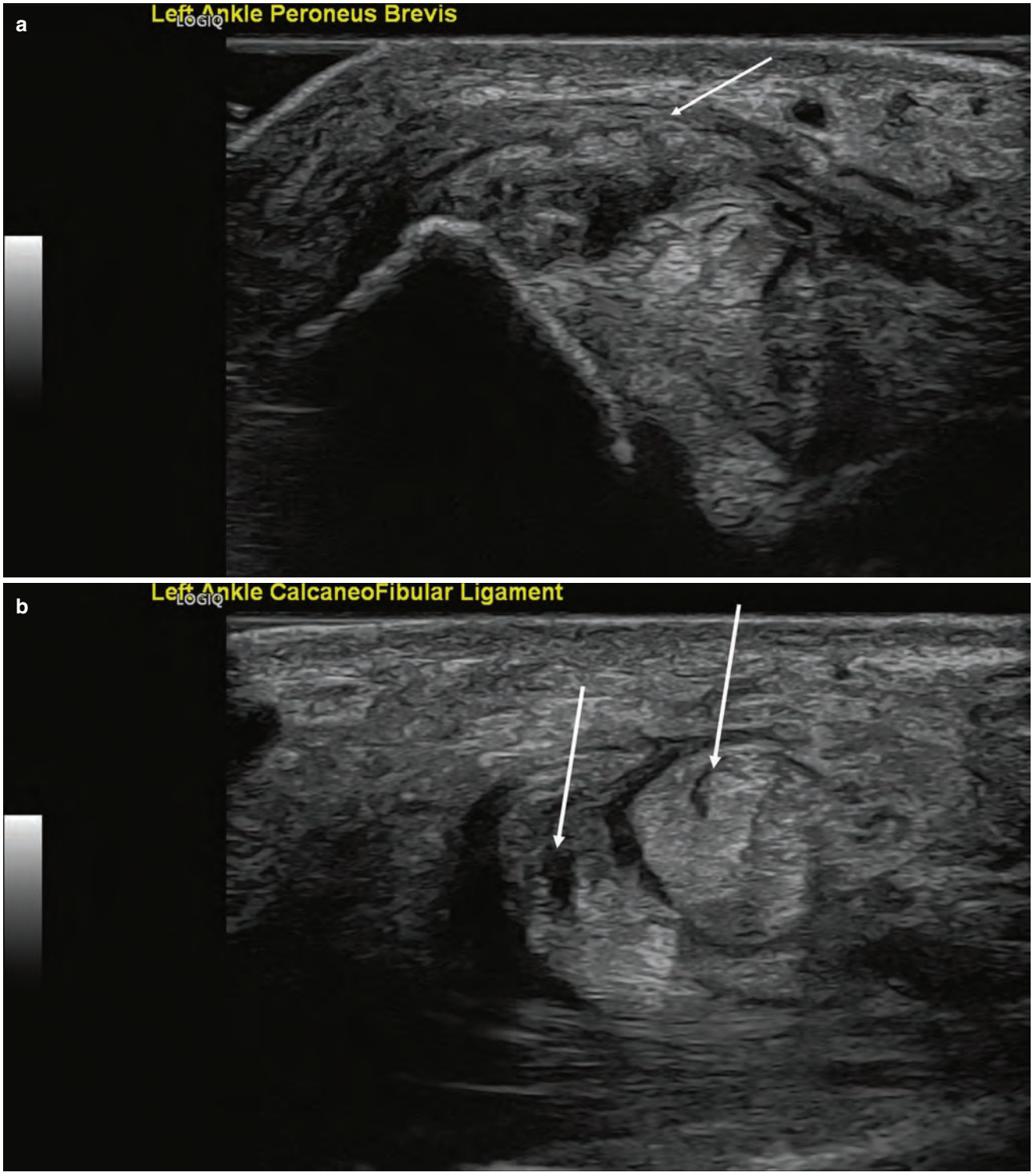

Fig. 16.12 An elite 55-year-old jockey. Peroneus longus and brevis tendinosis and superior peroneal retinacular injury. (**a**) Note the thickening of the superior peroneal retinaculum. (**b**) The peroneal tendons show central mucoid degeneration

the dorsum of the foot of the ball in soccer players kicking a ball. This can easily be seen by ultrasound examination ideally with a high-resolution small footplate probe such as 18–24 MHz. Microvascular imaging allows study of the normal blood supply to small nerves, and comparison of both sides will determine whether flow is abnormally increased.

Key Points

- The cause of a sudden flat foot deformity can be tibialis posterior tendon rupture, tendinosis or spring ligament rupture. These can all be determined by ultrasound.
- Nerves can be clearly seen on ultrasound examination with high-resolution (18–24 MHz) probes.

16.2.8 Muscle Injury

Diagnostic ultrasound may be used to assess muscle tears 6 h after injury. Before this, acute haemorrhage is echogenic and blends with the fibro-fatty interfaces of the muscle and is therefore invisible. This makes the use of pitch side ultrasound inaccurate as significant muscle damage can be overlooked. Within a few hours, liquefying haematoma forms. This is low in echogenicity and is easy to see within the muscle. It forms in the gap of the muscle injury. Ultrasound can be used to dynamically assess the size of the tear by contracting the muscle passively or actively; the movement involved is minimal and should not be enough to cause any pain. MRI can be useful in the initial phase of an injury but will overestimate the extent of injury after 24 h due to distant spread of muscle oedema in association with the injury. MRI is rarely accurate in distinguishing between partial- and full-thickness rupture. In chronic injury muscle atrophy is seen as a change in size with fatty infiltration (increased echogenicity) and best determined by comparing sides. MRI provides similar information but sometimes only one limb is examined preventing comparison. In those with chronic injury the ultrasound practitioner should always compare sides looking for chronic muscle change.

The technique of muscle ultrasound examination requires a lower frequency probe such as 8–12 MHz dependent on the depth and size of the muscle. It is best to use a fast sweeping motion over the muscle to detect the initial area of injury and then closing in on abnormal areas with slower movement to demonstrate more detail. Too much pressure can compress a liquefying haematoma making it more difficult to identify. Comparison with the opposite limb is essential to detect small areas of injury.

Diagnostic ultrasound can precisely identify scarring and myositis ossificans if the injuries are more established. Both these conditions are difficult to appreciate on MRI and are commonly overlooked. Scarring is of high echogenicity when established. Myositis ossificans is of high echogenicity and has acoustic shadowing behind it once it is established. The early calcification can be much easier to see using diagnostic ultrasound when compared to conventional radiography. Re-tearing can also be seen as low echogenicity and blurring of the normal muscle fibre pattern with vascularity in the region of a new tear [26].

Injuries may occur in any lower limb muscle group. The commonly seen injuries are of the hamstrings, quadriceps, adductors and calf muscles. Thigh muscle injury has been extensively researched in footballers. The presence of a musculotendinous injury or a large injury makes the time of returning to sport longer and the chance of a re-injury higher [35, 36].

Calf injuries commonly occur between the medial gastrocnemius and soleus muscles and are known as tennis leg. This can be mistaken for deep venous thrombosis or a ruptured popliteal cyst, but to the experienced ultrasound examiner, it is easy to distinguish between these disorders (Fig. 16.13).

Key Points

- Muscle injury may be invisible to ultrasound examination in the first 6 h after an injury as acute haemorrhage is echogenic and may mimic muscle.
- After 6 h, ultrasound accurately detects the injury as haematoma starts to liquefy. At this stage MRI may exaggerate the nature of the injury because of adjacent muscle oedema.

16.3 Guided Injections

Ultrasound is becoming essential to the safe guidance of all interventions in both the upper and lower limb. This is beyond the remit of this article but is an extension of its use once you become proficient [37, 38].

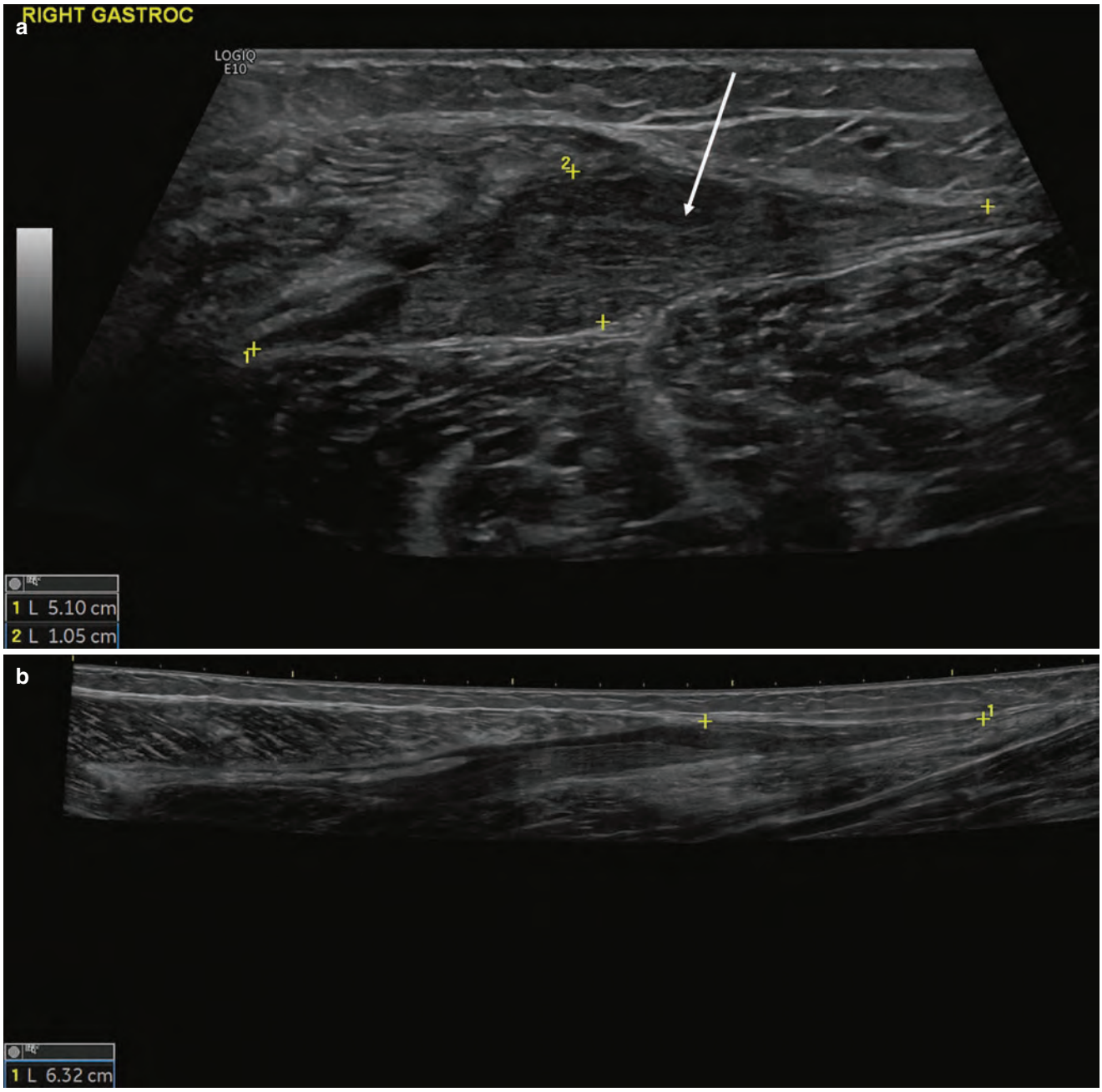

Fig. 16.13 A 50-year-old female skier. Injury in March 2020 just before lockdown for Covid 19. Stretching injury to the calf as she fell with ski moving forward. Imaged 5 months after injury as still symptomatic. (**a**) Poorly liquefied haematoma at site of injury between the gastrocnemius and soleus muscles. (**b**) Extended field of view ultrasound to show the amount of retraction of the medial gastrocnemius muscle with respect to the Achilles tendon

16.4 Concluding Remarks

Ultrasound can play a significant role in the evaluation of sports injuries. The most common application is evaluation of tendon pathology, such as tendinosis and tendon tear. While any tendon about the extremities can be evaluated, the high-resolution capabilities of ultrasound are especially ideal in evaluation of the distal extremities. The dynamic capabilities of ultrasound are also important showing tendon retraction in the setting of a full-thickness tendon tear, tendon subluxation and muscle hernias. Muscle injuries may also be evaluated for tear and haematoma although sensitivity is lower acutely after an injury. Ligaments may be assessed with ultrasound where dynamic imaging can also be used to demonstrate joint space gapping as an indicator of ligament tear. Dynamic assessment is also important in the evaluation of groin hernias. Ultrasound may be used to guide various procedures, such as injections and aspirations, as they relate to sports injuries.

Take Home Messages

- Ultrasound is effective in the evaluation of tendon and ligament injuries.
- Ultrasound may be limited in the early evaluation of muscle injury.
- Dynamic imaging is important in evaluation of muscle and ligament tears, tendon subluxation as well as various hernias.
- Ultrasound may be used to guide percutaneous procedures.

References

1. Schaeffeler C, Mueller D, Kirchhoff C, Wolf P, Rummeny EJ, Woertler K. Tears at the rotator cuff footprint: prevalence and imaging characteristics in 305 MR arthrograms of the shoulder. Eur Radiol. 2011;21(7):1477–84. Epub 2011/01/27. https://doi.org/10.1007/s00330-011-2066-x.
2. Jacobson JA. Shoulder US: anatomy, technique, and scanning pitfalls. Radiology. 2011;260(1):6–16. Epub 2011/06/24. https://doi.org/10.1148/radiol.11101082.
3. Galloway MT, Lalley AL, Shearn JT. The role of mechanical loading in tendon development, maintenance, injury, and repair. J Bone Joint Surg Am. 2013;95(17):1620–8. Epub 2013/09/06. https://doi.org/10.2106/JBJS.L.01004.
4. Buck FM, Grehn H, Hilbe M, Pfirrmann CW, Manzanell S, Hodler J. Magnetic resonance histologic correlation in rotator cuff tendons. J Magn Reson Imaging. 2010;32(1):165–72. Epub 2010/06/26. https://doi.org/10.1002/jmri.22222.
5. Kjellin I, Ho CP, Cervilla V, Haghighi P, Kerr R, Vangness CT, et al. Alterations in the supraspinatus tendon at MR imaging: correlation with histopathologic findings in cadavers. Radiology. 1991;181(3):837–41.
6. Jacobson JA, Lancaster S, Prasad A, van Holsbeeck MT, Craig JG, Kolowich P. Full-thickness and partial-thickness supraspinatus tendon tears: value of US signs in diagnosis. Radiology. 2004;230(1):234–42.
7. Wohlwend JR, van Holsbeeck M, Craig J, Shirazi K, Habra G, Jacobsen G, et al. The association between irregular greater tuberosities and rotator cuff tears: a sonographic study. AJR Am J Roentgenol. 1998;171(1):229–33.
8. Araki D, Miller RM, Fujimaki Y, Hoshino Y, Musahl V, Debski RE. Effect of tear location on propagation of isolated supraspinatus tendon tears during increasing levels of cyclic loading. J Bone Joint Surg Am. 2015;97(4):273–8. Epub 2015/02/20. https://doi.org/10.2106/JBJS.N.00062.
9. Park JS, Park HJ, Kim SH, Oh JH. Prognostic factors affecting rotator cuff healing after arthroscopic repair in small to medium-sized tears. Am J Sports Med. 2015;43(10):2386–92. Epub 2015/08/20. https://doi.org/10.1177/0363546515594449.
10. Skendzel JG, Jacobson JA, Carpenter JE, Miller BS. Long head of biceps brachii tendon evaluation: accuracy of preoperative ultrasound. AJR Am J Roentgenol. 2011;197(4):942–8. Epub 2011/09/24. https://doi.org/10.2214/AJR.10.5012.
11. Moser TP, Cardinal E, Bureau NJ, Guillin R, Lanneville P, Grabs D. The aponeurotic expansion of the supraspinatus tendon: anatomy and prevalence in a series of 150 shoulder MRIs. Skelet Radiol. 2015;44(2):223–31. Epub 2014/09/03. https://doi.org/10.1007/s00256-014-1993-4.
12. Hashiuchi T, Sakurai G, Morimoto M, Komei T, Takakura Y, Tanaka Y. Accuracy of the biceps tendon sheath injection: ultrasound-guided or unguided injection? A randomized controlled trial. J Shoulder Elb Surg. 2011;20(7):1069–73. Epub 2011/07/26. https://doi.org/10.1016/j.jse.2011.04.004.
13. van Holsbeeck M, Strouse PJ. Sonography of the shoulder: evaluation of the subacromial-subdeltoid bursa. AJR Am J Roentgenol. 1993;160(3):561–4. Epub 1993/03/01. https://doi.org/10.2214/ajr.160.3.8430553.
14. Daghir AA, Sookur PA, Shah S, Watson M. Dynamic ultrasound of the subacromial-subdeltoid bursa in patients with shoulder impingement: a comparison with normal volunteers. Skelet Radiol. 2012;41(9):1047–53. Epub 2011/10/15. https://doi.org/10.1007/s00256-011-1295-z.
15. Lobo Lda G, Fessell DP, Miller BS, Kelly A, Lee JY, Brandon C, et al. The role of sonography in differentiating full versus partial distal biceps tendon tears: correlation with surgical findings. AJR Am J Roentgenol. 2013;200(1):158–62. Epub 2012/12/21. https://doi.org/10.2214/AJR.11.7302.
16. Smith J, Finnoff JT, O'Driscoll SW, Lai JK. Sonographic evaluation of the distal biceps tendon using a medial approach: the pronator window. J Ultrasound Med. 2010;29(5):861–5. Epub 2010/04/30
17. Kalume Brigido M, De Maeseneer M, Jacobson JA, Jamadar DA, Morag Y, Marcelis S. Improved visualization of the radial insertion of the biceps tendon at ultrasound with a lateral approach. Eur Radiol. 2009;19(7):1817–21. Epub 2009/02/14. https://doi.org/10.1007/s00330-009-1321-x.
18. Downey R, Jacobson JA, Fessell DP, Tran N, Morag Y, Kim SM. Sonography of partial-thickness tears of the distal triceps brachii tendon. J Ultrasound Med. 2011;30(10):1351–6. Epub 2011/10/05
19. Potter HG, Hannafin JA, Morwessel RM, DiCarlo EF, O'Brien SJ, Altchek DW. Lateral epicondylitis: correlation of MR imaging, surgical, and histopathologic findings. Radiology. 1995;196(1):43–6.
20. Roedl JB, Gonzalez FM, Zoga AC, Morrison WB, Nevalainen MT, Ciccotti MG, et al. Potential utility of a combined approach with US and MR arthrography to image medial elbow pain in baseball players. Radiology. 2016;279(3):827–37. Epub 2016/05/18. https://doi.org/10.1148/radiol.2015151256.

21. De Maeseneer M, Marcelis S, Jager T, Girard C, Gest T, Jamadar D. Spectrum of normal and pathologic findings in the region of the first extensor compartment of the wrist: sonographic findings and correlations with dissections. J Ultrasound Med. 2009;28(6):779–86. Epub 2009/05/28
22. Lopez-Ben R, Lee DH, Nicolodi DJ. Boxer knuckle (injury of the extensor hood with extensor tendon subluxation): diagnosis with dynamic US—report of three cases. Radiology. 2003;228(3):642–6.
23. Klauser A, Frauscher F, Bodner G, Halpern EJ, Schocke MF, Springer P, et al. Finger pulley injuries in extreme rock climbers: depiction with dynamic US. Radiology. 2002;222(3):755–61.
24. Melville D, Jacobson JA, Haase S, Brandon C, Brigido MK, Fessell D. Ultrasound of displaced ulnar collateral ligament tears of the thumb: the Stener lesion revisited. Skelet Radiol. 2013;42(5):667–73. Epub 2012/09/25. https://doi.org/10.1007/s00256-012-1519-x.
25. Ebrahim FS, De Maeseneer M, Jager T, Marcelis S, Jamadar DA, Jacobson JA. US diagnosis of UCL tears of the thumb and Stener lesions: technique, pattern-based approach, and differential diagnosis. Radiographics. 2006;26(4):1007–20.
26. Allen GM. The use of ultrasound in athletes. Eur J Radiol. 2018;109:136–41. https://doi.org/10.1016/j.ejrad.2018.10.028.
27. Brandon CJ, Jacobson JA, Fessell D, Dong Q, Morag Y, Girish G, et al. Groin pain beyond the hip: how anatomy predisposes to injury as visualized by musculoskeletal ultrasound and MRI. AJR Am J Roentgenol. 2011;197(5):1190. https://doi.org/10.2214/AJR.10.4890.
28. Jacobson J, Khoury V, Brandon CJ. Ultrasound of the groin: techniques, pathology, and pitfalls. Am J Roentgenol. 2015;205(3):513–23. https://doi.org/10.2214/AJR.15.14523.
29. Vasileff WK, Nekhline M, Kolowich PA, Talpos GB, Eyler WR, van Holsbeeck M. Inguinal hernia in athletes: role of dynamic ultrasound. Sports Health. 2017;9(5):414–21. Epub 2017/07/22. https://doi.org/10.1177/1941738117717009.
30. Allen GM. Tendon and ligamentous trauma. In: Vanhoenacker FM, Maas, M., Gielen, J. L., editor. Imaging of orthopaedic sports injuries: Springer, New York; 2007. p. 61–72.
31. Rossi F, Dragoni S. Acute avulsion fractures of the pelvis in adolescent competitive athletes: prevalence, location and sports distribution of 203 cases collected. Skelet Radiol. 2001;30(3):127–31. Epub 2001/05/19. https://doi.org/10.1007/s002560000319.
32. Allen GM, Wilson DJ, Bullock SA, Watson M. Extremity CT and ultrasound in the assessment of ankle injuries: occult fractures and ligament injuries. Br J Radiol. 2020;93(1105):20180989. https://doi.org/10.1259/bjr.20180989.
33. Bianchi S, Becciolini M. Ultrasound features of ankle retinacula: normal appearance and pathologic findings. J Ultrasound Med. 2019;38(12):3321–34. https://doi.org/10.1002/jum.15026.
34. De Dea M, Loizou C, Allen G, Wilson D, Athanasou N, Uchihara Y, et al. Talonavicular ligament: prevalence of injury in ankle sprains, histological analysis and hypothesis of its biomechanical function. Br J Radiol. 2017;90(1071):20160816. https://doi.org/10.1259/bjr.20160816.
35. Ekstrand J, Askling C, Magnusson H, Mithoefer K. Return to play after thigh muscle injury in elite football players: implementation and validation of the Munich muscle injury classification. Br J Sports Med. 2013;47(12):769–74. https://doi.org/10.1136/bjsports-2012-092092.
36. Pollock N, Patel A, Chakraverty J, Suokas A, James SL, Chakraverty R. Time to return to full training is delayed and recurrence rate is higher in intratendinous ('c') acute hamstring injury in elite track and field athletes: clinical application of the British Athletics Muscle Injury Classification. Br J Sports Med. 2016;50(5):305–10. Epub 2016/02/19. https://doi.org/10.1136/bjsports-2015-094657.
37. Lee JC, Ahmed N, Allen GM. Image guided injection therapies in athletes—do they work and what should we be using? Eur J Radiol. 2019;110:193–202. https://doi.org/10.1016/j.ejrad.2018.12.001.
38. Allen GM, Wilson DJ. Ultrasound guided musculoskeletal injections. Amsterdam: Elsevier; 2018.

Peripheral Nerve Imaging

18

James F. Griffith and Roman Guggenberger

Learning Objectives

- To understand the ultrasound and MRI appearances of different nerve pathologies.
- To understand the complementary roles of US and MRI in evaluating different nerve pathologies.

18.1 Introduction

The main peripheral nerve abnormalities that lead to referral for imaging are, in order of frequency: entrapment, tumours, trauma, perineural fibrosis, neuralgic amyotrophy, and inflammatory neuropathy. These conditions are best imaged with either ultrasound or magnetic resonance imaging (MRI). Both modalities allow nerves to be seen in high resolution and have their own advantages that make them complimentary in peripheral nerve imaging. Ultrasound is more readily available, allows large segments of nerves to be imaged relatively quickly, and has a dynamic component. MR neurography (MRN) provides an excellent overview of the neural anatomic environment; enables more consistent visualisation of the smaller peripheral nerves, such as those in the foot; can visualise nerves in areas where transducer access is limited, such as the intraforaminal part of the brachial plexus; is less operator dependent; enables the functional capacity of nerves to be explored in greater depth through, for example, diffusion tensor imaging; and allows the effect of motor denervation, i.e. muscle atrophy, to be seen and quantified more accurately.

J. F. Griffith (✉)
Department of Imaging and Interventional Radiology, The Chinese University of Hong Kong, Shatin, Hong Kong

R. Guggenberger
Institut für Diagnostische und Interventionelle Radiologie, Universitätsspital Zurich, Zurich, Switzerland

This chapter discusses imaging of the peripheral nerves by ultrasound and MRI.

18.2 Peripheral Nerve Basics

Peripheral nerves range in diameter from 1 to 20 mm and are formed by multiple axons, grouped into fascicles which, in turn, are grouped into nerves. The endoneurium is the connective tissue surrounding the axon-Schwann cell unit and contains collagen fibres, fibroblasts, capillaries, and a few mast cells and macrophages. The perineurium binds groups of axon-Schwann cell units into nerve fascicles. The number and size of the nerve fascicles generally diminish as the nerve gets smaller more peripherally. The epineurium is the outermost connective tissue sheath that encloses all the nerve fascicles, providing mechanical support to the nerve and reducing friction with adjacent tissues [1]. The endoneurium and perineurium form a blood-nerve barrier akin to the blood-brain barrier. As such, peripheral nerves, except for the dorsal nerve root ganglia, do not enhance with intravenous contrast unless the barrier is compromised by inflammation or malignancy [2].

18.3 Pathophysiology Basics

Pathological nerves may show neural ± fascicular oedema, altered calibre, irregular contour, discontinuity, abnormal enhancement, perineural fibrosis, or rarely intraneural fatty replacement [3, 4]. In acute nerve pathologies, fascicular pattern is usually accentuated due to intra- and perineural oedema, leading to increased nerve calibre and signal intensity. With increasing chronicity, oedema subsides and fibrotic nerve changes lead to reorganisation of nerve tissue with decreased nerve diameter and loss of T2-hyperintensity on MRI. MR imaging is more sensitive at detecting target muscle denervation oedema or atrophy than ultrasound. Diffuse

J. Hodler et al. (eds.), *Musculoskeletal Diseases 2021–2024*, IDKD Springer Series,
https://doi.org/10.1007/978-3-030-71281-5_18

muscle oedema and contrast enhancement can be seen within 1 day of denervation. Both probably reflect increased muscle engorgement and increased muscle blood volume due to denervation. Muscle atrophy and fatty replacement are features of chronic denervation.

18.4 MR Neurography: Technical Considerations

MR neurography (MRN) aims to provide high-resolution high-contrast images of nerves. This is aided by suppression of the background fat as well as pulsation and breathing artefact suppression. While homogeneous fat suppression is challenging on 3T imaging, the increase in contrast-to-noise ratio and spatial resolution achieved by the higher field strength outweigh the issues with inadequate fat suppression. Dedicated peripheral coils ensure high-quality nerve detail and can, if necessary, be combined with surface coils when larger sections of the nerve need to be examined. For example, the brachial plexus is usually imaged with a combined head-neck coil to cover the cervical spine, foramina, and neck regions along with a torso coil to cover the parascapular and axillary regions.

Since nerves have a long (e.g. 80–100 ms) T2 signal and are usually surrounded by fat, fast or turbo spin-echo sequences with spectral saturation using the adiabatic inversion pulse and Dixon technique are preferred [5]. The Dixon technique allows larger areas to be imaged with homogenous fat suppression when, for example, imaging the brachial or lumbosacral plexuses.

Focal T2-weighted neural hyperintensity may occur if the course of the nerve changes relative to the B0-field into a plane higher than 55°. This is known as magic angle artefact which may also persist at TEs beyond 66 ms. Mild T2-hyperintensity of nerves can be seen in asymptomatic subjects [6]. If in doubt regarding the significance of any neural hyperintensity, comparison with the contralateral healthy side is helpful, as is assessing the target muscles for signs of denervation. Also, true pathologic intraneural T2-hyperintensity is usually higher than any maximal magic angle effect [7].

Recent advancements with extended echo train lengths and parallel imaging have enabled 3D T2-weighted imaging volumetric visualisation of nerves using fast or turbo spin-echo sequences in acceptable scan times [8, 9]. Suppression of adjacent vasculature can be achieved by motion-sensitised driven equilibrium or diffusion moment, improving the discrimination of small nerves in the extremities and skull base [10–12]. Contrast administration is not routinely used when imaging peripheral nerves though it can help to enhance vessel conspicuity and demonstrate inflammatory or neoplastic uptake on T1-weighted fat-suppressed images as well as simultaneously suppressing vessel signal on T2-weighted spin-echo and STIR images to increase neural delineation.

Diffusion tensor imaging (DTI) provides additional information on nerve integrity and can be a useful adjunct to standard MRN protocols. Random multidirectional motion of water molecules is restricted when the highly organised neural membranes are intact. The amount of restriction can be quantified by apparent diffusion coefficient (ADC) which is an estimate of mean water diffusivity in all directions. Diffusion can be further directionally quantified by fractional anisotropy with 0 being full isotropy and 1 being full anisotropy. Diffusion tractography, by connecting voxels of similar diffusivity, helps visually confirm neural integrity [13].

Key Point

- The highly organised structure of peripheral nerves is similar throughout the peripheral nervous system. Nearly all nerves look the same. Similarly, the ultrasound and MRI appearances of entrapment, tumour, injury, or inflammation tend to be similar irrespective of the nerve(s) affected.

18.5 Neural Entrapment

Carpal tunnel syndrome (CTS) is the commonest nerve entrapment. The main ultrasound and MR criterion of CTS is undue swelling of the median nerve. The carpal tunnel inlet and outlet are determined on ultrasound and MRI by direct visualisation of the transverse retinaculum. On ultrasound and MRI, one should measure the cross-sectional area (CSA) of the median nerve at the distal forearm, just proximal to the tunnel, at the tunnel inlet, at the tunnel outlet, and just distal to the tunnel.

The more swollen the median nerve, the more likely the possibility of CTS. The normal median nerve CSA at any of these locations on ultrasound is <10 mm^2. A median nerve CSA of >14 mm^2 at any of these locations is diagnostic of CTS [14]. Measurements between 10 and 14 mm^2 should be taken as suggestive of, but not diagnostic of, CTS. Ultrasound CSA measurements do not include the epineurium, and, hence, MRI measurements are about 20% greater than ultrasound measurements [15]. On MRI, a median nerve CSA > 15 mm^2 either proximal to or distal to the tunnel is a useful diagnostic criterion for CTS while a CSA > 19 mm^2 proximal to the tunnel is indicative of severe CTS [16]. Intraneural hyperaemia on ultrasound is a specific but insensitive ultrasound sign of neural compression. Other ultrasound and MR signs of CTS such as increased palmar retinacular bowing or retinacular thickness, loss of neural

fasciculation, flattening ratio, and reduction in carpal tunnel CSA are not specific enough to be very discriminatory on a case-by-case basis in everyday clinical practice.

Ultrasound is as sensitive as nerve conduction studies in confirming the presence of CTS. Patients with equivocal nerve conduction study findings for CTS will also usually have equivocal findings on ultrasound so the two examinations are not necessarily complimentary. Elastography and DTI studies have shown that CTS patients slower elasticity (i.e. stiffer) and median nerves with lower fractional anisotropy values (i.e. less unidirectional diffusion) though currently elastography and DTI do not provide additional information over that provided by CSA measurements alone.

Primary CTS is more common than secondary CTS due to, for example, tenosynovitis, ganglion cysts or other carpal tunnel masses, or crystal deposition within the carpal tunnel. All of these secondary causes can be screened with ultrasound or MRI, with MRI being particularly helpful in this regard.

Following carpal tunnel release, the median nerve will usually remain unduly swollen for at least 1 year following successful surgery and may never return to normal size despite good amelioration of symptoms [17]. This persistent median nerve swelling is due to neural fibrosis and congestion secondary to chronic compressive neuropathy. Therefore, a swollen median nerve following surgery on ultrasound or MRI should not be taken as a sign of incomplete decompression. Similarly, the retinaculum will reform in most patients at 3–12 months following surgery, though in a more elongated fashion such that the overall volume of the carpal tunnel is increased [17].

The next most common entrapment is *cubital tunnel syndrome* which occurs due to compression of the ulnar nerve either within the cubital tunnel deep to Osborne's ligament or within the cubital tunnel proper deep to the arcuate ligament. Any imaging of the cubital tunnel should extend from 8 cm proximal to the elbow joint, to include the arcade of Struthers, to 5 cm distal to the joint to include the ulnar nerves between the two heads of flexor carpi ulnaris [18].

Primary cubital tunnel syndrome is less common than secondary cubital tunnel syndrome due to, for example, a prominent anconeus epitrochlearis muscle osteophytosis, synovitis, or ganglion cysts encroaching from the ulnohumeral joint into the cubital tunnel. Secondary cubital tunnel syndrome tends to be mainly seen in older patients.

The greater the ulnar nerve CSA in the cubital tunnel, the more likely the diagnosis of cubital tunnel syndrome. The normal ulnar nerve CSA is <8 mm^2. An ulnar nerve CSA > 14 mm^2 at the cubital tunnel is considered diagnostic of cubital tunnel syndrome. CSA values between 8 and 12 mm^2 are suggestive of, but not diagnostic of, cubital tunnel syndrome.

Ultrasound also allows one to examine for ulnar nerve subluxation during elbow flexion more easily than MRI. Subluxation occurs due to a redundancy of Osborne's ligament. Although ulnar nerve subluxation is usually asymptomatic and can be seen in about one-fifth of healthy subjects, one can still appreciate how repeated subluxation of the ulnar nerve over the medial humeral epicondyle could lead to friction neuritis ('ulnar neuritis') in patients who frequently flex their elbows during daily, occupational, or sporting activities.

Although not discussed much in the literature, it is likely that two pathologies, namely, neural compression and inflammation, may act in isolation or in unison to produce symptoms of cubital tunnel syndrome. Some patients may have an inflamed ulnar nerve which is not compressed. This is different to other entrapment syndromes such as carpal tunnel syndrome, where the primary aetiology is solely that of neural compression. In this respect, MR has an advantage over ultrasound in allowing one to determine neural oedema by T2-hyperintensity. Adjacent muscle acts as an internal reference to standardise ulnar nerve signal intensity [19]. Then measure the contrast-to-noise ratio (CNR) as follows:

$$\mathrm{CNR} = \frac{\text{Ulnar nerve signal intensity} - \text{muscle signal intensity}}{\text{Standard deviation of air}}$$

A CNR of >50 has high accuracy for has high accuracy for cubital tunnel tunnel syndrome.

The third most common entrapment syndrome is *supinator syndrome* where the motor branch of the radial nerve (the posterior interosseous nerve) is entrapped at the inlet or just beyond the inlet of the supinator tunnel, known as the arcade of Frohse (Fig. 18.1). One will appreciate undue swelling of the deep branch of the radial nerve just proximal to or within the supinator tunnel. There is often also localised deep tenderness at this point.

Less frequent sites of neural entrapment include the suprascapular groove, the spinoglenoid notch (Fig. 18.2), the radial groove, the radial tunnel, Guyon's canal, the peroneal canal, and the tarsal tunnel.

Key Points

- Entrapment syndromes are common in the upper limb, uncommon in the lower limbs.
- At the relevant sites, the greater the degree of nerve swelling, the more likely the possibility of entrapment.
- The CSA of peripheral nerves on MRI is 20% larger than on ultrasound.
- Both ulnar nerve entrapment and friction neuritis can produce cubital tunnel syndrome symptoms.

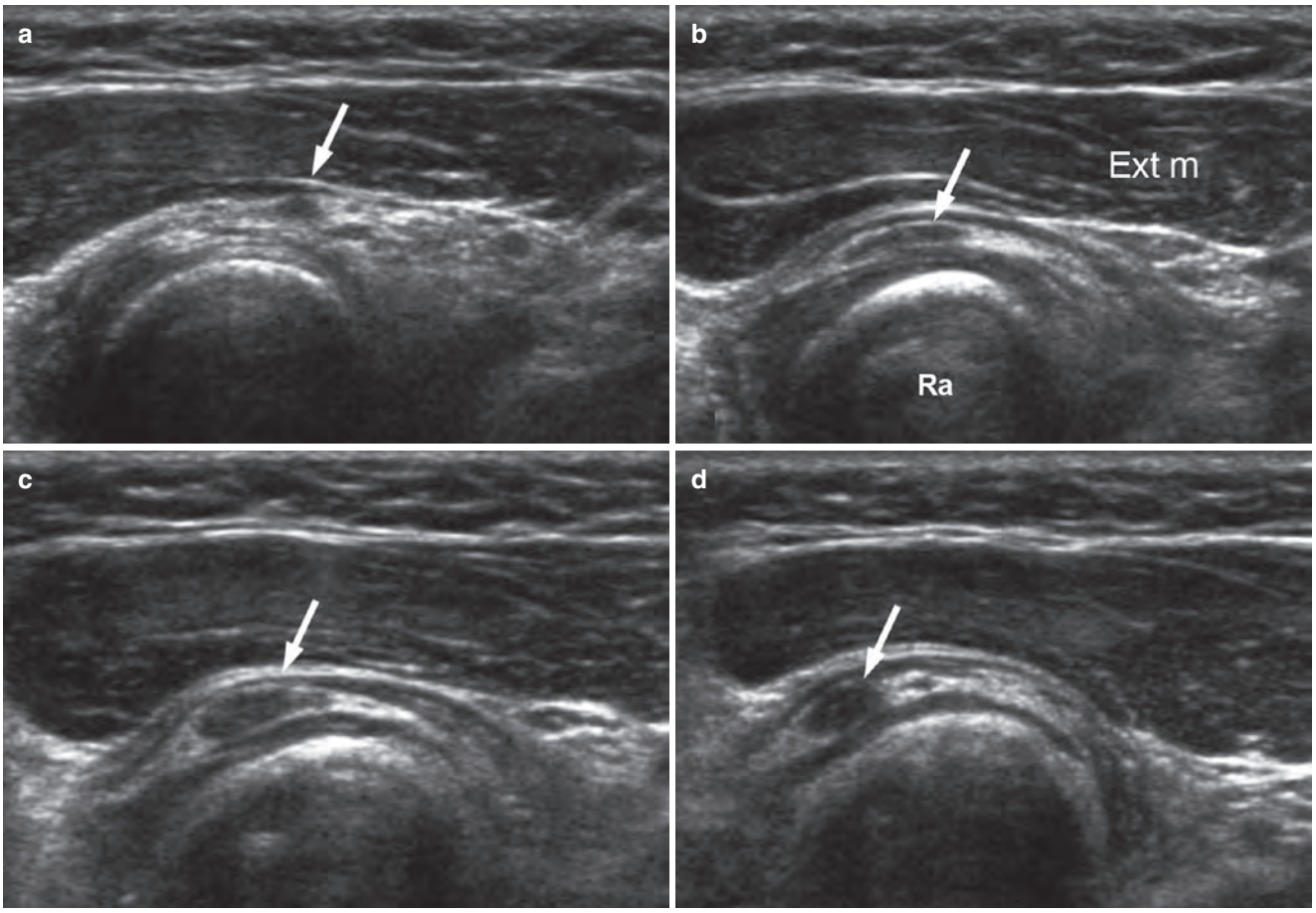

Fig. 18.1 Series of transverse ultrasound images showing posterior interosseous nerve (arrows) (**a**) proximal to and (**b**–**d**) within the supinator tunnel of a 9-year-old boy with quite abrupt onset of weakness of finger extension. The PIN is swollen within the supinator muscle ('supinator tunnel') located between the radial neck and the extensor forearm muscles. This swelling was due to an hourglass constriction at the arcade of Frohse confirmed surgically. PIN swelling is more commonly seen immediately proximal to the supinator tunnel inlet. Ext m Extensor carpi radialis brevis muscle

18.5.1 Tumours

More than 90% of peripheral nerve tumours are benign and more than 60% of these benign nerve sheath tumours are schwannomas. The next most common benign nerve sheath tumour is neurofibroma. Other benign nerve sheath tumours include intraneural lipoma and intraneural ganglia.

Schwannomas arise from Schwann cells, while neurofibroma comprises a mixture of neural cells. There are no known imaging features that allow one to accurately distinguish between a neurofibroma and schwannoma. As such, one should refer to the presence of a 'nerve sheath tumour' rather than a particular tumour type. Neural continuity is the most specific ultrasound or MR sign of a nerve sheath tumour (Fig. 18.3). Other less specific ultrasound or appearances are a fusiform or oblong-shaped mass, internal cystic, myxoid or haemorrhagic areas, posterior acoustic enhancement (on ultrasound), and moderate tumoural hyperaemia or enhancement. On MRI, the so-called target sign may be more suggestive of a schwannoma, while more fascicular patterns are seen with neurofibromas. Only about 70% of nerve sheath tumours have visible neural continuity on ultrasound examination, and it is only in this setting that one can make a definitive diagnosis of a nerve sheath tumour based on the ultrasound appearances alone. When neural continuity is present, one should ascertain whether the tumour is located eccentric or concentric to the parent nerve as this has a bearing on the success of surgical excision. Percutaneous biopsy of nerve sheath tumour is occasionally very painful and should not be undertaken when a confident diagnosis can be made based on ultrasound appearances alone provided malignancy is not suspected.

The remaining 30% of nerve sheath tumours do not have imaging appearances specific enough to make a definitive diagnosis based on ultrasound appearances alone. In this situation one can offer a probable or possible diagnosis of a nerve sheath tumour. Potential differential diagnoses are vascular leiomyomas, vascular malformation, glomus, fibroma,

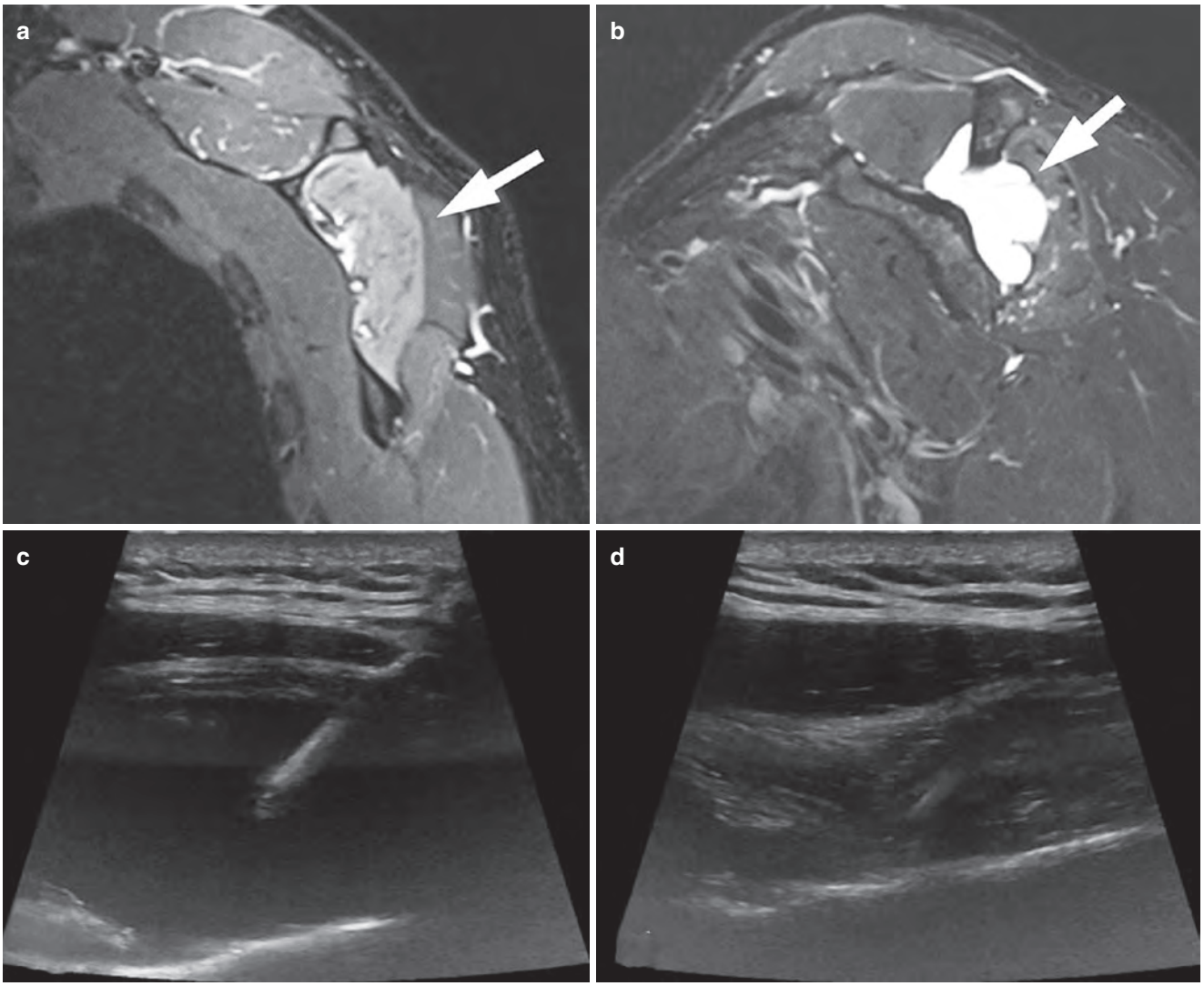

Fig. 18.2 Adult patient with increasing shoulder weakness while working overhead in vineyard. (**a**) MRN shows moderate infraspinatus denervation oedema (arrow) with (**b**) a large paralabral ganglion (arrow) causing suprascapular nerve compression in the spinoglenoid notch. This compression was relieved by US-guided cyst aspiration as seen on (**c**) pre- and (**d**) post-aspiration images

and ganglia. Appearances that would favour a nerve sheath tumour over these tumours are an oblong configuration to the mass, a regular margin, more pronounced internal speckling, and lack of vascular convergence.

Less common types of neurofibroma are diffuse and plexiform neurofibromas. Diffuse neurofibroma may be sporadic or associated with neurofibromatosis type I (NF1). They originate from the subcutaneous nerves and spread extensively along the subcutaneous connective tissue septae. One will see localised dermal and subcutaneous thickening, subcutaneous reticulation, and hyperaemia which can mimic localised cellulitis or panniculitis. Plexiform neurofibroma is only seen in NF1 and is associated with a moderate risk of malignant transformation. It has a more distinctive 'bags of worms' appearance with diffuse enlargement of nerves in a discrete lobulated mass and may occur in the subcutaneous as well as the deep tissues.

One in two malignant peripheral nerve sheath tumours (MPNST) occur in patients with NF1, while 1 in 20 patients with NFI will develop a MPNST. There are currently no imaging features that allow one to distinguish atypical nerve sheath tumours from MPNSTs [20] (Fig. 18.4). Both whole-body MRI with diffusion-weighted imaging and PET/CT imaging are currently being explored in this regard [20]. If there is clinical or imaging suspicion of MPNST, then a percutaneous biopsy should be undertaken to confirm or refute this possibility.

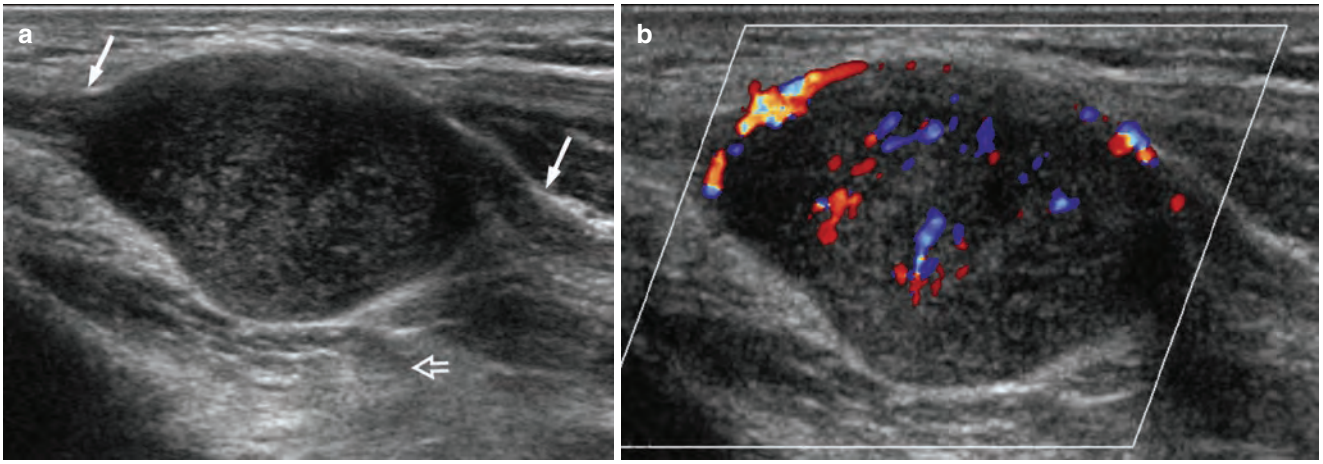

Fig. 18.3 Longitudinal ultrasound of distal forearm showing (**a**) medium-sized nerve sheath tumour arising eccentrically from the median nerve (arrows) with neural continuity and acoustic enhancement (open arrow). (**b**) The tumour shows moderate tumoural hyperaemia. These are diagnostic ultrasound appearances of a nerve sheath tumour

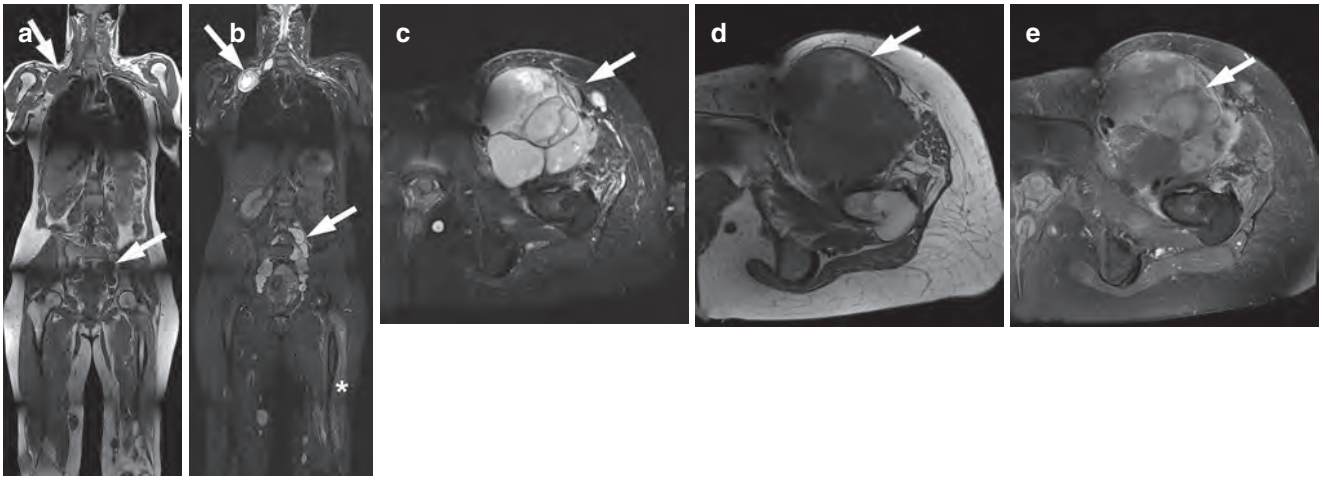

Fig. 18.4 Middle-aged women with hereditary schwannomatosis. (**a**) Multiple tumours are seen on T1-weighted and (**b**) T2-weighted STIR images (arrows). Severe denervation oedema and atrophy of the left quadriceps muscle is present (asterisk in **b**) as a consequence of a large dedifferentiated malignant schwannoma (confirmed histologically) of the femoral nerve with inhomogeneous signal on (**c**) T2-weighted STIR, (**d**) T1-weighted, and (**e**) T1-weighted fat saturated post-gad images

Key Points

- About 70% of nerve sheath tumours have neural continuity evident on imaging. Only in this setting, can one make a definite diagnosis based on imaging signs alone.
- Diagnostic accuracy of imaging for identifying nerve sheath tumours is much less when no neural continuity exists.
- Increase in size over time is the most reliable sign of the MPNST. If doubt exists, percutaneous biopsy is warranted.

18.5.2 Nerve Injury

Blunt injury to nerves usually recovers spontaneously and is not imaged. Conversely, sensory or motor denervation following a penetrating injury usually results in early surgical exploration without the need for imaging.

Imaging is, therefore, usually undertaken to investigate either traction injury or the delayed recognition of nerve injury following penetrating trauma. In traction injury, imaging should focus on those nerves which have been clinically compromised, while in penetrating trauma, imaging should focus on examination of those nerves close to the path of injury. A neuroma-in-continuity (NIC) or stump neuroma

can be seen some months following partial or complete nerve transection, respectively, and should not be mistaken for a nerve sheath tumour [21].

Features of nerve injury to ascertain on imaging are:

(a) Is the nerve visibly injured, i.e. is it not swollen or mild/moderately/severely swollen? What is the length of the affected segment? Is there perineural fibrosis, haematoma, or inflammation present? Is there neural adhesion? If perineural fibrosis is present, what percentage of the neural circumference is affected?
(b) Is there neural transection present and, if so, is this complete or incomplete?
(c) If neural transection is incomplete: what is the approximate percentage of neural transection. What is the length (in mm) of the gap between the retracted fibres? Is there any fibrosis or neuroma-in-continuity (NIC) present? What is the size of this NIC?
(d) If neural transection is complete: What is the length (in mm) of the gap between the retraced nerve endings? Is there any end fibrosis or end neuroma present at the cut ends of the nerve? If present, what is the size of the neuroma? What is the distance between the visibly normal sections of nerve at either end of the transection? (Fig. 18.5).

Peripheral nerve damage is usually graded according to Seddon and Sunderland, where corresponding signal changes can be seen on MRN (Table 18.1).

However, the Sunderland classification was devised on the basis of neural crush injury. Hence it does not apply to traction injury or penetrating injury which is the most common in practice. It does not, for example, include incomplete neural transection which is a common traumatic neural injury.

Key Points

- Most neural injury does not require imaging.
- The main points to consider are as follows: (1) is the nerve injured, i.e. swollen or with altered echotexture or signal intensity; (2) is there neural transection present and, if so, is it partial or complete; and (3) is there a neuroma present.
- A normal looking nerve or a mildly abnormal nerve on imaging has a good clinical outcome.

Table 18.1 Sunderland grade with commonly used terminology, neural integrity, and MR appearances

Grade	Terminology	Integrity	MRN
I	Neuropraxia	Intact	Hyperintense nerve
II	Axonotmesis (mild)	Axons torn	Hyperintense, thickened with prominent fascicles
III	Axonotmesis (moderate)	+ Endoneurium torn	
IV	Axonotmesis (severe)	+ Perineurium torn	Heterogeneous nerve
V	Neurotmesis	+ Epineurium torn	Complete nerve transection

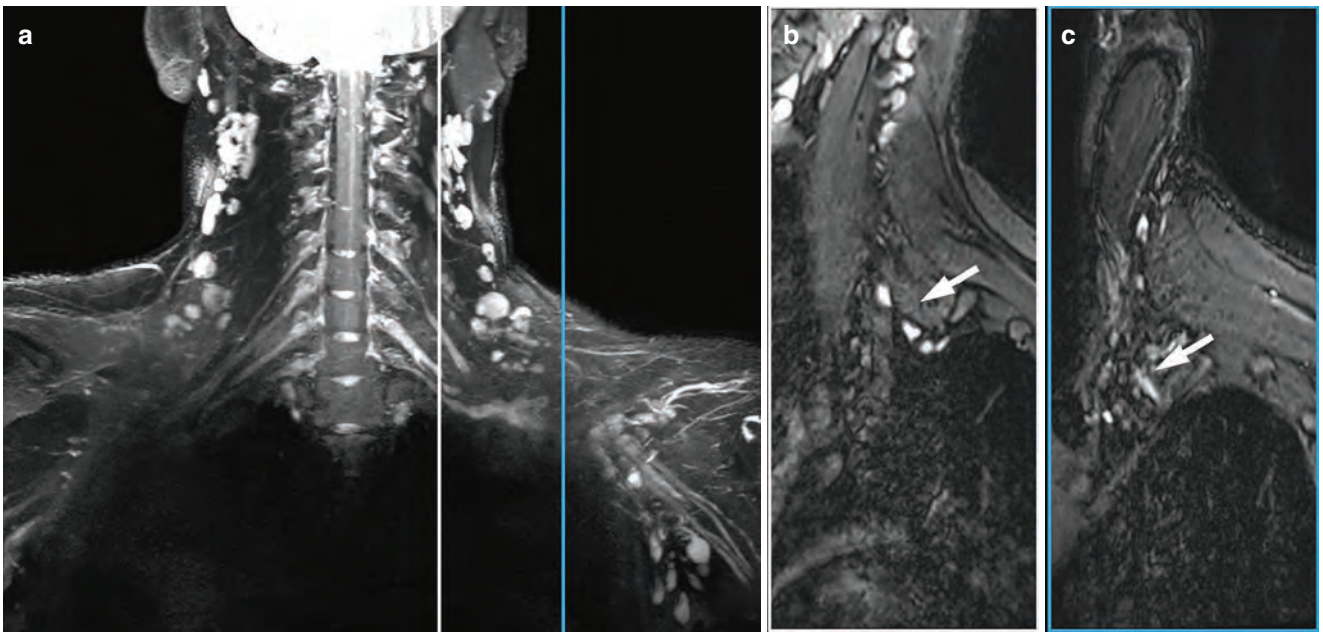

Fig. 18.5 Young man with transection of the entire left brachial plexus following an avalanche injury. (**a**) Coronal MIP of 3D SPACE STIR shows enlarged, retracted nerve stumps with (**b**) small stump neuroma formation (arrow) and (**c**) missing plexal structures more laterally (arrow)

18.5.3 Perineural Fibrosis

Perineural fibrosis is nearly always related to either prior radiation, surgery, or trauma. The most common site of post-irradiation perineural fibrosis is the brachial plexus, following irradiation for breast or nasopharyngeal carcinoma, usually with a 1–2-year latent period before symptoms emerge. The ultrasound and MR appearances of brachial plexopathy are as follows: increased size of the neural elements, poor delineation, obliterated or 'dirty' perineural fat, clumping or adhesions of the neural elements, intraneural or perineural hyperaemia/enhancement, and distortion of the neural and perineural tissues.

The main differential diagnosis, both clinically and on imaging, is metastatic infiltration of the brachial plexus. Metastatic infiltration of the brachial plexus is often, though not always, a feature of end-stage metastatic breast, head and neck, or lung carcinoma and appears, on imaging, as a discrete, often hyperaemic, mass infiltrating or adjacent to the brachial plexus. One may sometimes see metastatic infiltration of adjacent structures, such as the vertebrae or lung apices, as well as accompanying metastatic-type adenopathy. Occasionally, percutaneous biopsy may be necessary to distinguish between nodular post-irradiation fibrosis and metastatic disease. In such cases, this biopsy can be performed safely under ultrasound guidance.

Key Points

- Radiation is the most common cause of peripheral perineural fibrosis with the brachial plexus being most affected.
- Imaging appearances of perineural fibrosis are increased size, poor delineation, 'dirty' perineural fat, adhesion, hyperaemia/enhancement, and perineural distortion.

18.5.4 Neuralgic Amyotrophy

Neuralgic amyotrophy (or Parsonage-Turner syndrome) is preferable a term to 'brachial neuritis' as the nerves beyond the brachial plexus are not infrequently affected. Neuralgic amyotrophy is an inflammatory condition of unknown aetiology which, as the name implies, leads to both severe pain and muscle weakness, particularly in the periscapular region though also more peripherally in the upper limb. There is often a preceding trigger such as infection or vaccination. Neuralgic amyotrophy may wax and wane over several months with different nerves being affected. Usually only one side is affected, and even when both upper limbs are affected, it is typically sequential rather than simultaneous. The mixed suprascapular nerve is the most frequently affected nerve. A suprascapular nerve CSA of >4.2 mm^2 on ultrasound has a sensitivity of 86% and a specificity of 92% for neuralgic amyotrophy.

MRI is excellent at demonstrating the atrophic and denervation changes in the parascapular and other muscles (Fig. 18.6). Ultrasound, on the other hand, is particularly advantageous in allowing ready examination of potentially affected nerves beyond the brachial plexus. Extraplexal nerves that tend to be most affected are the long thoracic, axillary, median, and radial nerves as well as the anterior and posterior interosseous nerves. Affected nerves may show localised neural swelling ± neural fascicular entwinement ± hourglass constriction. These features can be appreciated on US and MR. The hourglass constriction is thought to result from a swollen inflamed nerve becoming twisted with limb movement and being unable to return to a normal position. Hourglass constriction requires surgical intervention. If one sees neural swelling on transverse ultrasound scanning, longitudinal scanning should be performed to evaluate the presence of incomplete or complete hourglass constriction. Similarly, on MRI if the nerve changes in diameter abruptly along its course along with MRN signal

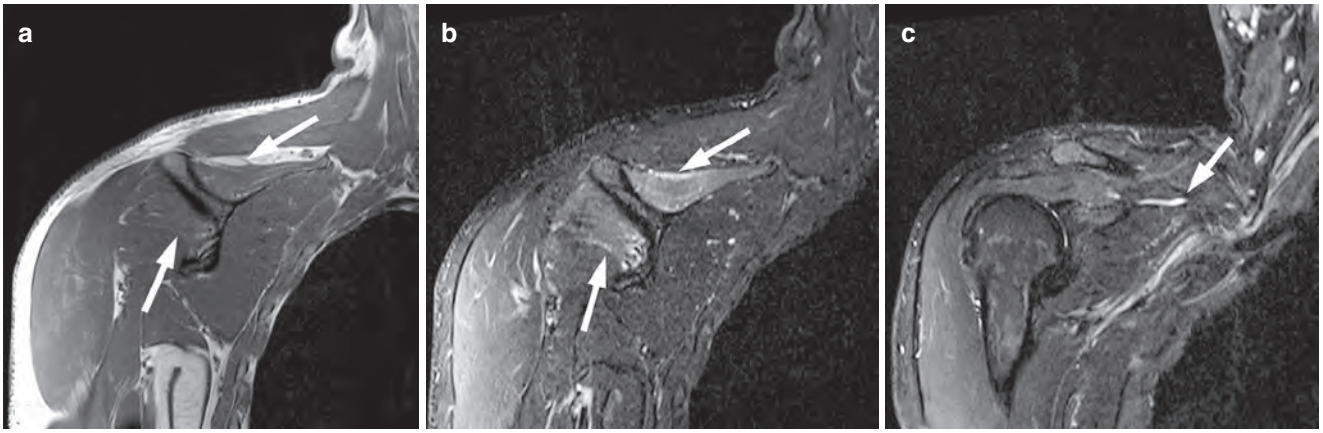

Fig. 18.6 In this patient with neuralgic amyotrophy, there is denervation oedema and moderate atrophy of the supraspinatus and infraspinatus muscles seen on both (**a**) T1-weighted (arrows) and (**b**) T2-weighted STIR images (arrows). (**c**) The suprascapular nerve is slightly thickened with a slightly irregular calibre (arrow) highly suggestive of neuralgic amyotrophy

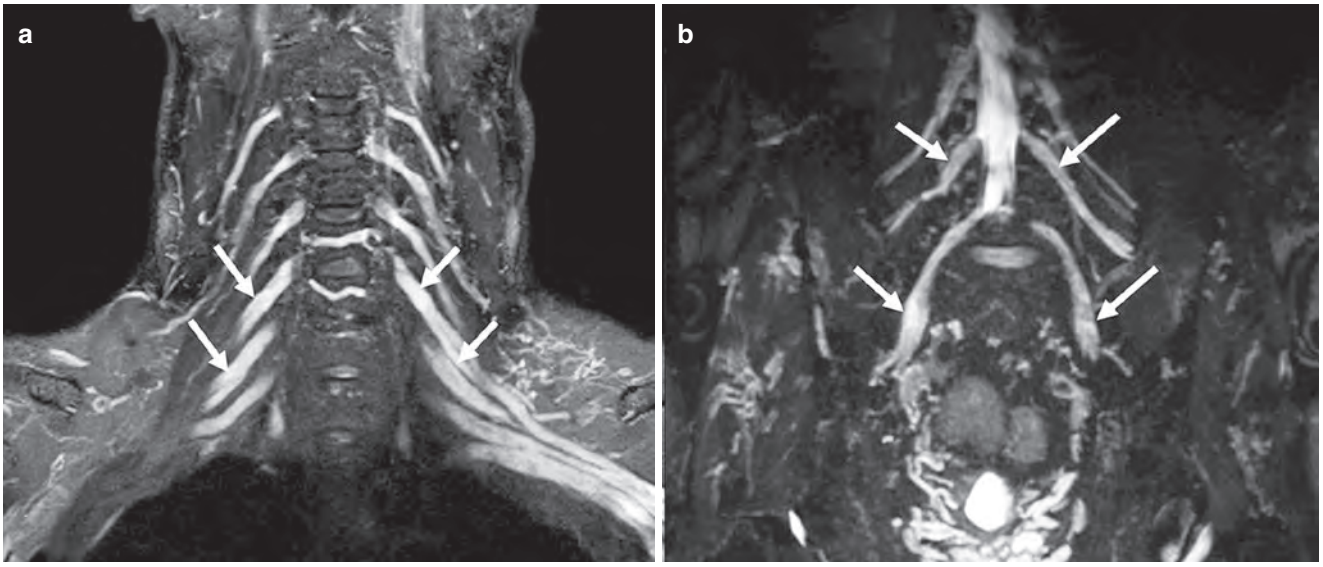

Fig. 18.7 MRN of patient with CIDP and characteristic enlargement of nerve roots and more peripheral plexal components on coronal MIP 3D SPACE STIR images, both in the (**a**) brachial (arrows) and (**b**) lumbosacral plexuses (arrows)

changes from hyper-, to hypo-, to hyperintensity, this may well represent focal hourglass constriction [22].

Key Points

- Neuralgic amyotrophy commonly affects the suprascapular nerve though extraplexal nerves are sometimes also affected.
- The imaging signs are neural swelling and, less frequently, fascicular entwinement ± hourglass constriction of an affected swollen nerve.
- MR is more accurate than US at showing target muscle denervation.

18.5.5 Inflammatory Neuropathy

Inflammatory neuropathies are amenable to anti-inflammatory treatment. The two main types of inflammatory neuropathy are chronic inflammatory demyelinating polyneuropathy (CIDP) and multifocal motor neuropathy (MMN). CIDP is a mixed neuropathy while MMN is predominantly motor. Both upper and lower limbs tend to be affected. Ultrasound and MR features are increased neural size and muscle denervation ± atrophy (Fig. 18.7). Any brachial trunk size of >8 mm^2 and swelling of the median nerve >13 mm^2 in the arm or >10 mm^2 in the forearm is 99% specific for inflammatory neuropathy [23]. Multiple sites of nerve swelling may be present.

Key Points

- Imaging is helpful in assessing inflammatory neuropathy.
- Bilateral, diffuse, and multifocal involvement is common.

18.6 Concluding Remarks

One can appreciate that imaging of the peripheral nerves comprises a wide pathological spectrum. Imaging has greatly increased our knowledge and perception of peripheral nerve disorders enabling these disorders to be diagnosed and treated with greater clarity and precision. When imaging the peripheral nerves, one needs to be particularly mindful of the patient's history regarding previous trauma, malignancy, surgery, irradiation, as well as neurological symptoms and deficit. Ultrasound and MRI are, in many instances, complementary in this regard with considerable clinical practical benefit.

Take Home Messages

- Ultrasound and MRI are incredibly helpful in the assessment of peripheral nerve disorders.
- High-resolution, targeted imaging is required.
- Usually either imaging modality will suffice, but to fully address some problems, both may be required and are usually complementary in this regard.

References

1. Filler AG, Maravilla KR, Tsuruda JS. MR neurography and muscle MR imaging for image diagnosis of disorders affecting the peripheral nerves and musculature. Neurol Clin. 2004;22:643–82.
2. Wasa J, Nishida Y, Tsukushi S, Shido Y, Sugiura H, Nakashima H, et al. MRI features in the differentiation of malignant peripheral nerve sheath tumors and neurofibromas. AJR Am J Roentgenol. 2010;194:1568–74.
3. Baumer P, Kele H, Kretschmer T, Koenig R, Pedro M, Bendszus M, et al. Thoracic outlet syndrome in 3T MR neurography fibrous bands causing discernible lesions of the lower brachial plexus. Eur Radiol. 2014;24:756–61.
4. Menorca RM, Fussell TS, Elfar JC. Nerve physiology: mechanisms of injury and recovery. Hand Clin. 2013;29:317–30.
5. Stanisz GJ, Midha R, Munro CA, Henkelman RM. MR properties of rat sciatic nerve following trauma. Magn Reson Med. 2001;45:415–20.
6. Husarik DB, Saupe N, Pfirrmann CW, Jost B, Hodler J, Zanetti M. Elbow nerves: MR findings in 60 asymptomatic subjects – normal anatomy, variants, and pitfalls. Radiology. 2009;252:148–56.
7. Kästel T, et al. Magic angle effect: a relevant artifact in MR neurography a 3T? AJNR Am J Neuroradiol. 2016;32(5):821–7.
8. Chhabra A, Lee PP, Bizzell C, Soldatos T. 3 Tesla MR neurography – technique, interpretation, and pitfalls. Skelet Radiol. 2011;40:1249–60.
9. Vargas MI, Viallon M, Nguyen D, Beaulieu JY, Delavelle J, Becker M. New approaches in imaging of the brachial plexus. Eur J Radiol. 2010;74:403–10.
10. Madhuranthakam AJ, Lenkinski RE. Technical advancements in MR neurography. Semin Musculoskelet Radiol. 2015;19:86–93.
11. Kasper JM, Wadhwa V, Scott KM, Rozen S, Xi Y, Chhabra A. SHINKEI – a novel 3D isotropic MR neurography technique: technical advantages over 3DIRTSE-based imaging. Eur Radiol. 2015;25:1672–7.
12. Chhabra A, Soldatos T, Subhawong TK, Machado AJ, Thawait SK, Wang KC, et al. The application of three-dimensional diffusion-weighted PSIF technique in peripheral nerve imaging of the distal extremities. J Magn Reson Imaging. 2011;34:962–7.
13. Guggenberger R, et al. Assessment of median nerve with MR neurography by using diffusion-tensor imaging: normative and pathologic diffusion values. Radiology. 2012;265:194–203.
14. Ng AWH, Griffith JF, Lee RKL, Tse WL, Wong CWY, Ho PC. Ultrasound carpal tunnel syndrome: additional criteria for diagnosis. Clin Radiol. 2018;73(2):214.e11–8.
15. Lee RKL, Griffith JF, Ng AWH, Tipoe GL, Chan AWH, Wong CWY, Tse WL, Ho PC. Cross-sectional area of the median nerve at the wrist: comparison of sonographic, MRI, and cadaveric measurements. J Clin Ultrasound. 2019;47(3):122–7.
16. Ng AWH, Griffith JF, Tong CSL, Law EKC, Tse WL, Wong CWY, Ho PC. MRI criteria for diagnosis and predicting severity of carpal tunnel syndrome. Skelet Radiol. 2020;49(3):397–405.
17. Ng AWH, Griffith JF, Tsai CSC, Tse WL, Mak M, Ho PC. MRI of the Carpal Tunnel 3 and 12 Months After Endoscopic Carpal Tunnel Release. AJR Am J Roentgenol. 2021;216(2):464–70.
18. Rhodes NG, Howe BM, Frick MA, Moran SL. MR imaging of the postsurgical cubital tunnel: an imaging review of the cubital tunnel, cubital tunnel syndrome, and associated surgical techniques. Skelet Radiol. 2019;48(10):1541–54.
19. Bäumer P, Dombert T, Staub F, Kaestel T, Bartsch AJ, Heiland S, Bendszus M, Pham M. Ulnar neuropathy at the elbow: MR neurography—nerve T2 signal increase and caliber. Radiology. 2011;260(1):199–206.
20. Ahlawat S, Blakeley JO, Langmead S, Belzberg AJ, Fayad LM. Current status and recommendations for imaging in neurofibromatosis type 1, neurofibromatosis type 2, and schwannomatosis. Skelet Radiol. 2020;49(2):199–219.
21. Chhabra A, Ahlawat S, Belzberg A, Andreseik G. Peripheral nerve injury grading simplified on MR neurography: as referenced to Seddon and Sunderland classifications. Indian J Radiol Imaging. 2014;24:217–24.
22. Sneag DB, Saltzman EB, Meister DW, Feinberg JH, Lee SK, Wolfe SW. MRI Bullseye sign: an indicator of peripheral nerve constriction in parsonage-turner syndrome. Muscle Nerve. 2017;56(1):99–106.
23. Goedee HS, van der Pol WL, van Asseldonk JH, Franssen H, Notermans NC, Vrancken AJ, van Es MA, Nikolakopoulos S, Visser LH, van den Berg LH. Diagnostic value of sonography in treatment-naive chronic inflammatory neuropathies. Neurology. 2017;88(2):143–51.

Chapter

Perspective Chapter: Musculoskeletal Ultrasound in Inflammatory Joint Diseases

Razvan Adrian Ionescu and Florentin Ananu Vreju

Abstract

Musculoskeletal ultrasound is a very important and useful tool in daily activity as a rheumatologist. It is also called "the stethoscope of rheumatologists." It enables the clinician to "see" into and around the joint, as ultrasound can penetrate any tissue except for bone. Even though ultrasound cannot penetrate bone, they are completely reflected by bony surfaces, which allows for the appreciation of bone integrity and the visualization of erosions. Another important aspect of using ultrasound for the evaluation of inflammatory joint diseases is the fact that it can depict inflammation within the musculoskeletal system (by depicting new vessel formation, using the Doppler effect), thus being able to contribute to the early and, even, very early diagnosis of inflammatory joint diseases and, conversely, to the early initiation of treatment that enables the prevention of irreversible disability.

Keywords: inflammation, joint, ultrasound, Doppler effect, B mode

1. Introduction

Ultrasonography (US) is a very important tool to be used in medicine. In rheumatology, its use is embedded in routine daily clinical practice and is called "the stethoscope of the rheumatologist."

There are some situations in which the "standard" approach to joint disease (i.e., anamnesis, clinical examination, lab tests, and radiographic examination) does not allow making the distinction between inflammatory and degenerative joint diseases, let alone the exact diagnosis of the diseases itself [1]. In such instances, there is a need for additional investigations to make the diagnosis. That is when the US was very helpful.

There are many advantages to using the US in rheumatology, especially inflammatory joint diseases. It is easy to use, it may be used on the bedside, it can be repeated, and it is sensitive to change. Musculoskeletal ultrasound (MSK-US) is the only rheumatological imaging modality that offers a dynamic examination while being a real-time examination, acquiring information as it happens. It is safe, fast, and non-invasive, while allowing for diagnostic procedures (e.g., arthrocentesis and biopsy) and treatment procedures (e.g., injection of different substances into the targeted area). But probably the most important advantage of MSK-US over any other imaging modality is its ability to diagnose the presence of inflammation, via using the Doppler

Multiple advantages of using MSK-US	
Reproducible	Very good acceptance
Good cost/effectiveness ratio	Easy doable
Improves sensitivity of clinical exam	Early detection of pathology
Real-time images	Very good acceptance
No radiation	Improved effectiveness of interventions

Table 1.
Advantages of MSK-US (modified from [2]).

module, as soon as the pathogenic process begins. Last, but not least, MSK-US allows simultaneous examination of multiple anatomical structures and increases the sensitivity of the clinical examination (**Table 1**) [2].

MSK-US is validated as a diagnostic tool for rheumatoid arthritis, crystal-induced arthritis, and psoriatic arthritis. It has also been validated for use as a follow-up tool in rheumatoid arthritis and psoriatic arthritis. Very important, because of its sensitivity to change, MSK-US is useful in evaluating response to treatment as well, in rheumatoid arthritis [3, 4]. When evaluating the metacarpophalangeal (MCP) joint for erosions, the intraobserver kappa statistic quotient is 0.75, while the interobserver kappa statistic quotient (which interprets agreement among different observers) is 0.76 [5]. Those quotients imply a good reliability of the observations and are comparable to those of radiologists scoring lesions on mammograms [5]. These reliabilities are dependent on multiple factors, one being the joint that is examined. Therefore, the kappa statistical quotient is 0.76 for the shoulder but 0.28 for the ankle/toes [6]. Another factor is the lesion that is evaluated: the overall agreement for tendon lesions and joint effusions is 91%. It is 83.5% for bursitis, 84% for tenosynovitis, and 87% for erosions [7]. In detecting knee synovitis, MSK-US is more sensitive than clinical examination [8].

There are some downsides to the use of MSK-US, too. The most important one is that it is operator-dependent. As shown above, sometimes, the inter-operator reliability is not that good. As such, there is a need for long, thorough, specialized, and continuous, time-consuming training to achieve expert levels, as it is a very dynamic field. Apart from the specialized operator, expert use of MSK-US involves the use of high-end machines, which are still quite expensive in some parts of the world. Due to the physical properties of ultrasound, they cannot penetrate bone. Consequently, MSK-US cannot be used to describe intra-osseous lesions, only cortical ones. Moreover, some anatomical regions are very difficult to explore on ultrasound [2].

The importance of MSK-US use in the context of inflammatory joint diseases is emphasized by its inclusion in EULAR's (European Alliance of Associations for Rheumatology) recommendations for the use of imaging in some of the inflammatory diseases management [9, 10].

2. Performing ultrasound examination

2.1 General principles

The most important thing about inflammatory joint diseases is to make the correct diagnosis and treatment as early as possible to avoid irreversible structural damage to

the joints. US can produce high-resolution images, distinguishing between different tissues and being able to assess bursae, tendons, ligaments, articular capsules, synovial proliferation, cartilage, and bone surface. Additionally, and of paramount importance, is the ability to assess inflammatory angiogenesis that characterizes inflammatory joint diseases.

EULAR's standardized procedures for ultrasound imaging in rheumatology [11] provide the general frame for a standardized MSK-US examination. Additionally, OMERACT (Outcome Measures in Rheumatology, former Outcome Measures in Rheumatoid Arthritis Clinical Trials) provides definitions for pathologic US findings [12].

When performing MSK-US, it is recommended we use linear transducers with a frequency ranging between 6 and 14 MHz for deep and intermediate structures and above 15 MHz for superficial ones [10]. There are two main modes to be used when performing MSK-US: B-mode, also termed gray scale (GS) mode, can provide anatomical information of the targeted region, and the Doppler mode (color Doppler or power Doppler) that allows for assessment of inflammatory angiogenesis [13]. When using Doppler mode, as little compression as possible is mandatory to avoid compression of very small vessels newly formed. Because blood flow in these vessels is very slow, the pulse repetition frequency should be less than 1 kHz.

Scanning joints should be performed with the probe oriented parallel or perpendicular to the surface of the bone (bony acoustic landmark) so that the cortical bone appears hyperechoic, bright, and sharp [11]. To avoid anisotropy, the probe should be tilted, angulated, and continually adjusted to maintain the ultrasound beam as perpendicular to the structure (usually a tendon) as possible, especially when the structure changes direction (as happens at the insertion site of tendons).

The probe can be used for compressing the region of interest, distinguishing between a liquid (compressible, that is displaceable) and a solid structure (non-compressible, that is non-displaceable) [11].

When performing MSK-US, a fair amount of gel should be used, especially when scanning superficial structures (e.g., extensor tendons of the hand). The orientation of the transducer is of paramount importance. If the structure to examine has a long axis in the craniocaudal orientation, then its most proximal part is placed on the left side of the screen. When in short axis view, the targeted region should be oriented on the screen as if the sonographist is looking at the patient [11].

MSK-US is a dynamic technique in that it can assess the region of interest in movement (passive or active) but also in that the probe should be translated, rotated, angulated, and tilted to allow the best assessment of the targeted region [11].

2.2 Structure examination and normal appearance

2.2.1 Tendons

The US examination of tendons shall be performed using linear probes with a frequency higher than 10 MHz. Because tendons are prone to anisotropy, care should be taken to maintain a perpendicular position of the probe onto the region of interest. This is particularly true for the attachment of the tendon to the bone (enthesis), where some tendons slightly change their orientation and any change of course of the tendon. Like any other structure examined in MSK-US, tendons should be examined in both longitudinal and transverse planes. In the transverse plane, one should be

Structure	US appearance
Tendon	Hyperechoic (to the subcutaneous surrounding tissue) fibrillar structure; L-parallel hyperechoic lines T-hyper/hypoechoic dots ("salt and pepper") No Doppler signal

Table 2.
US appearance of tendons. L, longitudinal view; T, transverse view (modified from [14, 15]).

aware of the small transonic image on the sides of the tendon, which is an artifact (tangential shadow) due to the curved shape of tendons in the transverse view. For tendons with synovial sheath, little probe pressure should be applied to avoid displacement (and missing) of small amounts of fluid in the sheath.

The normal appearance of a transverse scan of a tendon is that of a round/oval-shaped structure, resembling "salt and pepper" (hyper and hypoechoic) due to the fibrillar normal structure of a tendon. In longitudinal scans, they appear like fibrillar linear hyperechoic structures with a parallel disposition (**Table 2**).

Tendons must be examined on a gray scale (B-mode) and in Doppler mode to check for abnormal vascularization. Normal tendons do not have visible vessels. The examiner should pay attention to the Doppler settings for superficial or intermediate/profound tendons.

2.2.2 Enthesis

Enthesis is the complex region where a tendon, ligament, joint capsule, fascia, or muscle attaches to the bone [2]. Enthesis of interest in MSK-US are the fibrocartilaginous ones as they represent the target organ in spondylarthritis where the pathogenic process originates. Fibrocartilaginous entheses are a histologically complex structure of attachment to bone, so complex that the term "entheseal body" was coined at the beginning of the century [16, 17]. By the ultrasonographic definition, enthesis is the region where tendon, ligament, and joint capsule insert over the bone with regular edges and the same appearance and width as the rest of the tendon/ligament/capsule, having a fibrillar linear homogenous echogenicity [18]. The probe used for assessing enthesis is one with high frequency (>10 MHz). The normal US aspect of an enthesis in longitudinal view was aforementioned. In the transverse view, it is similar to the tendon/ligament/capsule it inserts. Nevertheless, when assessing an enthesis using US, one must assess all the components of the "entheseal body": the tendon, the bone underneath, the bursa (that frequently exists to lower friction between the tendon and the bone), and periarticular tissue [19]. For example, in the case of tendons, the US examination of the enthesis must consider the curvature enthesis usually taken when inserted into the bone. This can translate into malalignment of the transducer with the fibers of the enthesis, thus producing anisotropy. Therefore, whenever examining an enthesis, the probe must be slightly and continuously adjusted in its position over the enthesis. Doppler mode is mandatory, especially if spondyloarthritis is suspected (pay attention to the settings of the Doppler mode). Normal enthesis does not have visible vessels. The enthesis of interest in the evaluation of spondyloarthropathies is the insertion of the tricipital tendon on the olecranon, the insertion of the common extensor of the fingers tendon of the lateral humeral epicondyle, the insertion of the quadricipital tendon on the patella, the superior and inferior

insertions of the patellar tendon on the patella and the tibial tuberosity, respectively, the insertion of the Achilles tendon on the calcaneus, and the insertion of the plantar fascia on the inferior aspect of the calcaneus.

2.2.3 Cartilage

As normal cartilage is mainly made of water and has no intrinsic vasculature, the US beam will pass through it without almost any reflection; its normal appearance is, consequently, an intense hypoechoic structure. There are two types of cartilage that are of interest in MSK-US: hyaline cartilage and fibrocartilage. As hyaline cartilage lies over bones, which are totally impenetrable to US (thus constituting bony acoustic landmarks), it can be easily recognized because the profound interface between two structures with highly different acoustic impedance (bone and cartilage) produces an intense echo. Because of the very same physical reasons, the superficial border of the cartilage is more difficult to recognize since the difference in acoustic impedance between the cartilage and the surrounding intraarticular space is less [20]. Depicting the fibrocartilage is even more complicated (e.g., triangular fibrocartilage complex (TFFC) of the wrist). When assessing the cartilage, the choice of the probe's frequency depends on the depth of the region of interest: the deeper the region, the lower the frequency. The most frequently assessed hyaline cartilages in rheumatic inflammatory diseases are the femoral condyles cartilage and the cartilage of the head of the metacarpal bones. For both, the best position to assess them is in maximum flexion of the knee and of the metacarpophalangeal joints, respectively, because in this position they are best exposed from within other bony structures. As usual, they are examined in longitudinal and transverse view. The US examination must describe its transparency, homogeneity, thickness, the continuity of the interfaces (cartilage/adjacent soft tissue and cartilage/bone), and the subjacent bone profile. The most frequently assessed fibrocartilage is the triangular fibrocartilage complex of the wrist and the menisci of the knees. For the TFFC examination, the hand should be pronated and slightly deviated to the radial side, thus exposing the complex. It is examined only in the longitudinal view because the transverse approach does not bring much supplementary information [21]. As the TFFC is deep, the acoustic window is represented by the tendon of the sixth compartment of the extensor tendons of the hand, the extensor carpi ulnaris tendon, viewed in the longitudinal axis as well. The TFFC is viewed as a triangular, homogenous, hypoechoic (compared to the tendon above) structure lying between the distal head of the ulna and the triquetrum. Because the menisci are between the femur and the tibia, they are not completely depictable in any position. To view the external portion, the knee must be in a neutral position (extension) or slightly flexed (around 30 degrees), with the patient lying in dorsal decubitus [20]. They normally appear triangular shaped (basis—superficial, peak—deep), hypoechoic, homogenous structures. Normally, Doppler mode examination reveals no vessels in the cartilage.

2.2.4 Bone

Due to its abundance in calcium, bones cannot be assessed by US. Nevertheless, MSK-US is very accurate in assessing bone surface [22]. The frequency of the probe depends on the depth at which the bone is localized. The normal appearance of the cortical bone is as a hyperechoic continuous line that generates posterior acoustic shadowing and, sometimes, reverberation artifacts. Bones are examined on a gray scale

for the continuity and sharpness of their surface. Special attention must be given to the normal irregularities produced by the foramen nutritive, grooves for tendons or nerves, and sesamoid bones. Usually, most of these structures can be easily recognized, and the foramen nutritive is smooth and oblique to the diaphysis. Doppler mode is helpful in differentiating between nutritive vessels and inflammatory neoangiogenic vessels [23].

2.2.5 Joint capsule, synovial membrane, and joints

The joint capsule, which attaches to the bone at the end of the cartilage and is usually strengthened by ligaments, appears on MSK-US examination as a hypo/hyperechoic curved line above the joint visible in longitudinal view in B-mode examination. Its insertions (enthesis) are better seen than the mid portion.

Under normal conditions, the synovial membrane is extremely thin, so it cannot be visualized by US. It is visible only when it becomes thicker, as in chronic inflammatory joint disease. It is then when Doppler mode is most needed.

Examining a joint with US means examining the profile of the two bones that compose the articulation, the cartilage in between, the capsule, and the synovial membrane. In 2017, EULAR standardized procedures for ultrasound imaging [11]. As per these, the best way to perform wrist joint examination, bearing in mind that we are assessing two joints (radio-carpal and inter-carpal), is placing the transducer longitudinally, on the dorsal aspect, at the level of the radio-lunate and luno-capitate joints (corresponding to the third finger). For the metacarpophalangeal joint, the transducer is placed longitudinally over the midline of the joint and for the elbow joint the transducer is placed longitudinally on the anterior aspect over the coronoid fossa. All these techniques will allow for all or most of the above-mentioned structures to be visualized. The capsule of the glenohumeral joint is merely visible over the posterior recess of the joint. At the level of the ankle, the transducer should be placed over the anterior tibiotalar joint recess, while at the knee, the capsule is visible at the lateral and medial aspect of the tibiofemoral joint [11]. For the hip joint, the transducers should have low frequency and should be large enough to visualize the joint as much as possible. One should be aware that low-frequency transducers are not very reliable for Doppler mode use [24].

2.3 Pathological US findings

To understand and practice MSK-US in inflammatory joint diseases, it is mandatory to know the pathological findings that must be searched for.

Since MSK-US is operator-dependent, it should be as standardized as possible. In this respect, OMERACT has developed standardized definitions to be used when assessing and reporting an MSK-US examination to ensure maximum uniformity of reports [11]. Additionally, in 2005, the OMERACT Ultrasound Working Group (WG) initiated research on definitions and scoring of elementary lesions and US-detected pathologies [12] that have been updated along with the combined EULAR-OMERACT scoring system [25]. The result is a series of definitions and scoring systems for some of the inflammatory joint diseases and other rheumatic inflammatory or degenerative diseases that serve as a basis for diagnosing inflammatory joint diseases using MSK-US in clinical daily practice (**Tables 3** and **4**) [25].

There are inflammatory joint diseases in which some of the elementary US lesions are useful for diagnosis and/or treatment and are not inflammatory in nature but structural. Since they are used in daily clinical practice, their OMERACT definitions follow (**Table 5**).

Type of pathology	Description of US findings
Synovitis	Presence of hypoechoic synovial hypertrophy (SH) (regardless of presence of effusion or Doppler signal)
Tenosynovitis	Abnormal anechoic and/or hypoechoic (relative to the tendon) tendon sheath widening, related to tenosynovial abnormal fluid/hypertrophy. Doppler mode should be used only if there is peritendinous synovial sheath widening on B-mode; Doppler signal can be considered if in two perpendicular planes, within the peritendinous synovial sheath, excluding normal feeding vessel
Enthesitis	Hypoechoic and/or thickened insertion of the enthesis close to the bone (<2 mm from bony cortex) with Doppler signal (if active) and possible structural lesions
Erosion	Intra- and/or extra-articular discontinuity of bone cortex visible in two perpendicular planes (step-down discontinuity in [19])

Table 3.
OMERACT definitions for US-detected pathologies (modified after [25]).

US pathology	Elementary lesion
Synovitis	SH is defined as the presence of abnormal hypoechoic synovial tissue within the capsule that is not displaceable and poorly compressible and that may exhibit Doppler signals
Enthesitis	Hypoechoic increased thickness of enthesis (i.e., tendon insertion <2 mm from bony cortex) that exhibits Doppler signal
Tenosynovitis	Tenosynovial hypertrophy is the presence, in two perpendicular planes, within the synovial sheath, of abnormal hypoechoic (relative to tendon) tissue, not displaceable and poorly compressible, that may exhibit Doppler signal

Table 4.
OMERACT definitions of inflammatory elementary lesions composing the inflammatory US pathologies (modified from [25]).

Pathology	Structural elementary lesion
Enthesitis	Erosions, calcifications, enthesophytes at the level of the enthesis
Gout double contour	Abnormal hyperechoic band over the superficial margin of the hyaline cartilage, independent of the angle of insonation, regular/irregular, continuous/intermittent, that can be distinguished from the cartilage interface sign
Gout aggregate	Heterogenous hyperechoic foci maintain their high degree of reflectivity when the gain is minimized or the insonation angle is changed, which occasionally can generate posterior acoustic shadow
Gout tophus	Circumscribed, inhomogeneous, hyperechoic and/or hypoechoic aggregation, with/without posterior shadowing, which may be surrounded by a small anechoic rim
CPPD fibrocartilage	Hyperechoic deposits of variable shape, within the cartilage, fixed or moving along with the fibrocartilage during dynamic assessment
CPPD hyaline cartilage	Hyperechoic deposits of variable size and shape, without posterior shadowing, within the cartilage, fixed or moving along with the hyaline cartilage during dynamic assessment
CPPD tendon	Hyperechoic linear structures, generally without posterior shadowing, within the tendon, fixed or moving along with the tendon during dynamic assessment
CPPD synovial fluid	Hyperechoic deposits of variable size, without posterior shadowing, within the synovial fluid, mobile with joint movement and probe compression

Table 5.
Definitions of structural elementary lesions composing the inflammatory US pathologies (modified from [25]).

Based on those definitions, as previously mentioned, there is a EULAR-OMERACT combined scoring system [25], considering together gray scale appearance and Doppler signal, for synovitis (**Tables 6** and 7), tenosynovitis (**Table 8**), and enthesitis (**Tables 9** and **10**), separately.

Gray scale (SH) appearance	Grade 0 (normal)	No SH (irrespective of effusion)
	Grade 1 (minimal)	Minimal hypoechoic SH, up to the joint line
	Grade 2 (moderate)	Moderate hypoechoic SH protruding beyond the joint line with concave surface
	Grade 3 (severe)	Severe hypoechoic SH protruding beyond the joint line with convex surface
Doppler (PD) appearance	Grade 0 (normal)	No signals
	Grade 1 (minimal)	<3 single signals OR 1 confluent +2 single OR 2 confluent
	Grade 2 (moderate)	>grade1 BUT <50% of SH area covered by signals
	Grade 3 (severe)	>50% of SH area covered by signals

Table 6.
OMERACT scoring system for synovitis. SH, synovial hypertrophy; PD, power Doppler (modified from [25]).

Grade 0: normal	No SH + no PD
Grade 1: minimal synovitis	Grade 1 SH and/or ≤ grade 1PD
Grade 2: moderate synovitis	Grade 2 SH and/or ≤ grade 2 PD or Grade 1 SH + grade 2 PD
Grade 3: severe synovitis	Grade 3 SH and/or ≤ grade 3 PD or Grade 1 or 2 SH + grade 3 PD

Table 7.
EULAR-OMERACT combined scoring system for synovitis. EULAR, European Alliance of Associations for Rheumatology; OMERACT, Outcome Measures in Rheumatology; SH, synovial hypertrophy; PD, power Doppler (modified from [25]).

Grade	**B-mode (GS)**	**Doppler mode**
Grade 0	No tenosynovial widening	No Doppler signal
Grade 1	Minimal amount of an–/hypoechoic material within the tenosynovial sheath, in two perpendicular planes, localized or displaceable	Signals in one area of the widened sheath, in two perpendicular planes, excluding normal feeding vessel
Grade 2	Moderate amount of an–/hypoechoic material within the tenosynovial sheath	Signals in >1 area of the widened sheath, in two perpendicular planes, excluding normal feeding vessel
Grade 3	Severe amount of an–/hypoechoic material within the tenosynovial sheath	Signals filling most of the widened sheath in two perpendicular planes, excluding normal feeding vessel

Table 8.
OMERACT combined scoring system for tenosynovitis. GS, gray scale (modified from [25]).

Doppler	**0–3**
Hypoechogenicity	0/1
Thickened enthesis	0/1
Bone erosion	0/1
Enthesophyte or calcification	0/1

Table 9.
OMERACT combined scoring system for enthesitis with semiquantitative Doppler grading—part 1 (modified from [25]).

Grade 0	**0 Doppler signal**
Grade 1	< 2 punctiform Doppler signals with no confluent Doppler signal
Grade 2	2–4 punctiform Doppler signal OR 1 confluent Doppler signal
Grade 3	>4 punctiform Doppler signal OR > 1 confluent Doppler signal

Table 10.
OMERACT combined scoring system for enthesitis with semiquantitative Doppler grading—part 2 (modified from [25]).

All this data is mandatory for performing high-quality MSK-US. On one hand, they guide on "speaking the same language," and on the other hand, they allow appreciation of the efficacy of management of the disease, as they allow comparisons in the same patient between different points in time.

3. Ultrasound examination in rheumatic inflammatory joint diseases

3.1 Rheumatoid arthritis (RA)

The use of MSK-US in rheumatoid arthritis is frequent because it can provide valuable information on diagnosis, differential, disease severity, and monitoring disease course on treatment [26].

As a diagnostic tool, MSK-US can be used in undifferentiated arthritis to help a positive or a differential diagnosis [27]. This is especially important in seronegative patients whose disease could thus remain undiagnosed for a long time.

The features that US can depict in RA are synovial hypertrophy, cortical bone erosions, tenosynovitis and effusion. Padovano et al. showed that effusion without synovial hypertrophy should not be considered inflammatory in nature [28]. The presence of a Doppler signal within the thickened synovium is indicative of active inflammatory disease [29]; it, as well as features of tenosynovitis, predicts the risk of imaging progression of RA [30]. MSK-US is a more sensitive imaging modality for detecting erosions than X-ray examination [31]. MSK-US is very useful in depicting erosion on the fifth MTP joint and the second and fifth MCP joints. Even though the clinical relevance of a discovered erosion is variable (depending on its dimension and location), erosion at the fifth MTP increases the probability of RA diagnosis in arthritic patients [26].

MSK-US can also be used to evaluate disease progression in RA. It has been proven that a high baseline power Doppler US signal at the MCP level is predictive of the development of radiographic erosions over the next year [32].

It is well known that some patients, despite being in clinical remission, continue to progress radiologically [26]. Studies have shown that MSK-US is a very good imaging modality in assessing residual activity in RA patients: patients in clinical remission with residual power Doppler active synovitis are at high risk of progressive joint disease [33]. Moreover, these patients are at increased risk of relapse as compared to those power Doppler negative [34].

MSK-US scanning can be quite a time-consuming approach; that is why the number of joints to scan is always a question. This number depends on the clinical presentation, but there are studies pertaining to the choice and number of joints to be scanned in RA. Naredo et al. suggest the assessment of 12 joints (bilateral wrists, metacarpophalangeal, and proximal interphalangeal II and III of hands and knees) using power Doppler US, as it provides an overall assessment of joints' inflammation [35].

US has been proven to be useful in monitoring disease activity and response to treatment. It correlates strongly with disease activity score 28 joints (DAS28) and inflammatory serum markers (C-reactive protein and erythrocyte sedimentation rate) [36], and it is also sensible to therapy-induced change, thus being able to influence treatment decisions [37].

Combining clinical examination and MSK-US improves the diagnosis of RA patients, especially when radiology assessment is not conclusive. This allows for an early diagnosis, which is the key to avoiding permanent structural joint damage. It is useful in monitoring disease and appreciating the risk of disease flare (in patients in clinical remission) as well as in guiding treatment decisions.

3.2 Spondylarthritis (SpA)

US use in SpA is merely confined to peripheral SpA since in axial SpA, the US examination of the sacroiliac joints is limited to the posterior part of the joints, thus making magnetic resonance imaging the preferred modality to assess these joints [26]. In fact, US imaging has a greater sensitivity than other imaging modalities and clinical examination to detect peripheral involvement in SpA [33].

Using MSK-US in SpA is peripheral SpA is endorsed by EULAR in its recommendations for the use of imaging modalities in the diagnosis and management of SpA [9]. Published in 2015, these recommendations state that, in peripheral SpA, US can and should be used in diagnosing, monitoring disease activity, and evaluating structural damage.

The features associated with peripheral SpA that are assessable using MSK-US are arthritis, enthesitis, tenosynovitis, and dactylitis.

The US appearance of SpA arthritis is no different than RA's (**Table 3**). Using Doppler mode can confirm the intense inflammatory vascularization of the hypertrophied synovium, confirming active disease. This is also true for the US aspect of SpA tenosynovitis, with the additional comment that, in SpA, tenosynovitis is more frequent than in RA.

Enthesitis is considered the hallmark of SpA, since the pathogenic process of the disease appears to start at the level of the enthesis [38]. The definition, the US aspect, and the combined scoring system of enthesis have been described previously (see **Tables 3**, **9**, and **10**). Assessing entheseal inflammation has been long shown to have a very good diagnostic value in peripheral SpA [39]. It is noteworthy that, to define it as inflammatory, the lesion should be confined to less than 2 mm from the bone

cortex [40], and that structural bone lesions (enthesophytes and erosions) are seen in later stages, while the earlier lesions are those related to the tendon [41]. It should be emphasized that some structures are considered as "functional enthesis," even though they do not respect the "anatomical" definition in that we cannot find a fibrocartilaginous structure (e.g., the tendon areas around the pulleys) [10]. It is also noteworthy that peritendon inflammation of the extensor digitorum tendon (PTI pattern) and central slip tendon enthesitis at the level of the proximal interphalangeal joint are features specific for psoriatic arthritis (as a form of peripheral SpA) [38]. There are multiple US scores that can be used in assessing enthesitis as per the selection of sites to be assessed: MASEI (Madrid Sonography Enthesitis Index) [42], OMERACT US [40], and GUESS (Glasgow Ultrasound Enthesitis Score) [43].

Dactylitis is a very complex US inflammatory lesion, as it involves many structures; it consists of soft tissue edema, enthesitis of the superficial flexor of the finger tendon, peritendinous inflammation (PTI pattern of the extensor tendon), tenosynovitis of the flexor tendon and arthritis, all located in the same finger or toe, making it a pandigital involvement [44]. There is also a scoring system for dactylitis [45].

3.3 Crystal-induced arthritis

The use of MSK-US in crystal-related joint diseases is supported by its high sensitivity and specificity [46]. Both types of crystal deposits generate reflectivity, thus forming the US image.

Monosodium urate crystal deposits on the surface of the articular cartilage [47]. Because of that, they generate a hyperechoic band on that surface parallel to the contour of the head of the bone and move along with the bone, confirming it belongs to the cartilage. This is the "double contour" sign. The band is visible, irrespective of the angle of insonation (see also **Table 5**). Also, it is visible along the contours of the cartilage. The double contour sign is visible in most long-standing gouty patients; it is also reversible with treatment. Another US appearance of monosodium urate is the so-called "snowstorm appearance," which is the presence of numerous hyperechoic spots within an area of echogenicity. This is usually depicted when monosodium urate crystals are present within a synovial effusion. Another possible US finding that may be depicted in chronic gout is gout tophus, which appears as a heterogeneous mass containing hyperechoic foci. Sometimes, they must be differentiated from rheumatoid nodules. Tophi may be found inside tendons, joints, and bursae [46, 48].

In diagnosing calcium pyrophosphate deposits, MSK-US is an accurate tool with a high likelihood ratio and better sensitivity than X-rays [49, 50]. Calcium pyrophosphate crystals deposit inside the hyaline cartilage of the joints (intraarticular), in contrast to monosodium urate crystals (which, as previously noted, are located on the surface of the cartilage). Their appearance is classical at the wrist level, where they can be depicted inside the triangular cartilage and at the knee level (inside the cartilage and the menisci). They can also be viewed inside the hip and the acromioclavicular joints [49, 50].

As with all other MSK-US examinations, the evaluation of deposits must be done both in B-mode and in Doppler mode to assess the presence of inflammation associated with the deposit itself. Also, the evaluation must be performed in 2 perpendicular planes, especially when it is referring to the consequences of the presence of crystal deposits, that is, erosion; as well as with other MSK pathologies

potentially producing erosions, lesions produce by crystal deposits must be confirmed in both perpendicular planes.

4. Discussion

Having such a versatile imaging tool in rheumatology as MSK-US represents a very good advantage for clinician rheumatologists. Knowing how to use it is mandatory nowadays. As it is validated for diagnosis in its early stages of inflammatory joint diseases, as well as for follow-up and evaluation of treatment efficacy, MSK-US has to be and is incorporated into daily routine practice.

On the other hand, one must not over-emphasize the role of MSK-US in inflammatory joint diseases since there are some downsides to it. Probably the most important problem with this imaging technique is the need for good training, especially long training. Moreover, no matter the quality of the training, any US image is clearly operator-dependent. This is illustrated by the differences in agreement that arise when several experimented experts examine the same joint in the same patient. It is noteworthy, though, that these "disagreements" also depend on other factors, such as the joint examined.

One of the important advantages of MSK-US is the possibility of exploring joints dynamically. The possibility of examining joint movement while it happens allows for viewing details that can provide diagnostic clues. Moreover, MSK-US is the only at-hand imaging method that permits interventional maneuvers, whether diagnostic or therapeutic.

Of course, MSK-US cannot examine every joint in the body, even in the context of inflammatory joint diseases. That is because of the anatomical situation of some joints, as is the case of the sacroiliac joint, whose inflammatory state in the context of spondyloarthritis is US accessible with great difficulty, even though they are superficially located under the skin. This brings us to the fact that MSK-US, like any other investigation, should be carefully chosen, in the appropriate context, of an inflammatory joint disease. The previous example, pertaining to the sacroiliac joints, is conclusive: in case of suspicion of involvement of those joints, as part of a axial spondyloarthritis, one should prefer magnetic resonance imaging over any other imaging technique, including MSK-US, for diagnostic purposes. On the other hand, if there is a suspicion of enthesitis also in the context of spondyloarthritis, one should choose US over any other imaging method for confirming the peripheral involvement.

5. Conclusions

Ultrasound is a very useful tool for the practicing rheumatologist. It is at hand, rapid, non-invasive, cost-effective, repeatable and allows for dynamic evaluation. It can be used for diagnosis, monitoring and treatment decision making. Its use has opened a new window to the diagnosis and also to a more profound understanding of pathogenetic mechanisms of inflammatory joint diseases, thus allowing for an early diagnosis, followed by an early treatment and, hence, avoidance of irreversible joint damage and disability. It has become an extension of the clinical examination ("rheumatologist's extended finger" [51]) enabling the treating physician with a more profound view of processes to be influenced by the various and effective treatments of inflammatory joint diseases. Thus, performing musculoskeletal ultrasound is mandatory for any clinician working in the field of rheumatology.

Conflict of interest

The authors declare no conflict of interest.

Author details

Razvan Adrian Ionescu[1*] and Florentin Ananu Vreju[2]

1 "Carol Davila" University of Medicine and Pharmacy, Colentina Clinical Hospital, Bucharest, Romania

2 Craiova University of Medicine and Pharmacy, Craiova County Emergency Hospital, Craiova, Romania

References

[1] Kaeley GS, Bakewell C, Deodhar A. The importance of ultrasound in identifying and differentiating patients with early inflammatory arthritis: A narrative review. Arthritis Research & Therapy. 2020;**22**(1):1-10. DOI: 10.1186/s13075-019-2050-4

[2] Mata Arnaiz MC, de Miguel ME. Utilidad de la ecografia en la evaluacion de las entesis perifericas en las espondiloarthritis. Reumatologia Clinica. 2014;**10**:113-119

[3] Haavardsholm EA, AgaAB OIC, et al. Ultrasound in management of rheumatoid arthritis: ARCTIC randomized controlled strategy trial. BMJ. 2016;**354**:i4205

[4] Dale J, Stirling A, Zhang R, et al. Targeting ultrasound remission in early rheumatoid arthritis: The results of the TaSER study, a randomized clinical trial. Annals of the Rheumatic Diseases. 2016;**75**:1043

[5] Antonio AL, Crespi CM. Predictors of interobserver agreement in breast imaging using the brest imaging reporting and data system. Breast Cancer Research and Treatment. 2010;**120**:539

[6] Scheel AK, Schmidt WA, Hermann KG, et al. Interobserver reliability of rheumatologists performing musculoskeletal ultrasonography: Results from a EULAR "train the trainers" course. Annals of the Rheumatic Diseases. 2005;**64**:1043

[7] Naredo E, Moller I, Moragues C, et al. Interobserver reliability in musculoskeletal ultrasonography: Results from a "Teach the Teachers" rheumatologist course. Annals of the Rheumatic Diseases. 2006;**65**:14

[8] Karim Z, Wakefield RJ, Qiunn M, et al. Validation and reproductibility of ultrasonography in the detection of synovitis in the knee: A comparison with arthroscopy and clinical examination. Arthritis and Rheumatism. 2004;**50**:387

[9] Mandl P, Navarro-Compan V, Terslev L, et al. EULAR recommendations for the use of imaging in the diagnosis and management of spondylarthritis in clinical practice. Annals of the Rheumatic Diseases. 2015;**74**(7):1327-1339

[10] Colebatch AN, Edwards CJ, Østergaard M, et al. EULAR recommendations for the use of imaging of the joints in the clinical management of rheumatoid arthritis. Annals of the Rheumatic Diseases. 2013;**72**(6):804-814. DOI: 10/1136/annrheumdis-2012-203158

[11] Moller I, Janta I, Backhaus M, et al. The 2017 EULAR standardized procedures for ultrasound imaging in rheumatology. Annals of the Rheumatic Diseases. 2017;**0**:1-6

[12] Wakefield RJ, Balint PV, Szkudlarek M, et al. Musculoskeletal ultrasound including definitions for ultrasonographic pathology. The Journal of Rheumatology. 2005;**32**(12):2485-2487

[13] Vreju F, Ciurea M, Rosu A, et al. Power Doppler sonography, a non-invasive method of assessment of the synovial inflammation in patients with early rheumatoid arthritis. Romanian Journal of Morphology and Embryology. 2011;**52**(2):637-643

[14] Naredo E, d'Agostino MA, Wakwfield RJ, et al. OMERACT ultrasound task force. Reliability of a consensus based ultrasound score for

tenosynovitis in rheumatoid arthritis. Annals of the Rheumatic Diseases. 2013;**72**:1328-1334

[15] Micu M. Tendoanele. In: Fodor D, editor. Ecografie Musculoscheletala vol 1: Semiologia normala si patologica a structurilor musculoscheletale. Bucuresti: Librex Publishing; 2017. pp. 37-48

[16] Benjamin M, McGonagle D. The anatomical basis for disease localization in seronegative spondyloarthropathy at enthesis and related sites. Journal of Anatomy. 2001;**199**:503-526

[17] Benjamin M, Moriggl B, Brenner E, et al. The enthesis organ concept. Why enthesopathies may not present as a focal insertional disorder. Arthritis and Rheumatism. 2004;**50**:3306-3313

[18] Terslev L, Naredo E, Iagnocco A, et al. Defining enthesitis in spondyloarthritis by ultrasound: Results of a Delphi process and of a reliability reading exercise. Athritis Care Research. 2014;**66**:741-748

[19] Vlad V. Enteza. In: Fodor D, editor. Ecografie Musculoscheletala vol 1: Semiologia normala si patologica a structurilor musculoscheletale. Bucuresti: Librex Publishing; 2017. pp. 57-64

[20] Felea I, Tamas M-M. Cartilajul. In: Fodor D, editor. Ecografie Musculoscheletala vol 1: Semiologia normala si patologica a structurilor musculoscheletale. Bucuresti: Librex Publishing; 2017. pp. 71-80

[21] Taljanovic MS, Goldberg MR, Sheppard E, et al. US of intrinsic and extrinsic wrist ligaments and triangular fibrocartilage complex—Normal anatomy and imaging technique. Radiographics. 2011;**e44**:1-26

[22] Zamorani MP, Valle M. Bone and joint. In: Bianchi S, Martinoli C, editors. Ultrasound of the Musculoskeletal System. Springer Science & Business Media. Germany: Springer-Verlag Berlin Heidelberg; 2007. pp. 137-185

[23] Vreju FA. Osul, periostul. In: Fodor D, editor. Ecografie Musculoscheletala vol 1: Semiologia normala si patologica a structurilor musculoscheletale. Bucuresti: Librex Publishing; 2017. pp. 103-110

[24] Vlad V, Berghea F. Articulatiile sinoviale. In: Fodor D, editor. Ecografie Musculoscheletala vol 1: Semiologia normala si patologica a structurilor musculoscheletale. Bucuresti: Librex Publishing; 2017. pp. 91-101

[25] Bruyn GA, Iagnocco A, Naredo E, et al. OMERACT definitions for ultrasonographic pathologies and elementary lesions of rheumatic disorders 15 years on. The Journal of Rheumatology. 2019;**46**(10):1388-1393. DOI: 10.3899/jrheum.181095

[26] D'Agostino MA, Padovano I, Iagnocco A. Imaging. In: Bijlsma JWJ, Hahula E, editors. EULAR Textbook on Rheumatic Diseases. 3rd ed. London: BML Publishing Group Ltd; 2018. pp. 122-157

[27] Gutierrez M, Bertolazzi C, Castillo E, et al. Ultrasound as a useful tool on the diagnosis of rheumatoid arthritis in patients with undifferentiated arthritis. Journal of Clinical Rheumatology. 2019;**25**(5):203-208. DOI: 10.1097/RHU.0000000000001034

[28] Padovano I, Constantino F, Breban M, et al. Prevalence of ultrasound synovial inflammation in heathy subjects. Annals of the Rheumatic Diseases. 2016;**75**(10):181901823. DOI: 10.1136/annrheum dis-2015-208103

[29] Iagnocco A, Ceccarelli F, Perricone C, et al. The role of ultrasound in rheumatology. Seminars in Ultrasound, CT, and MR. 2011;**32**(2):66-73. DOI: 10.1053/j.sult.2010.11.004

[30] Lillegraven S, Bøyesen P, Hammer HB, et al. Tenosynovitis of the extensor carpi ulnaris tendon predicts erosive progression in early rheumatoid arthritis. Annals of the Rheumatic Diseases. 2011;**70**(11):2049-2050. DOI: 11.1136/ard.2011.151316

[31] Grassi W, Filippucci E. Ultrasonography and the rheumatologist. Current Opinion in Rheumatology. 2007;**19**(1):55-60. DOI: 10.1097/BOR.0b013e3280119648

[32] Taylor PC, Steure A, Gruber J, et al. Comparison of ultrasonographic assessment of synovitis and joint vascularity with radiographic evaluation in a randomized, placebo-controlled study of infliximab therapy in early rheumatoid arthritis. Arthritis and Rheumatism. 2004;**50**(4):1107-1116. DOI: 10.1002/art.20123

[33] Brown AK, Quinn MA, Karim Z, et al. Presence of significant synovitis in rheumatoid arthritis patients with disease-modifying antirheumatic drug-induced clinical remission: Evidence from an imaging study may explain structural progression. Arthritis and Rheumatism. 2006;**54**(12):3761-3773. DOI: 10.1002/art.22190

[34] Foltz V, Gandjbakhch F, Etchepare F, et al. Power Doppler ultrasound, but not low-field magnetic resonance imaging predicts relapse and radiographic disease progression in rheumatoid arthritis patients with low levels of disease activity. Arthritis and Rheumatism. 2012;**64**(1):67-76

[35] Naredo E, D'Agostino MA, Wakefield RJ, et al. Reliability of a consensus-based ultrasound score for tenosynovitis in rheumatoid arthritis. Annals of the Rheumatic Diseases. 2013;**71**(8):1328-1334. DOI: 10.1136/annrheumdis-2012-202092

[36] Damjaniv N, Radunovic G, Prodanovic S, et al. Construct validity and reliability of ultrasound disease activity score in assessing joint inflammation in RA: Comparison with DAS28. Rheumatology. 2012;**51**(1):120-128. DOI: 10.1093/rheumatology/ker255

[37] Sifeuntes-Cantu C, Contrearas-Yanez I, Saldarriaga L, et al. The added value of musculoskeletal ultrasound to clinical evaluation in the treatment decision of rheumatoid arthritis outpatients: Physician experience matters. BMC Muculoskeletal Disorder. 2017;**18**(1):1-10. DOI: 10.1186/s12891-017-1747-2

[38] Zabotti A, Salvin S, Quartuccio L, et al. Differentiation between early rheumatoid and early psoriatic arthritis by the ultrasonographic study of the synovio-entheseal complex of the small joints of the hands. Clinical and Experimental Rheumatology. 2016;**34**(3):459-465

[39] D'Agostina MA, Said-Nahal R, Hacquard-Bouder C, et al. Assessment of peripheral enthesitis in the spondylarthropathies by ultrasonography combined with power Doppler: A cross sectional study. Arthritis and Rheumatism. 2003;**48**(2):523-533. DOI: 10.1002/art.10812

[40] Balint PV, Terslev L, Aegerter P, et al. OMERACT ultrasound task force members. Reliability of a consensus-based ultrasound definition and scoring for enthesitis in spondyloarthritis and psoriatic arthritis. Annals of the Rheumatic Diseases.

2018;**77**(2):1730-1735. DOI: 10.1136/annrheumdis-2018-213609

[41] Gutierrez M, Filippucci E, De Angelis R, et al. A sonographic spectrum of psoriatic arthritis: "The five targets". Clinical Rheumatology. 2010;**29**(2):133-142. DOI: 10.1007/s10067-009-1292-y

[42] Macia-Villa C, Falcao S, Medina J, et al. A descriptive and reliability analysis of elemental lesions and power Doppler subtypes. Scandinavian Journal of Rheumatology. 2019;**48**(6):454-459

[43] Balint PV, Kane D, Wilson H, et al. Ultrasonography of entheseal insertions in the lower limb in spondylarthropathy. Annals of the Rheumatic Diseases. 2002;**61**(10):905-910. DOI: 10.1136/ard.61.10.905

[44] Kaeley GS. Enthesitis in psoriatic arthritis (part 2): Imaging. Rheumatology. 2020;**59**(1):i5-i20

[45] Zabotti A, Sakellariou G, Tinazzi I, et al. Novel and reliable DACTylitis global Sonographic (DACTOS) score in psoriatic arthritis. Annals of the Rheumatic Diseases. 2020;**79**:1037-1043

[46] Christiansen RN, Ostergaard M, Terslev L. Ulttasonography in gout: Utility in diagnosing and monitoring. Clinical and Experimental Rheumatology. 2018;**36**:S61-S67

[47] Grassi W, Meenagh G, Pascual E, et al. "Crystal-clear" sonographic assessment of gout and calcium deposition disease. Seminars in Arthritis and Rheumatism. 2006;**36**(3):197-202. DOI: 10.1016/j.semarthrit.2006.08.001

[48] Neogi T, Jansen TLTA, Dalbeth N, et al. 2015 gout classification criteria: An America College of Rheumatology/European League Against Rheumatism collaborative initiative. Annals of the Rheumatic Diseases. 2015;**74**(10):1789-1798

[49] Zhang W, Doherty M, Bardin T, et al. European league against rheumatism recommendations for calcium pyrophosphate deposition. Part I: Terminology and diagnosis. Annals of the Rheumatic Diseases. 2011;**70**(4):563-570. DOI: 10.1136/ard.2010.139105

[50] Filipou G, Scanu A, Adinolfi A, et al. Criterion validity of ultrasound in the identification of calcium pyrophosphate crystal deposits at the knee: An OMERACT ultrasound study. Annals of the Rheumatic Diseases. 2020;**80**(2):261-267. DOI: 10.1136/annrheumdis-2020-217998

[51] Manger B, Kalden J. Joint and connective tissue ultrasonography—A bedside rheumatological procedure? Arthritis and Rheumatism. 1995;**38**:736-742